

Study the male reproductive biology of a marine invertebrate *Galeolaria caespitosa* and investigate its potential as a bio-indicator species of coastal marine pollution

Yonggang Lv

B.Biotech (Hons)

A thesis submitted in partial fulfilment of the requirements for the degree
of Doctor of Philosophy

School of Environmental and Life Sciences
Faculty of Science and Information Technology
The University of Newcastle, Australia

31 August, 2016

Statement of Originality

The thesis contains no material which has been accepted for the award of any other degree or diploma in any university or other tertiary institution and, to the best of my knowledge and belief, contains no material previously published or written by another person, except where due reference has been made in the text. I give consent to the final version of my thesis being made available worldwide when deposited in the University's Digital Repository, subject to the provisions of the Copyright Act 1968.

Signature: _____

Date: _____

Manuscripts for Publication

Yonggang Lv, R. John Aitken & Minjie Lin. Detailed analysis of the male reproductive system in a potential bio-indicator species – the marine invertebrate *Galeolaria caespitosa* (Polychaeta: Serpulidae). Submitted to PLOS ONE.

Yonggang Lv, R. John Aitken & Minjie Lin. Ultrastructural investigation and *in vitro* induction of spermatid differentiation in a potential bio-indicator species – the marine invertebrate *Galeolaria caespitosa* (Polychaeta: Serpulidae). Ready for submission to PLOS ONE.

Yonggang Lv, Minjie Lin & R. John Aitken. Dibutyl phthalate-impaired spermatozoa induced embryonic malformation in a potential bio-indicator species – the marine invertebrate *Galeolaria caespitosa* (Polychaeta: Serpulidae). Ready for submission.

Abstract

The history of marine pollution can be traced back to the very beginning of human civilisation. Nevertheless, this issue did not raise serious concern until a threshold level was reached with devastating consequences for the marine ecosystem. In recent years, bio-indicator species have been gradually embraced as one of the most effective approaches to predict, monitor and assess marine contamination. The statistics acquired from biomonitoring not only facilitate determination of the biological significance of man-made hazardous substances on marine ecosystems but also establish an important foundation for marine wildlife conservation and public health management.

The focal species in this PhD project is an Australian native marine invertebrate *Galeolaria caespitosa*, which is recognised as a potential bio-indicator species for coastal marine pollution and a model organism for use in laboratory toxicity tests, due to a number of remarkable life history characteristics it exhibits. According to a range of recent studies, the gametes of *G. caespitosa*, particularly its spermatozoa, and the processes of fertilisation, embryogenesis and larval development were susceptible to marine contaminants and could be utilised as sensitive indicators of pollutants in the immediate environment. Nevertheless, the reproductive biology of this species, particularly the male reproductive system, has only been superficially described. This knowledge gap has created an opportunity to undertake a comprehensive investigation of reproduction and embryonic development in this species including the sensitivity of these processes to common environmental contaminants.

(1) Utilising serial histological sections and electron microscopic techniques, the male reproductive system in *G. caespitosa* was reconstructed and the general pattern of

spermatogenesis was established. This study for the first time established a comprehensive model of male reproductive system in polychaetes, with the function of each compartment being elucidated in detail. In addition, clear similarities were found between the male reproductive system in this simple invertebrate and human beings in terms of the structure and function.

(2) As the differentiation of round spermatids in *G. caespitosa* took place in the germinal fluid without any physical support from nurse cells, spermiogenesis in this species was regarded as a convenient model for studying the underlying mechanisms of this complex differentiation process. Therefore, spermiogenesis was analysed in detail at the ultrastructural level and a preliminary study was performed to reproduce the differentiation of spermatids *in vitro*. This *in vitro* study revealed that the regulators of spermiogenesis in *G. caespitosa* were gender-specific and involved proteinaceous constituents thereby providing a basis for future studies addressing the molecular regulation of this complex differentiation process.

(3) Exposure of spermatozoa to low levels of dibutyl phthalate (DBP) led to impaired embryogenesis and developmental abnormalities that adhered to a common pattern featuring asymmetrical division of the blastomeres. This study yielded important information on the mechanisms underlying DBP-induced embryonic arrest and abnormality, highlighting the reproductive toxicity that DBP exhibits towards the gametes of aquatic invertebrates and providing novel insights into the role that sperm centrioles play in early embryogenesis.

(4) By examining the adverse effects of common marine pollutants on early embryogenesis, it was clear that the stress response of spermatozoa, which was reflected

by defects in the subsequent embryogenesis, could be utilised as a sensitive indicator for detecting certain chemicals, such as bisphenol A, DBP and a range of alkylphenols.

Table of Contents

Statement of Originality	I
Manuscripts for Publication.....	II
Abstract	III
Table of Contents	VI
Chapter 1	1
1.1 Research Background	2
1.1.1 Coastal water pollution – a global concern.....	2
1.1.2 The use of bio-indicator species for marine pollution monitoring	3
1.1.3 Sessile broadcast-spawning polychaetes as bio-indicators.....	5
1.1.4 <i>Galeolaria caespitosa</i> – a potential bio-indicator species	10
1.1.5 Male reproductive system and sperm production	18
1.1.6 Contaminant-induced oxidative damage in male germline	30
2. Research Objectives	39
Chapter 2	42
2.1 Overview	43
2.2 Introduction	44
2.3 Materials and Methods.....	45
2.3.1 Sample collection and maintenance.....	45
2.3.2 Serial paraffin sections for light microscopy.....	46
2.3.3 Transmission electron microscopy	47
2.3.4 Scanning electron microscopy.....	48
2.3.5 Live cell observation	48
2.3.6 Statistical analysis.....	48
2.4 Results	50
2.4.1 Male reproductive system in <i>Galeolaria caespitosa</i>	50
2.4.2 Seminiferous epithelium compartment.....	53
2.4.3 Nurse cell compartments	55
2.4.4 Efferent duct compartments.....	57
2.4.5 Germ cell differentiation in <i>Galeolaria caespitosa</i>	59
2.5 Discussion.....	69
Chapter 3	76

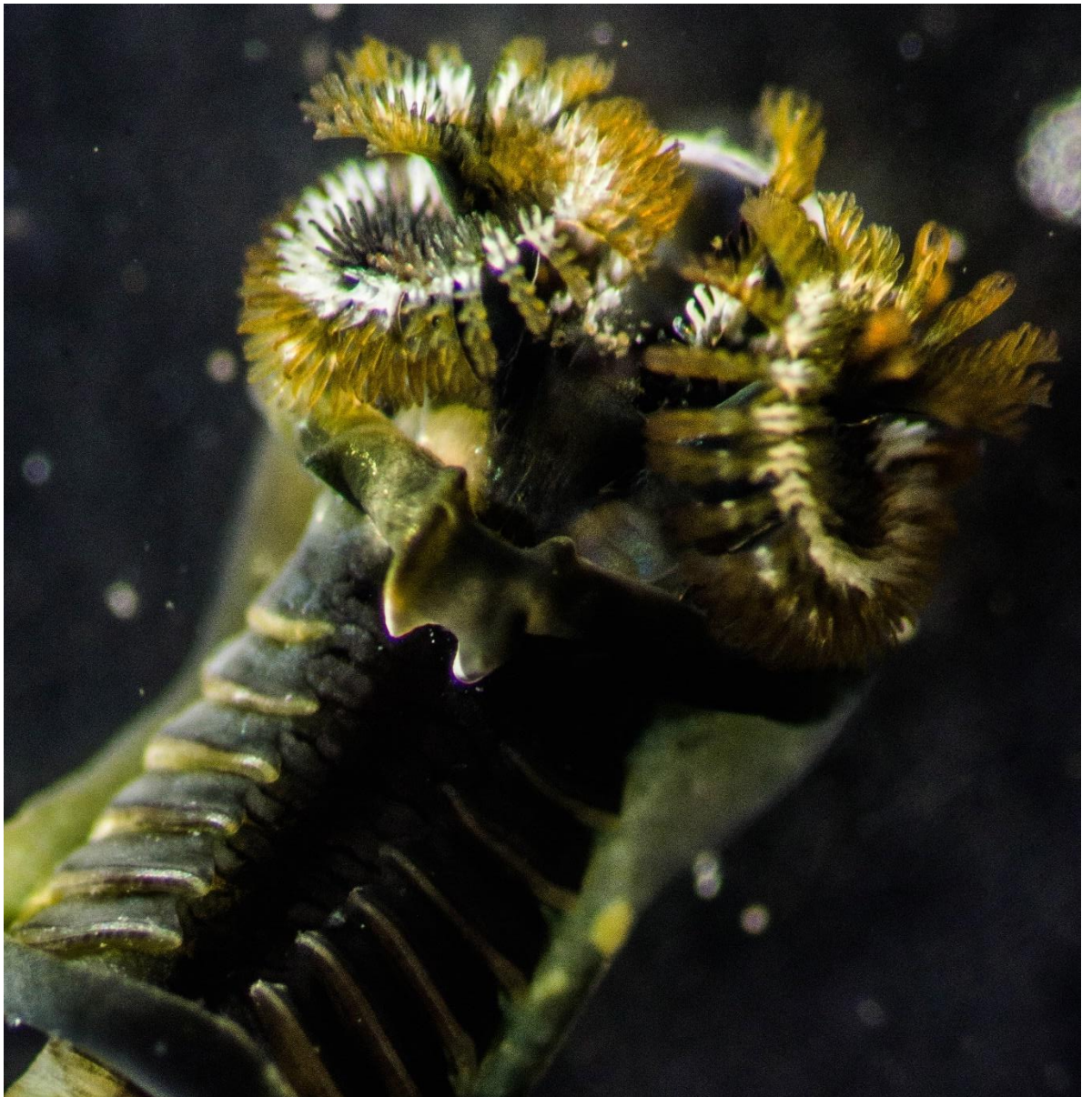
3.1 Overview	77
3.2 Introduction	79
3.3 Materials and Methods	79
3.3.1 Sample collection and maintenance	79
3.3.2 Transmission electron microscopy	79
3.3.3 <i>In vitro</i> culture of spermatids	80
3.3.4 Statistical analysis	82
3.4 Results	82
3.4.1 Step 1 spermatids	82
3.4.2 Step 2 spermatids	84
3.4.3 Step 3 spermatids	87
3.4.4 Step 4 spermatids	88
3.4.5 Step 5 spermatids	90
3.4.6 Step 6 spermatids	91
3.4.7 Step 7 spermatids	93
3.4.8 Step 8 spermatids	95
3.4.9 Step 9 spermatids	97
3.4.10 Step 10 spermatids	98
3.4.11 Spermatozoa.....	101
3.4.12 Pattern of spermatid differentiation	103
3.4.13 Induction of spermatid differentiation <i>in vitro</i>	106
3.5 Discussion.....	117
Chapter 4.....	126
4.1 Overview	127
4.2 Introduction	128
4.3 Materials and Methods	130
4.3.1 Sample collection and maintenance	130
4.3.2 Toxicity tests	130
4.3.3 Confocal microscopy	132
4.3.4 Sperm analyses.....	135
4.3.5 Statistical analysis	138
4.4 Results	140
4.4.1 DBP caused embryogenesis arrest and malformation by impairing the male germline	140

4.4.2 DBP-impaired spermatozoa produced malformed embryos with a typical pattern of abnormality.....	146
4.4.3 The typically malformed embryos contained abnormal mitotic spindles and underwent defective chromosome segregation during the first cleavage	148
4.4.4 The non-dividing blastomere in the typically malformed embryos was unable to assemble contractile actin ring during the second cleavage	153
4.4.5 DBP induced acrosome and centriole damage in the spermatozoa which respectively led to embryonic arrest and malformation.....	154
4.5 Discussion.....	165
Chapter 5	174
5.1 Overview	175
5.2 Introduction	177
5.3 Materials and Methods.....	179
5.3.1 Sample collection and maintenance.....	179
5.3.2 Toxicity tests	179
5.3.3 Statistical analysis.....	181
5.4 Results	182
5.4.1 Bisphenol A	183
5.4.2 Alkylphenols.....	186
5.4.3 Phthalate esters	194
5.5 Discussion.....	205
5.5.1 Bisphenol A	205
5.5.2 Alkylphenols.....	210
5.5.3 Phthalate esters	211
Chapter 6	215
6.1 General discussion.....	216
6.1.1 Established a comprehensive model of male reproductive system and spermatogenesis in broadcast-spawning polychaetes	216
6.1.2 Discovered the similarities between the male reproductive system of vertebrates and invertebrates	217
6.1.3 Demonstrated that the differentiation of spermatids was intrinsically programmed	218
6.1.4 Unlocked the mechanism of embryonic disruption originated from phthalate ester-induced sperm impairment	219
6.1.5 Demonstrated the sensitivity of spermatozoa to a range of marine pollutants	220
6.2 Future directions	220

6.2.1 Investigate the self-renewal process of spermatogonial stem cells in <i>G. caespitosa</i>	220
6.2.2 Optimise the system for differentiating spermatids <i>in vitro</i>	221
6.2.3 Investigate the changes that DBP-induced in sperm centrioles	222
6.2.4 Assess the sensitivity of <i>G. caespitosa</i> to effluents in laboratory and field studies..	222
References	223
Appendix	i

Chapter 1

Literature review and research aims



1.1 Research Background

1.1.1 Coastal water pollution – a global concern

With the rapid development of coastal industries, agriculture and marine transportation, the pressure of human activities on the marine environment has been dramatically intensified, causing devastating impacts on the structure and functioning of marine ecosystems (Torres *et al.*, 2008). Such anthropogenic-induced interventions jeopardise the products and services that the ecosystems provide, which in turn poses potential risks to human well-being through a biomagnification process (Islam and Tanaka, 2004).

Among various types of marine pollution, the discharge of domestic, commercial and industrial effluents containing complex mixtures of hazardous chemicals to marine waters has been recognised as one of the major human-derived disturbances of the environment. Exposure to toxic contaminants has been held to bring about a series of sub-lethal effects on marine organisms, such as metabolic disorder, reproductive disruption, growth inhibition and embryonic abnormality (Sindermann, 1979). As a consequence, the current rate of species extinction has accelerated to approximately 1,000 to 10,000 times the background extinction rate (Derraik, 2002).

Although marine pollution has provoked much concern in recent decades, the production and emission of marine pollutants have not ceased. Pollutants are ubiquitously found in coastal waters, which are located near the primary sources of these dangerous substances, such as coastal refineries and sewage outlets. In addition, human populations in coastal areas are growing faster than those in inland regions, resulting in coastal environments and ecosystems being subjected to elevated anthropogenic pressure. Given these circumstances, the prediction, monitoring and evaluation of coastal water pollution has

become an immediate requirement for the sustainable management and conservation of existing fisheries and marine resources (Islam and Tanaka, 2004).

1.1.2 The use of bio-indicator species for marine pollution monitoring

Globally, the detection and assessment of marine pollution is mainly dependent on chemical measurements of contaminants in water, sediments and marine biota (Rainbow, 1995; Rainbow, 2006). It is generally believed that such chemical analyses can accurately and efficiently reflect the severity of marine pollution. However, the statistics obtained from chemical measurements, alone, cannot provide an effective basis for determining the actual damage that the pollution has caused to the marine ecosystem (Long *et al.*, 1995). To estimate the potential for adverse biological effects, the chemistry statistics have to be interpreted, resulting in the generation of massive, complex datasets (Zhou *et al.*, 2007). Besides, risk assessments established on the basis of these data can sometimes be misleading, as pollutants are normally found in trace amounts in the water body and at elevated levels in sediments (Long *et al.*, 1995; Torres *et al.*, 2008). Comparatively speaking, the analysis of accumulated pollutants in cells, body fluids, tissues, and organs of marine biota is of ecotoxicological relevance, as the contamination levels in these organisms provide a relative measure of pollutant bioavailability, integrated over the preceding period of time (Beiras *et al.*, 2003; Galloway *et al.*, 2002; Markert *et al.*, 2003; Rainbow, 2006). The measurement of pollutants in marine biota also helps to determine the risks that marine species at higher trophic levels, and even humans, would take by consuming the contaminated edible species (Chiarelli and Roccheri, 2014). In this context it should be recognised that the concentration of chemical residues in marine organisms as a consequence of foraging activity is variable, and determined by the physical properties of pollutants as well as such factors as the ingestion rate and gut uptake

efficiency of the host species (Leppänen, 1995). A representative example for a programmed biomonitoring system is the “Mussel Watch”, which was adopted by environmental organisations in the late twentieth century to assess the extent of marine contamination economically. This approach, along with many other traditional investigations were all dedicated to the measurements of pollutant concentrations in the organisms rather than the resultant adverse ecological impacts (Goldberg and Bertine, 2000).

Over the last several decades, the use of bio-indicator species has been gradually embraced and popularised to determine the biological significance of various marine pollutants and to acquire information for marine wildlife conservation and public health management (Long *et al.*, 1995; Sany *et al.*, 2014). More significantly, these species can be utilised to reflect the ecological status of local environment and to exhibit early warning signs for ecosystem dysfunction through their quantifiable biochemical, physiological or ecological responses to the pollutants (Au, 2004).

To unleash the full potential of a bio-indicator species in reflecting ecological status, an appropriate stress response should be selected based on the properties of the target contaminants (Au, 2004). Stress responses of marine organisms to pollutants are initiated at low levels of biological organisation and propagated upward through higher levels (Adams, 2005). Host responses at low organisational levels, such as elevated expression of cytochrome P450 and loss of DNA integrity, are sensitive, specific and easy to determine and reproduce, but less realistic and have no direct relationship with ecological changes (Au, 2004; Sarkar *et al.*, 2006). In contrast, responses at higher levels of biological organisation, such as decreased population size and disturbed sex ratio, can directly reflect the ecosystem status. However, these responses are comparatively

complicated to analyse and cannot be detected until severe environmental degradation has occurred. Comparatively, host responses at intermediate levels of biological organisation, such as reproductive dysfunction and defective early development, are readily measurable and reproducible, and are able to provide early warnings of ecological change and dysfunction (Adams, 2005; Au, 2004). Besides, the investigation into such stress responses allows an extrapolation from individual to population responses and also provides researchers with opportunities to elucidate the underlying molecular or biochemical mechanisms (Au, 2004).

1.1.3 Sessile broadcast-spawning polychaetes as bio-indicators

Polychaetes are segmented invertebrates characterised by the presence of a well-distinguished prostomium bearing specialised sense organs and/or feeding appendages, followed by a segmented trunk dividing into thoracic and abdominal regions. Each trunk segment has a pair of parapodia with associated chaetae (Fauchald and Rouse 1997). These organisms form the largest taxon in Annelida with more than 13,000 species in 83 families that have been documented to date (Hutchings, 1998). Polychaetes are generally marine; their ability to survive in a wide range of environmental conditions enables them to reside all marine habitats, ranging from intertidal to abyssal benthic zone (Rouse, 1998). These segmented worms play an important role in the normal functioning of marine ecosystems, because they not only are ubiquitously distributed in the marine environment, but also occupy numerous trophic levels in various ecosystems, from primary consumers to top predators.

Polychaetes exhibit distinct life history characteristics that endow these organisms with significant potential as model species in laboratory toxicity testing and marine pollution

monitoring (Dean, 2008). These characteristics include, but are not limited to, their body size, sedentary lifestyle, unique feeding habits, bioaccumulation ability, short life cycle, broadcast-spawning strategy and enormous reproductive capacity, as well as the vulnerability of their gametes, fertilisation and early development (i.e. embryogenesis and larval development) to a wide range of pollutants.

1.1.3.1 Ideal body size

A wide range of marine invertebrates, especially polychaete species are particularly suitable for both laboratory toxicological tests and culture purposes, because of their ideal body size. Polychaetes are macroscopic, so microscopic equipment is not required if the study only involves whole-body analyses. Furthermore, they are much smaller than most marine vertebrates, reducing the amount of laboratory space and toxicants are required for analysis. Polychaetes can also be readily cultured and maintained over many generations in the laboratory, which facilitates the continuous observation and monitoring of individual stress responses to environmental toxicants (Dean, 2008). The drawback for using smaller organisms in pollution monitoring is a corresponding reduction in the concentrations of toxicants they are prone to accumulate (Ahn *et al.*, 2001). However, larger body sizes are usually associated with a decrease in the vulnerability of the host species to pollutants (Bremner, 2008).

1.1.3.2 Sedentary lifestyle

The sessile polychaetes, which generally dwell in the sediments or adhere to hard surfaces, are relatively inert compared with their larvae which are capable of long distance transport (Dean, 2008). Such sedentary lifestyle renders them being chronically exposed to hazardous substances in the local environment rather than episodic exposures of most

vagile species (Dean, 2008; Melville and Pulkownik, 2006). Therefore, any change in the fitness of the local invertebrate community can be effectively reflected in these sessile polychaetes (Boening, 1999; Dean, 2008). Compared with sedentary species, migratory species are relatively difficult to collect and require an investigation into the duration of time that they have stayed in the local area prior to sampling (Burger and Gochfeld, 2004). Moreover, a considerable portion of sedentary polychaetes (e.g. serpulids) act as fouling species that tend to form dense assemblages on natural and artificial hard substrates, such as rock revetments, docks, pier piling and ship hull. This remarkable capacity to colonise artificial surfaces enables researchers to perform replicate measurements on the stressors that alter the settlement, colonisation and survival rates of the fouling communities. The use of artificial substrates also minimises variation due to physical differences between independent sampling sites (e.g. type of substrate and light penetration), so that the parameters measured should only reflect changes in water quality, rather than the physical characteristics of the habitat (Saliu and Ovuorie, 2007).

1.1.3.3 Feeding habits and bioaccumulation ability

The feeding strategies that polychaetes exhibit also makes them promising bio-indicator species (Dean, 2008; Giangrande *et al.*, 2005). The filter-feeding polychaetes maximise their exposure to dissolved hazardous substances in the aqueous environment as they process a large amount of water exchange during foraging activities (Dean, 2008). By contrast, the deposit-feeding polychaetes are in intimate contact with the sediments and directly uptake particulate contaminants that settle onto the nearby substrate (Dean, 2008; Rainbow, 1995). In light of these considerations, a suitable polychaete can be selected, based on the physical properties of the target contaminant, such as its water solubility and the size of particles that it forms in the water body or in sediments.

Polychaetes, along with many other marine invertebrates possess the ability to accumulate toxic contaminants in their cells, body fluids, tissues, and organs. The concentrations of deleterious materials accumulated in polychaetes are proportional to the levels of those substances in the local environment (Pocklington and Wells, 1992). This ability makes them good indicators of the presence and bioaccumulation potential of these materials. The direct ingestion of particulate contaminants has been regarded as the primary route for bioaccumulation of toxicants (Leppänen, 1995). As a consequence, the ingested contaminants will be desorbed in the intestine and subsequently absorbed across the intestinal wall. Apart from feeding activities, toxicants can also be accumulated in the host species through water ventilation during respiration, or through direct contact with contaminated water or sediment, during which the toxicants passively diffuse through the body surface (Leppänen, 1995; Weston *et al.*, 2000). Due to their different diets and habitats, the accumulation of toxicants in deposit-feeders is related to the concentration of contaminants in the sediment, while the bioaccumulation in filter-feeding species is more likely to reflect the pollutant concentrations in the water body (Dean, 2008).

1.1.3.4 Short life cycle

A considerable proportion of marine polychaetes can accomplish their entire life cycle in a matter of weeks. In reproductive and developmental toxicity testing, more toxicants or effluent samples can be examined within a given time using these polychaetes rather than alternative species with longer life cycle. Moreover, short-lived organisms are able to respond more promptly to any pollutant-induced sub-lethal effects on gene expression, fecundity, growth rate or longevity through changes in their population (Kennedy and Jacoby, 1999).

1.1.3.5 Broadcast-spawning strategy and enormous reproductive capacity

Although polychaete species are diverse in their spawning strategies, broadcast-spawners account for the majority of them. The broadcast-spawning polychaetes shed their gametes directly into the surrounding water column and the subsequent fertilisation largely relies on turbulent-stirring processes in the flow to bring the gametes together (Crimaldi, 2012). This feature renders the gametes of broadcast-spawners vulnerable to being directly and chronically exposed to hazardous substances in the local environment before, during and after fertilisation. Nevertheless, the fertilisation rates achieved by these species are strongly limited by the long-term dilution of gamete concentration in the water column. Such dilution effects are mitigated by the parent organisms forming dense aggregations, releasing gametes in a viscous matrix that can persist under low flow conditions, spawning synchronously and producing large quantities of viable gametes (Crimaldi, 2012; Kupriyanova, 2006; Marshall and Bolton, 2007; Oliver and Babcock, 1992). This enormous reproductive capacity of polychaetes also enables researchers to access a virtually unlimited number of gametes for toxicological purposes.

1.1.3.6 Vulnerability to pollutants

Undoubtedly, different polychaetes respond to the various hazardous contaminants in diverse ways. In previous laboratory and field ecotoxicological studies, a large number of polychaetes were found to exhibit high sensitivity to a wide range of marine toxicants [e.g. heavy metals (Reish *et al.*, 1976), polycyclic aromatic hydrocarbons (Rossi and Neff, 1978) and tributyltin (Lau *et al.*, 2007; Moore *et al.*, 1991)]. Such sensitivity is generally expressed through changes in their reproduction, growth and mortality which, in turn, facilitates the evaluation of pollution-induced adverse impacts at the individual, population and community levels. In most case, polychaete gametes are more susceptible

to the action of toxicants than the adults, suggesting that contaminant-derived defects in fertilisation and early development can serve as sensitive indicators of the presence of pollutants (Dean, 2008). For example, toxicity tests conducted by Gopalakrishnan *et al.* (2008) revealed that fertilisation, embryogenesis and larval development of the polychaete *Hydroides elegans* were extremely susceptible to heavy metals.

1.1.4 *Galeolaria caespitosa* – a potential bio-indicator species

In Australia, the coastal areas support the majority of the residents, with more than 82% people living within 50 km of the coastline. Such a high density of population results in overwhelming human pressures on the coastal environment (Birch, 2000). In this case, establishing a comprehensive biomonitoring system for predicting, assessing and managing the ecological status of coastal areas in Australia becomes an immediate need. The focal species in the current PhD project is an Australian native marine invertebrate *Galeolaria caespitosa* (Polychaeta: Serpulidae), which has great potential as a candidate species for coastal pollution biomonitoring. In this section, basic information on this marine polychaete will be provided, with an emphasis on elucidating its potential as a model species for both pollution monitoring and laboratory toxicity testing.

1.1.4.1 Broad geographical distribution

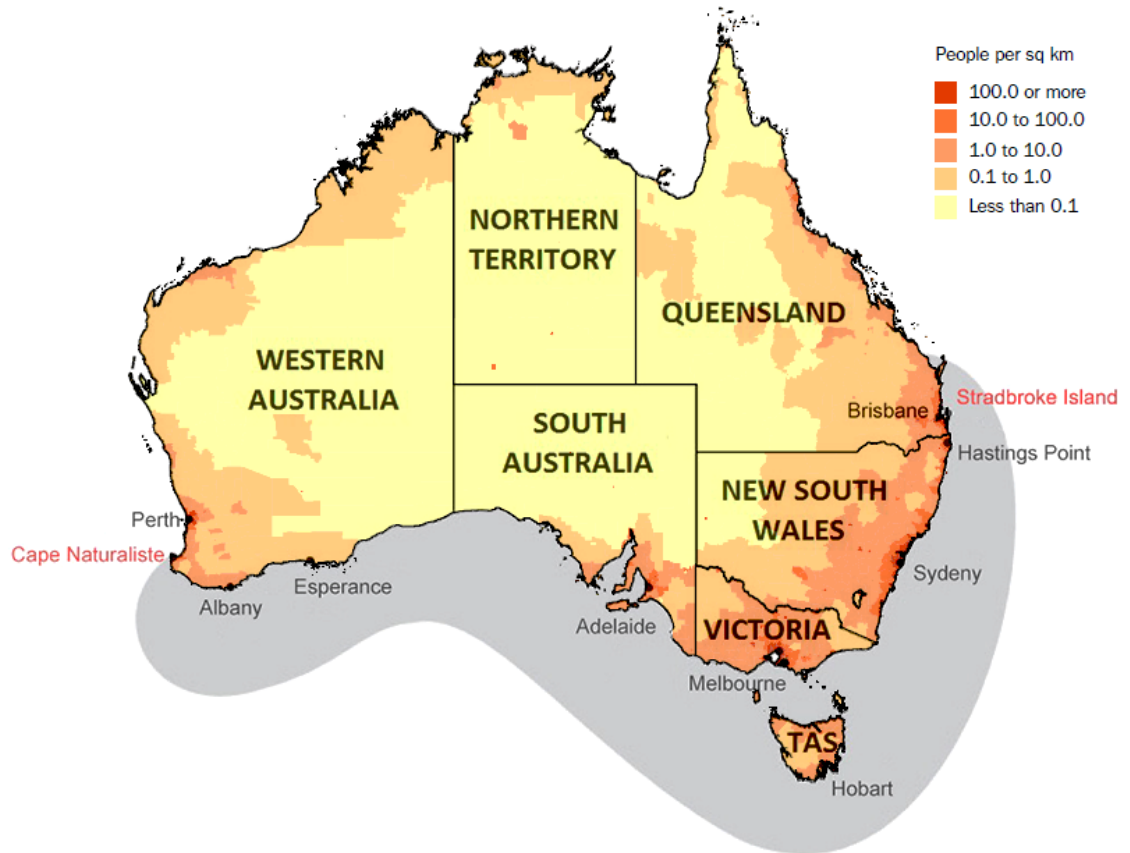


Figure 1.1 The geographical distribution of human population (yellow- to red-coloured areas) and *Galeolaria caespitosa* (shaded area) in Australia. The Australia's residents are generally concentrated along the south-eastern and south-western coasts, as well as the entire coastline of Tasmania. *G. caespitosa* can be found mainly in the southern part of the continent from Stradbroke Island in Queensland to Cape Naturaliste in Western Australia. Adapted from Halt *et al.* (2009) and Australian Bureau of Statistics (2010).

G. caespitosa is endemic to the southern coast of Australia, with a continuous range over 4,500 kilometres (Halt *et al.*, 2009; Styan *et al.*, 2008). Specifically, its geographical distribution initially occurs at the eastern coast of the continent, stretches westwards along the whole southern coast, and terminates at the south-eastern coast of Australia (**Figure 1.1**). According to the statistics released by Australian Bureau of Statistics in 2010, Australia's population is heavily centralised with the majority of population living along

the south-eastern and south-western coasts. Interestingly, *G. caespitosa* can be found in most of the densely populated coastal areas, which are labelled with orange (10 to 100 people/km²) and red (≥ 100 people/km²) in the map (**Figure 1.1**). Such a coincidence between the geographical distribution of human beings and *G. caespitosa* suggests that this species may be an effective indicator for human-derived pollution in coastal regions.

1.1.4.2 Sedentary intertidal lifestyle



Figure 1.2 Aggregation of the tubeworm *G. caespitosa* (Wilson's Promontory, Victoria). *G. caespitosa* dwells in dense calcareous tubes and colonises hard surfaces in the intertidal zone of the seashore. Photo by Dr Jeff Shimeta, used with permission.

G. caespitosa is a sessile tubeworm accommodated within white calcareous tubes (**Error! Reference source not found.**) that form 5 to 15 cm thick assemblages on hard substrates with an extremely high density of up to 10 individuals per cm³ (Halt *et al.*, 2009; Styan

et al., 2008). They can be easily collected from pier pilings and rock revetments in low to mid intertidal regions of the seashore (Minchinton, 1997; Ross and Bidwell, 2001). Benthic polychaetes are widely accepted as suitable indicators of marine pollution, as they live in close proximity to the sediments, where most marine toxicants eventually end up (Giangrande *et al.*, 2005). Nonetheless, intertidal polychaetes are also considered as candidate bio-indicators, due to the fact that they are subject to more intensive pressures derived from urbanisation.

1.1.4.3 Small body size and broadcast-spawning strategy

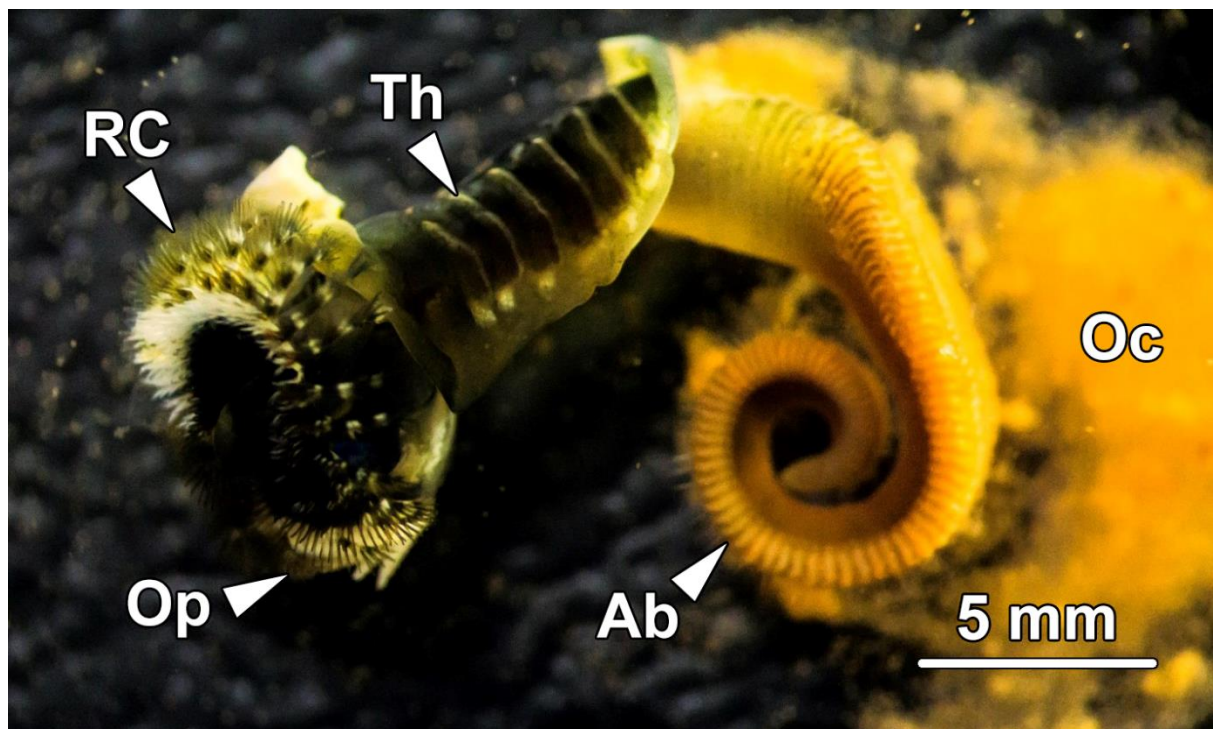


Figure 1.3 An adult female *G. caespitosa* in natural seawater with spawned oocytes (Oc). *G. caespitosa* is comprised of a head bearing a prostomial radiolar crown (RC) and an operculum (Op), a segmented thorax (Th) and a segmented abdomen (Ab). The female adults are characterised by their conspicuous orange abdomen. On exposing to seawater, mature *G. caespitosa* spontaneously releases large amounts of viable gametes. Photo by Yonggang Lv.

G. caespitosa has a relatively small body size which is approximately 10 to 30 mm in length and 0.8 to 2.7 mm in thoracic width (Halt *et al.*, 2009). It consists of a head bearing

a prostomial radiolar crown and an operculum, a thorax and a segmented abdomen (Error! Reference source not found.). This species is dioecious, gender being distinguishable by the orange colour of the female abdomen and creamy white colour of the male abdomen (Andrews and Anderson, 1962; Kupriyanova and Havenhand, 2005). The conspicuous colours of their abdomens are due to the presence of viable free-floating gametes throughout the year (Kupriyanova, 2006).

As a model broadcast-spawning species, *G. caespitosa* releases gametes directly into the water column, where fertilisation occurs externally (Marshall and Evans, 2005b). Such a spawning strategy coupled with the relative immobility of the parent organism, results in the gametes of *G. caespitosa* being directly exposed to toxic substances in surrounding seawater before, during and after fertilisation. During laboratory toxicity tests, *G. caespitosa* can be readily stimulated to spawn gametes by simply extracting the worms from their tubes and exposing them to natural seawater in small petri dishes (Kupriyanova, 2006; Marshall and Evans, 2005a; Ross and Bidwell, 2001).

1.1.4.4 Immediate acclimation to laboratory conditions

The acclimation period allows the test organisms to stabilise in a novel laboratory environment. As a result of being frequently used in routine toxicity studies, it is of immense importance for a bio-indicator species to quickly adapt to laboratory conditions. Ross and Bidwell (2001) found in their study that *G. caespitosa* is amenable to laboratory holding and can be maintained for at least 2 weeks in aerated tanks without jeopardising the viability of its gametes. As a model species, it has an excellent ability to accommodate foreign environments as manifested by the high fertilisation rates (~ 98%) that have been achieved under laboratory conditions, without any acclimation period prior to the test (Ross and Bidwell, 2001).

1.1.4.5 Rapid early development

The embryonic development in *G. caespitosa* was first studied by Andrews and Anderson (1962) and its larval development, metamorphosis and settlement were described by Marsden and Anderson (1981). Immature oocytes, which are characterised by the presence of a prominent nucleus called the germinal vesicle, can be sometimes observed mixing with mature ones (**Figure 1.4A**). These oocytes cannot be fertilised before the breakdown of the germinal vesicle. The unfertilised eggs of *G. caespitosa* exhibit a polyhedron shape on being released, but immediately transform into a spherical shape after immersion in seawater, with a diameter of approximately 65 μm . The colour of eggs ranges from pale pink to yellowish in reflected light, and appears to be brown under transmitted light (Andrews and Anderson, 1962). The success of fertilisation in *G. caespitosa* is indicated by the presence of a fertilisation membrane, which appears as a thickened jelly layer lifted from the egg surface (**Figure 1.4B**; Andrews and Anderson, 1962).

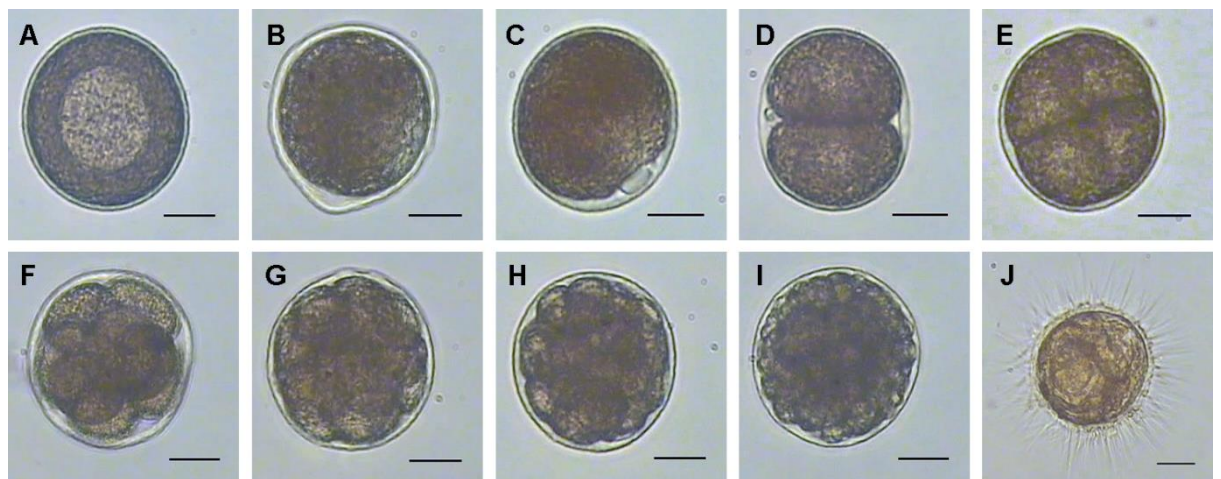


Figure 1.4 The normal early embryogenesis in *G. caespitosa*. (A) An immature oocyte with a distinct vesicle. (B) A fertilised egg with lifted envelope at the site of sperm penetration. (C) The discharge of first polar body occurs about 30 to 45 min after fertilisation. (D) The discharge of second polar body occurs soon after that of the first one. The fertilised egg bisects into two about

1.5 h after fertilisation. **(E)** The fertilised egg divides into four cells about 2 h after fertilisation. **(F)** The fertilised egg enters the 8-cell stage about 2.5 h after fertilisation. **(G)** The fertilised egg develops into a 16-cell embryo about 3 h after fertilisation. **(H)** The fertilised egg divides into 32 blastomeres about 3.5 h after fertilisation. **(I)** The fertilised egg develops into a blastula about 5 h after fertilisation. **(J)** The fertilised egg develops into a trochophore larva with motile external cilia about 18 h after fertilisation. Photo by Yonggang Lv. Scale bars = 20 μm .

The fertilised egg of *G. caespitosa* follows a pattern of equal and spiral cleavage, during which blastomeres synchronously divide. Early embryogenesis is extremely rapid, taking only 1.5 h for a fertilised egg to develop into a 2-cell embryo and 5 h into a blastula (**Figure 1.4C to I**). Gastrulation occurs thereafter, with features can be difficult to discern under light microscope conditions due to dramatic increases in cell density and decreases in cell size. It only takes about 18 h for a fertilised egg to develop into a planktotrophic trochophore, which is characterised by conspicuous internal organs and active external cilia (**Figure 1.4J**; Marsden and Anderson, 1981). The planktotrophic larvae of *G. caespitosa* develop for up to three weeks and settle gregariously in response to cues from conspecifics (Andrews and Anderson, 1962; Halt *et al.*, 2009; Marsden and Anderson, 1981). The rapid early development in *G. caespitosa* enables researchers to access a virtually unlimited number of embryos with minimal incubation time and to perform rapid assessments to reveal the effects of marine pollutants on its early development.

1.1.4.6 Capacity to accumulate trace metals

As a typical filter-feeding species, *G. caespitosa* has the ability to accumulate toxic substances through the uptake of suspended particulate matter during the water exchange involved in foraging activities. Concentrations of ten trace metals in the whole tissue of *G. caespitosa* and other seven common coastal Australian polychaetes (*Australonereis ehlersi*, *Australonuphis parateres*, *Lumbrinereis* spp., *Marphysa* spp., *Notomastus*

estuaries, Scoloplos simplex, and Sigalion spp.) collected from uncontaminated sites were examined by Waring *et al.* (2006) to determine their bioaccumulation ability. The concentrations of mercury, silver and zinc accumulated in *G. caespitosa* were significantly higher than in seven other species and the concentrations of manganese, copper, cadmium were the second highest among the eight species tested. In contrast, the concentrations of arsenic, lead and selenium in *G. caespitosa* were moderately high among all species and the concentration of cobalt was lower than other seven species. This study clearly demonstrated that *G. caespitosa* has the capacity to accumulate certain trace metals.

1.1.4.7 Vulnerability of gametes and larvae to pollutants

Another important reason for *G. caespitosa* being regarded as a bio-indicator species is that it has exhibited sensitive responses in a series of previous toxicity tests. According to the toxicity tests conducted by Hollows *et al.* (2007), the fertilisation in *G. caespitosa* was extraordinarily susceptible to low concentrations of copper (25 to 50 µg/L). The success rates of fertilisation were significantly decreased with the presence of copper under both laboratory and field conditions. Wisely and Blick (1967) tested the larval mortality of seven invertebrates, including two bryozoans (*Watersipora cucullata* and *Bugula neritina*), two tubeworms (*Spiuorbis lamellose* and *G. caespitosa*), two bivalve molluscs (*Mytilus edulis planulatus* and *Crassostrea commercialis*), and a brine shrimp (*Artemia salina*), when being exposed to mercury and copper solutions. The larvae of bivalve molluscs and brine shrimp were found to have the most significant sensitivity to these heavy metals; the larvae of *G. caespitosa* were more vulnerable compared with those of the two bryozoans and the other serpulid tubeworm *Spiuorbis lamellosa*. Ross and Bidwell (2001) analysed the effects of gamete exposure to copper and a complex

effluent produced by a lead smelter. The toxicity of the two toxicants were manifested by the median effective concentrations (EC₅₀) for 48-h larval development. The larval development in *G. caespitosa* exhibited low EC₅₀ values ranging from 16 to 40 µg/L of copper solutions. Compared with those of other tested organisms (*Isochrysis* sp., *Nitzschia closterium* and *Mytilus edulis*), the larvae of *G. caespitosa* exhibited the most sensitive response to the effluent.

Overall, these toxicological studies reveal that the reproduction and development in *G. caespitosa*, particularly its fertilisation process, was susceptible to a range of trace elements and heavy metals, highlighting the feasibility of utilising its gametes and early development as indicators for coastal pollution monitoring. It has been suggested that using the bio-indicator species that have been intensively studied in the past can facilitate the interpretation of resultant biomonitoring data (Ward and Jacoby, 1992). Without sufficient knowledge on the designated stress response at a certain biological organisation level, one can hardly evaluate the parallel stress to the indicator species at a different biological level. With regard to our focal species *G. caespitosa*, its reproductive biology, particular the male reproductive biology has been poorly elucidated. Therefore, in the following section, a comprehensive review of the male reproductive biology will be provided, with an emphasis on spermatogenesis and spermatozoa.

1.1.5 Male reproductive system and sperm production

The reproductive characteristics of polychaetes are extremely diverse, which may not only because of their remarkable plasticity and adaptability to a broad range of habitats, but also attributed to the simplicity of their reproductive system (Eckelbarger *et al.*, 2001; Hutchings, 1998). The reproductive biology of polychaetes has been generally studied

from several aspects, such as gametogenesis, spawning strategy, fertilisation mode, embryogenesis and larval development (Giangrande, 1997). A comprehensive investigation of male reproductive biology in polychaetes could potentially provide new insights into the elaborate process of sperm production in the male reproductive system and establish a knowledge basis for any future research involving their reproduction. Nevertheless, only a limited number of publications have described the pattern of spermatogenesis in polychaetes in detail or studied the structure and function of the male reproductive system. Given the insufficient knowledge in polychaetes, the following section focuses on human testicular anatomy and mammalian spermatogenesis and relates this information to our current understanding of the male reproductive system in polychaetes.

1.1.5.1 Testicular structure and function in mammalian species

The testes in mammalian species are surrounded by a thick fibrous capsule, the tunica albuginea, and divided by connective tissue septa into 200 to 300 pyramid-shaped intercommunicating compartments, which are known as lobuli testes. Each lobe contains one or more highly convoluted seminiferous tubules, which are internally lined with the seminiferous epithelium, where spermatogenesis occurs (Johnson and Everitt, 2007). Spermatogenic cells first appear at the basement membrane of the seminiferous epithelium and migrate peripherally towards the lumen during differentiation. The fully differentiated spermatozoa detach from the seminiferous epithelium and travel through the lumen of seminiferous tubules in testicular fluid. These newly released sperm cells are immotile and are passively transported out from the seminiferous tubules through tubuli recti, or the straight seminiferous tubules, which are solely lined by Sertoli cells (Henrikson and Mazurkiewicz, 1997; Johnson and Everitt, 2007). The spermatozoa then

enter the rete testis, which is a network of anastomosing channels lined by cuboidal to columnar epithelium with short microvilli and a single cilium on the luminal surface (Cormack, 2001). Spermatozoa exit the testis through the efferent ducts (“vasa efferentia” in **Figure 1.5**) and are then transported into the highly coiled ductus epididymis. The efferent ducts possess a thin circular layer of smooth muscle beneath the basal lamina of the epithelium containing ciliated columnar and non-ciliated cuboidal epithelial cells. The transportation of spermatozoa through the efferent ducts is conducted by ciliary action and the peristaltic contraction of smooth muscle (Haschek *et al.*, 2010). During the passage through the ductus epididymis, the spermatozoa accomplish their final maturation, including the completion of sperm morphogenesis and acquisition of the ability to move and fertilise oocytes. The epididymis also functions as a reservoir for the storage and sustenance of mature spermatozoa (Cooper, 1986a; Cooper, 1986b; Johnson and Everitt, 2007).

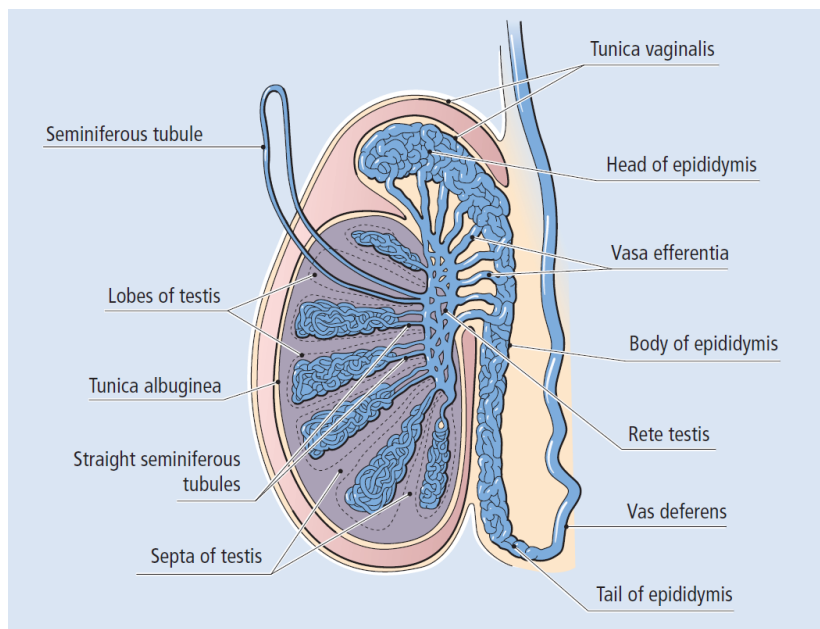


Figure 1.5 A diagram illustrates the testicular structure in humans. The human testis is surrounded by a closed serous sac known as *tunica vaginalis* derived from peritoneum during descent of testis. Deep to the tunica vaginalis there is a thick white fibrous connective tissue

capsule, the *tunica albuginea*, which completely encloses the testis. The testis is internally divided by *interlobular septa* into about 250 pyramidal compartments, the *lobuli testis*. Each lobe of testis contains one to four highly convoluted *seminiferous tubules*, which are internally lined by a complex stratified epithelium containing spermatogenic and supporting cells. The hilar ends of the coiled seminiferous tubules transform into *straight seminiferous tubules* that connect to the *rete testis*, which in turn connects to the *head of epididymis* through the *vasa efferentia*. Spermatozoa accomplish the final maturation during their migration through the *body of epididymis*. They are stored in the *tail of epididymis* and eventually exit the testis from the *vas deferens*. Illustration by Johnson and Everitt (2007).

1.1.5.2 General pattern of spermatogenesis

Spermatogenesis is a highly complex but orderly arranged process, during which diploid spermatogonial stem cells undergoes a series of mitotic and meiotic divisions and transforms into highly specialised haploid spermatozoa (Phillips *et al.*, 2010; Wistuba *et al.*, 2007). The ultimate purpose of spermatogenesis is to establish and maintain a daily output of functional spermatozoa that act as efficient delivery vehicles for paternal DNA and other factors to oocytes (Chu and Shakes, 2013; Sutovsky and Manandhar, 2006). Although the pattern of spermatogenesis varies considerably across species, it can be generally summarised into three major phases: mitotic propagation of spermatogonial stem cells in the proliferative (or mitotic) phase, genetic recombination of spermatocytes in the meiotic phase and morphological transformation of round spermatids into specialised functional spermatozoa in the spermiogenic phase (Oatley and Brinster, 2008; Phillips *et al.*, 2010).

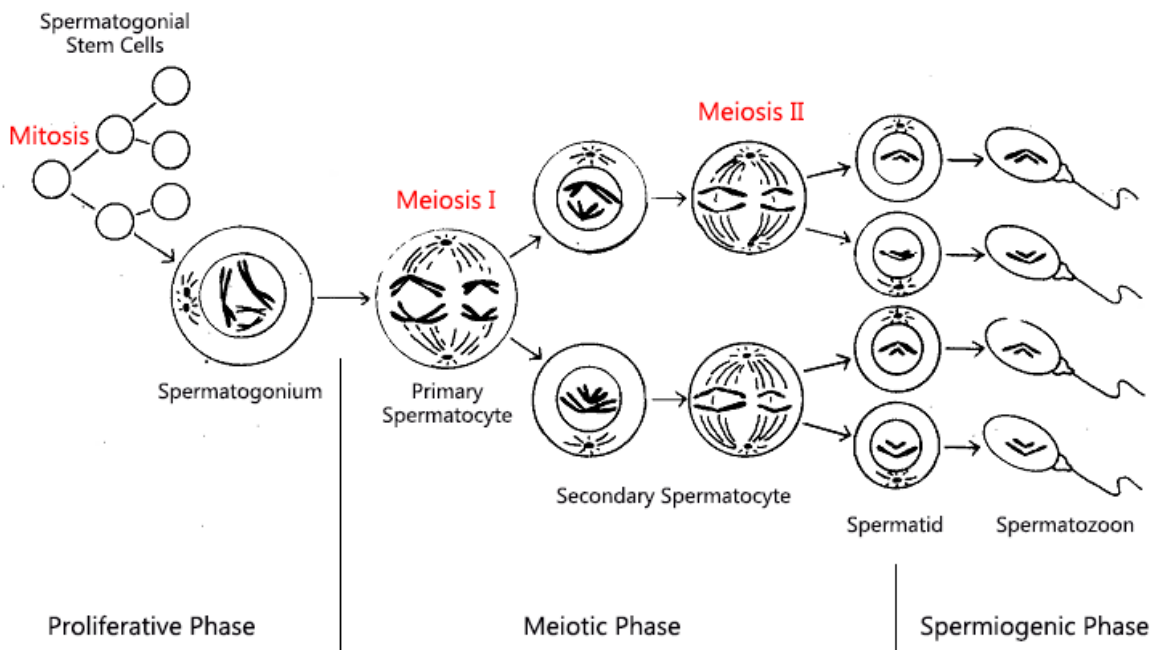


Figure 1.6 The general pattern of spermatogenesis. The spermatogenesis can be generally divided into three phases: proliferative phase, meiotic phase and spermiogenic phase.

The entire process of spermatogenesis in mammalian species occurs while embedded in the recesses of Sertoli cells, which are roughly pyramid-shaped supporting cells lying within the seminiferous epithelium. These nurse cells provide nutritional and structural support for the germ cells (Gupta, 2005). During spermatogenesis, the germ cells gradually migrate away from the basement membrane and move towards the lumen of the seminiferous tubule. The seminiferous epithelium is separated into basal and adluminal compartments by a blood-testis barrier created by tight junctions binding neighbouring Sertoli cells together (**Figure 1.7**). Spatially, the basal compartments contain spermatogonia that are in direct contact with the basement membrane and primary spermatocytes up to the preleptotene stage of the first meiotic division. The following meiotic divisions of spermatocytes (i.e. meiotic phase), differentiation of round spermatids (i.e. spermiogenic phase) and detachment of spermatozoa from Sertoli cells

(i.e. spermiation) all occur in a specialised microenvironment behind the blood-testis barrier in the adluminal compartment (Johnson and Everitt, 2007; Roosen-Runge, 1977).

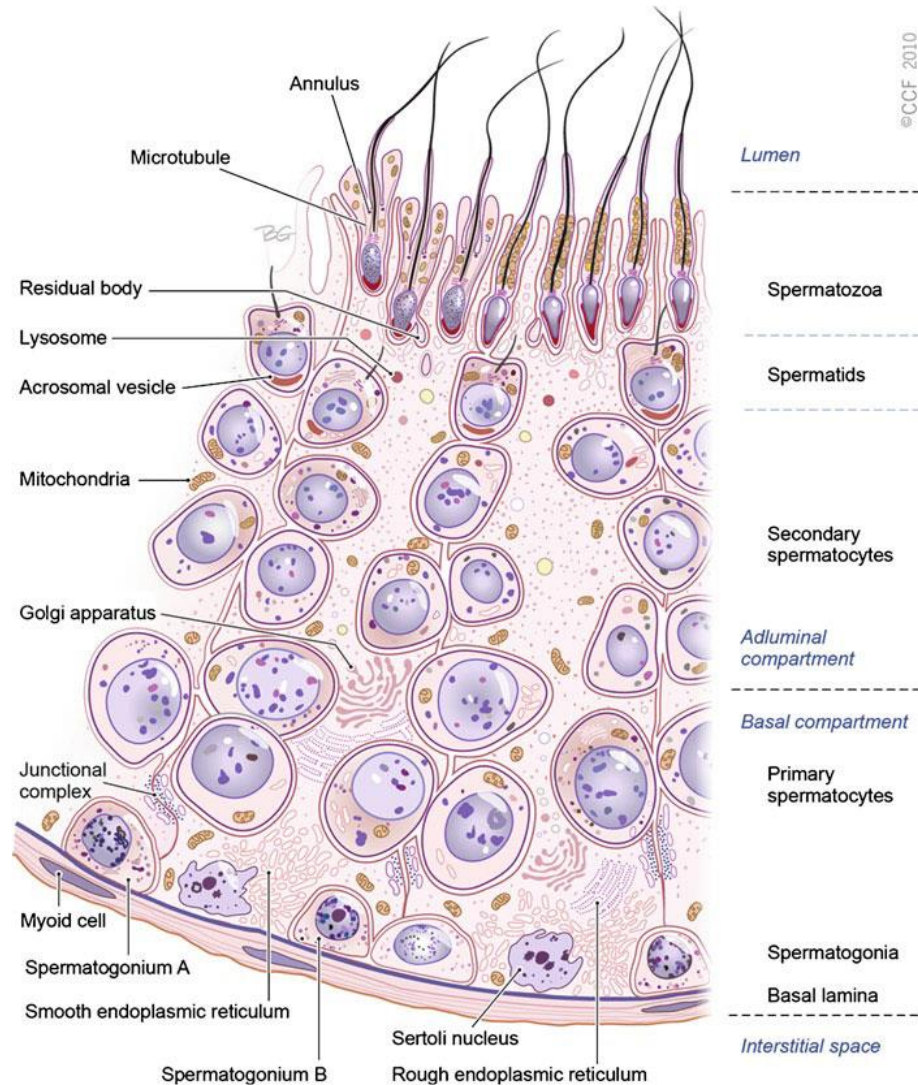


Figure 1.7 A diagram illustrates the cross section of seminiferous epithelium in the seminiferous tubule. The wall of the seminiferous tubule consists of myoid cells separated from the seminiferous epithelium by a basement membrane (Kierszenbaum and Tres, 2015). Tight junctional complexes between adjoining Sertoli cells compartmentalise the seminiferous epithelium into a basal compartment and an adluminal compartment. The junctional complexes separate young germ cells, i.e. spermatogonia and preleptotene spermatocytes, from later spermatogenic cells (Ravindranath *et al.*, 2003). Newly formed spermatozoa are released to the lumen of seminiferous tubule. Photo by Sharma and Agarwal (2011).

Proliferative phase

Spermatogonial stem cells are relatively rare in the seminiferous epithelium, because they are heavily outnumbered by the differentiating spermatogonia, spermatocytes, spermatids and spermatozoa that they produce (Phillips *et al.*, 2010). During the mitotic phase, the spermatogonial stem cells, which act as the foundation of spermatogenesis, confront two fate decisions – proliferation and differentiation (de Rooij, 2001). While a portion of spermatogonia undergo self-renewing divisions to proliferate, the remainder are committed to differentiating divisions to form primary spermatocytes, which subsequently enter meiotic divisions to reduce their chromosomal complement by half (de Kretser *et al.*, 1998). Spermatogonial stem cells achieve prolonged tissue homeostasis by maintaining an appropriate equilibrium between these two divisions, so that the proliferative demand of the testis to generate a constant supply of spermatozoa can be fulfilled (Oatley and Brinster, 2008). This balance is generally regulated by species-specific intrinsic gene expression and can be affected by extrinsic environmental stimuli (de Kretser *et al.*, 1998; Oatley and Brinster, 2008). In mammalian species, the nuclear division (i.e. karyokinesis) of spermatogonia is completed thoroughly but the cytoplasmic division (i.e. cytokinesis) remains incomplete. This incomplete cytokinesis results in the retention of cytoplasmic bridges between germ cells, forming a syncytium whereby germ cell clones readily communicate with each other through the exchange of ions, proteins and mRNAs (de Rooij and Grootegoed, 1998; Greenbaum *et al.*, 2011; Haglund *et al.*, 2011). Such communication ensures the synchronisation of sperm cell growth and differentiation throughout the entire spermatogenic process (Phillips *et al.*, 2010).

The mitotic division of spermatogonial stem cells can be either a symmetric or an asymmetric process (de Rooij, 2001). The symmetric model suggests that a

spermatogonial stem cell divides to produce either two new stem cells that have the capacity to undergo further self-renewal or two differentiating spermatogonia connected by a cytoplasmic bridge which are destined for differentiation into spermatozoa. However, the asymmetrical theory suggests that the division of a spermatogonial stem cell results in one self-renewing stem cell and one non-stem differentiating daughter cell (de Rooij, 2001; Oatley and Brinster, 2008). Whether the spermatogonial division is symmetric or asymmetric in mammals is currently unknown and is a topic of debate (Sofikitis *et al.*, 2008).

Meiotic phase

Following the completion of the proliferative phase of germ cell development, differentiating spermatogonia develop into primary spermatocytes that are committed to commencing the meiotic phase of spermatogenesis. Each primary spermatocyte undergoes two successive meiotic divisions to yield four round spermatids, during which the haploidisation of the genome occurs (Wistuba *et al.*, 2007). The first meiotic division can be subdivided into preleptotene, leptotene, zygotene, pachytene, diplotene and diakinesis phases. Primary spermatocytes at different meiotic phases are readily distinguished by their positions within the seminiferous epithelium, the appearance of heterochromatin and the presence of synaptonemal complexes in the nucleus (Hess and de Franca, 2008). The first meiotic division accomplishes the segregation of homologous chromosomes to opposite ends of the primary spermatocyte. Through cytokinesis, the primary spermatocyte divides into two secondary spermatocytes, each of which only contains a single set of chromosomes, while each chromosome consists of two chromatids joining together at the centromere. The two chromatids then separate and migrate towards the opposite ends of the cell on the completion of the second meiotic division and the

secondary spermatocytes divide generating four round haploid spermatids per primary spermatocyte (**Figure 1.6**).

Spermiogenic phase

On completion of the meiotic phase, the round spermatids undergo dramatic morphological changes and transform into elongated spermatozoa with highly compacted chromatin (de Kretser *et al.*, 1998; Hess and de Franca, 2008; Oatley and Brinster, 2008). This complex differentiation process is characterised by major morphological events including condensation of chromatin, formation of the acrosome, elongation of the flagellum and elimination of excessive cytoplasm (de Kretser *et al.*, 1998). Temporally, the entire spermiogenesis can be divided into Golgi phase, cap phase, acrosomal phase and maturation phase.

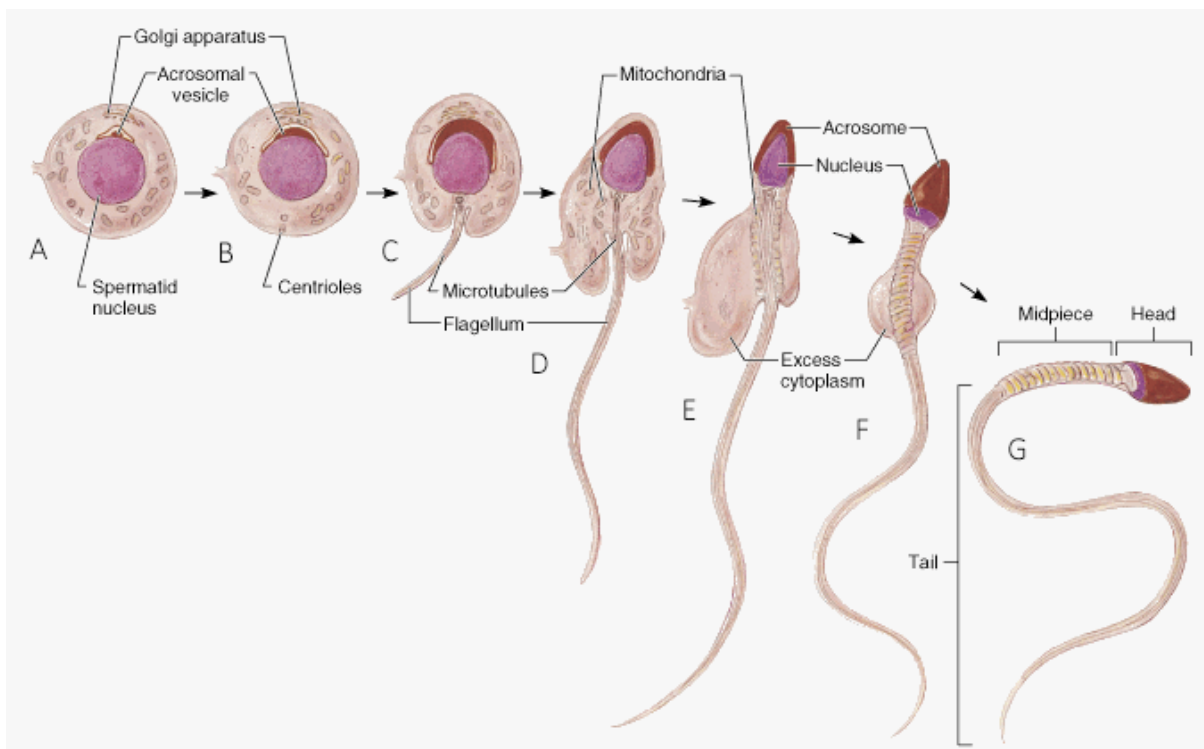


Figure 1.8 Differentiation of spermatids in mammalian species. Spermatid differentiation occurs in four stages: (A - C) Golgi phase, (D) cap phase, (E) acrosomal phase and (F - G) maturation phase. (A) Numerous proacrosomal granules appear adjacent to the Golgi apparatus

and coalesce to form a single acrosomal granule within the acrosomal vesicle. The acrosomal vesicle comes into intimate contact with an indentation of the nucleus during Golgi phase. **(B)** The acrosomal vesicle flattens and spreads over the anterior region of the nucleus. Meanwhile, the centrioles migrate to the posterior pole of the spermatid and leave the vicinity of the nucleus. **(C)** As the acrosomal vesicle is being formed, the distal centriole gives rise to a formative flagellum. **(D)** The acrosomal vesicle enlarges to cover two thirds the nuclear surface and becomes known as the acrosome. In the meantime, the flagellum further elongates and mitochondria gathers at the posterior pole of the spermatid to form a mitochondria sheath. **(E)** Mitochondria migrate to form a helical sheath around the outer dense fibres. **(F)** Excess cytoplasm is extruded from the cell body and the connecting cytoplasmic bridge is ruptured. **(G)** Spermatozoa are formed after the elimination of excess cytoplasm. Photo by Marieb (2000).

Golgi phase: The initiation of cytodifferentiation of round spermatids is indicated by the presence of small proacrosomal granules at the trans face of the Golgi complex (Gupta, 2005). These granules coalesce to form a single acrosomal granule within an acrosomal vesicle. The vesicle increases in size and subsequently comes into intimate contact with an indentation of the nucleus, which marks the anterior pole of the future sperm head (**Figure 1.8A**). The acrosomal granule adheres to the inner acrosomal membrane and becomes hemispherical in shape. Such structure remains distinct throughout the remainder of spermiogenesis (Tulsiani, 2003). At this stage, a pair of centrioles can be found near both the Golgi complex and the acrosomal vesicle. The centrioles migrate to the posterior pole of the spermatids (**Figure 1.8B**) and the distal centriole gradually becomes oriented perpendicularly to the cell surface and gives rise to a flagellum that protrudes out of the cell body (**Figure 1.8C**). Cytoplasmic tubules arise and form a cylindrical sheath, the manchette, which facilitates the shaping and elongation of the nucleus. The manchette contains a large number of parallel arrays of microtubules extending caudally from spermatid nucleus and attaches to the cell membrane at the posterior margin of the acrosomal cap.

Cap phase: The cap phase of spermiogenesis commences soon after the acrosomal vesicle makes contact with the nuclear envelope. During this phase, the attachment site between the acrosomal vesicle and the nucleus extends distally towards the caudal end of the nucleus until it covers approximately two thirds of the nuclear surface (Gartner *et al.*, 2010). The enlargement of the acrosomal vesicle is accomplished by the addition of glycoprotein-rich contents into the forming acrosomal system. The synthesis of such glycoproteins involved in acrosome formation initiates in pachytene spermatocytes and continues throughout the entire spermiogenic process (Tulsiani, 2003). In the meantime, the proximal centriole attaches to the nuclear envelope, which later forms the connecting piece in the neck region of the spermatozoa (**Figure 1.8D**). With the assistance of the manchette, the nuclei of spermatids elongate. The mitochondria, which were initially randomly dispersed throughout the entire cytoplasm, migrate towards the developing flagellum to form a mitochondrial sheath.

Acrosomal phase: The acrosome completes its differentiation during the acrosomal phase. The flagellum further develops, with nine coarse outer dense fibres forming surrounding the axial filament. A fibrous sheath, the annulus, appears around the distal part of the flagellum, corresponding to the future principal piece of the tail. The mitochondria gather around the segment of the flagellum between the annulus and nucleus and arrange helically around it to form the mitochondrial sheath of the midpiece (**Figure 1.8E**).

Maturation phase: With the completion of flagellum formation, the excess cytoplasm is released from the spermatozoa in the form of residual bodies, which contain abundant fine granules, lipid droplets and degenerating organelles (**Figure 1.8F**). The residual body appears as a distinct bulge formed by caudal movement of cytoplasmic material in

spermatids. The majority of the residual bodies are phagocytosed by the Sertoli cells, while a small portion of them are released into the lumen of the seminiferous tubule (Lipshultz *et al.*, 2009).

The spermiogenic phase is concluded at spermiation, during which the elongated spermatozoa lose their cytoplasmic connections with adjacent cells, detach from the seminiferous epithelium and travel along the lumen of the seminiferous tubule in the testicular fluid secreted by Sertoli cells (**Figure 1.8G**).

1.1.5.3 Spermatozoa in polychaetes

The great range of different reproductive modes in polychaetes is not only reflected in the various methods of gamete release and diverse patterns of embryonic development, but also in the different structures of gametes, especially sperm morphologies (Rouse, 2005). Polychaete spermatozoa were distinguished by Jamieson and Rouse (1989) into three morphological types: ect-aquasperm, ent-aquasperm, and introsperm. This classification of polychaete spermatozoa was demonstrated to be correlated with their sperm transfer patterns and fertilisation strategies (Rouse, 2005). In comparison with introsperm, which rarely come into contact with water, both ect-aquasperm and ent-aquasperm devote a certain amount of time in the water. Ect-aquasperm is liberated freely into the ambient water where they fertilize the eggs, whereas ent-aquasperm and introsperm are transferred to the females *via* spermatophores or copulation (Jamieson and Rouse, 1989). Ect-aquasperm, which are associated with broadcast spawning, generally have a short or bullet-shaped head (less than 5 μm), a midpiece with four to six mitochondria, and a long flagellum with the typical $9 \times 2 + 2$ microtubular arrangement. Modification of this basic morphology by moderate (4 - 8 μm) or extreme ($\sim 48 \mu\text{m}$) elongation of the nucleus and development of a complex acrosome is usually associated with fertilisation within the

polychaete tube, spermatophore transfer, pseudocopulation, or copulation. The sperm head is sometimes slightly elongated in ect-aquasperm. The structure of the midpiece is the most distinct difference between ect-aquasperm and ent-aquasperm. The midpiece of ect-aquasperm is short and generally has four to six mitochondria surrounding the centrioles, while that of ent-aquasperm is relatively long and complicated (Jamieson and Rouse, 1989).

1.1.6 Contaminant-induced oxidative damage in male germline

Contaminant-induced production of reactive oxygen species (ROS) and the resultant oxidative stress has been determined as one of the most prevalent forms of toxicity in marine organisms exposed to pollution (Livingstone, 2003). It has been well demonstrated by our laboratory that human spermatozoa are extraordinarily vulnerable to oxidative stress due to their abundant endowment with polyunsaturated fatty acids and DNA, which are major substrates for free radical attack as well as their capacity for the spontaneous production of ROS. Owing to the extremely limited cytoplasmic space, spermatozoa also contain minor amount of cytosolic antioxidant enzymes (e.g. catalase, SOD and glutathione peroxidase) that protect them from oxidative damage (Aitken *et al.*, 2010a). The study conducted by Lewis and Galloway (2009) highlighted oxidative damage in spermatozoa is not limited to humans and other mammalian species, but also occurs in marine invertebrates.

Similar to all other cells living under aerobic conditions, spermatozoa are constantly subject to the oxygen paradox: oxygen derivatives are essential for triggering signal transduction cascades in certain physiological processes, but they will cause detrimental effects on the cells if present to excess. Spermatozoa can spontaneously generate a range

of ROS, which refers to metabolites originating from oxygen reduction, such as superoxide anion, hydrogen peroxide and hydroxyl radical. With a small amount of ROS, a cascade of protein tyrosine phosphorylation can be effectively triggered which facilitates sperm capacitation and sperm-oocyte fusion (Aitken *et al.*, 2010a; Baumber *et al.*, 2000). The normal function of spermatozoa requires a steady concentration of ROS balanced by the relative rates of ROS generation and elimination, but this dynamic equilibrium can be easily disturbed, leading to elevated ROS levels (Lushchak, 2011). Excessive production of free radicals and reactive metabolites, which overwhelms the limited antioxidant defences in spermatozoa, is known to induce oxidative stress on sperm cellular constituents, including lipid peroxidation in sperm plasma membrane, DNA strand breakage in the sperm nucleus, and protein damage in the axonemal cytoskeleton (Aitken *et al.*, 2010b; Gharagozloo and Aitken, 2011; Misra *et al.*, 2009; Sharma and Agarwal, 1996; Xing, 2012). In this section, we will look into the mechanisms of ROS production and consequential oxidative damages in the spermatozoa of marine invertebrates.

In marine environments, the amounts of ROS production are remarkably increased by the existence of an extensive range of artificial xenobiotics in chemical contaminants (Livingstone 2001). Organic contaminants are potential anthropogenic-related sources that facilitate the production of enhanced ROS and other pro-oxidant free radicals, and include redox cycling compounds (quinones, nitroaromatics, nitroamines, bipyridyl herbicides), polynuclear aromatic hydrocarbons (PAHs; benzene, PAH oxidation products), halogenated hydrocarbons (bromobenzene, dibromomethane, polychlorobiphenyls, lindane), dioxins, pentachlorophenol, and heavy metals [Al, As, Cd, Cr, Hg, Ni; (Livingstone, 2001; Livingstone, 2003)]. In response to these pollutants, ROS

can be directly or indirectly generated *via* various potential mechanisms, resulting in oxidative damage.

1.1.6.2 Generation of reactive oxygen species in aerobic organisms

The paradox of aerobic life is that higher eukaryotic aerobic organisms cannot exist without oxygen, yet oxygen is inherently dangerous to their existence (Davies, 1995; de Lamirande and Gagnon, 1995). The basic cellular metabolism of aerobic organisms has been demonstrated to be related to the generation of a whole array of radical and non-radical oxidants, which are commonly referred to as reactive oxygen species (Livingstone, 2001; Valavanidis *et al.*, 2006). Radical oxidants include superoxide anion ($O_2^{\bullet-}$), hydroxyl (OH^{\bullet}), peroxy (RO_2^{\bullet}), and hydroperoxyl (HO_2^{\bullet}) radicals (Bayr, 2005; de Lamirande and Gagnon, 1995; Livingstone, 2001). Non-radical oxidants include hydrogen peroxide (H_2O_2), hypochlorous acid ($HOCl$), ozone (O_3), and peroxynitrite ($ONOO^-$), which can be easily converted into radical forms (Bayr, 2005; Livingstone, 2001).

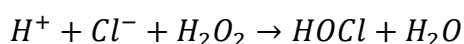
Through a non-enzymatic, univalent, reduction pathway, oxygen undergoes four successive one-electron reductions resulting in the generation of several reactive intermediates (shown in **Reaction 1**; Davies, 1995). The first one-electron reduction of oxygen generates the superoxide anion. The addition of a second electron and two protons generates the non-radical oxidant hydrogen peroxide. The third electron addition produces the highly reactive hydroxyl radical and simultaneously releases a hydroxide ion. The fourth electron addition accompanied by two protons harmlessly generates two water molecules.



The reactivity of different ROS varies considerably: some of these molecules are extremely reactive (hydroxyl radical), while some others are less reactive (hydrogen peroxide and superoxide anion; Davies, 1995; Livingstone, 2001). The superoxide anion, which is created from molecular oxygen by the addition of an electron, is a mild reductant with relatively low reactivity in spite of being a free radical (see **Reaction 1**; Davies, 1995). The formation of superoxide takes place spontaneously, especially in the electron-rich aerobic environment in the vicinity of the inner mitochondrial membrane in association with the respiratory electron transport chain (Nordberg and Arnér, 2001). Superoxide (as well as hydrogen peroxide) is also produced endogenously by flavoenzymes, e.g. xanthine oxidase activated in ischemia-reperfusion. Other superoxide-producing enzymes are lipoxygenase and cyclooxygenase. The family of NADPH-dependent oxidases found in a variety of cell types including phagocytic cells, is a membrane-associated enzyme complex, specialised to deliver high levels of ROS production. Enzymes similar to components of this complex are also present in non-phagocytic cells where their functions are related to signal transduction. Two molecules of superoxide can also rapidly dismutate to hydrogen peroxide and molecular oxygen and this reaction is further accelerated by superoxide dismutase (Davies, 1995; Nordberg and Arnér, 2001).

Hydrogen peroxide is not a free radical oxidant but is nonetheless of great significance mainly due to its capacity to penetrate biological membranes (Nordberg and Arnér, 2001).

It plays a radical forming role as an intermediate in the production of more reactive ROS molecules including hypochlorous acid by the action of myeloperoxidase (**Reaction 2**), an enzyme present in the phagosomes of neutrophils and, most importantly, formation of OH^\bullet via the redox activity. Another important function of H_2O_2 is indicated in its role as an intracellular signalling molecule. H_2O_2 once produced by the above mentioned mechanisms is removed by at least three antioxidant enzyme systems, namely catalases, glutathione peroxidases, and peroxiredoxins (Livingstone, 2001; Nordberg and Arnér, 2001).

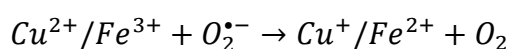


Reaction 2

Hydroxyl radical can instantly and indiscriminately react with virtually all organic molecules, the detected strong toxic effects only being limited by its extremely short half-life (de Lamirande *et al.*, 1997; Livingstone, 2001; Sies, 1997). This radical can be derived from hydrogen peroxide in the Fenton reaction catalysed by metal ions (Fe^{2+} or Cu^+), found bound in complex with different proteins or other molecules (see **Reaction 3**; Nordberg and Arnér, 2001; Valavanidis *et al.*, 2006). Superoxide also contributes to the connection with **Reaction 4** by recycling those metal ions (Nordberg and Arnér, 2001). The sum of **Reactions 3** and **4** is the Haber-Weiss reaction (**Reaction 5**).



Reaction 3



Reaction 4



Reaction 5

ROS generation is the product of multiple mechanisms in biological system. In most cases, they are produced as by-products of oxygen metabolism. Over 95% of the oxygen consumed by organisms undergoes a concerted tetravalent reduction to produce energy in a reaction catalysed by cytochrome *c* oxidase in the mitochondrial electron transport chain. Cytochrome oxidase is the terminal electron acceptor in the chain and must give up its reducing equivalents in order to allow continued electron transport; if electrons stop flowing through the chain the proton motive force dissipates, and ATP production cannot continue. Thus, the major role of oxygen for all aerobic organisms is simply to act as a sink or dumping ground for electrons (Nordberg and Arnér, 2001). The predominant source of ROS generation in spermatozoa has been demonstrated to be obtained from electron leakage in the mitochondrial electron transport chain during cellular respiration, with approximately 2% of consumed oxygen being converted to superoxide anion *via* this route (Aitken *et al.*, 2012a; Koppers *et al.*, 2008). However, this cell type also features other free radical generating pathways including highly specialized NADPH oxidases (Aitken *et al.*, 1997; Aitken *et al.*, 2003; Musset *et al.*, 2012).

1.1.6.3 ROS-induced lipid peroxidation

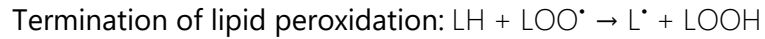
Membrane phospholipids of aerobic organisms are continually subjected to oxidant challenges from endogenous and exogenous sources, while peroxidised membranes and lipid peroxidation products represent constant threats to aerobic cells. Cells contain antioxidant compounds such as vitamin E for preventing the initiation of peroxidation and a variety of mechanisms for maintaining membrane integrity and homeostasis by repairing oxidatively damaged lipid components (Sies, 1997). The process of lipid

peroxidation is composed of a set of chain reactions, especially for polyunsaturated fatty acids, which are very sensitive to oxidative reactions by ROS because of their double bonds (Aitken *et al.*, 2010a).

The oxidation of lipids is one of the most frequently utilized approaches to detect oxidative stress in most organisms, especially the invertebrate species, which contain large quantities of lipids with a polyunsaturated structure, that is vulnerable to oxidative attack (Aitken *et al.*, 2010a; Lushchak, 2011). The oxidation of lipids generally results in the production of peroxides *via* a process known as lipid peroxidation. In aerobic organisms, membrane phospholipids are continuously targeted by oxidants originating from endogenous and exogenous sources (Valavanidis *et al.*, 2006). Peroxidised membranes, the fluidity of which has been impaired as a result of oxidative attack, are rigid and lack both permeability and integrity (Chen and Yu, 1994; Valavanidis *et al.*, 2006). 4-Hydroxynonenal (HNE) is a commonly used membrane lipid peroxidation indicator because it can be easily detected and quantified by means of several methods (Poli *et al.*, 2008). It is an aldehyde product that is generated during membrane lipid peroxidation, as a result of the degradation of ω -6 polyunsaturated fatty acids (Blanc *et al.*, 1998; Doi *et al.*, 2004).

The process of lipid peroxidation consists of a series of free radical chain reactions, particularly for those polyunsaturated fatty acids which are very sensitive to oxidative reactions by ROS due to their double bonds (Halliwell and Chirico, 1993; Valavanidis *et al.*, 2006).





In light of the above reactions, polyunsaturated lipid (*LH*) is initially oxidized by ROS, resulting in the generation of carbon-centred lipid radical (*L*[•]). Carbon-centred lipid radicals, in turn, react with oxygen to form the corresponding lipid peroxy radical (*LOO*[•]). Finally, polyunsaturated lipids react again with *LOO*[•], leading to the formation of *L*[•] and lipid hydroperoxide (*LOOH*). The resulting *LOOH* is readily degraded into several reactive species including lipid alkoxy radicals (*LO*[•]), aldehydes, alkanes, lipid epoxides, and alcohols. These lipid peroxidation products form DNA adducts which can trigger mutations, modified patterns of gene expression, and induce apoptosis (Valavanidis *et al.*, 2006).

1.1.6.4 ROS-induced DNA damage

The DNA in spermatozoa is also particularly vulnerable to ROS-induced oxidative damage. DNA damage is usually regarded as the formation of oxidative nucleic acid base modifications including single-strand breaks, double strand breaks or chromosomal aberrations (Halliwell and Aruoma, 1991; Higuchi, 2003; Yakes and Van Houten, 1997). Two main mechanisms of ROS-induced DNA damage have been described by Halliwell and Aruoma (1991). First, hydrogen peroxide penetrates the nucleus easily *via* biological membranes and reacts with metal ions to form *OH*[•]. Second, ROS triggers a series of metabolic cellular events that lead to the activation of nuclease enzymes, which finally cleave the DNA sugar-phosphate backbone (Halliwell and Aruoma, 1991). Alternatively, ROS may induce increases in intracellular free calcium ions (*Ca*²⁺), which might fragment DNA by activating *Ca*²⁺-dependent endonucleases. The reaction of intracellular ROS with DNA results in numerous forms of base damage, the most

abundant lesion of DNA which is utilised extensively as a biomarker for cellular oxidative stress being 8-hydroxy-2'-deoxyguanosine (8-OH-dG), or its oxidation product 8-oxo-2'-deoxyguanosine [8-oxo-dG; (Beal, 1995; Cooke *et al.*, 2003; Valavanidis *et al.*, 2006)].

Large amounts of ROS are generated during mitochondrial oxidative phosphorylation, suggesting mitochondrial DNA (mtDNA) may accumulate more oxidative DNA damage in comparison with nuclear DNA (Desai *et al.*, 2010; Valavanidis *et al.*, 2006; Yakes and Van Houten, 1997). Additionally, the mitochondrial genome is more susceptible to DNA damage than nuclear DNA due to **(i)** a lack of complex chromatin organisation, which serves as a protective barrier against ROS-induced damage, **(ii)** a lack of DNA repair capacity, **(iii)** the existence of localised metal ions that can act as the catalysts in ROS production and **(iv)** the stimulation of ROS reactions due to damage to the electron transport chain or as a consequence of lipid peroxidation (Yakes and Van Houten, 1997).

1.1.6.5 ROS-induced protein damage

Protein damage has recently become a popular measurement of oxidative stress (Chevion *et al.*, 2000; Lushchak, 2011). Among the various incidences of protein oxidation, protein carbonyl content is the most widely used marker (Chevion *et al.*, 2000). Protein oxidation reactions encompass a variety of propagating radicals and ROS, which result in oxidative alterations to amino acid side chains, peptide fragmentation, reactions of peptides with lipids and carbohydrate oxidation products, and formation of carbonyl derivatives of proteins (Berlett and Stadtman, 1997; Valavanidis *et al.*, 2006).

The oxidation of amino acid residues in protein can be generalised into two major mechanisms, ionizing radiation and metal ion-catalysed oxidation reactions (Cabiscol *et al.*, 2000). The impacts of ionizing radiation on proteins can be attributable to the

hydroxyl radicals formed by the radiolysis of water, followed by reaction with the α -hydrogen atom of an amino acid residue to produce a carbon-centred radical. In the presence of oxygen, the alkoxy radical is then generated, which induces cleavage of peptide bonds (Hawkins and Davies, 2001). Metal-catalysed oxidation of proteins has been described as a post-translational modification mechanism, featuring the introduction of a metal cation, which results in the formation of carbonyl groups in the side-chains of amino acids at the cation-binding site. The reaction with molecular oxygen or H₂O₂ then results in the production of active oxygen species which oxidise amino acid residues in the immediate vicinity (Cabiscol *et al.*, 2000; Lenz *et al.*, 1996).

Overall, invertebrate spermatozoa are particularly susceptible to oxidative damage due to their simplistic structure, high contents of polyunsaturated fatty acids in the acrosome and membranes, as well as the active generation of ROS by the mitochondria (Desai *et al.*, 2010; Lewis and Galloway, 2010).

2. Research Objectives

Aim 1: To investigate the functional anatomy of the male reproductive system and elucidate the pattern of spermatogenesis in *G. caespitosa*

In light of a comprehensive review of the related literature on *G. caespitosa*, the male reproductive system of this species remains poorly studied at present and there is no published paper on elucidating its pattern of spermatogenesis. In order to acquire a preliminary knowledge of its male reproductive biology, the initial aim of my PhD project was **(1)** to investigate the structure and function of the male reproductive system and **(2)** to establish the pattern of germ cell differentiation, as well as the dynamic transportation of the spermatogenic cells in the male tract during and after spermatogenesis.

Aim 2: To describe the spermiogenesis in *G. caespitosa* at the ultrastructural level and reproduce the differentiation of spermatids *in vitro*

Unlocking the underlying mechanisms that regulate the complex differentiation of male germ cells from diploid spermatogonial stem cells through mitosis and meiosis to give rise to haploid mature spermatozoa has been explored with extensively over the last century (Parks *et al.*, 2003). Unlike the majority of the other cell types, male germs cells in mammalian species are highly dependent upon mature Sertoli cells and in intimate contact with other integrated somatic cells which are located within an intact seminiferous epithelium. Although much information underlying spermatogenesis in mammals has been revealed through gene manipulation, there is still a need for the establishment of *in vitro* culture system to acquire a comprehensive understanding of the process of sperm production.

Based on the results obtained from the first part of my PhD project, the male reproductive system in *G. caespitosa* was relatively simple compared with that in mammalian species and the entire spermiogenesis in this species occurred while individual germ cells moved freely within the germinal chamber. Therefore, the second aim of my project was (1) to elucidate the differentiation of round spermatids at the ultrastructural level, (2) to establish an artificial culture system to support the differentiation of spermatids *in vitro*. The establishment of this *in vitro* culture system is of great significance for the future study of spermiogenesis, as it provides convenient model to uncover the cell signalling pathways involved in this complex differentiation process.

Aim 3: To uncover the mechanisms of how the dibutyl phthalate-impaired spermatozoa lead to embryonic arrest and malformation

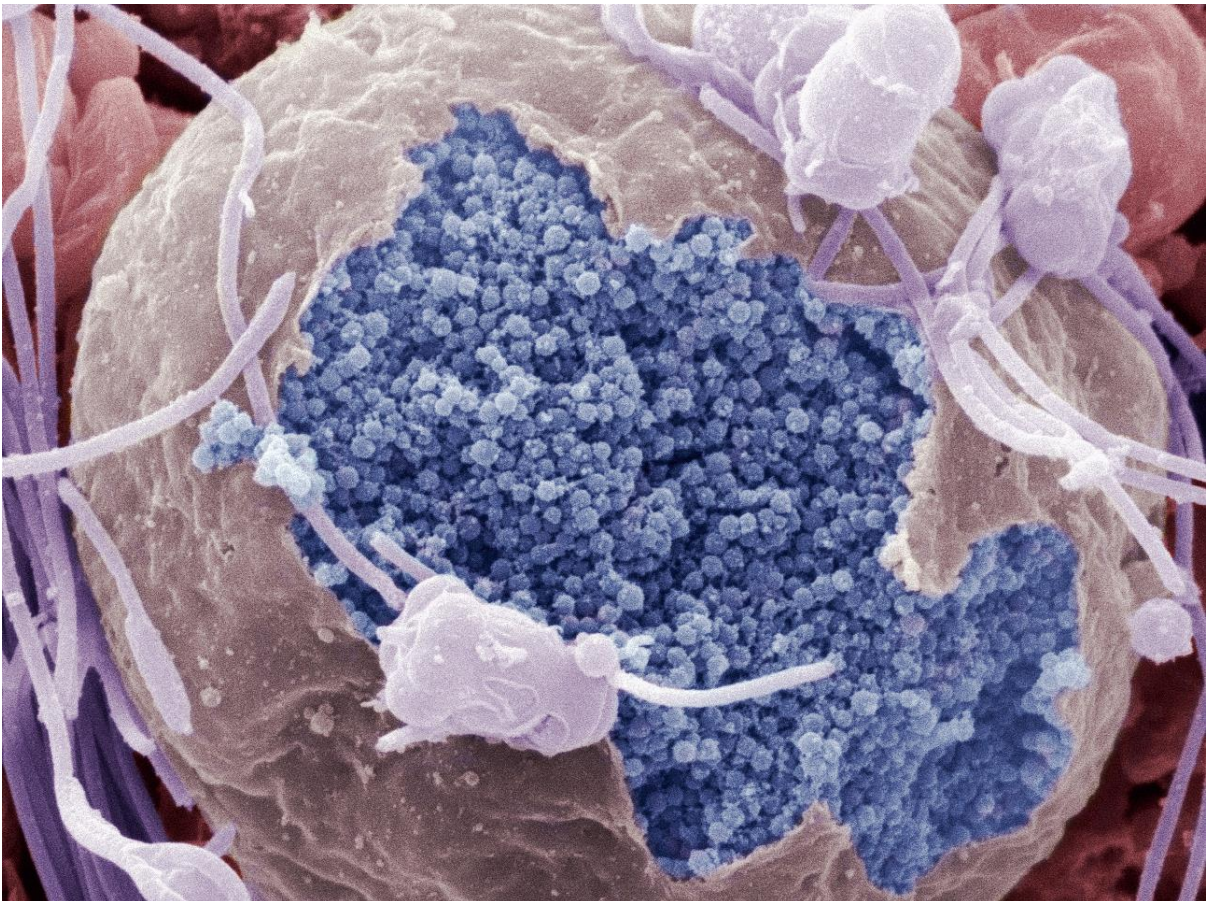
The third aim of my project was (1) to investigate the adverse effects of gamete exposure to a widely applied plasticiser dibutyl phthalate on the subsequent early embryonic development and (2) to uncover the mechanisms of how pre-fertilisation exposure to graded concentrations of dibutyl phthalate resulted in embryonic arrest and abnormality.

Aim 4: To analyse the effects of a range of representative marine pollutants on the gamete function and early embryogenesis in *G. caespitosa*

With the purpose of evaluating the potential of *G. caespitosa* as a bio-indicator species for coastal pollution, the effects of a range of representative marine pollutants on the gamete function and subsequent early embryogenesis in *G. caespitosa* were analysed. The pollutant-induced reproductive defects, including sperm dysfunction, embryonic arrest and developmental abnormality, provide a basis for detecting and assessing pollutant-induced changes in the environment.

Chapter 2

Functional anatomy of the male reproductive system and the pattern of spermatogenesis in *Galeolaria caespitosa*



2.1 Overview

Utilising histological techniques, the gross and functional anatomy of the male reproductive system in the marine invertebrate *Galeolaria caespitosa* has been elucidated for the first time, with an emphasis on the pattern of its spermatogenesis and dynamic process of sperm transportation. The abdomen of *G. caespitosa* was divided by intersegmental septa into over 80 trunk segments. Each segment served as a germinal chamber with a C-shaped gonadal arrangement consisting of several distinct compartments: a seminiferous epithelium (SE) compartment located in the centre of the chamber, with each of its two ends connecting to a nurse cell (NC) compartment and then an efferent duct (ED) compartment. The SE compartment contained a multilayered seminiferous epithelium where spermatogenesis was initiated. Spermatids were released in pairs into the lumen of the SE compartment and then transported to the NC compartment where they underwent spermiogenesis with the support of secretory vesicles released by the nurse cells. Spermatozoa were stored in the ED compartment and subsequently released into the seawater through the vas deferens. Unlike vertebrates where spermatozoa differentiated in close proximity to the nurse cell population (i.e. Sertoli cells), the sperm cells of *G. caespitosa* exhibited no direct contact with supporting cells at any spermatogenic stage. This finding suggested that the spermatogenesis in *G. caespitosa* was more dependent on intrinsic developmental programming than most species. Notwithstanding such differences, there were clear parallels between the male reproductive system of *G. caespitosa* and mammals, in terms of the structure and function. The independence of spermatogenic cells from supporting cells in *G. caespitosa* raised the possibility of inducing the spermiogenesis *in vitro*, which would provide a useful tool

to dissect the mechanisms underlying this complex cell differentiation process in invertebrates and other higher order animals.

2.2 Introduction

As mentioned in previous section, a number of life history characteristics that the marine invertebrate *Galeolaria caespitosa* exhibits endow this species great potential as a bio-indicator species of coastal marine pollution (see **Section 1.1.4, Chapter 1**). A series of previous toxicity tests demonstrated its capacity to accumulate toxic substances in marine environment (Waring *et al.*, 2006) and the susceptibility of its reproductive activities (e.g. fertilisation, embryogenesis and larval development) to a range of marine pollutants (Hollows *et al.*, 2007; Ross and Bidwell, 2001; Wisely and Blick, 1967). Such findings imply that the gametes, as well as those post-fertilisation events of *G. caespitosa* can serve as sensitive indicators for certain contaminants.

More recently, research demonstrated that the behaviour of spermatozoa in *G. caespitosa* effectively reflected the subsequent success of fertilisation, which therefore could act as effective bio-indicators for water quality monitoring (Falkenberg *et al.*, 2016; Schlegel *et al.*, 2014). The study conducted by Schlegel *et al.* (2014) indicated that the motility and swimming speed of spermatozoa significantly decreased when being exposed to both near-future ($\Delta\text{pH} = 0.3$) and far-future ($\Delta\text{pH} = 0.5$) ocean acidification scenarios, which resulted in decreased fertilisation success. Such sensitive response that spermatozoa exhibited to minor pH changes could provide early warning alerts for the CO₂-induced ocean acidification. Falkenberg *et al.* (2016) proposed a bioassay system for water quality monitoring – Sperm Accumulated Against Surface (SAAS), which provided a novel and rapid method for the measurement of sperm motility. During their study, they discovered

that motile spermatozoa of *G. caespitosa* tended to actively accumulate at the lower surface of tissue culture well-plates, whereas the immotile ones were not able to adhere to the bottom surface. A strong positive correlation was also detected between the number of spermatozoa accumulated against the well-plate surface and the success rate of fertilisation, indicating that the employment of SAAS could reliably reflect the fertilisation capacity of the spermatozoa (Falkenberg *et al.*, 2016). Such sperm bioassays are more sensitive compared with embryotoxicity tests, in terms of their capacity to detect low levels of marine contamination, as spermatozoa are usually more vulnerable to contaminants. Slight variations in sperm behaviour may not be effectively manifested in the subsequent early development, given the enormous number of gametes that broadcast-spawners produce.

The behaviour of spermatozoa and other reproductive activities in *G. caespitosa* has been repeatedly demonstrated to have significant potential in monitoring and evaluating coastal water quality and ecosystem status. However, male reproductive biology, particularly the structure of male reproductive system and pattern of spermatogenesis remain largely unknown. In this chapter, a detailed analysis of the male reproductive system in *G. caespitosa* has been undertaken, revealing novel developmental features that support the use of this organism as a model species in an ecotoxicology context.

2.3 Materials and Methods

2.3.1 Sample collection and maintenance

Aggregations of *Galeolaria caespitosa* were collected freshly at low tides from intertidal rock revetments at Merewether Beach (32°56'34"S, 151°45'9"E), Merewether, New South Wales, Australia. The tubeworms were transported to the laboratory within 1 h

after the collection and maintained in an aerated polyethylene bucket with natural seawater obtained from the collection site. Samples were reared at constant room temperature of 20 ± 2 °C and supplied with a 12-h light/12-h dark illumination cycle. All samples used in this study were fixed within 48 h of collection.

2.3.2 Serial paraffin sections for light microscopy

Male adults were carefully extracted from their calcareous tubes using fine forceps and fixed in 10% neutral buffered formalin (Sigma-Aldrich, Castle Hill, Australia) for at least 48 h at room temperature. The volume of formalin was over 20 times that of the specimen on a weight per volume (2 mL of formalin per 100 mg of *G. caespitosa*). The fixative was replaced with fresh when the solution became obviously cloudy during the 48 h of fixation period. The fixed worms were transferred to 70% (v/v) acetone in phosphate buffer and dehydrated for 45 min at room temperature. After that, the samples were dehydrated in 90% acetone twice followed by dehydration three times in 100% acetone for 45 min each. To remove the dehydrating agent, the specimens were then washed in 50% xylene in acetone (v/v) for 45 min, followed by another two washes in 100% xylene. To replace the xylene residue in the specimens with paraffin wax, the worms were infiltrated for four cycles and embedded in paraffin wax at the melting point of between 54 - 58 °C. Serial sections were cut along the longitudinal body axis of animals at a thickness of 5 µm using a Leica RM 2145 microtome (Leica, Heidelberg, Germany) and mounted onto microscope slides. Every fourth serial section was double-stained with Harris' haematoxylin and eosin. The slides were then viewed and photographed under a Zeiss Axiovert S100 inverted microscope with a Zeiss AxioCam MRm camera (Carl Zeiss, Oberkochen, Germany).

2.3.3 Transmission electron microscopy

After being extracted from their calcareous tubes, the whole worms were immediately immersed in 2.5% (v/v) glutaraldehyde (ProSciTech, Queensland, Australia) in artificial seawater (28.32 g NaCl, 0.77 g KCl, 5.41 g MgCl₂·6H₂O, 7.13 g MgSO₄·7H₂O, 1.18 g CaCl₂ and 0.2 g NaHCO₃ in 1 L distilled water) with an osmolality of 1,140 mOsm/kg and pH at 7.4 at room temperature for 1 h. The abdomen of each worm was cut into cubes no more than 1 mm³ in size. The specimens were then transferred to freshly made fixative and fixed at 4 °C overnight. Fixed specimens were washed and post-fixed in 1% (v/v) osmium tetroxide in artificial seawater (pH 7.4) for 2 h. After dehydration through an ascending acetone series, the specimens were infiltrated with 50% (v/v) Spurr's resin embedding medium (ProSciTech, Queensland, Australia) in absolute acetone on a rotator at room temperature overnight. The resin medium was then replaced with 100% Spurr's resin and the specimens were infiltrated for a further 12 h. The specimens were then embedded in freshly made 100% Spurr's resin in polyethylene embedding capsules or moulds (ProSciTech, Queensland, Australia) and polymerised in an oven at 65 °C for 24 h. Resin blocks were cut into semi-thin sections on a Reichert Ultracut S Microtome (Leica, Wien, Austria) with freshly made glass knives or a diamond knife (Diatome, Bienne, Switzerland). Semi-thin sections were stained with 0.5% (w/v) toluidine blue (BDH Chemicals, Kilsyth, Australia) in absolute ethanol and observed under the Zeiss Axiovert S100 microscope (Carl Zeiss, Oberkochen, Germany). Ultra-thin sections at a thickness of 60 nm were cut and stained with aqueous saturated uranyl acetate and Reynolds' lead citrate (BDH Chemicals, Poole, England) and examined under a JEM-2100EX II transmission electron microscope (JEOL, Tokyo, Japan) at 80 kV.

2.3.4 Scanning electron microscopy

For SEM specimens, whole male worms were fixed in 2.5% glutaraldehyde and 1% osmium tetroxide, followed by dehydration through a graded series of ethanol solutions. In order to remove excess liquid in the specimens, critical point drying was employed using liquid carbon dioxide as the transition solvent. Dried specimens were mounted on anodised aluminium stubs, coated with gold-palladium using a SPI Module™ Sputter Coater and then examined under a Philips XL30 scanning electron microscope (Philips, Eindhoven, Netherlands).

2.3.5 Live cell observation

Adult male *G. caespitosa* were extracted from their calcareous tubes and immersed in filtered natural seawater. The worms spontaneously released their spermatozoa on being exposed to seawater. They were allowed to sit for at least 10 min until the spawning ceased. After that, the worms were rinsed vigorously in seawater and transferred to clean seawater. More spermatozoa, along with a considerable amount of spermatids, were stimulated to release by puncturing the abdominal wall with a syringe needle and gently pressing the abdomen using a pair of forceps. The released sperm solution was collected using Pasteur pipettes and examined under the Zeiss Axiovert S100 microscope (Carl Zeiss, Oberkochen, Germany). Images of spermatids were captured using the equipped Zeiss AxioCam MRm camera (Carl Zeiss, Oberkochen, Germany).

2.3.6 Statistical analysis

Cellular and nuclear diameters of spermatogonia and spermatocytes are presented as mean \pm SE, which were calculated from at least 20 samples of each cell type. The statistical difference between the sizes of spermatogonia and spermatocytes was

determined using the student's t-test. The difference was recognised as statistically significant if the P value was less than 0.05. All statistical analyses were performed using Microsoft Excel 2013 (Microsoft Corporation, Redmond, USA).

2.4 Results

2.4.1 Male reproductive system in *Galeolaria caespitosa*

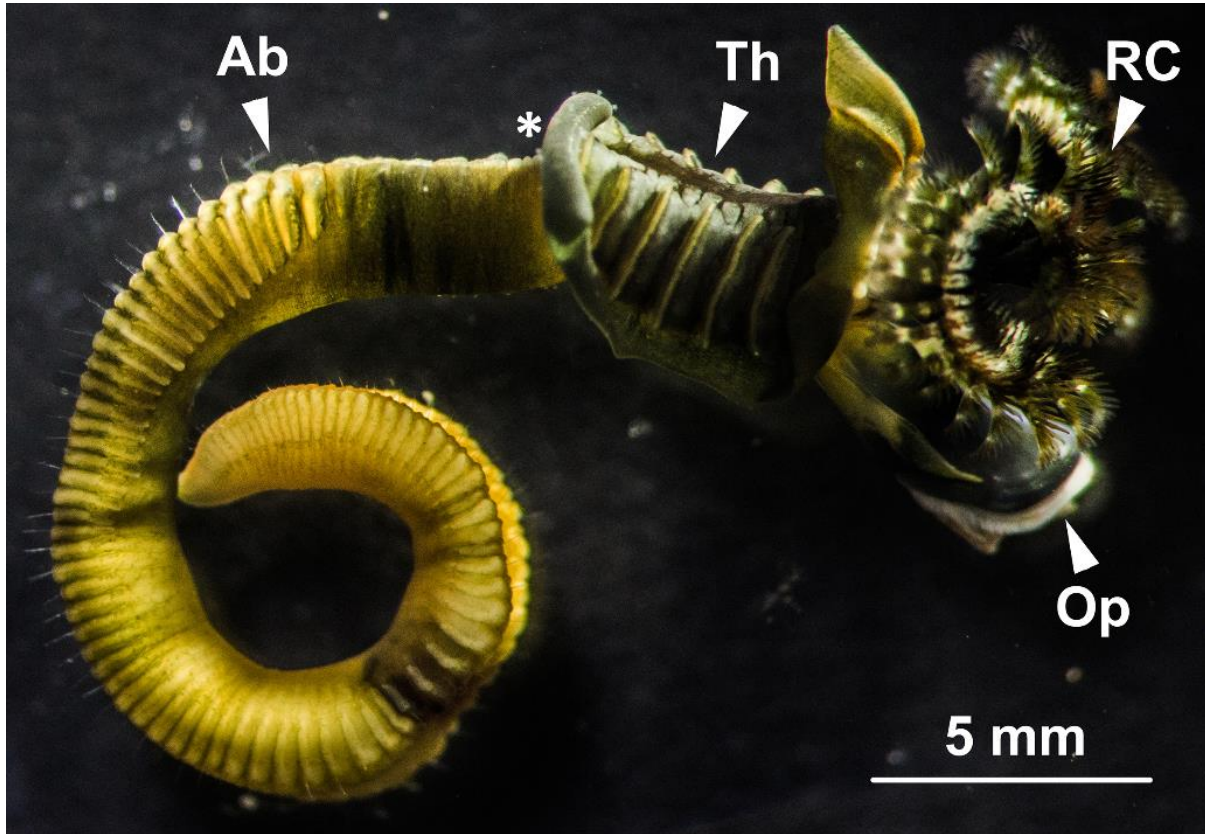


Figure 2.1 A male *G. caespitosa* extracted from its calcareous tube. *G. caespitosa* consisted of a conspicuous head bearing a radiolar crown (RC) and an operculum (Op), a thorax (Th) and a segmented abdomen (Ab). The main sperm duct (or vas deferens) lay along the mid-ventral region of the abdomen with an opening (*) located at the junction of the abdomen and thorax.

Male *G. caespitosa* was composed of a head bearing a prostomial radiolar crown (RC) and an operculum (Op), a six-segmented thorax (Th), and a creamy white abdomen (Ab; **Figure 2.1**). The abdomen of adult *G. caespitosa* was divided into over 80 trunk segments by intersegmental septa (IS) which consisted of a thin layer of interlacing connective tissue (**Figure 2.2**). Each abdominal segment surrounded an unsegmented intestine (I) and a coiled main artery that ran the whole length of the abdomen. Except for the first five to six segments next to the thorax, all other abdominal segments served as germinal

chambers (GC) where the spermatogenesis occurred. These chambers were always filled with sperm cells (SC) at various stages of spermatogenesis. The head-end intersegmental septum formed the “floor” of each germinal chamber, whereas the tail-end septum formed the “ceiling”.

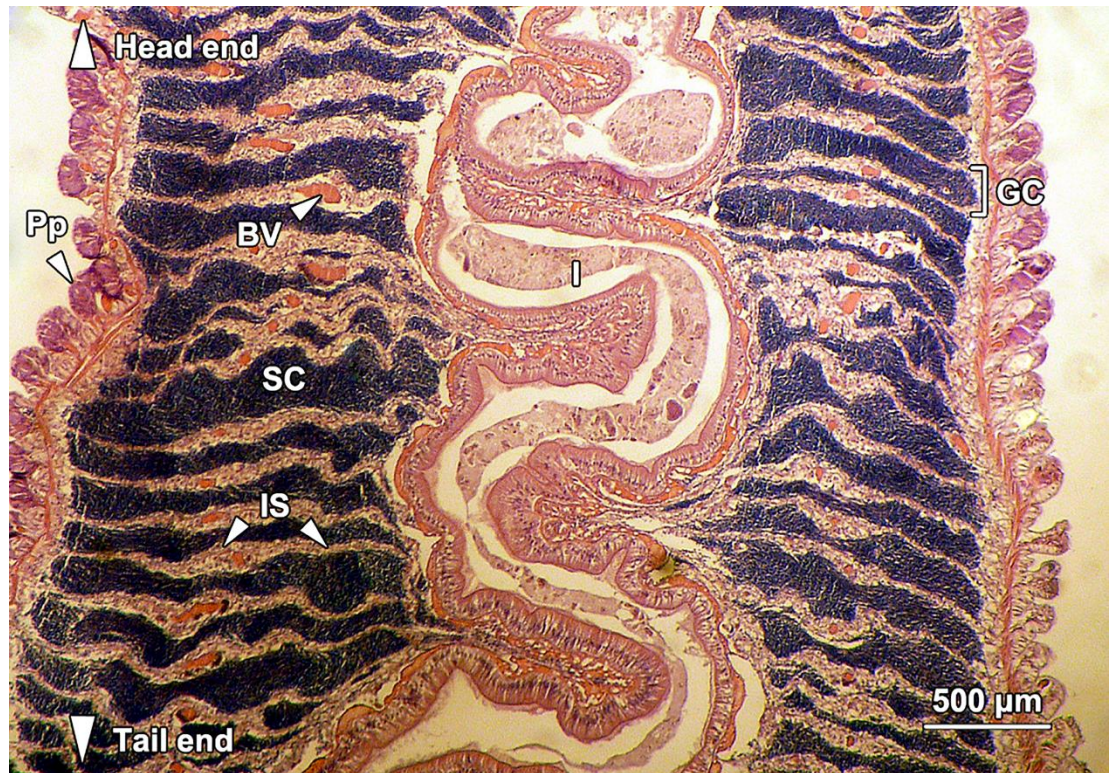


Figure 2.2 A longitudinal section through the abdomen of *G. caespitosa*. Internally, a coiled intestine (I) ran the whole length of the abdomen. The abdomen was divided into over 80 trunk segments by the intersegmental septa (IS). Each segment externally bore a pair of parapodia (Pp). Blood vessels (BV) were located within the intersegmental septa. The abdominal segments served as germinal chambers (GC) where the spermatogenesis occurred. These germinal chambers were filled up with sperm cells (SC) at various spermatogenic stages.

Transversely, the germinal chambers appeared as a C-shaped tubule which consisted of three morphologically distinct compartments: one seminiferous epithelium (SE) compartment, two nurse cell (NC) compartments and two efferent duct (ED) compartments. The SE compartment was located at the centre of the C-shaped chamber with the two NC compartments at each end. Then each of the NC compartments was

linked to an ED compartment. Finally, the two ED compartments joined together to form the unsegmented vas deferens (VD), which ran through the whole abdomen with an opening situated at the joint between thoracic and abdominal regions (**Figure 2.3**).

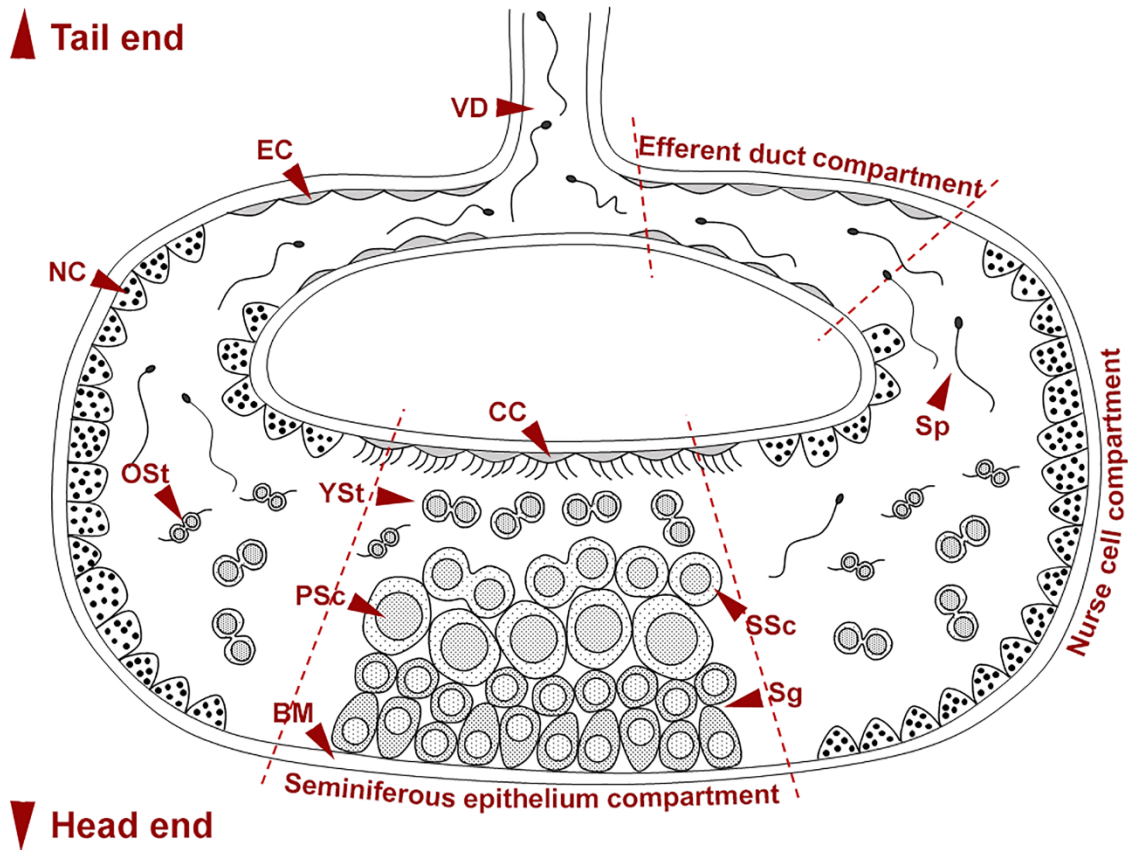


Figure 2.3 A schematic diagram showing a germinal chamber of the male reproductive system in *G. caespitosa*. The C-shaped germinal chamber was divided into three distinct compartments: one seminiferous epithelium compartment, two nurse cell compartments and two efferent duct compartments. Spermatogenesis occurred in the seminiferous epithelium compartment and spermatogonia (Sg) initially appeared on the basement membrane (BM) of the germinal chamber. The spermatogonia underwent a series of mitotic divisions and subsequently developed into primary spermatocytes (PSc) which produced secondary spermatocytes (SSc) through the first meiotic division. Each secondary spermatocyte further produced a pair of young spermatids (YSt) through the second meiotic division. The paired young spermatids were released from the seminiferous epithelium and migrated into the nurse cell compartments where they underwent spermiogenesis and differentiated into older spermatids (OSt) and spermatozoa (Sp). The spermatozoa then migrated towards the efferent duct compartments and were finally released

into the seawater through the vas deferens (VD). CC, ciliated cells; EC, squamous epithelial cells; NC, nurse cells.

2.4.2 Seminiferous epithelium compartment

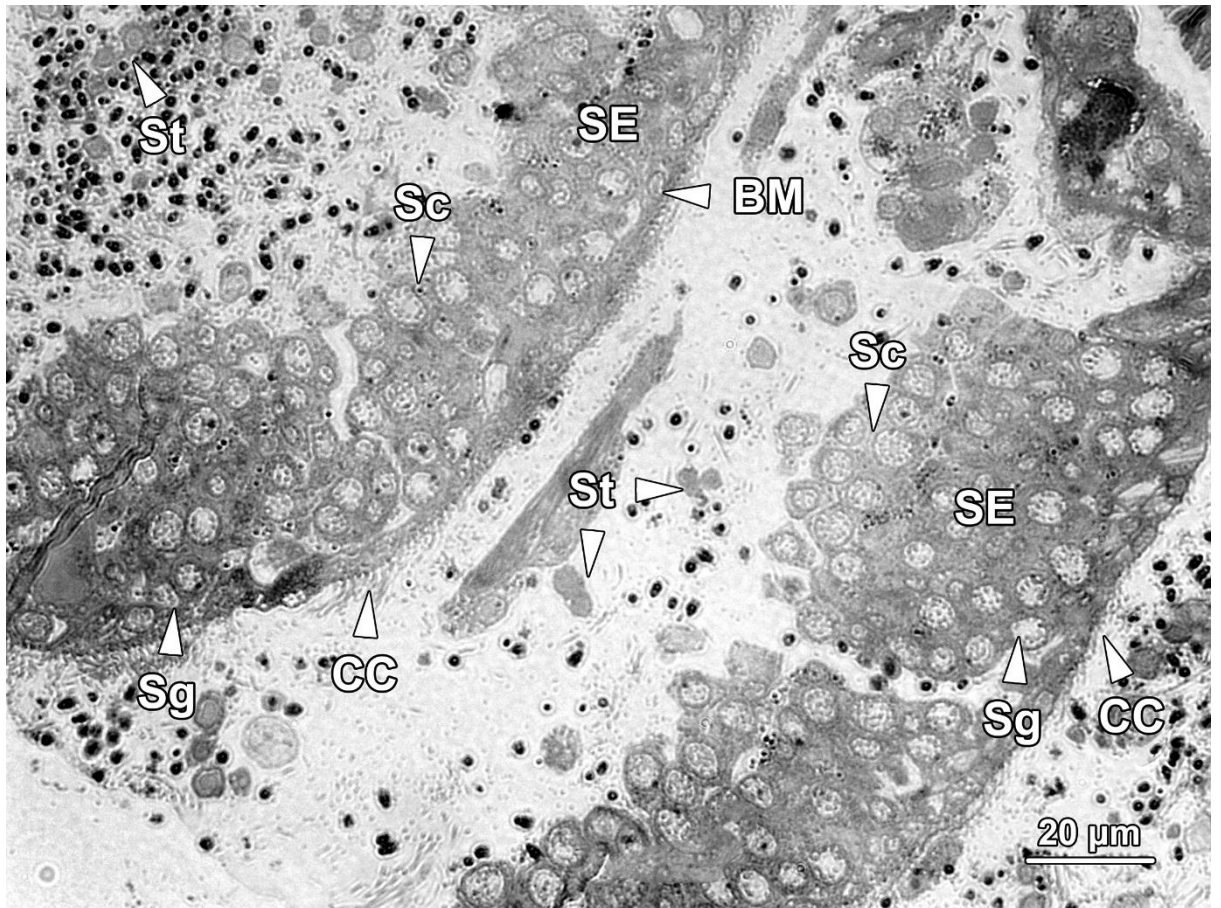


Figure 2.4 A longitudinal section of two neighbouring seminiferous epithelium compartments. The floor of the compartment was layered with seminiferous epithelium (SE), whereas the ceiling was covered by a monolayer of ciliated cells (CC). The seminiferous epithelium contained layers of spermatogonia (Sg) and spermatocytes (Sc). Spermatogonia occupied the initial layers near the basement membrane (BM), while spermatocytes with a larger size and paler colour were located in the upper layers close to the lumen. Paired spermatids (St) detached from the seminiferous epithelium and completed the remainder of spermatogenesis in the lumen of the germinal chamber.

Spermatogenesis was orchestrated in this compartment. The seminiferous epithelium (SE) sat on the basement membrane (BM) of the chamber floor and contained spermatogonia (Sg) and spermatocytes (Sc) only, which were densely packed in multilayers (**Figure 2.4**).

Spermatogonia were located in the bottom layers, in close apposition to the basement membrane, while primary and secondary spermatocytes were in the top layers. Spermatids (St) had never been found within the seminiferous epithelium, but were abundant in the lumen, close to the ceiling of the SE compartment (**Figure 2.4**). Thus, the mitotic and meiotic divisions of spermatogenesis occurred within the seminiferous epithelium, while the entire process of spermiogenesis, during which haploid round spermatids differentiated into functional spermatozoa (Sp), occurred in the lumen outside the epithelium. Blood vessels (BV) were frequently observed adjacent to the seminiferous epithelium, but there was no direct contact between them (**Figure 2.5**). No nurse cells were observed in the SE compartment. The ceiling of the SE compartment was covered by a monolayer of ciliated epithelial cells (CC; **Figure 2.4** and **2.5**), which facilitated the transportation of freely floating spermatids at various stages from the SE compartment to the NC compartments.

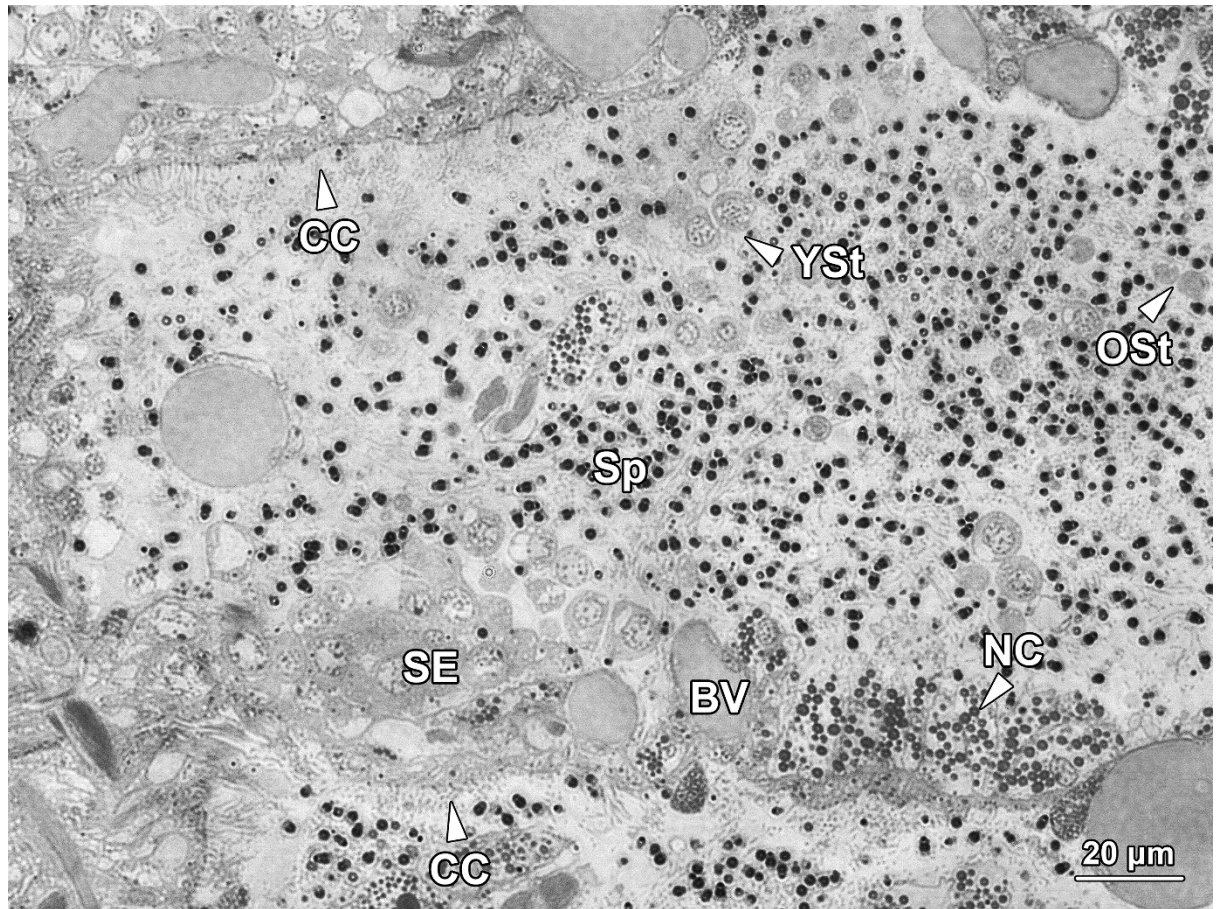


Figure 2.5 A longitudinal section of the connecting area between the seminiferous epithelium compartment (SE, on the left) and a nurse cell compartment (NC, on the right) in a germinal chamber. Young (YSt) and older spermatids (OSt) were observed floating freely in the lumen and were mixed with numerous spermatozoa (Sp) and granules secreted by the nurse cells. Noticeably, neither nurse cells nor blood vessels (BV) exhibited any physical connection with germ cells.

2.4.3 Nurse cell compartments

The two NC compartments were located at each end of the SE compartment. The wall of this compartment was tightly packed with spherical- to ovoid-shaped nurse cells (**Figure 2.5** and **2.6A**). These cells averaged $15.81 \pm 0.70 \mu\text{m}$ in diameter and contained a large number of electron-dense spherical granules with a diameter of approximately $1.72 \pm 0.055 \mu\text{m}$ (**Figure 2.6B**). These nurse cells supported the differentiating spermatids by releasing their cellular contents into the lumen, rather than through any sort of direct

contact. Noticeably, the lumen of NC compartments contained an enormous number of individual or paired spermatids at different stages of spermiogenesis, as well as spherical granules released from nurse cells (**Figure 2.5**).

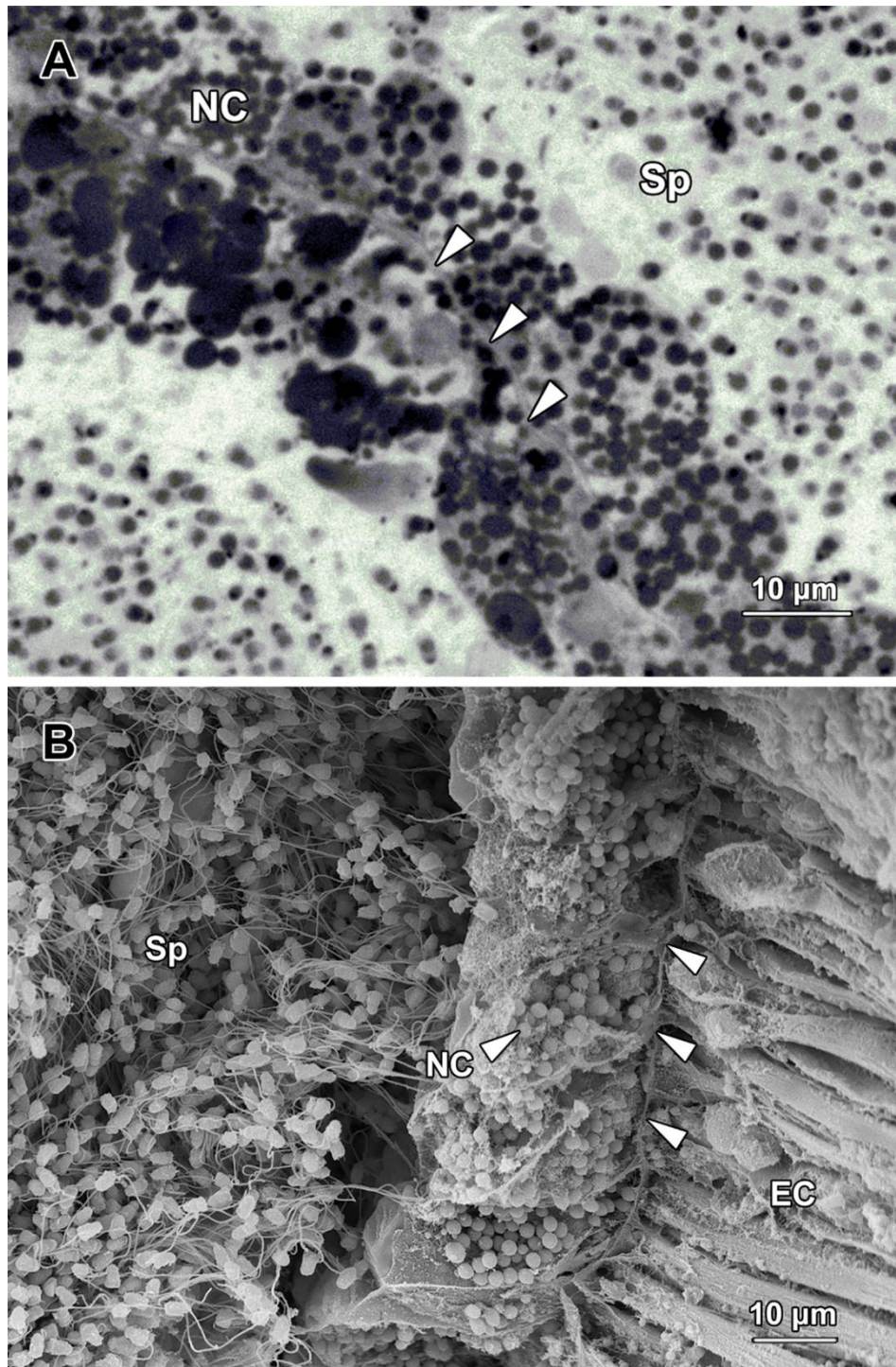


Figure 2.6 (A) A light micrograph showing nurse cells (NC) lining the border (arrowheads) of two nurse cell compartments. The nurse cells were filled with spherical granules which were released to the lumen to support the differentiation of spermatids. Sp, spermatozoa. **(B)** A scanning electron micrograph showing a portion of a nurse cell compartment filled with spermatozoa (Sp). The nurse cells (NC) were densely distributed along the wall of the compartment (arrowheads), with epithelial cells (EC) of digestive tract on the other side.

2.4.4 Efferent duct compartments

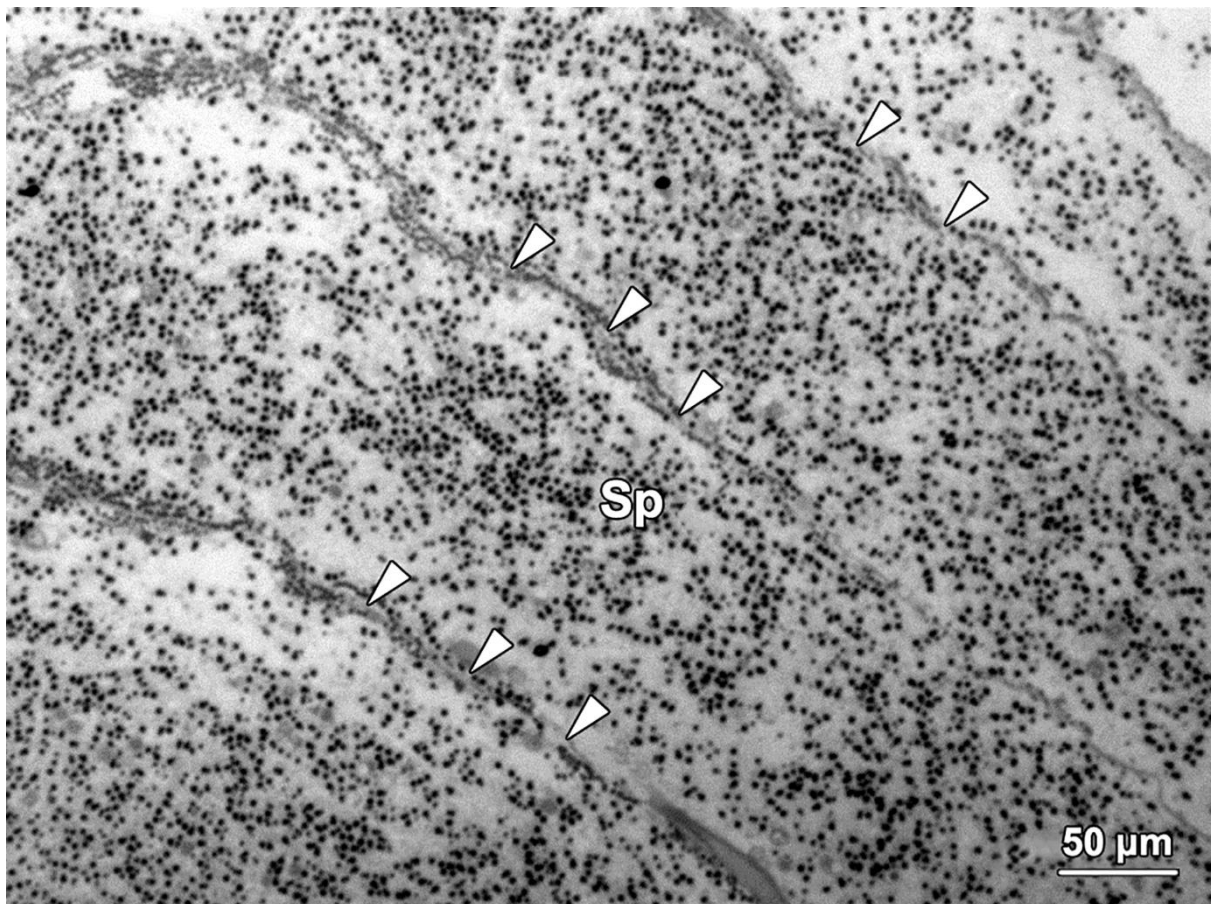


Figure 2.7 A light micrograph showing four neighbouring efferent duct compartments containing large numbers of spermatozoa (Sp) and spherical granules secreted by nurse cells. Each side of the intersegmental septa (arrowheads) in this compartment were covered by a thin layer of epithelial cells.

The two ED compartments were located at each end of the C-shaped germinal chamber and connected the NC compartments with the vas deferens (**Figure 2.3**). The wall of ED compartments encompassed a layer of thin intersegmental septa and a layer of squamous

epithelial cells (**Figure 2.7**). The lumen of ED compartments contained large numbers of spermatozoa (Sp) and few spermatids. The two ED compartments joined a thin, unsegmented vas deferens which lined the inner surface of the mid-ventral body wall. The wall of efferent duct at the junction of the ED compartment and vas deferens was thicker than that in other regions of this compartment (**Figure 2.8**). With the muscle contraction of the abdominal region, spermatozoa in each germinal chamber were transported from the efferent ducts into the vas deferens, and were finally released into the water column from the opening of the vas deferens situated at the joint between thoracic and abdominal regions (**Figure 2.1**).

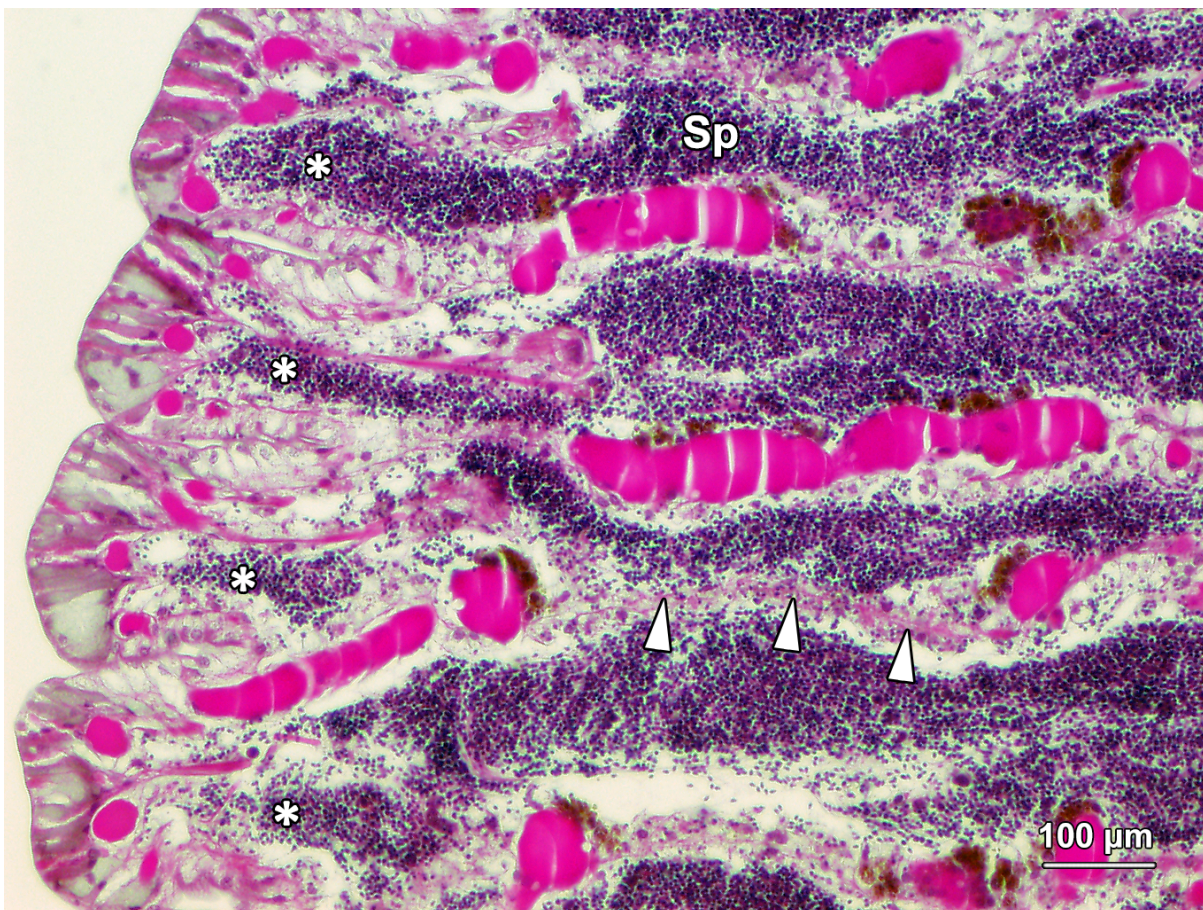


Figure 2.8 A light micrograph showing efferent duct compartments connecting to the vas deferens (*) at the terminus of each C-shaped germinal chamber. The wall of the efferent duct in this region (arrowheads) was comparatively thicker than that in other regions of this

compartment. It consisted of muscle cells that facilitated migration of spermatozoa from the efferent ducts to the vas deferens.

2.4.5 Germ cell differentiation in *Galeolaria caespitosa*

2.4.5.1 Pattern of spermatogenesis

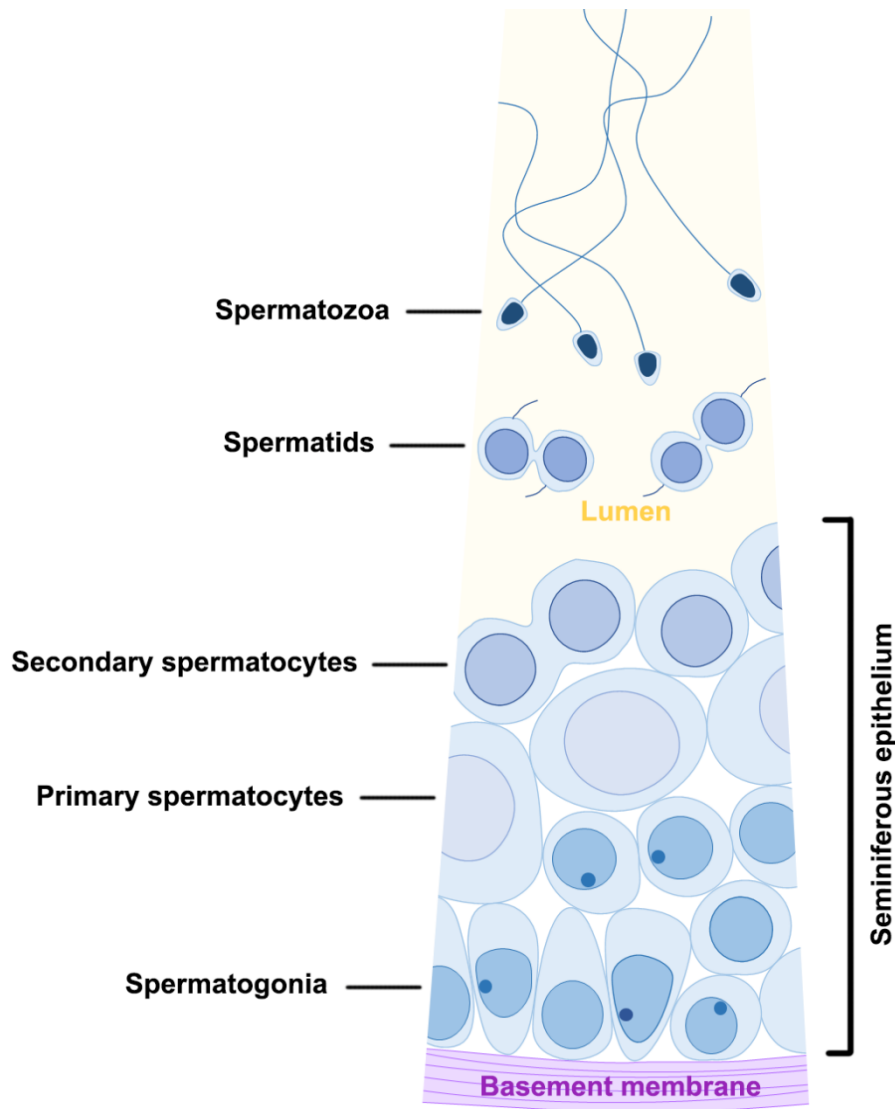


Figure 2.9 A diagram showing the pattern of spermatogenesis in *G. caespitosa*. Spermatogonia were in clusters and in close apposition to the basement membrane of the SE compartment. They underwent mitotic divisions and developed into primary spermatocytes while migrating away from the basement membrane. A primary spermatocyte divided into a pair of secondary spermatocytes through the first meiotic division and each secondary spermatocyte then further divided into a pair of spermatids after the second meiotic division. The paired spermatids subsequently detached from the seminiferous epithelium and completed spermiogenesis while

floating freely in the lumen of the germinal chamber. No direct contact between germ cells and nurse cells was observed at any spermatogenic stage.

Figure 2.3 and **2.9** collectively illustrated the pattern of sperm production in *G. caespitosa*. Spermatogenesis initially occurred in the seminiferous epithelium located on the floor of the SE compartment. Spermatogonia were basally located in the seminiferous epithelium but after a series of mitotic divisions, they ascended to the upper layers and divided into primary spermatocytes, which subsequently formed secondary spermatocytes through the first meiotic division. During the second meiotic division, each secondary spermatocyte divided into a pair of spermatids connected by a cytoplasmic bridge. These newly formed spermatids were maintained in pairs when they detached from the seminiferous epithelium and were released into the lumen of SE compartment. Paired spermatids completed the remainder of spermatogenesis while floating freely in the lumen of germinal chamber.

With the assistance of ciliated cells on the ceiling of each SE compartment, paired young spermatids (YSt; **Figure 2.5**) migrated into the NC compartments situated at both ends of the SE compartment. They were mixed with granules secreted by the nurse cells and continued to develop into older spermatids (OSt) and spermatozoa in the NC compartments. The newly formed spermatozoa (Sp) migrated towards and were stored in the ED compartments (**Figure 2.7**). The spermatozoa completed spermiogenesis and entered into the vas deferens with the help of the epithelial cells (EC) on the wall of ED compartments (**Figure 2.3**). For fertilisation, spermatozoa were released into seawater through the opening of vas deferens (VD) by rhythmic contractions of the vas deferens and abdominal muscles (**Figure 2.1**).

On the basis of both light and electron microscopic observations, the germ cells at various spermatogenesis stages in *G. caespitosa* were classified as follows.

2.4.5.2 Spermatogonia

Spermatogonia could only be found in the bottom layers of the seminiferous epithelium located in the SE compartment of each germinal chamber. Based on their positions, cell size and ultrastructural morphology, spermatogonia were subdivided into two types.

Type A spermatogonia were firmly adherent to the basement membrane (**Figure 2.10A**). They were approximately $8.46 \pm 1.63 \mu\text{m}$ in diameter with a nucleus about $5.2 \pm 0.8 \mu\text{m}$ in diameter. These spermatogonia were ovoid to fusiform in shape, with an oval nucleus (N) filled up with mostly sparse granular euchromatin and a few randomly distributed heterochromatin blocks. One or two small nucleoli (Nu) could sometimes be observed in the nucleus. The cytoplasm of type A spermatogonia was abundant in volume, however, few organelles were observed except for a large quantity of oval- to round-shaped mitochondria (M) and a continuous profile of rough endoplasmic reticulum (RER) lying in close proximity to the nucleus. The mitochondria were preferentially congregated in the basal cytoplasm of type A spermatogonia which was the aspect directed towards the basement membrane.

Type B spermatogonia (SgB) were found away from the basement membrane (**Figure 2.10B**); they were smaller in size but outnumber the type A spermatogonia (SgA) in the seminiferous epithelium, which indicated they were the offspring of type A

spermatogonia. Type B spermatogonia averaged $6.89 \pm 1.04 \mu\text{m}$ in diameter and possessed a nucleus about $4.4 \pm 0.69 \mu\text{m}$ in diameter. The differences in cellular and nuclear sizes between these two types of spermatogonia were statistically significant ($P < 0.001$). Morphologically, type B spermatogonia possessed relatively more ribosomes in the cytoplasm and the inner membrane of its nuclear envelope was scattered with more abundant heterochromatin blocks, which made the nuclear membrane less obvious compared with type A spermatogonia. Rather than ovoid or fusiform in shape, the type B spermatogonia appeared more spherical in shape. Similarly, they also contained a considerable number of mitochondria (M) in their cytoplasm and a conspicuous profile of rough endoplasmic reticulum (RER) surrounding the nucleus (**Figure 2.10B**). The nucleus (N) of type B spermatogonia was spherical in shape and contained a prominent eccentric nucleolus (Nu).

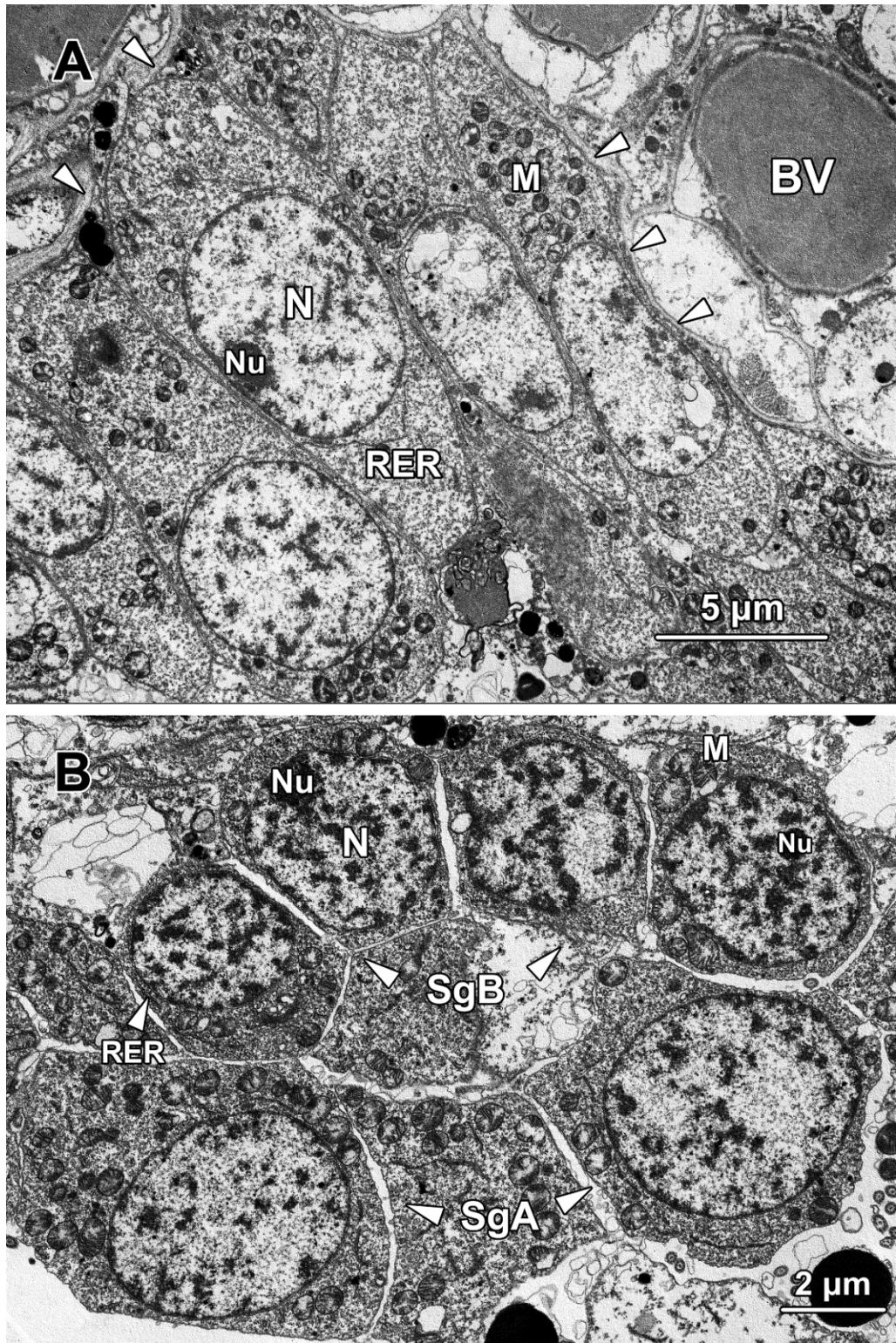


Figure 2.10 (A) A transmission electron micrograph showing a layer of type A spermatogonia packed along the basement membrane (arrowheads) of the SE compartment. The type A spermatogonia had no physical contact with the blood vessel (BV). Numerous mitochondria (M) tended to cluster in the basal cytoplasm while the nucleus (N) contained irregularly scattered clumps of chromatin blocks and an eccentrically located nucleolus (Nu).

RER, rough endoplasmic reticulum. **(B) A transmission electron micrograph showing two type A spermatogonia (SgA, the lower row) and four type B spermatogonia (SgB, the upper row).** Type B spermatogonia were frequently found one or two layers away from the basement membrane. Irregularly accumulated chromatin could be observed lining the inner nuclear membrane and in the centre of the nucleus. A conspicuous nucleolus (Nu) was frequently observed in the nucleus adhering to the nuclear membrane of type B spermatogonia. M, mitochondria; RER, rough endoplasmic reticulum.

2.4.5.3 Spermatocytes

Primary spermatocytes were the end products of a series of mitotic divisions of spermatogonia and were layered on the top of the type B spermatogonia. Primary spermatocytes had an ovoid to fusiform shape about $8.1 \pm 0.21 \mu\text{m}$ in diameter and an oval nucleus about $5.99 \pm 0.16 \mu\text{m}$ in diameter (**Figure 2.11**). The primary spermatocytes were significant larger than the size of type B spermatogonia ($P < 0.05$). As the formation of primary spermatocytes involved a dramatic growth in cell volume, the cytoplasm was much more abundant than their precursors. The ribosomes appeared to be sparsely distributed throughout the cytoplasm, along with a small number of glycogen particles (Gl; **Figure 2.11**). Late zygotene/early pachytene primary spermatocytes could be characterised by the presence of the synaptonemal complex, a structure composed of proteins that form a central shaft and two lateral bars associated with homologous chromosomes. The chromatin which previously lined the inner membrane of nuclear envelope disappeared at this stage and the double-membrane structure of nuclear envelope became conspicuous. The remaining portion of the nucleus was occupied with sparsely distributed euchromatin. A small number of mitochondria (M) and a conspicuous Golgi complex (GC) with secreted single membrane-bound vesicles and multivesicular bodies (MB) could be observed in the perinuclear area (**Figure 2.11**).

The first meiotic division of a primary spermatocyte generated two secondary spermatocytes. However, secondary spermatocytes were seldom observed during our ultrastructural investigation, suggesting that the second meiotic division was a quick process which only lasted for a short period of time.

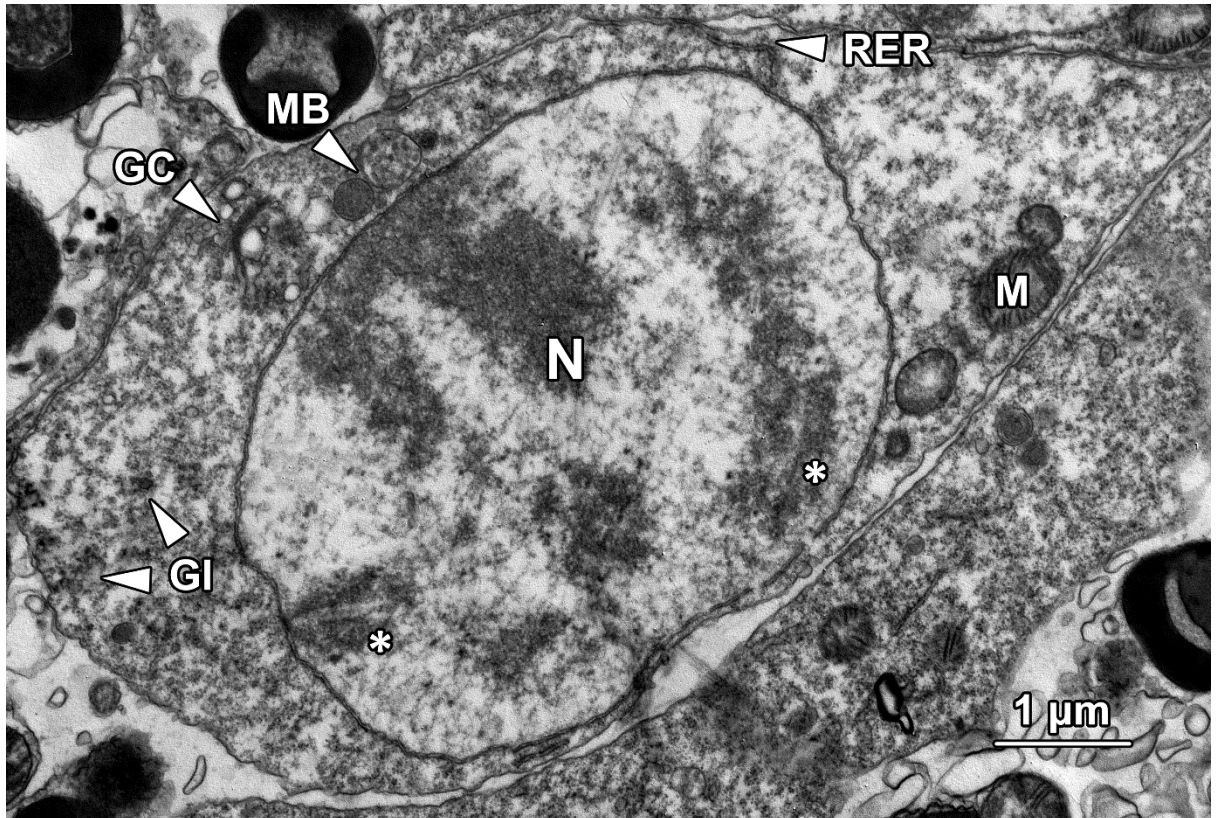


Figure 2.11 A transmission electron micrograph showing a primary spermatocyte at late zygotene/early pachytene stage of the first meiotic division. The most distinctive feature of the primary spermatocyte at this stage was the presence of synaptonemal complexes (*) in the nucleus. A Golgi complex with secreted irregular-sized vesicles and multivesicular bodies (MB) could be observed. Mitochondria (M) and glycogen (GI) were scattered throughout the cytoplasm. RER, rough endoplasmic reticulum.

2.4.5.4 Spermatids

The newly formed young spermatids (YSt) were frequently found in pairs in the lumen of SE and NC compartments (**Figure 2.5**). The spermatids remained in pairs during early spermiogenesis and separated into individual spermatozoa after shedding most of their

cytoplasm in the final stages of spermiogenesis. Based on their light microscope appearance, spermatids were divided into two major groups: non-flagellated young spermatids and flagellated older spermatids.

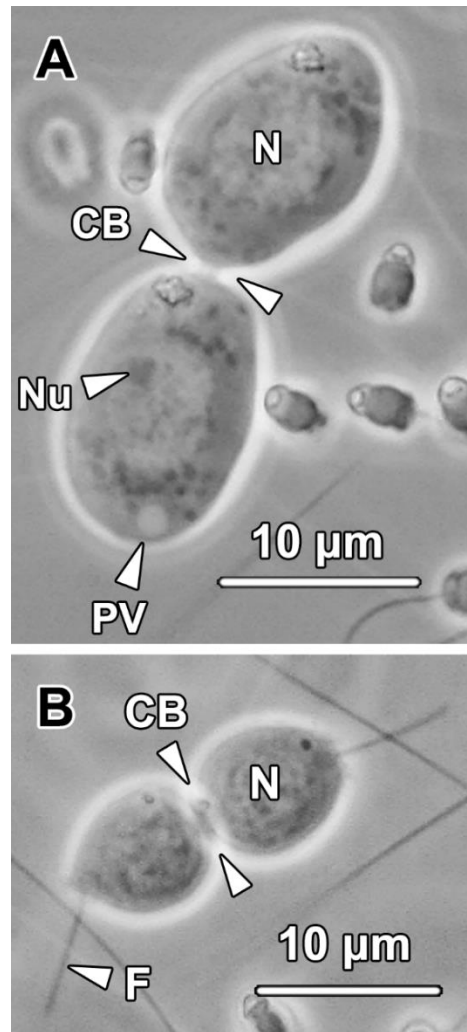


Figure 2.12 (A) A light micrograph of a pair of young spermatids connected by a cytoplasmic bridge (CB). A proacrosomal vacuole (PV), which was the precursor of acrosome, could be seen adjacent to the oval- to spherical-shaped nucleus (N). A distinct nucleolus (Nu) was eccentrically situated in the nucleus. No flagellum had formed at this stage. **(B) A light micrograph of a pair of older spermatids connected by a cytoplasmic bridge (CB).** At this stage, a forming sperm flagellum (F) was observed protruding from the posterior cytoplasm of the older spermatids. The older spermatids contained comparatively less cytoplasm and a spherical-shaped nucleus (N).

Non-flagellated young spermatids were found in pairs and connected by a common cytoplasmic bridge (CB; **Figure 2.12A**). They contained relatively abundant cytoplasm and were ovoid in shape with an oval- to spherical-shaped nucleus. A spherical proacrosomal vacuole (PV) could be observed in the posterior end of the cytoplasm opposite the cytoplasmic bridge. A distinct nucleolus (Nu) was frequently found eccentrically located in the nucleus (N), or even attached to the nuclear membrane (**Figure 2.12A**).

Flagellated older spermatids remained in pairs (**Figure 2.12B**). Compared with the younger spermatids, the older ones were more spherical in shape and contained less cytoplasm and a spherical nucleus (N) with denser chromatin. Noticeably, these round spermatids possessed an elongating flagellum (F) which protruded out of the cell body.

2.4.5.5 Spermatozoa

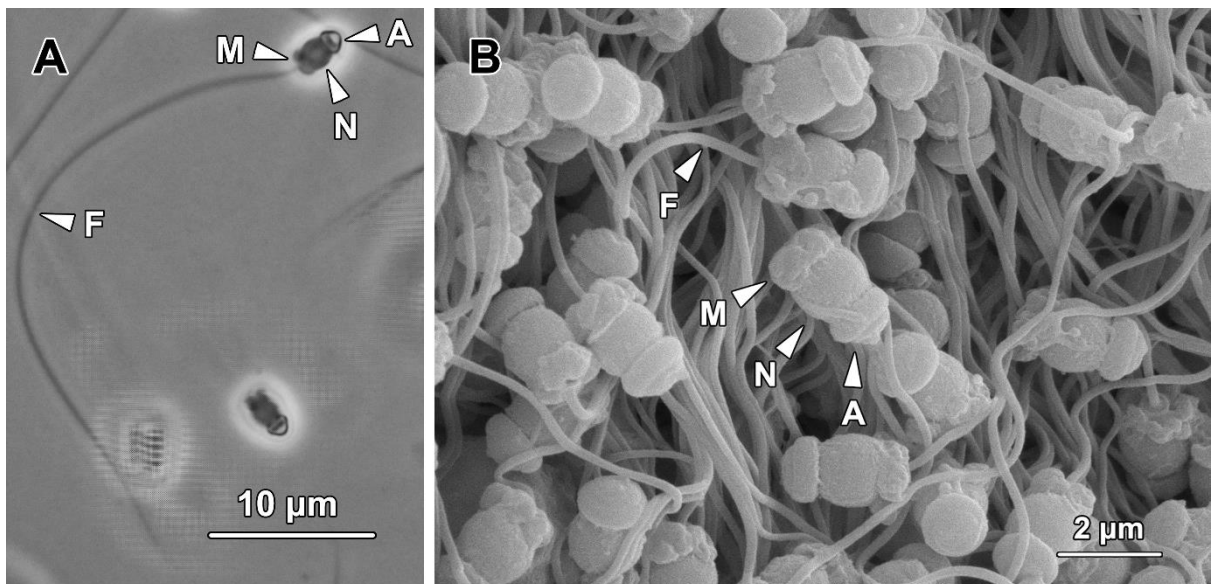


Fig 2.13 (A) A light micrograph of a spermatozoon. They consisted of a cap-like acrosome (A), an oval-shaped nucleus (N), a short midpiece (M) containing four round mitochondria and a developed flagellum (F) about 45 μm in length. **(B) A scanning electron micrograph showing**

bundles of spermatozoa stored in the lumen of the ED compartment. A, acrosome; M, midpiece; N, nucleus; F, flagellum.

Spermatozoa in *G. caespitosa* could be observed mainly in the ED compartments of each germinal chamber (**Figure 2.7**). In both the efferent duct and vas deferens, the spermatozoa were mixed with a large number of spherical granules secreted by the nurse cells (**Figure 2.5**). Each spermatozoon consisted of a cap-like acrosome (A), an oval nucleus (N), a short midpiece (M) containing four round mitochondria, and an elongated flagellum (F; **Figure 2.13**). In live spermatozoa, the longitudinal length of the sperm head (including the acrosome, nucleus and midpiece) was approximately 3.35 μm and the length of flagellum is about 45 μm .

2.5 Discussion

Galeolaria caespitosa is categorised into the annelid class Polychaeta, which comprises over 15,000 discovered species in 83 families (Eckelbarger *et al.*, 2001; Hutchings, 1998). The reproductive characteristics and feeding strategies in polychaetes are extremely diverse, which may be attributed to the simplicity of their reproductive system and their remarkable plasticity and adaptability to a broad range of habitats (Giangrande, 1997; Wilson, 1991). Although the reproductive biology of a considerable number of polychaetes has been documented previously, the structure of their male reproductive system has not been comprehensively described in detail. The pattern of spermatogenesis, in particular the formation and differentiation of spermatogonia, has been neglected by a majority of studies. This is possibly because the identification of spermatogenic stages is relatively difficult in polychaetes given the ability of developing germ cells to detach from the seminiferous epithelium and are mixed with other cells at various stages of differentiation in the coelomic cavity.

In the present chapter, the pattern of spermatogenesis within the male reproductive tract of *G. caespitosa* has been described for the first time. In *G. caespitosa*, the spermatogonia originate in the seminiferous epithelium lining the basement membrane of the germinal centre and are liberated into the lumen after the second meiotic division to complete the entirety of spermiogenesis while floating freely in the lumen. The germinal epithelium in *G. caespitosa* appears as densely packed cell layers, where the type A and B spermatogonia occupy a position in close apposition to the basement membrane while primary and secondary spermatocytes are situated in the upper layers close to the lumen. The spermatogonia are tightly packed together, whereas the spermatocytes gradually lose intercellular adhesion generating cell layers with a less compacted appearance.

In other studied polychaetes, the structure and function of their testes are various and can be categorised into three distinct groups: complex, simple and non-definitive. Only a small number of polychaetes possess complex testes [e.g. *Branchiopolynoe cf. seepensis* (Van Dover *et al.*, 1999), *Petitia amphophthalma* (Bührmann *et al.*, 1996)], where developing sperm cells are retained until the completion of spermiogenesis. These relatively complex testes are believed to facilitate sperm storage (Van Dover *et al.*, 1999) and tend to be associated with internal fertilisation; their spermatozoa being transported into the female reproductive tract with the help of spermathecae (Hilário *et al.*, 2005).

By contrast, a large number of polychaetes possess simple testes surrounded by a thin layer of sheath/peritoneal cells or a simple layer of germinal epithelium, such as *Amathys lutzi* (Blake and Van Dover, 2005), *Marenzelleria viridis* (Bochert, 1996), *Parergodrillus heideri* (Purschke, 2002), *Phragmatopoma lapidosa* (Eckelbarger, 1984), *Pomatoceros triqueter* and *Pomatoceros lamarckii* (Cotter *et al.*, 2003), *Polydora* spp. and *Steblospio benedicti* (Rice, 1981) and *Stygocapitella subterranea* (Purschke and Fursman, 2005). In addition, polychaetes with non-definitive testes, where the spermatogonia develop in cell clusters and are not invested by any epithelial or sheath cells, are also very common, such as in *Capitella* spp., *Capitomastus* spp. and *Capitellides* spp. (Eckelbarger and Grassle, 1987), *Gorgoniapolynoe caeciliae* (Eckelbarger *et al.*, 2005), *Platynereis massiliensis* (Lücht and Pfannenstiel, 1989), *Sabella spallanzanii* (Currie *et al.*, 2000; Giangrande *et al.*, 2000), *Vanadis formosa* and *Krohnia lepidota* (Rice and Eckelbarger, 1989). In *G. caespitosa*, the spermatogonial stem cells arise from unbound seminiferous epithelium and can therefore be categorised as a non-definitive testis. These studies on polychaetes with simpler testes indicate that the general pattern of their spermatogenesis is quite similar: spermatogenesis initially occurring in the testes after which spermatogenic cells

are released into the coelomic cavity to complete their differentiation in relative isolation (Rouse, 1998). Different from the species with complex testes, polychaetes with simple or non-definitive testes have no consistency in their fertilisation strategy or sperm transfer mode, suggesting that the reproductive strategy of any given annelid species is not necessarily related to the complexity of their testes.

In the abdominal region of *G. caespitosa*, blood vessels can be found embedded in the intersegmental septa and situated near the seminiferous epithelium, but there is no physical contact between the blood vessels and any type of sperm cells. In contrast, in most studied polychaetes, the seminiferous epithelia, or even the entire testes have been found in intimate association with blood vessels such as the nephridial blood vessel [e.g. *Amathys lutzii* (Blake and Van Dover, 2005) and *Marenzelleria viridis* (Bochert, 1996)], peritoneal blood vessel [e.g. *Phragmatopoma lapidosa* (Eckelbarger, 1984)], genital blood vessel [e.g. *Hesiocaeca methanicola* (Eckelbarger *et al.*, 2001)] and parapodial blood vessel [e.g. *Steblospio benedicti* (Rice, 1981)]. In most cases, spermatogonial stem cells are the only sperm cell type that have been observed directly attaching to the blood vessel, i.e. spermatogonia migrate peripherally during mitotic divisions and lose the direct connection with the circulation. However, in some polychaete species, such as *Gorgoniapolynoe caeciliae* (Eckelbarger *et al.*, 2005), the sperm cells remain attached to the blood vessels until early spermiogenesis. In *Capitella* spp., clusters of blood cells have been observed near the testes in the coelomic cavity (Eckelbarger and Grassle, 1987). It is presumed that these ramified blood vessels nourish the early spermatogenic cells through intimate contact.

Although polychaetes with simpler testes display a similar pattern of spermatogenesis, the timing of germ cell detachment from the seminiferous epithelium is different. A

number of previous studies have found that germ cells are released from the epithelium during the final mitotic division or before the onset of the first meiotic division [e.g. *Amathys lutzi* (Blake and Van Dover, 2005), *Marenzelleria viridis* (Bochert, 1996), *Phragmatopoma lapidosa* (Eckelbarger, 1984) and *Steblospio benedicti* (Rice, 1981)]. The sperm cells in these species are released into the coelomic cavity early as spermatogonia. Noticeably, either the spermatogonia [e.g. *Amathys lutzi* (Blake and Van Dover, 2005)] or the spermatocytes [e.g. *Marenzelleria viridis* (Bochert, 1996), *Phragmatopoma lapidosa* (Eckelbarger, 1984) and *Steblospio benedicti* (Rice, 1981)] in such species are in pairs and connected by a cytophore or cytoplasmic bridge. Distinct from these observations, sperm detachment from the seminiferous epithelium in *G. caespitosa* happens after the completion of second meiotic division. Moreover, no cytoplasmic bridge has been observed between spermatogonia or spermatocytes in *G. caespitosa*. In *Hydroides dianthus*, *Serpula vermicularis* and *Vermiliopsis infundibulum*, which are also serpulid polychaetes exhibiting similar reproductive characters (e.g. fertilisation strategy and sperm structure) with *G. caespitosa*, sperm detachment may happen after the completion of mitotic divisions due to the absence of spermatogonia in the coelomic cavity and similarly, no cytoplasmic bridge has been detected between spermatocytes (Gherardi *et al.*, 2011). Either way, these studies demonstrate that a significant portion of the spermatogenic process, occurs in the testicular lumen/coelomic cavity in these polychaete species.

In the germinal chambers of *G. caespitosa*, the whole ceiling of the seminiferous epithelium compartment is covered by a layer of ciliated epithelial cells, which facilitate the transportation of spermatids towards the nurse cell compartment. Ciliated intersegmental septa have also been observed in *Capitella* spp. (Eckelbarger and Grassle,

1987), *Parergodrilus heideri* (Purschke, 2002) and *Phragmatopoma lapidosa* (Eckelbarger, 1984). The ciliated cells in these species, including the ones in *G. caespitosa*, exhibit a cubic to columnar shape and contain a spherical nucleus situated at the basal cytoplasm. Multiple cilia protrude from the anterior surface of the ciliated cells, whereas the basal surface of the cells firmly adheres to the intersegmental septum. Such ciliated epithelial cells have seldom been reported in other polychaete species. Nevertheless, they have been neglected or mistakenly recognised as sperm flagella in some polychaetes, as the histological sections presented in association with these studies do demonstrate the existence of ciliary structures [e.g. *Pomatoceros lamarckii* (Cotter *et al.*, 2003) and *Serpula vermicularis* (Gherardi *et al.*, 2011)].

In *G. caespitosa*, individual secondary spermatocyte divides into a pair of spermatids connected by a common cytoplasmic bridge during the second meiotic division. The paired spermatids then undergo spermiogenesis simultaneously (**Figure 2.12A and B**). In contrast, in some polychaetes, a pair of secondary spermatocytes connected by a common cytoplasmic bridge develop into a tetrad of spermatids rather than two individual pairs of spermatids, such as in *Asetocalamyzas laoncola* (Vortsepneva *et al.*, 2006), *Marenzelleria viridis* (Bochert, 1996), *Phragmatopoma lapidosa* (Eckelbarger, 1984) and *Steblospio benedicti* (Rice, 1981). Additionally, in a considerable number of other polychaetes, such as *Amathys lutzi* (Blake and Van Dover, 2005), *Boccardiella hamata* (Reunov *et al.*, 2010), *Capitella* spp. (Eckelbarger and Grassle, 1987) and *Methanoaricia dendrobranchiata* (Eckelbarger and Young, 2002), a large number of spermatocytes have been observed held together by a cytophore which tends to persist during the following spermiogenesis.

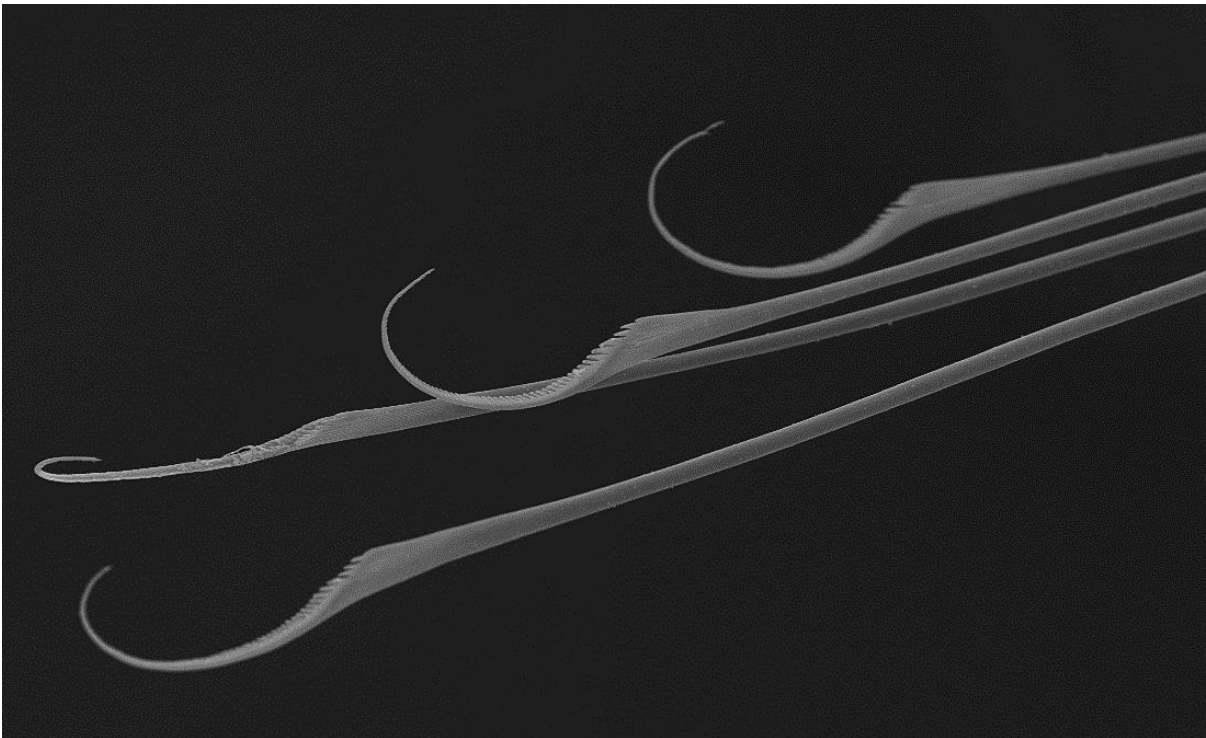
Apart from the support provided by blood vessels, no other type of supporting cell for sperm differentiation has been reported in any other polychaete species so far. Remarkably, nurse cells have been found in this study, occupying a considerable part of each germinal chamber in *G. caespitosa*. The entire wall of the two NC compartments is covered by these supporting cells, which contain numerous electron-dense granules (**Figure 2.6**). The nurse cells indirectly support spermiogenesis by releasing their cellular contents into the lumen. According to *in vitro* culture studies we have conducted on the spermatids, the fluid extracted from the germinal chamber of *G. caespitosa* can support the further development of young spermatids (unpublished observation). Therefore, the nurse cells are believed to play an important role in the development of spermatids in *G. caespitosa*. The electron-dense granules released by the nurse cells of *G. caespitosa* are not only found in the NC compartments, but also in the efferent duct compartments and vas deferens, suggesting that these granules may also be involved in maintaining the viability of spermatozoa during their transport and storage within the male reproductive tract.

Spermatogenesis in *G. caespitosa* does not appear to involve intimate contact with any other cell type, as no supporting cells has been detected in direct association with any spermatogenic stage or during spermiogenesis. The haploid germ cells of *G. caespitosa* are found floating independently in the lumen of the germinal chamber. In contrast, spermatogenesis in vertebrates is completely dependent on intimate contact with Sertoli cells (Jones and Lin, 1992). This relative independence from supporting cells in *G. caespitosa* endow this species great potential to be a model species for uncovering the molecular mechanisms underpinning sperm differentiation, particularly the complex process of spermatid differentiation, using *in vitro* cell culture systems.

In summary, the germinal chamber of *G. caespitosa* appears as a C-shaped tubule surrounding the main artery and intestine that run the whole length of the abdomen. A similar male reproductive system can be observed in histological sections of abdominal segments in *Aonides oxycephala* (Radashevsky *et al.*, 2011), *Branchiomma luctuosum* (Licciano *et al.*, 2002) and *Sabella spallanzanii* (Giangrande *et al.*, 2000). Based on morphological and functional differences, the germinal chamber in *G. caespitosa* has been divided into three distinct compartments, including an SE compartment, two NC compartments and two ED compartments. The two ED compartments situated at the two ends of the C-shaped germinal chamber join together to the vas deferens. Interestingly, this arrangement of compartments in the germinal chamber of *G. caespitosa* resembles the arrangement of the seminiferous tubule in mammalian testes. Thus the U-shaped seminiferous tubule in the human also has two openings running side by side to join the rete testis, efferent duct, and then the vas deferens (Bloom and Fawcett, 1975). This simple sessile annelid may therefore not only serve as a model bio-indicator species capable of revealing the presence of reproductive toxicants in the marine environment but might also be used to shed light on such fundamental processes as spermiogenesis that will be inform our understanding of male reproduction across a wide range of species, including man.

Chapter 3

Ultrastructural investigation of spermiogenesis and *in vitro* differentiation of spermatids in *Galeolaria caespitosa*



3.1 Overview

In this chapter, spermiogenesis in the marine invertebrate *Galeolaria caespitosa* has been elucidated in detail at the ultrastructural level and a substantial portion of this complex differentiation process has been successfully reproduced *in vitro*. Using transmission electron microscopy, ten steps of spermatid differentiation were identified based on morphological events such as formation of acrosome, condensation of the nucleus, elongation of the flagellum and elimination of excess cytoplasm. On completion of the second meiosis, newly formed spermatids are detached from the seminiferous epithelium and released to the lumen of each germinal chamber. These young spermatids are present in pairs and interconnected by a cytoplasmic bridge throughout the entire spermiogenic process.

The differentiation of spermatids was temporally divided into three phases: Golgi phase, acrosomal phase and maturation phase. During the Golgi phase, proacrosomal vesicles appeared in close proximity to a conspicuous Golgi complex located at the posterior pole of the spermatids and gradually coalesced into a proacrosomal vacuole. Meanwhile, the two centrioles, which were initially located near the nuclear membrane, migrated towards the cytoplasmic membrane. The distal centriole subsequently docked onto the plasma membrane and gave rise to a formative flagellum. The acrosome accomplished a major portion of its differentiation process during the acrosome phase. At the same time, the distal centriole inserted into the shallow implantation fossa formed at the posterior end of the nucleus. The mitochondria fused with each other to form larger spherical-shaped ones. The larger mitochondria then migrated and adhered to the concave surface of the nucleus at the posterior pole. The acrosome began to migrate towards the apex of the spermatids after the adherence of the mitochondria. During the maturation phase, the acrosome

finalised its migration and differentiation, the nucleus accomplished its condensation and the excess cytoplasm was extruded from the spermatids as residual bodies. As a consequence, the cytoplasmic bridge between spermatids was ruptured and the spermatids developed into individual spermatozoa.

The independence of spermiogenesis from supporting cells in *G. caespitosa* provided us a convenient model for reproducing this complex differentiation process *in vitro*, which has been difficult to achieve in mammalian species. In this study, we successfully induced the step 1-3 spermatids to differentiate into the step 7-9 spermatids in both male germinal fluid and 10% foetal bovine serum in RPMI 1640 medium, but failed to reproduce this process in female or boiled male germinal fluids. Therefore, the key regulators of spermiogenesis in *G. caespitosa* were gender-specific and contained protein substances. These findings established a fundamental basis for the future studies regarding the molecular mechanisms of spermatid differentiation in this species and even other higher animals.

3.2 Introduction

This study described in **Chapter 2** demonstrated that the spermatogenesis in *G. caespitosa* does not involve physical connection with any sort of supporting cells; hence, it was more dependent on intrinsic developmental programming compared with most species. Noticeably, the entire process of spermiogenesis, during which round spermatids differentiated into highly specialised spermatozoa, occurred while the gametes were floating freely in the lumen of the germinal chamber. Such independence from supporting cells made the spermiogenesis in *G. caespitosa* a convenient model to uncover the molecular mechanisms underlying this complex differentiation process. The study presented in this chapter describes spermiogenesis in *G. caespitosa* at the ultrastructural level and provided an opportunity to recapitulate differentiation of spermatids *in vitro*.

3.3 Materials and Methods

3.3.1 Sample collection and maintenance

Aggregations of *G. caespitosa* were collected freshly at low tides from intertidal rock revetments at Merewether beach (32°56'34"S, 151°45'9"E), Merewether, New South Wales, Australia. The tubeworms were transported to the laboratory within 1 h after collection and maintained in an aerated polyethylene bucket with natural seawater obtained from the collection sites. Samples were reared at constant room temperature of 20 ± 2 °C and supplied with a 12-h light/12-h dark illumination cycle. All samples used in this study were fixed within 48 h of collection.

3.3.2 Transmission electron microscopy

As described in **Section 2.3.3, Chapter 2**, male *G. caespitosa* were fixed in glutaraldehyde, dehydrated through a graded series of acetone concentrations and

embedded in Spurr's resin. The resin blocks were sectioned under a microtome and ultrathin sections were stained with uranyl acetate and lead citrate and examined by transmission electron microscopy.

3.3.3 *In vitro* culture of spermatids

Adult male *G. caespitosa* were extracted from their calcareous tubes and immediately immersed in filtered natural seawater. The worms spontaneously released their spermatozoa on being exposed to seawater. They were allowed to sit for at least 10 min until the spawning ceased. After that, the worms were rinsed vigorously in seawater and transferred to clean seawater. More spermatozoa, along with a considerable amount of spermatids, were stimulated to release by puncturing the abdominal wall with a syringe needle and gently pressing the abdomen using a pair of forceps. To enrich the spermatids, 1.5 mL of the sperm solution collected from at least 10 male adults was applied to the top of a discontinuous Percoll gradient (10%, 20%, 30% and 40% Percoll in artificial seawater of 1.5 mL each) in a 15 mL Falcon tube and centrifuged at 500 g for 20 min. The centrifugation process separated the cells into two distinct fractions: a thick fraction that was rich in spermatozoa and a thin fraction contained spermatids at various differentiation steps. The thin fraction was carefully transferred to a 1.5 mL Eppendorf tube using transfer pipettes. The Percoll was then eliminated by centrifugation at 500 g for 5 min and the resultant germ cell pellet was resuspended in culture medium.

The isolated spermatids were cultured respectively in male germinal fluid, boiled male germinal fluid, female germinal fluid, and 10% foetal bovine serum (FBS; Sigma Aldrich, Castle Hill, Australia) in RPMI 1640 media (Thermo Fisher Scientific, North Ryde, Australia) to test their capacity to induce the differentiation of spermatids *in vitro*. Except

for the male germinal fluid, the osmolality of all other culture media was tested and adjusted to that of the male germinal fluid (1135 mOsm/kg) using artificial seawater.

To obtain the male and female germinal fluids, adult worms were extracted from their tubes and placed on a dry petri dish. To stimulate the release of germinal fluid, the abdominal wall was lightly punctured using a 30G × 0.5 in syringe needle and then gently pressed using a pair of forceps. During this process the digestive tract and the main artery were not disturbed in order to avoid contamination by their contents. The germinal fluid was collected using a Hamilton® 7000.5KHs 0.5 µL syringe (Sigma Aldrich, Castle Hill, Australia) and pooled together into a 1.5 mL Eppendorf tube. About 20 to 30 adult worms were used for each attempt at cell culture so that at least 100 µL of germinal fluid could be obtained. The germinal fluid was then centrifuged at 19,083 g for 5 min and the supernatant was transferred to a clean Eppendorf tube. 1 µL of purified spermatids and 1 µL of 10,000 U/mL Penicillin-Streptomycin (Thermo Fisher Scientific, North Ryde, Australia) were added to 98 µL of the male or female germinal fluid and mixed thoroughly. Using a Pasteur pipette, the purified spermatids in the germinal fluid were immediately transferred to a microscope side chamber made with a 40 mm × 22 mm HybriWell™ hybridization sealing chamber (Thermo Fisher Scientific, North Ryde, Australia). To minimise evaporation of the culture medium, the two ports of the slide chamber were sealed firmly by two seal-tabs.

The sperm cells were cultured inside a Zeiss microscopic physiological chamber (Carl Zeiss, Oberkochen, Germany) with 5% CO₂ and 100% humidity air at 21 °C for up to 36 h. The slide chamber was kept in the dark by wrapping the physiological chamber with aluminium foil. The cultured spermatids were examined under a Zeiss Axiovert S100 microscope (Carl Zeiss, Oberkochen, Germany) equipped with a Zeiss AxioCam MRm

camera (Carl Zeiss, Oberkochen, Germany) at 0 h, 12 h, 24 h and 36 h during the incubation. The percentages of spermatids at different stages were counted from a hundred randomly selected cells under the microscope.

3.3.4 Statistical analysis

All data presented in this article were generated from at least three biological replicates to meet the requirements for statistical validity. The measurements of spermatids and their subcellular organelles are all presented as mean \pm SE, which were calculated from at least 20 samples from each step of spermatid development. The statistical difference between spermatids at different developmental steps was determined using the Student's t-test. Differences were recognised as statistically significant if the *P* value was less than 0.05. All statistical analyses were performed using Microsoft Excel 2013 (Microsoft Corporation, Redmond, USA).

3.4 Results

Spermatids have been classified into ten steps based on the morphological development of the acrosome, nucleus, flagellum and other organelles at the ultrastructural level.

3.4.1 Step 1 spermatids

During the second meiotic division of spermatogenesis, each secondary spermatocyte divided into a pair of step 1 spermatids, which were interconnected by a common cytoplasmic bridge. At this stage of development, these spermatids became detached from the seminiferous epithelium to float freely in the lumen of the germinal chamber.

Step 1 spermatids were ovoid in shape with an average cellular diameter of $6.4 \pm 0.46 \mu\text{m}$ (**Figure 3.1A**). The nucleus (N) was spherical- to oval-shaped and approximately $4.38 \pm$

0.46 μm in diameter. Small patches of dense heterochromatin were randomly scattered in the nucleoplasm and lined the inner nuclear membrane. Euchromatin was sparse and evenly distributed throughout the nucleoplasm. The nucleus contained one or two prominent eccentric nucleoli (Nu).

In the perinuclear region of the cytoplasm, a well-developed Golgi complex (GC) was observed, with a large amount of secretory small membrane-bound vesicles (V) and multivesicular bodies (MB) at its concave surface (**Figure 3.1B**). These vesicles later fused with each other to form a proacrosomal vacuole. A pair of centrioles (C) was located in close proximity to both the nuclear membrane and the Golgi complex (**Figure 3.1A**). Spherical-shaped mitochondria (M) with an average diameter of $0.44 \pm 0.06 \mu\text{m}$ were clustered near the Golgi complex (**Figure 3.1A**). Rough endoplasmic reticulum (RER) was randomly distributed throughout the whole cytoplasm (**Figure 3.1B**). Bundles of microtubules (Mt) surrounded the nucleus and formed the circular manchette that facilitated shaping of the nucleus (**Figure 3.1C**).

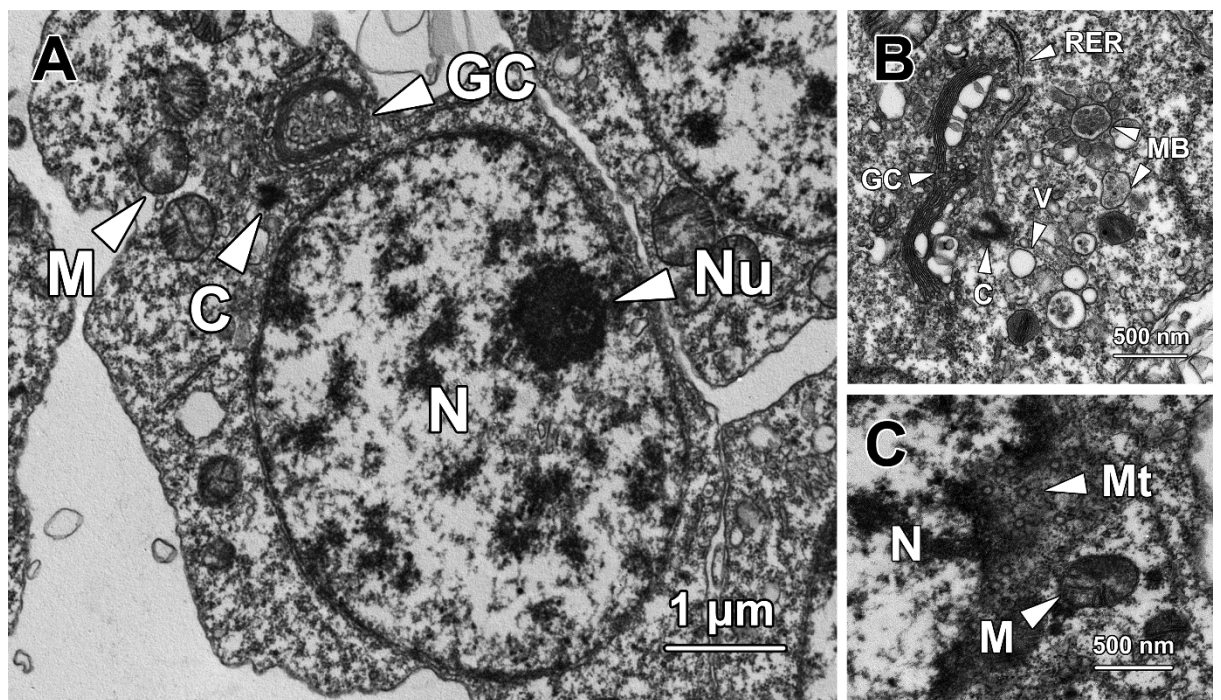


Figure 3.1 Transmission electron micrographs of step 1 spermatids. (A) Step 1 spermatids were ovoid in shape with an oval nucleus (N) containing one or two eccentric nucleoli (Nu) and a large number of randomly dispersed small patches of chromatin. A well-developed Golgi complex (GC) was found in close proximity to the nucleus. A pair of centrioles (C) resided adjacent to both the Golgi complex and the nuclear membrane. Spherical mitochondria (M) were in clusters in the cytoplasm. (B) Numerous small membrane-bound vesicles (V) and multivesicular bodies (MB) were presented at the concave surface of the Golgi complex (GC). Centrioles (C) were also found next to the Golgi complex. Rough endoplasmic reticulum (RER) was randomly distributed in the cytoplasm. (C) Bundles of microtubules (Mt) were found tightly surrounding the nucleus, forming a circular manchette that facilitated the shaping of the nucleus (N). M, mitochondria.

3.4.2 Step 2 spermatids

Step 2 spermatids remained oval-shaped with a spherical to oval nucleus (**Figure 3.2A**). The average cellular and nuclear diameters of step 2 spermatids were $5.89 \pm 0.41 \mu\text{m}$ and $4.15 \pm 0.42 \mu\text{m}$ respectively. While their cellular size was significantly smaller than that of step 1 spermatids ($P < 0.001$), the nuclear size has no significant difference compared with that of their immediate precursors ($P > 0.05$). Dense clumps of chromatin were randomly dispersed throughout the nucleus and also lined the inner nuclear membrane. A conspicuous nucleolus (Nu) was eccentrically situated in the nucleoplasm.

Step 2 spermatids were characterised by the formation of the proacrosomal vacuole (PV), which was generated by coalescence of the small membrane-bound vesicles secreted by the Golgi complex (GC). The proacrosomal vacuole at this stage was spherical in shape with a nearly electron-lucent matrix (**Figure 3.2A**). The two centrioles continuously migrated away from the nuclear membrane and gradually approached the cytoplasmic membrane, during which the two centrioles oriented parallel instead of perpendicular to each other. The centriole that was in close association with the plasma membrane was the distal centriole (DC), which later gave rise to the sperm flagellum; the centriole relatively

distant from the plasma membrane was the proximal centriole (PC; **Figure 3.2B**). Spherical-shaped mitochondria (M) are randomly dispersed around the periphery of the nucleus while continuous profiles of rough endoplasmic reticulum (RER) tightly surrounded the nucleus (**Figure 3.2A**).

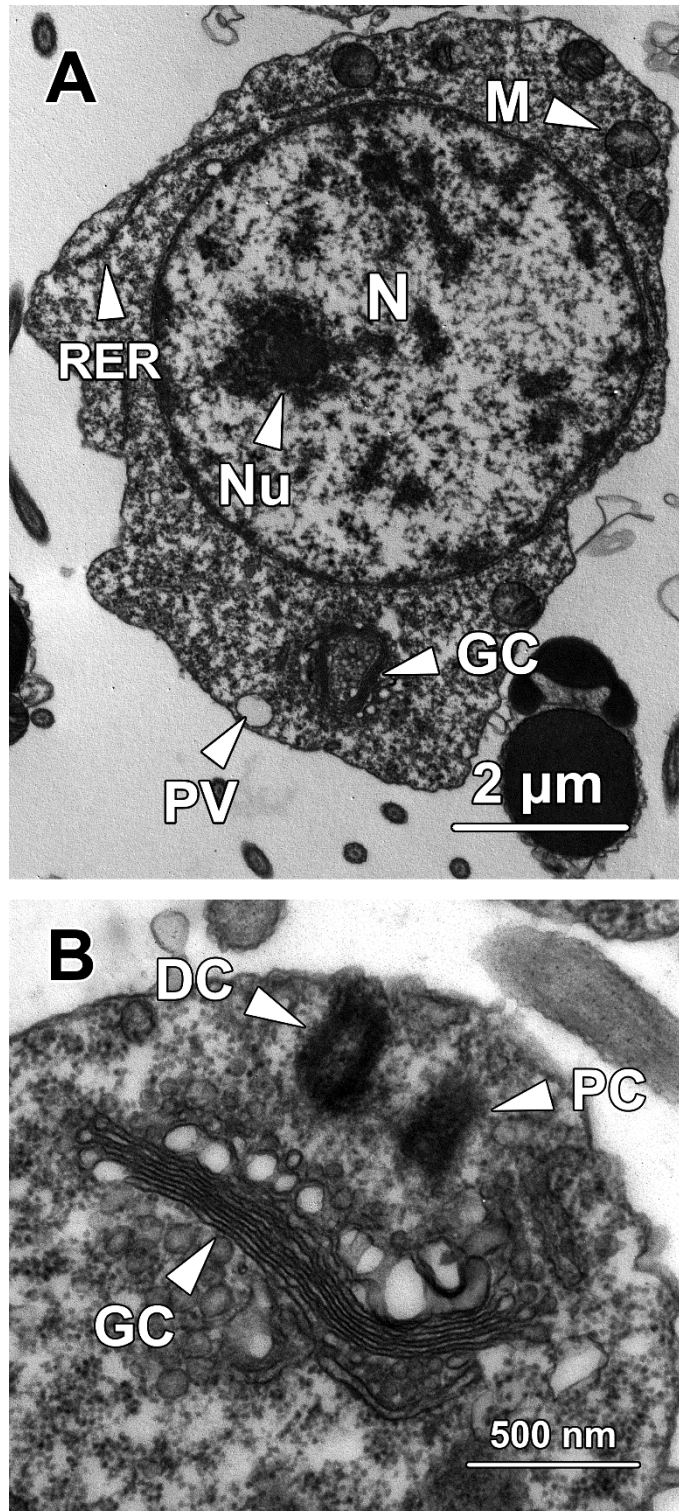


Figure 3.2 Transmission electron micrographs of step 2 spermatids. (A) Step 2 spermatids were oval-shaped with a spherical to oval nucleus (N) containing an eccentric nucleolus (Nu) and small clumps of chromatin. In the periphery of the nucleus, a distinct Golgi complex (GC) was observed adjacent to a spherical proacrosomal vacuole (PV) with an electron-lucent matrix, which originated from the fusion of small membrane-bound vesicles. Continuous profiles of rough

endoplasmic reticulum (RER) were found running around the nucleus. Spherical mitochondria (M) were randomly dispersed throughout the cytoplasm. (B) The two centrioles in step 2 spermatids remained in close proximity to the Golgi complex (GC) but became relatively distant from the nucleus. While the distal centriole (DC) approached the plasma membrane, the proximal centriole (PC) oriented parallel to the former and was relatively distant from the cell membrane.

3.4.3 Step 3 spermatids

Step 3 spermatids had a cellular diameter of $6.01 \pm 0.51 \mu\text{m}$ and a nuclear diameter of $3.87 \pm 0.45 \mu\text{m}$, which were similar to that of the step 2 spermatids ($P > 0.05$). Distinct from the irregular-shaped small chromatin blocks in the nucleoplasm of step 1 or 2 spermatids, the chromatin blocks in step 3 spermatids exhibited a rod-like appearance. The chromatin that clumped against the inner nuclear membrane became thicker than that in step 2 spermatids (**Figure 3.3A**).

The proacrosomal vacuole (PV) remained adjacent to the Golgi complex (GC) but became larger as more Golgi-derived vesicles fused with it. At this stage, a small patch of electron-dense material formed eccentrically in the poorly stained matrix of the proacrosomal vacuole (**Figure 3.3A**). Although both of the two centrioles remained close to the Golgi complex, the distal centriole (DC) docked onto the plasma membrane where the flagellum would subsequently form. The proximal centriole (PC) oriented almost perpendicularly to the distal centriole (**Figure 3.3B**). Different from the mitochondria in younger spermatids, which were all spherical in shape, a portion of the mitochondria (M) in step 3 spermatids exhibited a rod-shaped appearance (**Figure 3.3A**); the long axis was about $0.91 \pm 0.16 \mu\text{m}$ and short axis was averagely $0.38 \pm 0.13 \mu\text{m}$. Noticeably, the long axis of these mitochondria was approximately twice as long as the diameter of the spherical-shaped mitochondria, whereas the short axis had no significant difference compared with the diameter of spherical mitochondria ($P > 0.05$). At this step, the

spermatids remained in pairs and were interconnected by a cytoplasmic bridge (CB; **Figure 3.3C**).

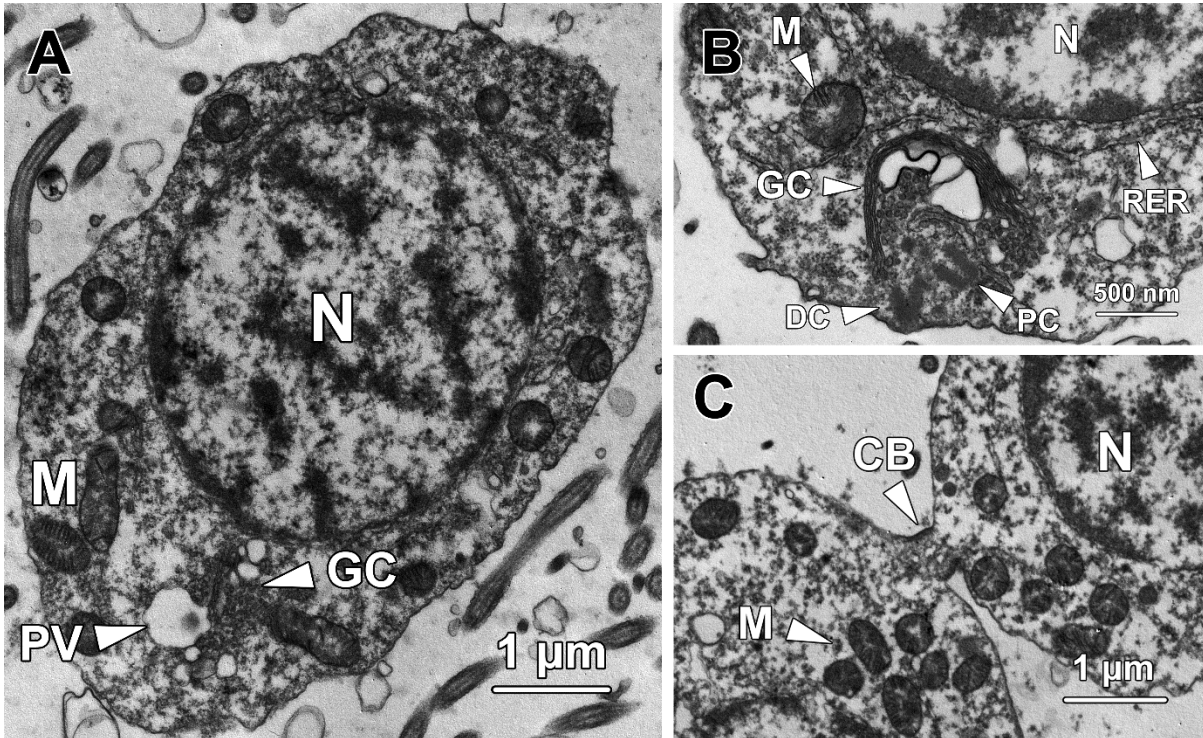


Figure 3.3 Transmission electron micrographs of step 3 spermatids. (A) Similar to their immediate precursors, step 3 spermatids remained ovoid in shape with a spherical- to oval-shaped nucleus (N) containing rod-shaped chromatin blocks. Thick patches of chromatin also attached to the inner nuclear membrane. Next to the Golgi complex (GC), a spherical proacrosomal vacuole (PV) was observed containing a patch of electron-dense material. A portion of mitochondria (M) transformed to a rod-shape in step 3 spermatids. (B) Both the proximal (PC) and distal centrioles (DC) remained in close proximity to the Golgi complex (GC) and started to orient perpendicularly to each other. Rough endoplasmic reticulum (RER) was found surrounding the nucleus (N). M, mitochondria. (C) The step 3 spermatids were in pairs and interconnected by a cytoplasmic bridge (CB). Mitochondria (M) were clustered at the cytoplasm near the cytoplasmic bridge. N, nucleus.

3.4.4 Step 4 spermatids

Step 4 spermatids were spherical in shape containing a spherical nucleus (**Figure 3.4A**).

They exhibited similar cellular and nuclear sizes to those of step 3 spermatids ($P > 0.05$).

The average cellular and nuclear diameters of step 4 spermatids were $5.7 \pm 0.45 \mu\text{m}$ and $4.04 \pm 0.5 \mu\text{m}$ respectively. The chromatin blocks remained rod-shaped, but were sparser compared with those in step 3 spermatids, indicating the commencement of chromosome decondensation in step 4 spermatids.

The step 4 spermatids were characterised by the formation of proacrosome and flagellum. The patch of electron-dense material in the proacrosomal matrix (**Figure 3.4B**) expanded and eventually occupied the majority of the proacrosomal matrix, thereby transforming the proacrosomal vacuole into a proacrosome (P; **Figure 3.4B**). Meanwhile, the proacrosome came into closer proximity with the plasma membrane compared with step 3 spermatids. The distal centriole (DC), which resided near the Golgi complex (GC) protruded out of the cytoplasm to form a flagellum (F; **Figure 3.4C**).

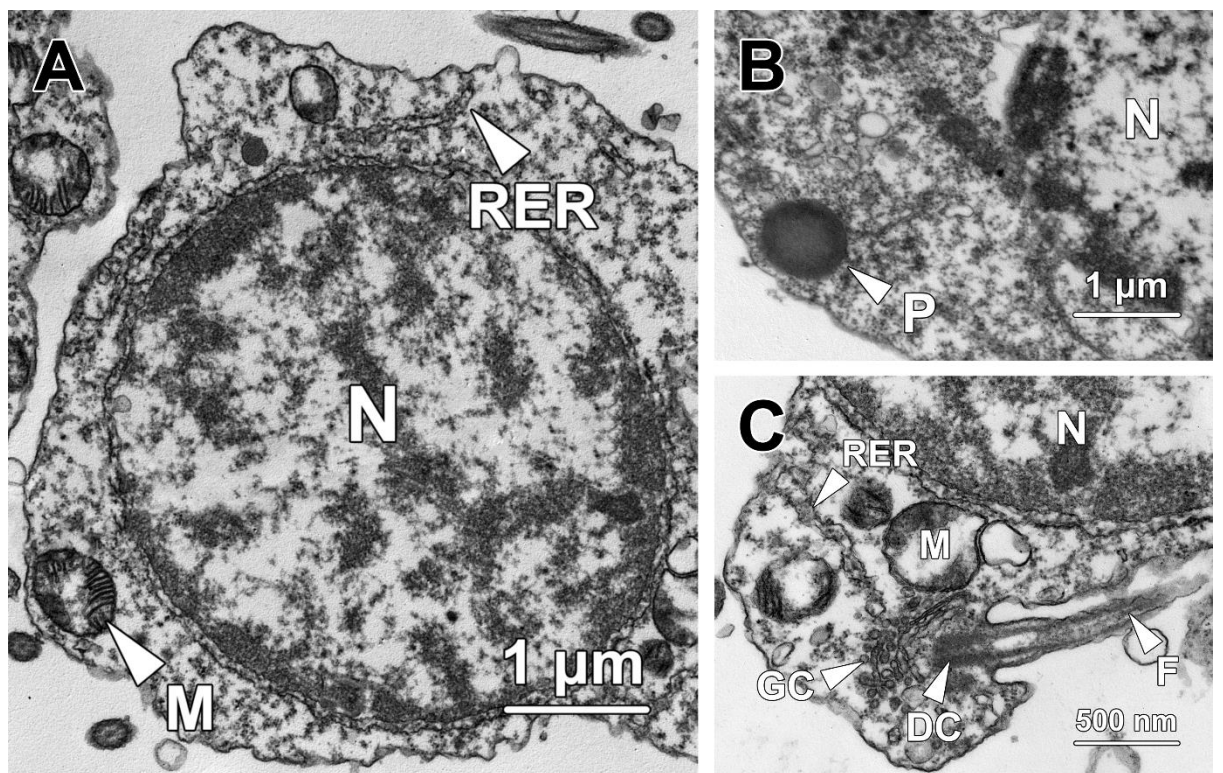


Figure 3.4 Transmission electron micrographs of step 4 spermatids. (A) Chromatin blocks in the nucleus (N) of step 4 spermatids remained rod-shaped but became sparser than those in

previous step, indicating the chromosome decondensation commenced at this stage. Mitochondria (M) and rough endoplasmic reticulum (RER) are randomly distributed throughout the cytoplasm. (B) The proacrosomal vacuole transformed into a proacrosome (P) in step 4 spermatids, with its matrix being mostly occupied by the electron-dense material. N, nucleus. (C) The distal centriole (DC) next to the Golgi complex (GC) formed a flagellum (F) protruding out of step 4 spermatids. N, nucleus; RER, rough endoplasmic reticulum.

3.4.5 Step 5 spermatids

Step 5 spermatids had a cellular diameter of $4.81 \pm 0.64 \mu\text{m}$ and a nuclear diameter of $3.35 \pm 0.51 \mu\text{m}$, both of which were significantly smaller than those of step 4 spermatids ($P < 0.01$). The chromosomes were further decondensed and transformed into a retiform pattern at this stage (Figure 3.5A).

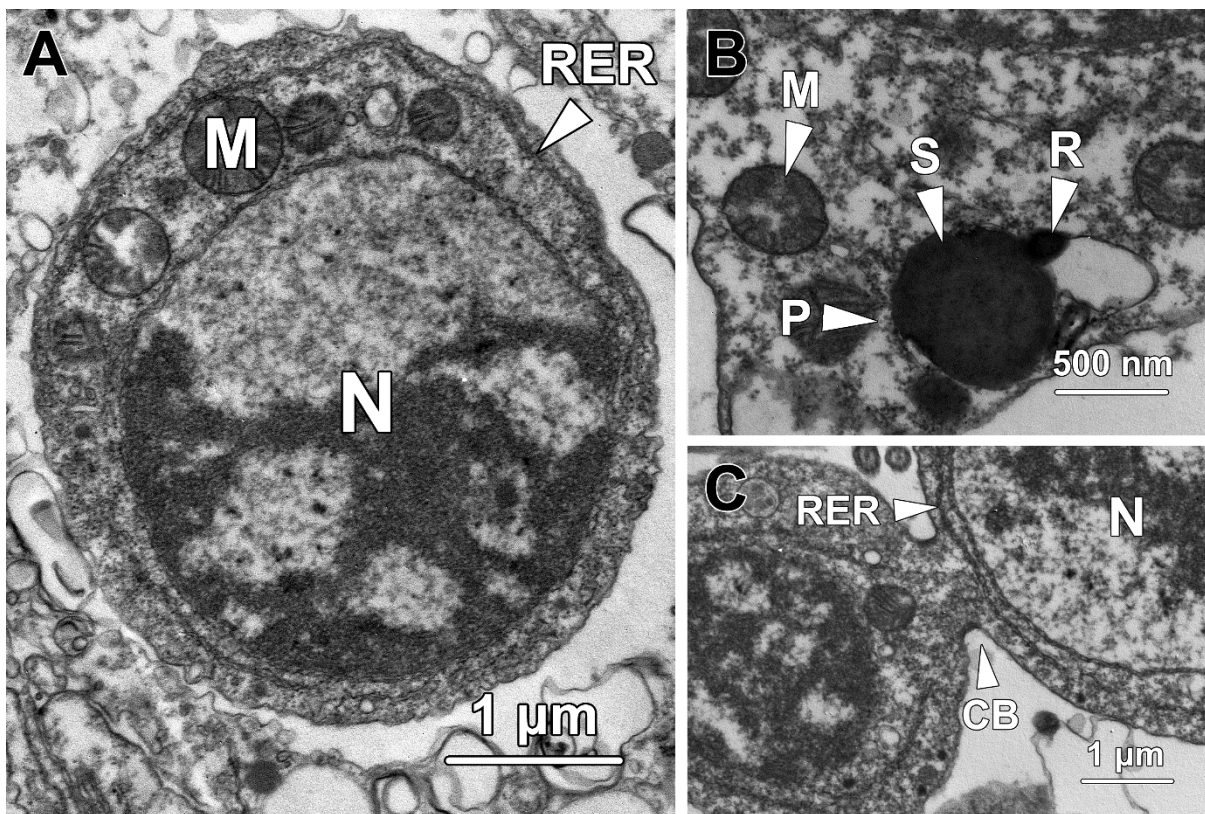


Figure 3.5 Transmission electron micrographs of step 5 spermatids. (A) As the nuclear size (N) of step 5 spermatids decreased, the decondensed chromosomes were aggregated into a retiform pattern. Large spherical-shaped mitochondria (M) were observed gathering at one end of the spermatids. RER, rough endoplasmic reticulum. (B) In the proacrosome (P) of step 5

spermatids, a ring-shaped structure (R) formed surrounding the sphere (S) at the centre. In the longitudinal section, the proacrosome appeared as two small spheres located at each side of a large sphere. M, mitochondria; N, nucleus. (C) Step 5 spermatids remained interconnected by a cytoplasmic bridge (CB). A continuous profile of rough endoplasmic reticulum (RER) was found surrounding the nucleus.

The proacrosome in step 5 spermatids transformed from a simple sphere into its mature form, a ring-shaped deposit of electron-dense material (R) surrounding the sphere (S) at the centre, which appeared as two small electron-dense spheres residing at each side of a large sphere in longitudinal section (**Figure 3.5B**). A small number of extremely large mitochondria (M) with a diameter of over 500 nm clustered at one end of the spermatid (**Figure 3.5A**), which later formed the mitochondrial sheath surrounding the midpiece of the sperm flagellum. The step 5 spermatids were still in pairs and connected by a cytoplasmic bridge (CB; **Figure 3.5C**).

3.4.6 Step 6 spermatids

Compared with step 5 spermatids, both the cellular and nuclear diameters further decreased significantly in step 6 spermatids, which were $2.81 \pm 0.25 \mu\text{m}$ ($P < 0.01$) and $2 \pm 0.18 \mu\text{m}$ ($P < 0.001$) respectively. The chromatin continued to dencondense and transformed into larger chromatin blocks that occupied almost half volume of the whole nucleoplasm (**Figure 3.6A**).

In step 6 spermatids, the proacrosome still appeared as a spherical vacuole containing a central sphere (S) and a ring-like structure (R). The proacrosomal matrix, which was electron-lucent in step 3 spermatids, started to be occupied by coarse granules. The proacrosome further approached the plasma membrane, with its membrane firmly adhering to the cell membrane (**Figure 3.6B**). In step 6 spermatids, a shallow depression formed at the posterior pole of the nucleus, which was the implantation fossa (*) for the

proximal centriole (**Figure 3.6A**). While the proximal centriole gradually came to lie in close proximity to the implantation fossa, the formative flagellum (F) originated from the distal centriole (DC) and was further elongated (**Figure 3.6C**). The formation of the implantation fossa marked the posterior end of the cell, where the proximal centriole and flagellum resided and the mitochondrial sheath later formed. At this stage, the large spherical-shaped mitochondria (M) were still situated away from the centrioles (**Figure 3.6A**).

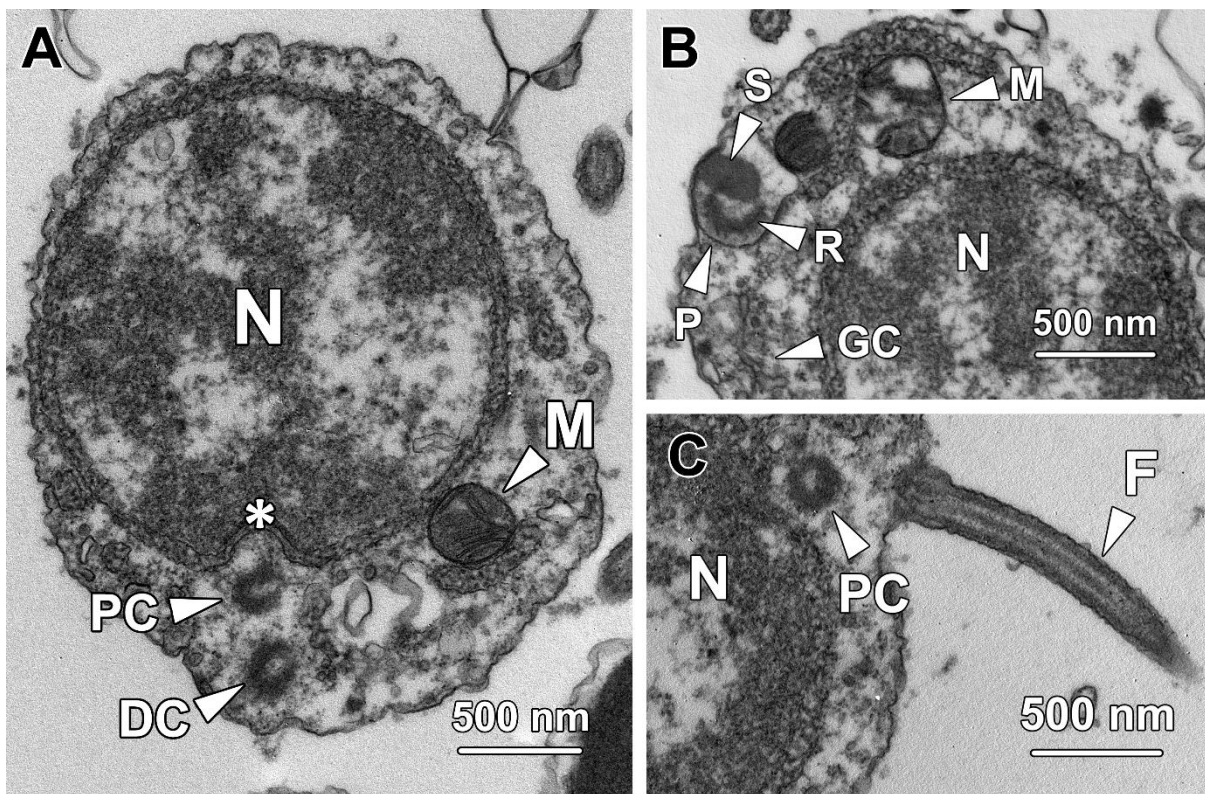


Figure 3.6 Transmission electron micrographs of step 6 spermatids. (A) An implantation fossa (*), which appeared as a shallow depression, formed at the posterior end of the nucleus (N). The proximal centriole (PC) was in close proximity to the implantation fossa while the distal centriole remained docking to the cytoplasmic membrane. Large spherical-shaped mitochondria (M) migrated towards the pole where the centrioles resided. (B) This electron micrograph was cross-sectioned through a small portion of the proacrosome, showing fragments of both the ring-shaped structure (R) and the central sphere (S). The proacrosomal matrix became being occupied by coarse granules. A portion of the proacrosome adhered to the cytoplasmic membrane. Large

spherical mitochondria were found next to the proacrosome. N, nucleus. (C) As the proximal centriole (PC) embedding into the implantation fossa, the flagellum (F) extended from the distal centriole and was further elongated. N, nucleus.

3.4.7 Step 7 spermatids

The nuclei of step 7 spermatids were spherical in shape and contained an irregular-shaped chromatin block with a coarse granular appearance (**Figure 3.7A**). The large heterochromatin block, which attached to the posterior pole of the inner nuclear membrane, occupied the majority of the nucleoplasm and the remaining portion of the nucleus was occupied by sparse euchromatin.

In step 7 spermatids, the acrosome (A) transformed from the spherical into an inverted-bowl or hemispherical shape (**Figure 3.7B**). The anterior membrane of the acrosome was arc-shaped and fully attached to the plasma membrane. The posterior membrane of the acrosome was relatively flat and in close proximity to the large spherical mitochondria (**Figure 3.7B**), indicating the acrosome was located next to the flagellum at this step. In the acrosome, both the central sphere (S) and the ring-shaped structure (R) were situated close to the posterior membrane but relatively away from the anterior membrane. Noticeably, a small number of electron-denser particles lined the interior border of the ring. The acrosomal matrix at this step was completely fill up with coarse granules (**Figure 3.7B**).

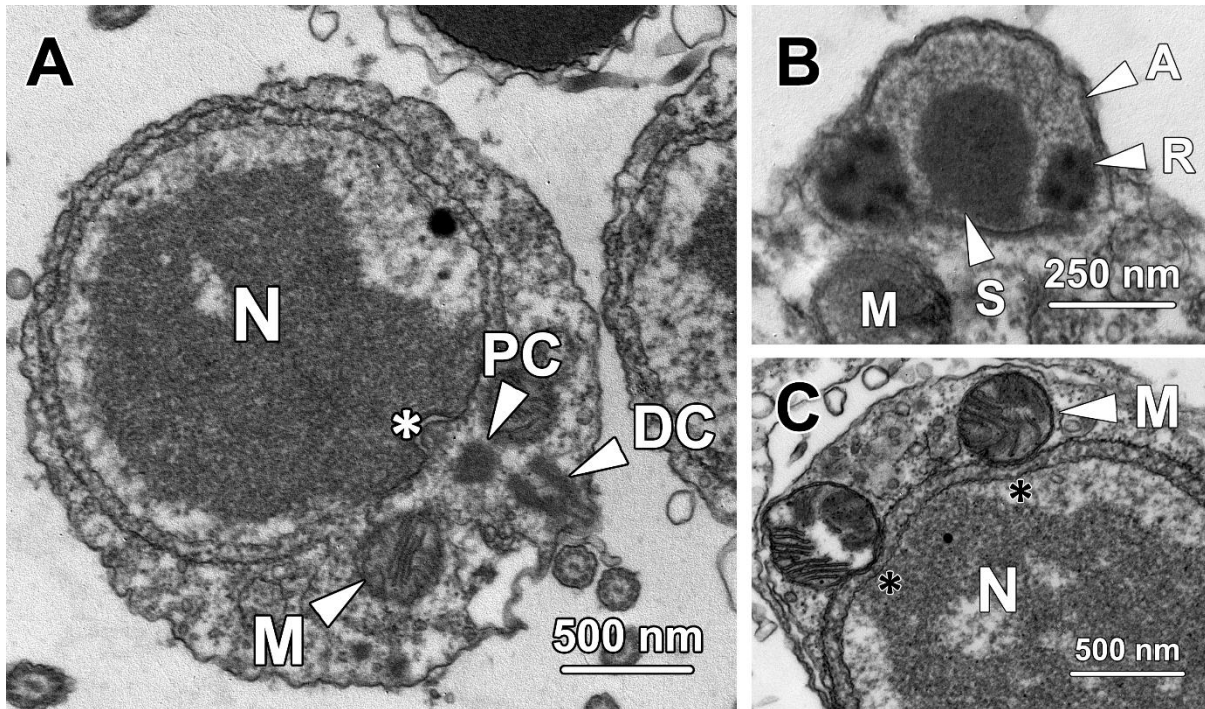


Figure 3.7 Transmission electron micrographs of step 7 spermatids. (A) The chromatin in the nucleus of step 7 spermatids exhibited a coarse granular form and aggregated into a large irregular-shaped block. The chromatin block attached to the posterior end of the nucleus (N), where an implantation fossa (*, white asterisk) had formed. The proximal centriole (PC) remained in close proximity to the fossa and oriented perpendicularly to the distal centriole (DC). The large spherical-shaped mitochondria (M) became surrounded the centrioles and started to form the mitochondrial sheath at the base of the flagellum. (B) The acrosome (A) transformed into an inverted-bowl shape with its anterior region tightly adhered to the cell membrane. In the acrosomal matrix, both the central sphere (S) and the ring-shaped structure (R) attached to the inner posterior membrane of the acrosome. The acrosome was located adjacent to large spherical mitochondria (M) which were forming the mitochondrial sheath of the flagellum. (C) Where the mitochondria (M) approached the nuclear membrane, the nuclear envelope curved inward to form depressions (*, black asterisks). N, nucleus.

In step 7 spermatids, the large spherical-shaped mitochondria translocated to the pole where the centrioles resided and started to form the mitochondrial sheath surrounding the base of the flagellum (**Figure 3.7A**). Simultaneously, the mitochondria gradually approached the nucleus and the corresponding portions of nuclear membrane curved

inward to form concaves (*, black asterisks) to accommodate these mitochondria (**Figure 3.7C**).

3.4.8 Step 8 spermatids

Spherical-shaped step 8 spermatids were still in pairs and interconnected by a cytoplasmic bridge (CB; **Figure 3.8A**). The nucleus remained roughly spherical but the chromatin block transformed into an oval shape. The chromatin gradually condensed from a coarse granular form (**Figure 3.8B**) to a dense homogeneous granular form (**Figure 3.8A** and **C**). The remaining portion of the nucleoplasm was occupied by sparse euchromatin.

The acrosome of step 8 spermatids remained adjacent to the mitochondria and flagellum at the posterior pole of the cytoplasm (**Figure 3.8A**). In the acrosome, the central sphere transformed into a hemisphere (Hs) whose flat side firmly attached to the inner posterior membrane (**Figure 3.8B**). The posterior membrane was approximate flat with a gentle posteriorly directed curve. The ring-like structure (R), which was interiorly lined with conspicuous darker particles, also came in direct contact with the acrosomal membrane on both sides (**Figure 3.8B**). The coarse granules that occupied the entire acrosomal matrix became denser compared with step 8 spermatids. As differentiation proceeded, the central hemisphere (Hs) increased its volume and gradually occupied the whole acrosomal matrix (**Figure 3.8B** to **C**). Simultaneously, the central hemisphere, along with the adherent portion of posterior membrane, ascended anteriorly, resulting in the formation of a shallow cylinder-shaped indentation at the posterior pole of the acrosome (**Figure 3.8C**). Noticeably, the posterior membrane adjacent to the hemisphere was lined with a thin band of dense granular materials, which later would become the subacrosomal materials (**Figure 3.8B** and **C**).

The proximal centriole (PC) in step 8 spermatids remained perpendicular to the flagellum (F) and continued the implantation process by extending its microtubules into the implantation fossa (*, see the lower spermatid in **Figure 3.8A**). The spherical mitochondria firmly adhered to the concave surface at the posterior end of the nucleus and formed the mitochondria sheath that surrounded the proximal centriole and the flagellum (**Figure 3.8A**).

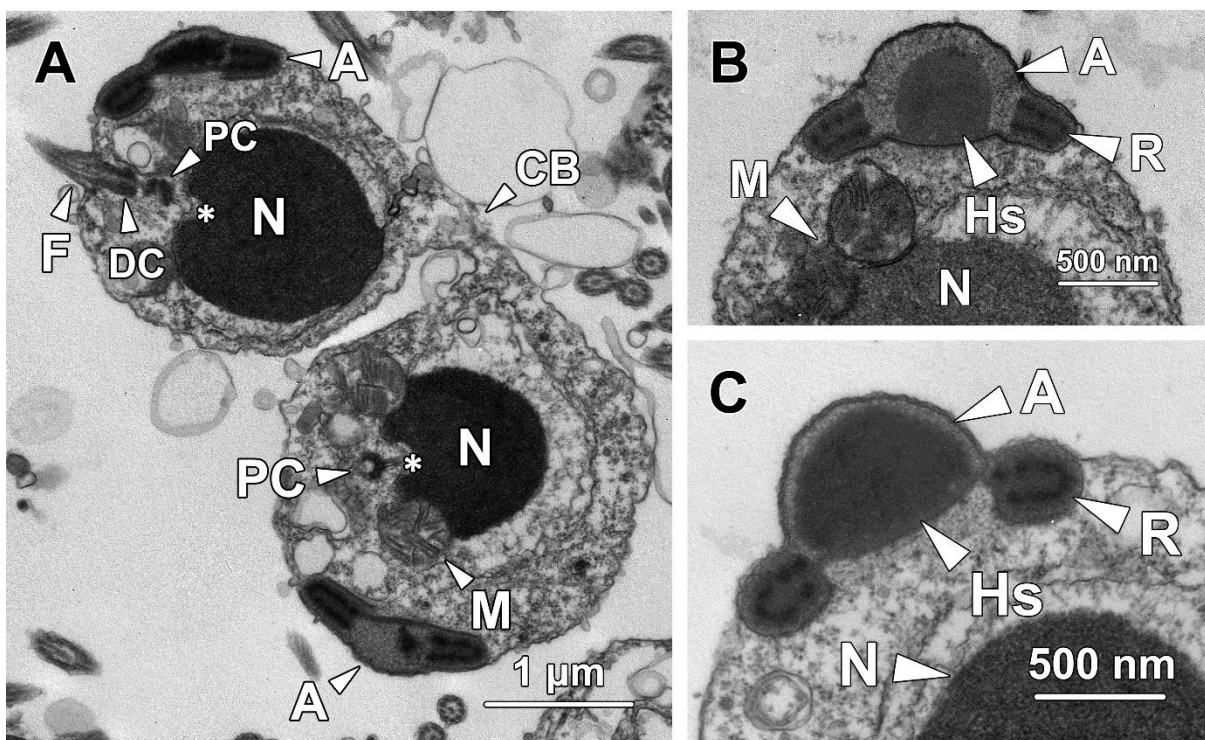


Figure 3.8 Transmission electron micrographs of step 8 spermatids. (A) Step 8 spermatids were still interconnected by a cytoplasmic bridge (CB). The nucleus (N) remained spherical in shape while the chromatin block transformed into an oval shape with a highly condensed homogeneous appearance. The proximal centriole (PC) extended its microtubules into the implantation fossa (*) and oriented perpendicularly to the flagellum (F) originated from the distal centriole (DC). The developing acrosome (A) remained adjacent to the flagellum at this stage. (B) The central sphere firmly attached to the posterior membrane of the acrosome (A) and transformed into a hemisphere (Hs). The ring-like structure (R), with darker particles lining its interior border, also became directly contacted with the acrosomal membrane on both sides. The acrosomal matrix was filled up with densely packed coarse granules. M, mitochondria; N, nucleus. (C) As the morphogenesis of the acrosome proceeded, the central hemisphere (Hs) increased its

volume and ascended towards the anterior membrane, resulting in the formation of an indentation at the posterior end of the acrosome. N, nucleus; R, ring-shaped structure.

3.4.9 Step 9 spermatids

Step 9 spermatids remained in pairs and were interconnected by a cytoplasmic bridge (**Figure 3.9A**). The chromatin in the nucleus accomplished its condensation and exhibited a homogeneous granular appearance.

Instead of residing adjacent to the flagellum at the posterior cytoplasm, the acrosome was found half way to the anterior region of step 9 spermatids (**Figure 3.9B**), suggesting that anterior migration of the acrosome commenced on completion of chromatin condensation. In the acrosome, the central hemisphere (Hs) further expanded and occupied the entire acrosomal matrix coming into direct contact with the ring-like structure at both sides (**Figure 3.9A and B**). The electron density was identical throughout the entire acrosome, except for the darker particles lining the interior border of the ring structure. Similar to that in step 8 spermatids, the posterior membrane of the acrosome was still externally lined with a thin band of dense granular material.

In step 9 spermatids, clusters of irregular-shaped vesicles were randomly dispersed in the cytoplasm, which formed the residual bodies (RB) containing excess cytoplasm that would be subsequently expelled from the spermatids (**Figure 3.9A and B**).

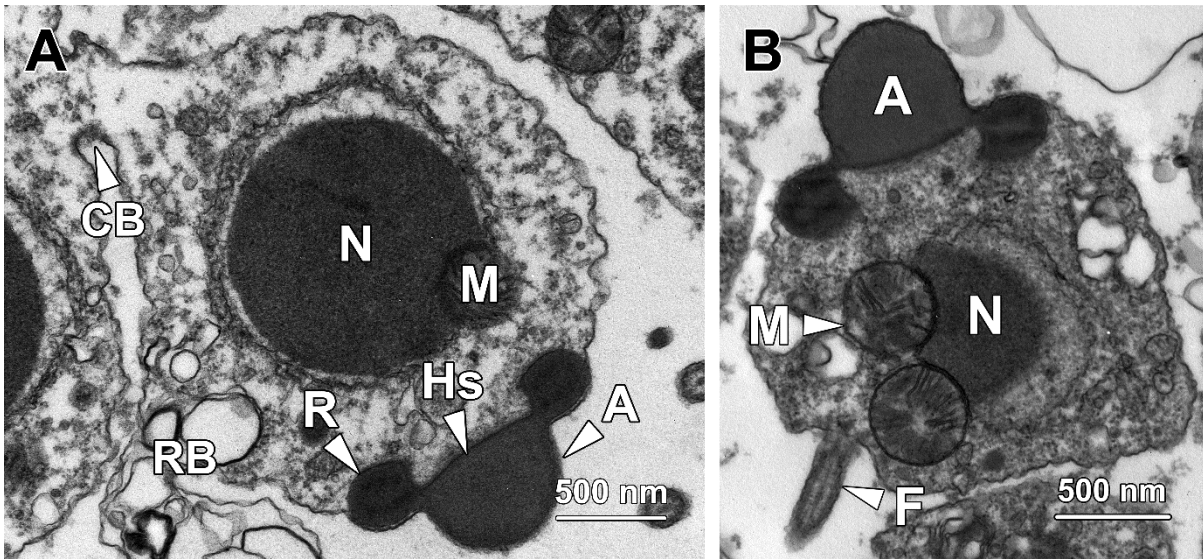


Figure 3.9 Transmission electron micrographs of step 9 spermatids. (A) Step 9 spermatids were still in pairs and interconnected by a cytoplasmic bridge (CB). The central hemisphere (Hs) in the acrosome occupied the entire acrosomal matrix and connected to the ring-like structure (R) on both sides. The whole acrosome exhibited an identical electron density except for the darker particles lining the interior border of the ring structure. Multiple irregular-shaped residual bodies (RB) containing excess cytoplasm appeared in step 9 spermatids. M, mitochondria; N, nucleus. (B) In step 9 spermatids, the acrosome (A) started to migrate towards the anterior end of the cytoplasm, which was opposite to the pole that the flagellum (F) and mitochondria (M) resided. The mitochondria remained firmly adherent to depressions at the posterior end of the nucleus (N).

3.4.10 Step 10 spermatids

The nucleus of step 10 spermatids was oval-shaped and contained fully condensed chromatin with a homogeneous granular appearance (**Figure 3.10A**).

The acrosome reached the anterior pole of the cytoplasm, which was opposite to the midpiece and flagellum (**Figure 3.10A**). The entire acrosome was filled with homogeneous electron-dense materials. The darker particles previously lining the interior border spread throughout the entire ring, resulting in the ring-shaped structure to be darker compared with the hemisphere. Noticeably, the posterior end of the acrosome became closer to but never attached to the nucleus, forming a subacrosomal space between the

acrosome and the nuclear membrane (**Figure 3.10A**). At this stage, the subacrosomal space only contained sparse granules and only the posterior membrane of the acrosome was lined with dense granular materials. The formation of the mitochondrial sheath was also completed in step 10 spermatids, with four spherical mitochondria tightly surrounding the proximal centriole (PC; **Figure 3.10B**).

Noticeably, early step 10 spermatids were maintained in pairs connected by a cytoplasmic bridge (CB; **Figure 3.10B**). With the continuous expulsion of residual bodies containing excess cytoplasm, the cytoplasmic bridge collapsed and each pair of spermatids became two independent spermatozoa at the end of step 10 (**Figure 3.10C**). As a result, the cytoplasm in the spermatozoa was extremely limited and barely contained any ribosomes.

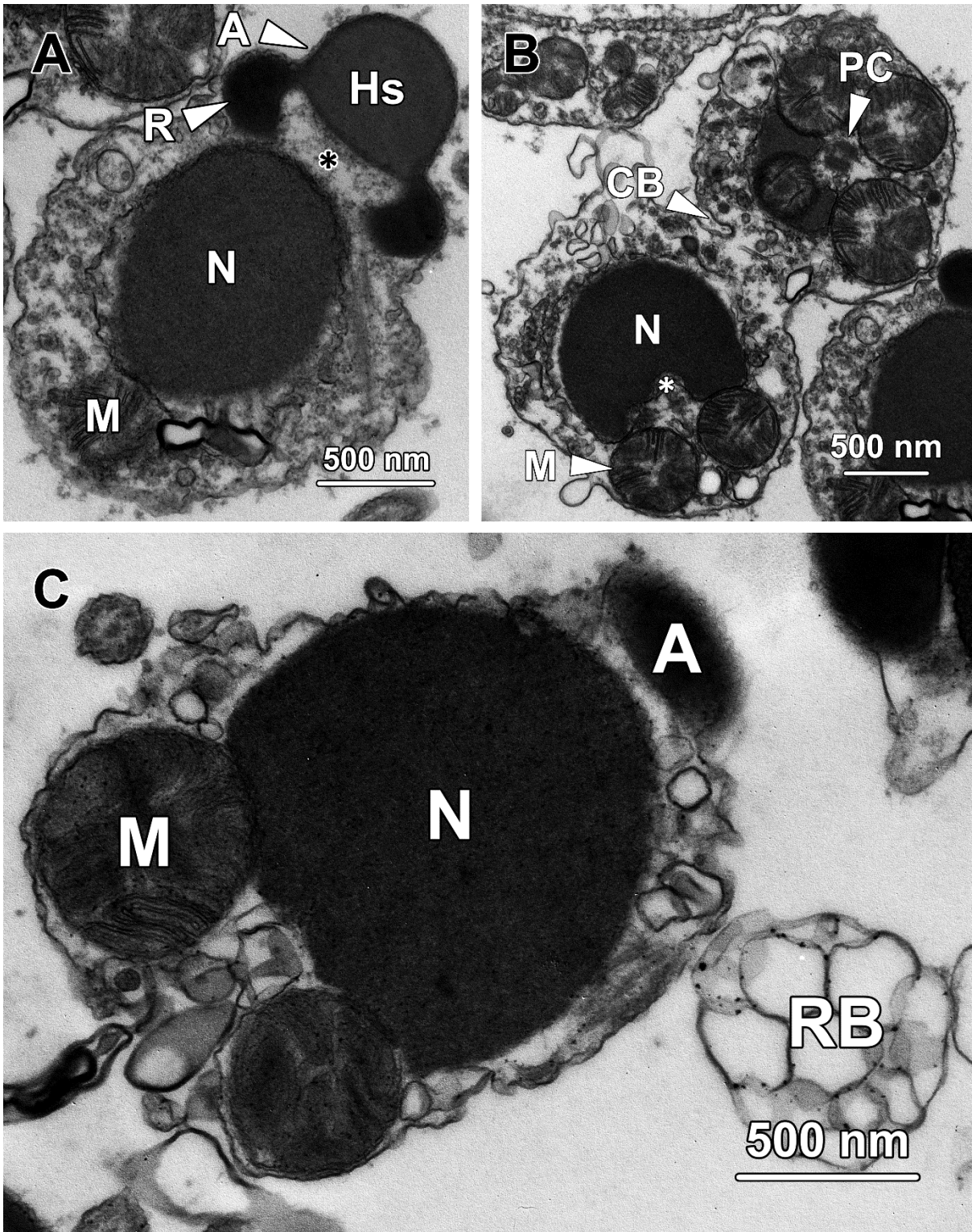


Figure 3.10 Transmission electron micrographs of step 10 spermatids. (A) The oval-shaped nucleus (N) was occupied by fully condensed homogeneous granular chromatin. The acrosome (A) reached the apex of the cytoplasm in step 10 spermatids, which was opposite to the pole that the mitochondria (M) and flagellum resided. As the dark particles spread throughout the ring-like structure, the ring appeared darker compared with the central hemisphere. (B) Early step 10

spermatids remained in pairs and were interconnected by a cytoplasmic bridge (CB). The cytoplasm contained clusters of irregular-shaped vesicles, indicating the continuous formation and expulsion of residual bodies. The formation of mitochondrial sheath was accomplished, with four spherical mitochondria (M) surrounding the proximal centriole (PC). *, implantation fossa. (C) In late step 10 spermatids, numerous clusters of irregular-shaped vesicles were found inside and adjacent to the cytoplasm, suggesting the discharge of residual bodies (RB) occurred dramatically at this stage. With the elimination of excess cytoplasm, the cytoplasmic bridge that connected the spermatids disintegrated, resulting in the formation of two independent spermatozoa. A, acrosome; M, mitochondria; N, nucleus.

3.4.11 Spermatozoa

From the head to the tail, the spermatozoa in *G. caespitosa* consisted of a cap-like acrosome (A), an oval nucleus (N) containing fully condensed homogeneous chromatin, a short midpiece containing four spherical mitochondria and an elongated flagellum (**Figure 3.11**). The acrosome exhibited a homogeneous appearance with evenly distributed electron density. The posterior end of the acrosome was in close proximity to but not directly attached to the nucleus, forming a subacrosomal space (*, black asterisk; **Figure 3.11A**) that contained electron-dense fibrillary materials in an homogeneous granular subacrosomal matrix (**Figure 3.11A and B**). At the posterior end of the nucleus, the proximal centriole was inserted into the shallow implantation fossa (*, white asterisk; **Figure 3.11A**). The four spherical mitochondria firmly adhered to corresponding depressions of the nucleus and surrounded the base of the flagellum, where the annulus, an electron-dense ring-shaped structure formed (**Figure 3.11A and C**).

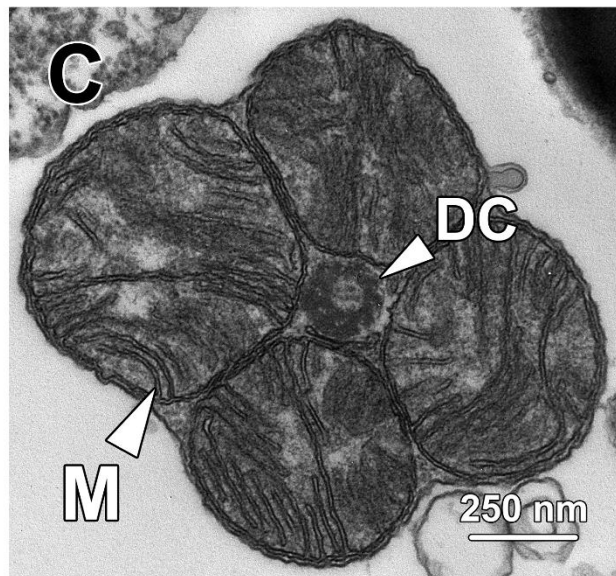
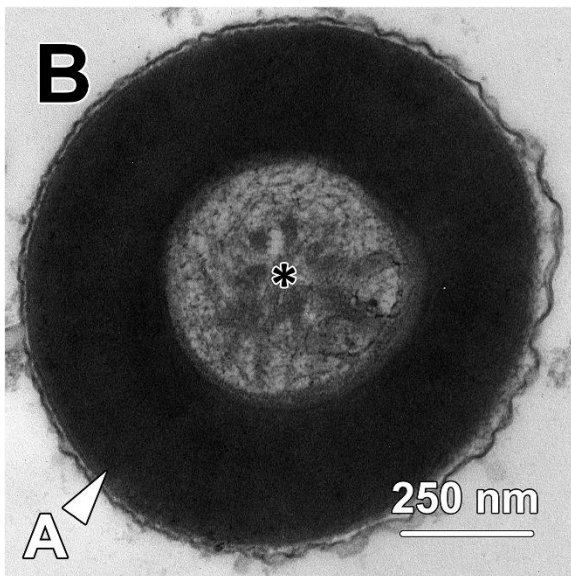
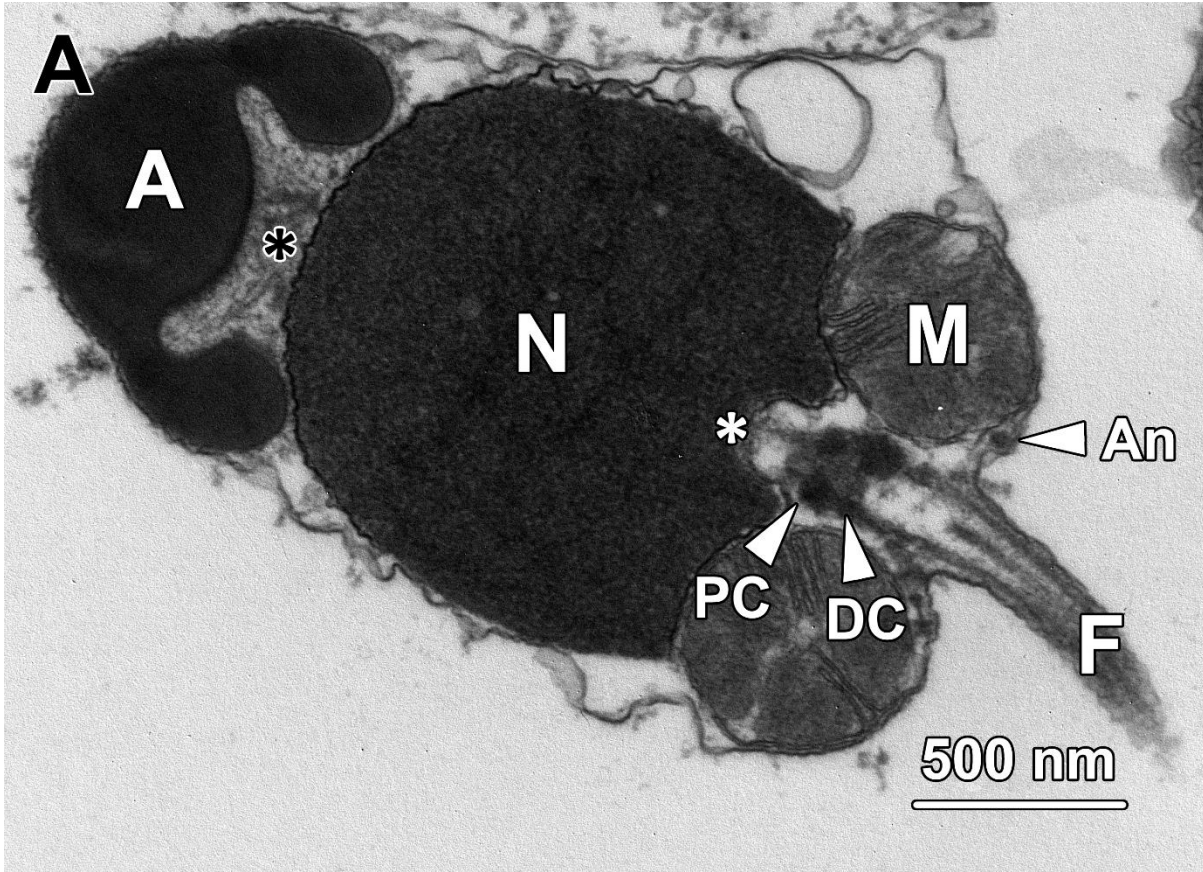


Figure 3.11 Transmission electron micrographs of spermatozoa. (A) Spermatozoa consisted of a cap-like acrosome (A), an oval nucleus (N), a short midpiece containing four spherical mitochondria (M) and an elongated flagellum (F). A subacrosomal space (*, black asterisk) formed between the acrosome and the nucleus, containing evenly distributed electron-dense fibrillary subacrosomal material. The proximal centriole (PC) was inserted into the implantation fossa (*, white asterisk) formed at the posterior end of the nucleus. The four mitochondria lodged

in concave recesses at the posterior nuclear margin and surrounded the base of the flagellum, where the annulus (An) formed. **(B)** A transverse section through the ring structure at the base of the acrosome showed the fibrillary content of the subacrosomal space (*, black asterisk). **(C)** A transverse section through the midpiece showed four spherical mitochondria (M) encircling the base of the flagellum.

3.4.12 Pattern of spermatid differentiation

Temporally, the entire spermiogenesis in *G. caespitosa* could be divided into three phases: Golgi phase (**Figure 3.12A to B**), acrosomal phase (**Figure 3.12C to E**) and maturation phase (**Figure 3.12F to G**).

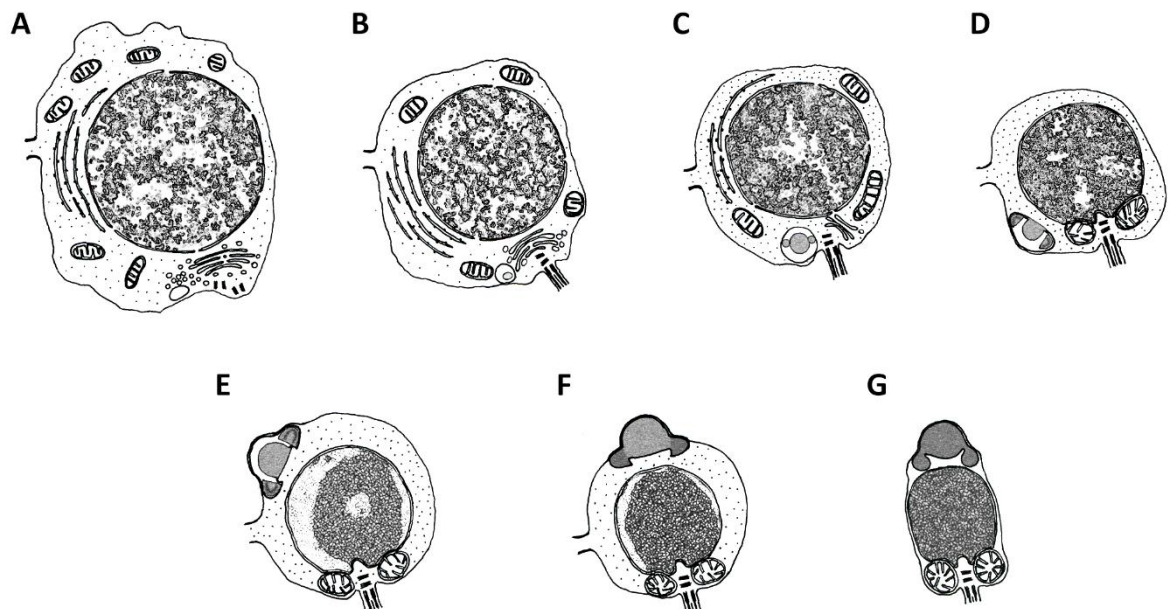


Figure 3.12 Illustrations showing the pattern of spermiogenesis in *G. caespitosa*. The spermiogenesis was temporally divided into **(A - B)** Golgi phase, **(C - E)** acrosomal phase and **(F - G)** maturation phase. **(A)** In early Golgi phase, a large number of single-membrane bound vesicles were observed adjacent to a conspicuous Golgi complex. These vesicles gradually merged into an electron-lucent proacrosomal vacuole. A pair of centrioles, which were initially located in close proximity to the nuclear membrane, migrated towards the cell membrane. **(B)** In the late Golgi phase, the fusion of proacrosomal vesicles ceased and a patch of electron-dense material formed in the matrix of the proacrosomal vacuole. The distal centriole docked to the cell membrane, where a formative flagellum subsequently protruded out. **(C)** In early acrosomal phase, the Golgi complex became no longer involved in the differentiation of the acrosome and the

proacrosomal vacuole transformed into a proacrosome containing a large sphere surrounded by a ring-like structure. The chromosomes decondensed into rod-shaped chromatin blocks and occupied half volume of the nucleoplasm. **(D)** The proacrosome transformed into an inverted-bowl shaped acrosome, during which both the central sphere and the ring structure attached to the inner posterior membrane of the acrosome. The proximal centriole came into intimate contact with the implantation fossa formed at the posterior end of the nucleus. After the fusion of mitochondria, they migrated to and adhered to concave recesses of the nucleus at the posterior pole. The acrosome started to migrate towards the anterior pole of the cytoplasm after the adherence of the mitochondria. **(E)** In the late acrosomal phase, the acrosome almost reached the most anterior aspect of the spermatids. The chromatin condensed into a rough oval-shaped chromatin block. **(F)** In early maturation phase, the acrosome has accomplished the majority of its differentiation, during which the central hemisphere came to occupy the entire matrix of the acrosome. **(G)** In the late maturation phase, acrosome differentiation was completed and the nucleus was fully condensed. The excess cytoplasm was completely eliminated from the spermatid through the extrusion of residual bodies. The cytoplasmic bridge between the spermatids ruptured and the spermatids developed into individual spermatozoa.

The Golgi phase involved the formation and growth of proacrosomal vacuole, the migration of the centrioles and the formation of flagellum. The acrosome first appeared as a large amount of single-membrane bound proacrosomal vesicles at the posterior pole of the spermatids (**Figure 3.12A**). These vesicles could be found in close apposition to the concave surface of a prominent Golgi complex and subsequently coalesced into an electron-lucent proacrosomal vacuole containing a patch of electron-dense material (**Figure 3.12B**). The two centrioles were initially found situated closely to the nuclear membrane. As the proacrosomal vacuole increased in its volume, both the proximal and distal centrioles gradually migrated towards the plasma membrane. After the distal centriole docked with the cell membrane, it gave rise to a formative flagellum that protruded out of the cell body (**Figure 3.12B**).

During the acrosomal phase, the acrosome accomplished a majority of its differentiation and the nucleus decreased in size in association with chromatin condensation. In the early

acrosomal phase, the proacrosomal vacuole transformed into a proacrosome, which contained a large sphere surrounded by a ring-shaped structure (**Figure 3.12C**). When the spermatids entered into the late acrosomal phase, the acrosome transformed into a more mature form, during which the entire acrosome differentiated into an inverted-bowl shape and both the central sphere and the ring structure adhered to the inner posterior membrane of the acrosome (**Figure 3.12D**). In the meantime, the sperm flagellum further elongated and the proximal centriole inserted into a shallow implantation fossa formed at the posterior end of the nucleus (**Figure 3.12D**). Remarkably, the mitochondria, which used to be randomly dispersed throughout the cytoplasm during the Golgi phase, fused with each other to form larger spherical-shaped mitochondria. These larger mitochondria gradually migrated towards the posterior end of the cytoplasm, where the flagellum and acrosome were located, and then lodged into concave recesses formed at the posterior pole of the nucleus (**Figure 3.12D**). After adherence of the mitochondria, the acrosome started to migrate towards the anterior pole of the spermatid (**Figure 3.12D to E**). With the migration of the acrosome, the chromatin was dramatically condensed and formed into a rough oval-shaped chromatin block (**Figure 3.12E**).

Spermiogenesis in *G. caespitosa* was concluded during the maturation phase, during which the acrosome finalised its migration and differentiation, the nucleus accomplished its condensation and excess cytoplasm was extruded from the spermatids in the form of residual bodies (**Figure 3.12F to G**). With the elimination of residual bodies, the cytoplasmic bridge that connected the spermatids broke down and the spermatids became independent from each other and developed into spermatozoa (**Figure 3.12G**).

3.4.13 Induction of spermatid differentiation *in vitro*

After being purified through discontinued Percoll gradients, three major types of spermatids were commonly found in the culture media: spherical- to oval-shaped spermatids with no flagellum (step 1-3 spermatids; **Figure 3.13A**); spherical-shaped spermatids with short flagellum (step 4-6 spermatids; **Figure 3.13B**); spherical-shaped spermatids with conspicuous acrosome, condensed nucleus and elongated flagellum (step 7-9 spermatids; **Figure 3.13C**). In addition, a small number of spermatozoa remain in the culture medium (**Figure 3.13D**). The percentage each type of differentiating spermatids accounted for was recorded at 0 h, 12 h, 24 h and 36 h respectively after incubation. These data were used to determine whether the applied culture medium was effective in inducing spermiogenesis *in vitro*, or not.

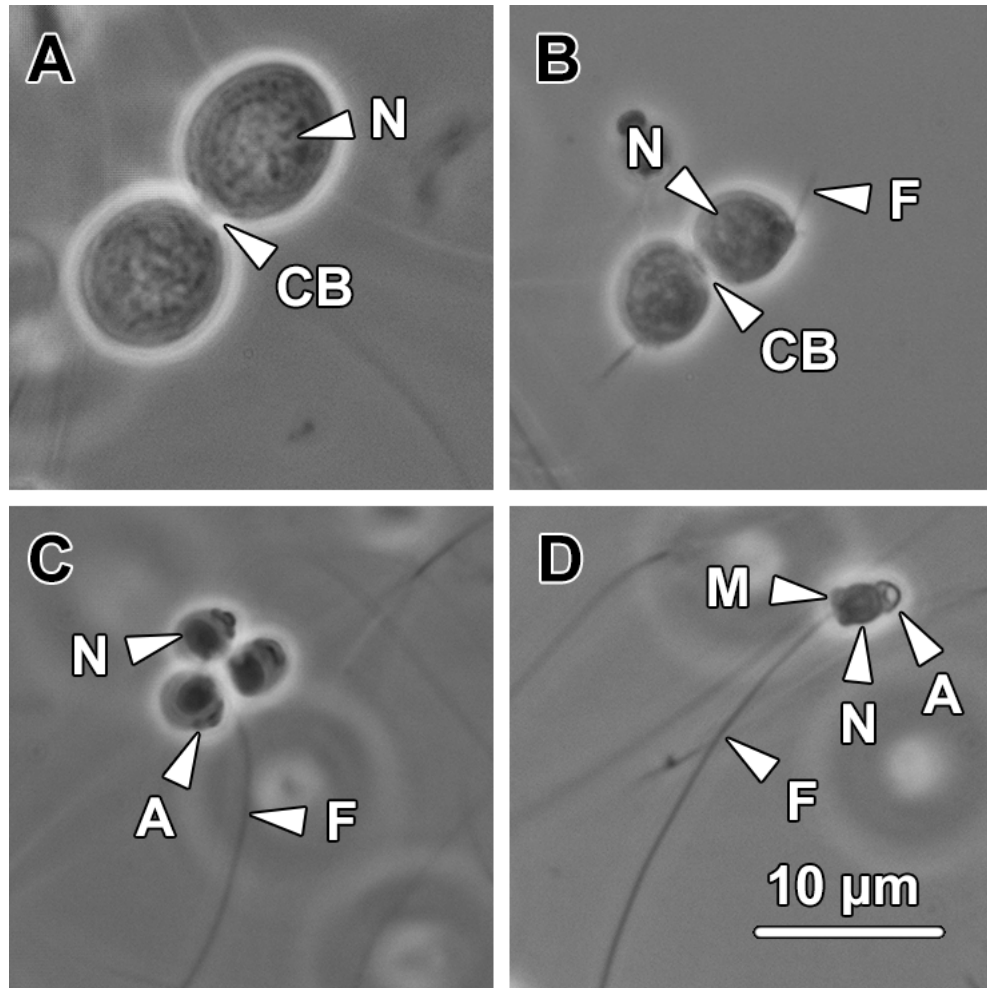


Figure 3.13 Representative types of spermatids and spermatozoa in the culture media. (A) Step 1-3 spermatids. The spermatids at these steps are a spherical to oval in shape. They are in pairs and interconnected by a cytoplasmic bridge (CB). N, nucleus. (B) Step 4-6 spermatids. Spermatids at these steps remain in pairs and being connected by a cytoplasmic bridge (CB). A short flagellum (F) protrudes from the posterior end of each spermatid. N, nucleus. (C) Step 7-9 spermatids. The spermatids at these steps are spherical in shape and contain a cap-like acrosome (A), a condensed nucleus (N) and an elongated flagellum (F). The acrosome resides at or near the posterior end of the spermatids. (D) Spermatozoa. Spermatozoa consist of a cap-like acrosome (A), an oval-shaped nucleus (N), a short midpiece (M) and a flagellum (F).

Regardless of the type of the culture medium, before differentiating into step 4-6 spermatids, the paired step 1-3 spermatids were found to undergo cytoplasmic fusion (Figure 3.14A and B). The cytoplasmic bridge connecting the paired spermatids

disappeared and the two spermatids fused into a larger spherical-shaped cell (**Figure 3.14C and D**). The entire fusion process lasted for approximately 45 min.

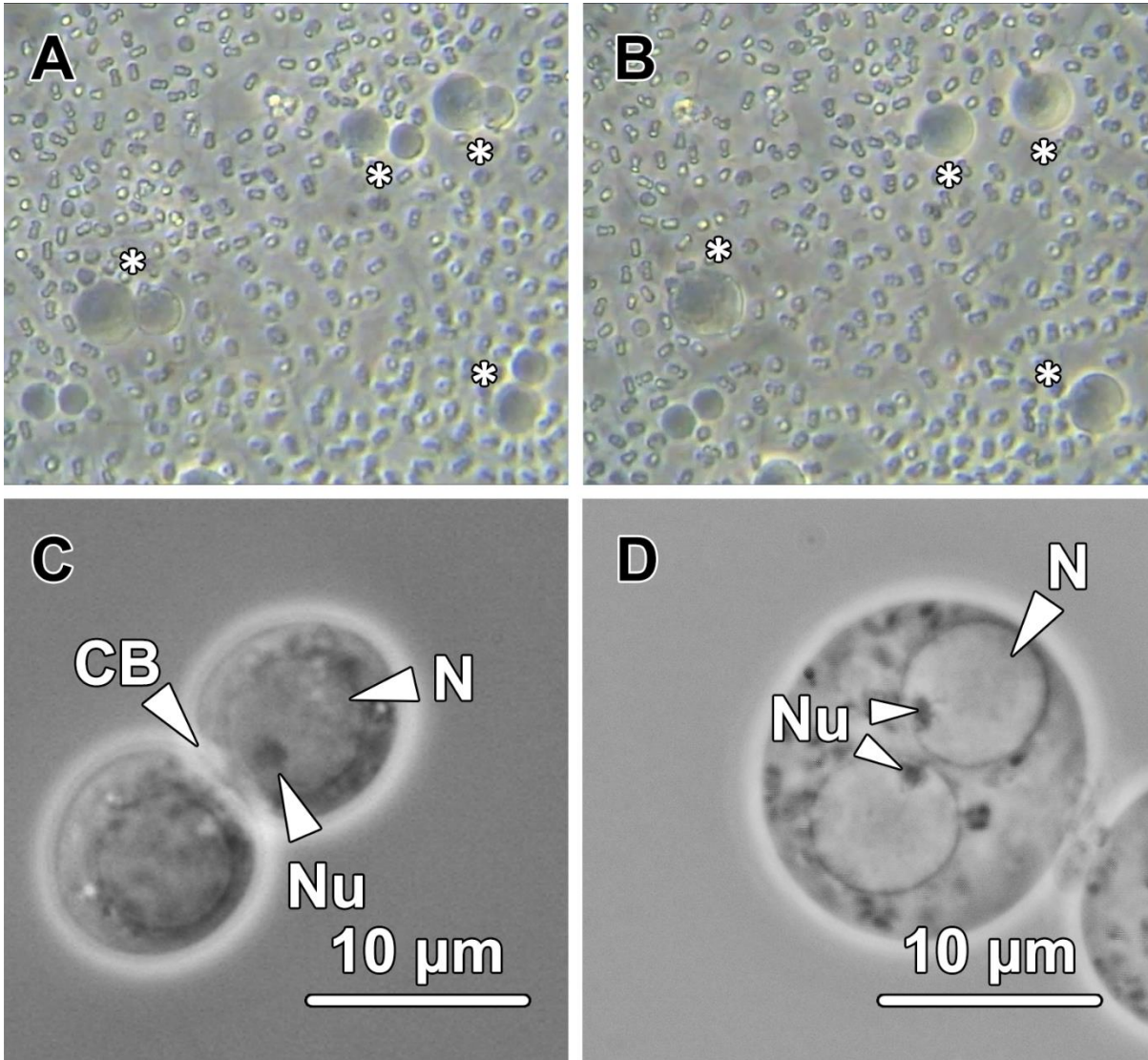


Figure 3.14 Step 1-3 spermatids underwent cytoplasmic fusion during *in vitro* differentiation in male germinal fluid. (A - B) These images were taken from a video recording the *in vitro* differentiation of spermatids. As these cells had not been purified through discontinued Percoll gradients, a large number of spermatozoa remain mixing with the spermatids. The step 1-3 spermatids (*) were found to undergo cytoplasmic fusion in the *in vitro* culture system. (C) The step 1-3 spermatids were initially in pairs and interconnected by a common cytoplasmic bridge (CB). A prominent nucleolus (Nu) was sometimes observed residing eccentrically in the nucleus (N). (D) After the cytoplasmic fusion, the spermatids appeared as a large spherical-shaped cell containing two nuclei (N), with each nucleus possesses an eccentric nucleolus (Nu).

Since the spermiogenesis in *G. caespitosa* occurs while floating freely in the germinal fluid, we first attempted to induce the differentiation of spermatids *in vitro* using germinal fluid obtained from male adults. Within 36 h of incubation, the percentage of step 1-3 spermatids dramatically decreased from 11.33% to 0.67% ($P < 0.01$) while the average percentage of step 7-9 spermatids increased dramatically from 27.33% to 44% during the first 24 h and remained constant during the last 12 h of incubation (**Figure 3.15**). The average percentage of step 4-6 spermatids slightly decreased from 52% to 47.33% in the first 12 h and maintained at around 45% during the remaining 24 h of incubation (**Figure 3.15**). The ratios of these three types of spermatids at the four time points indicated that the male germinal fluid was able to support the differentiation of step 1-3 spermatids to step 7-9 spermatids within 36 h. However, the percentage of spermatozoa remained nearly the same (~ 10%) during the entire 36 h-incubation (**Figure 3.15**), suggesting the male germinal fluid under current culture conditions was unable to support the differentiation of step 7-9 spermatids into spermatozoa.

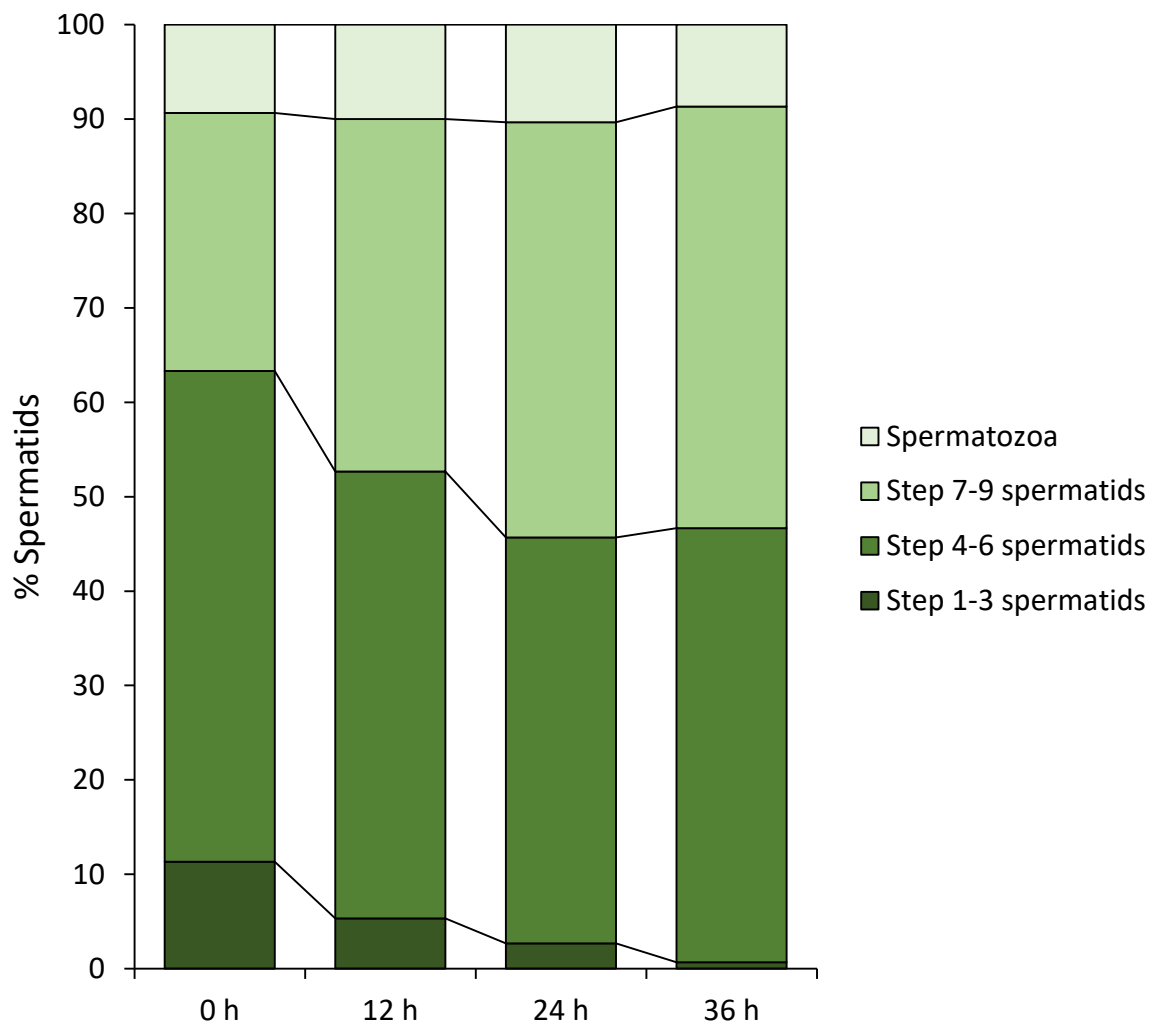


Figure 3.15 The male germinal fluid was able to induce a substantial portion of spermatid differentiation *in vitro*. After 36 h of incubation in the male germinal fluid, the average percentage of step 1-3 spermatids decreased from 11.33% to 0.67%, whereas that of step 7-9 increased from 27.33% to 44.67%. The percentages of step 4-6 slightly reduced from 52% to 47.33% in the first 12 h and became constant afterwards. The percentage of spermatozoa remained almost unchanged (~ 10%) during the entire 36 h-incubation, indicating no new spermatozoon generated in this culture media.

To determine whether any protein regulator of spermiogenesis existed in the male germinal fluid, the spermatids were cultivated in boiled male germinal fluid under the same culture conditions. Throughout the 36 h of incubation, the average percentages of all four types of sperm cells were generally unchanged ($P > 0.05$; **Figure 3.16**). As the boiled male germinal fluid failed to support the differentiation of spermatids *in vitro*, the

regulators of spermiogenesis in the male germinal fluid of *G. caespitosa* most likely contained protein molecules. Since no significant degeneration of spermatids occurred during the 36 h of incubation in the boiled male germinal fluid, it is also suggested that this culture medium was able to maintain the viability of spermatids for at least 36 h – but not their differentiation.

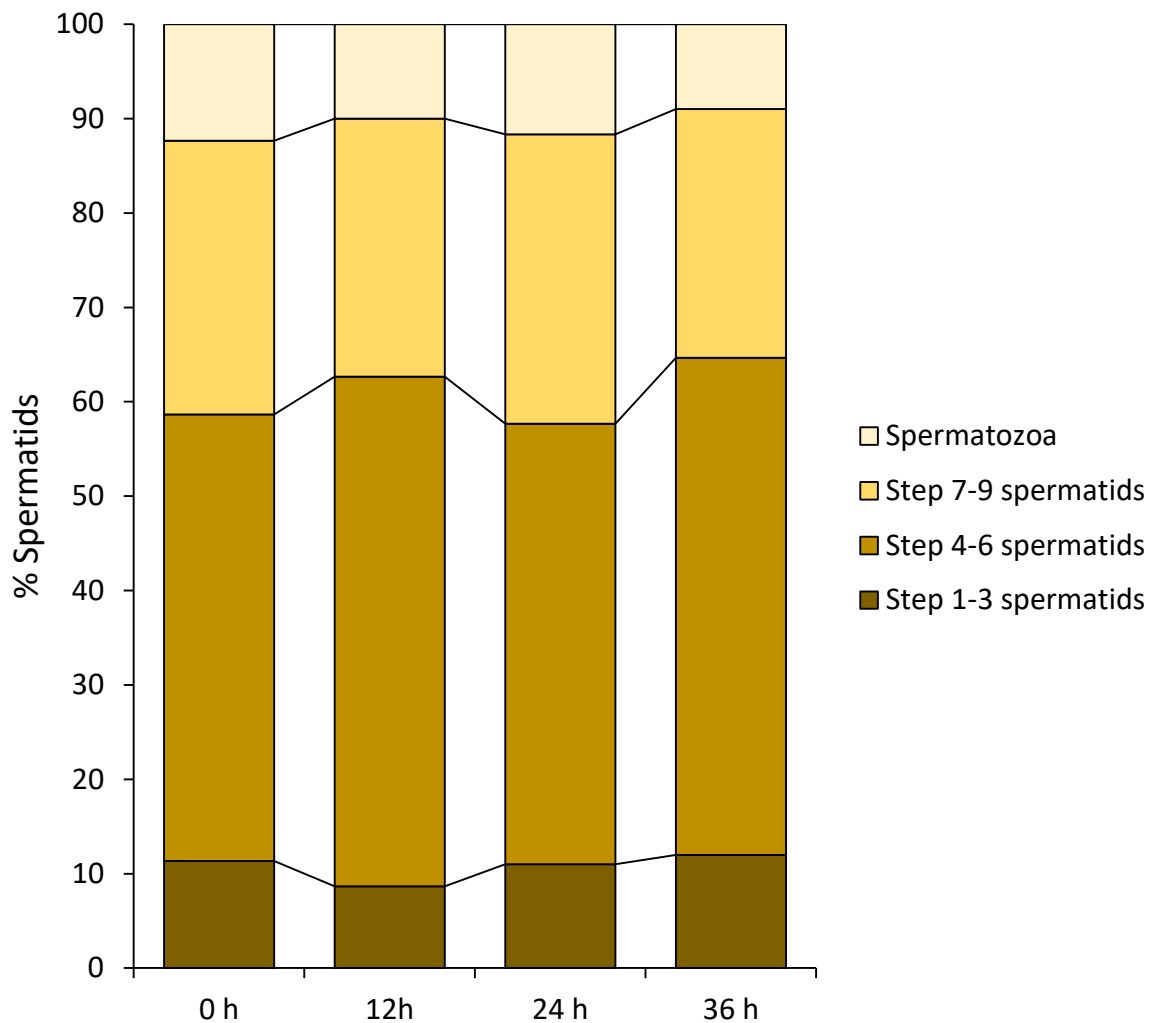


Figure 3.16 The boiled male germinal fluid lost its capacity to support the differentiation of spermatids *in vitro*. During the 36 h of incubation in the boiled male germinal fluid, no significant change of the average percentages was detected in all four types of sperm cells ($P > 0.05$). It indicated that the boiled male germinal fluid could not induce the young spermatids to differentiate *in vitro*, but could maintain the viability of the spermatids for at least 36 h.

To determine whether the regulators of spermiogenesis were gender-specific, spermatids were then incubated in female germinal fluid under the same culture conditions. Within 24 h of incubation, the percentages of the four types of sperm cells exhibited no significant change ($P > 0.05$; **Figure 3.17**), suggesting the female germinal fluid could not support the differentiation of spermatids. The spermatids cultured in the female germinal fluid started to degenerate within 24 h after incubation, making it impossible to obtain any data at 36 h of incubation.

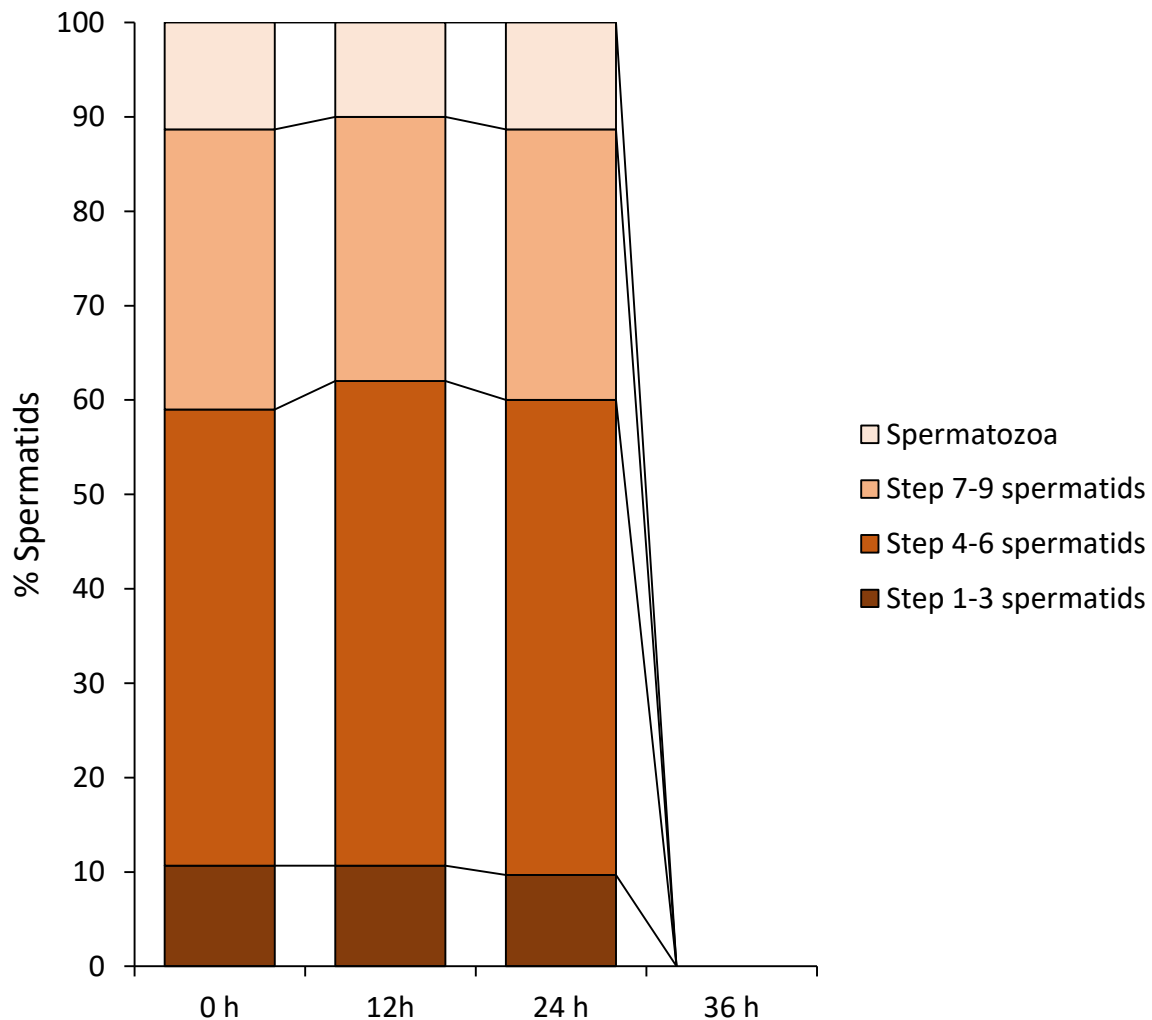


Figure 3.17 The female germinal fluid was unable to induce the differentiation of spermatids *in vitro*. During the first 24 h of incubation, the percentages of step 1-3 spermatids, step 7-9

spermatids and spermatozoa were almost unchanged ($P > 0.05$). The spermatids degenerated after 24 h-incubation in the female germinal fluid; therefore, the data at 36 h were not applicable.

The spermatids were finally incubated in 10% foetal bovine serum in RPMI 1640 medium (RPMI + FBS) under the same *in vitro* culture conditions. Within 36 h of incubation, the percentage of step 1-3 spermatids reduced from 10% to 0% ($P < 0.01$; **Figure 3.18**) while the percentage of step 7-9 spermatids increased from 28% to 39.33% ($P < 0.01$; **Figure 3.18**). The percentages of step 4-6 spermatids and spermatozoa were almost constant, which were about 55% and 7% respectively ($P > 0.05$; **Figure 3.18**). These data demonstrate that similar to the male germinal fluid, the RPMI + FBS could also support the differentiation of step 1-3 spermatids into step 7-9 spermatids within 36 h of incubation but not into spermatozoa under the current *in vitro* culture conditions.

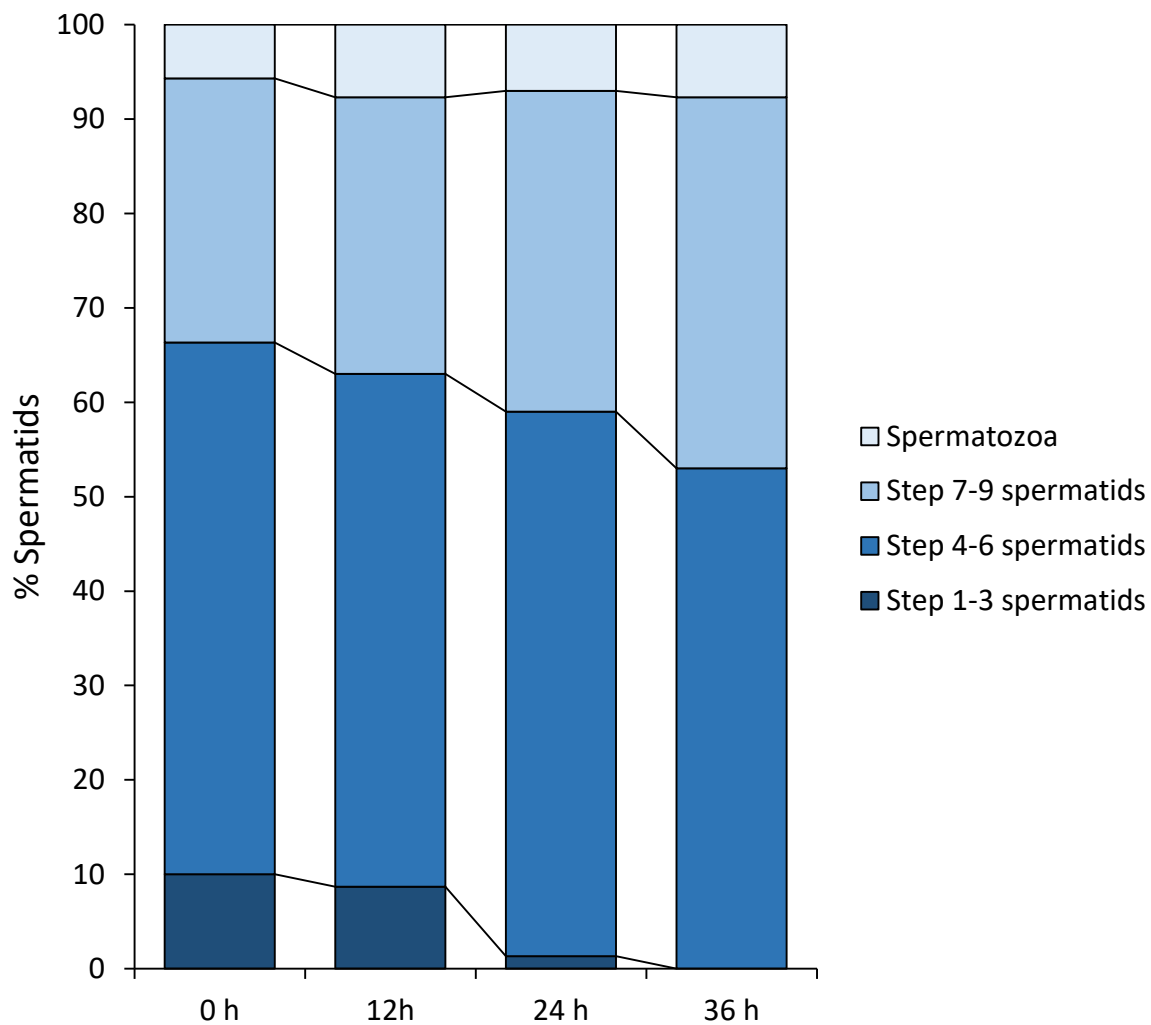


Figure 3.18 10% foetal bovine serum in RPMI 1640 medium was able to induce a substantial portion of spermatid differentiation *in vitro*. After 36 h of incubation in this culture medium, the percentage of step 1-3 spermatids decreased from 10% to 0% while that of step 7-9 spermatids increased from 28% to 39.33%. The average percentages of step 4-5 spermatids and spermatozoa exhibited no significant change, which remained about 55% and 7% respectively ($P > 0.05$).

The effectiveness of the four culture media in inducing spermiogenesis *in vitro* was reflected by the changes of the percentages of step 7-9 spermatids in the culture media. At the beginning of the culture attempts, the percentages of these spermatids were not significantly different (**Figure 3.19**; $P > 0.05$). During the 36 h of incubation, the percentages of step 7-9 spermatids increased in both male germinal fluid (MGF) and

RPMI + FBS. In contrast, the ratios of step 7-9 spermatids in female germinal fluid (FGF) and boiled MGF remained almost constant (**Figure 3.19**). After 36 h of incubation, the average percentage of step 7-9 spermatids in MGF became the highest among the four culture media while that in RPMI + FBS was the second highest. This implies that the artificial culture medium RPMI + FBS might not be as effective as the natural medium MGF in terms of the capacity to induce spermiogenesis *in vitro*. However, no statistical significance could be detected between the percentages of step 7-9 spermatids in these two culture media. The FGF and boiled MGF had no capacity to induce the young spermatids to develop into older step 7-9 spermatids and the former could not support the survival of spermatids for 36 h *in vitro* (**Figure 3.19**).

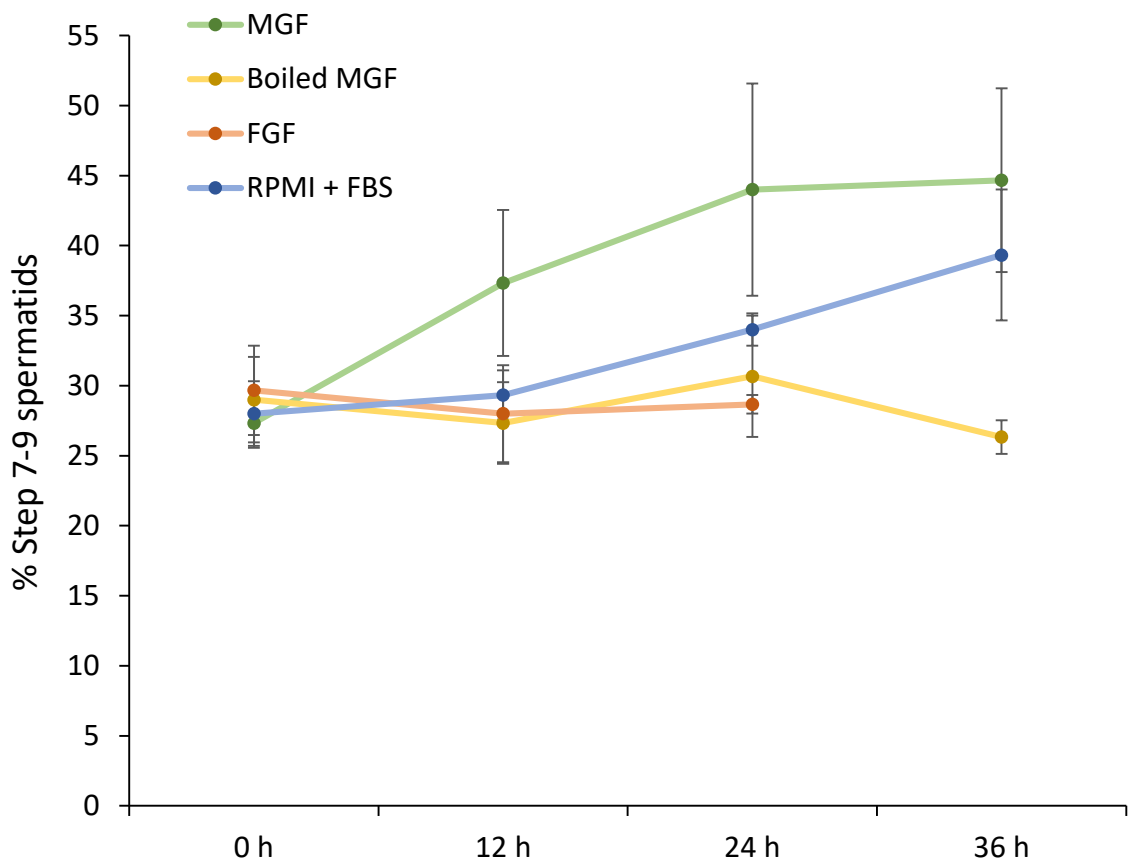


Figure 3.19 Comparison between the capacity of the four culture media to induce spermatid differentiation *in vitro*. The average percentages of step 7-9 spermatids at four different time points were used as an indicator for determining the effectiveness of the four culture media, including male germinal fluid (MGF), boiled male germinal fluid (boiled MGF), female germinal fluid (FGF) and 10% foetal bovine serum in RPMI 1640 medium (RPMI + FBS). The average percentage of step 7-9 spermatids in MGF continuously increased to 44.67% at the end of the incubation, while that in RPMI + FBS achieved a percentage of 39.33% in a similar increasing tendency. Comparatively, the ratios of the spermatids had no significant change in the FGF and boiled MGF during the entire incubation. The FGF even could not maintain the viability of the spermatids after 24 h of incubation.

3.5 Discussion

The spermiogenesis in the marine invertebrate *Galeolaria caespitosa* has been elucidated in detail in this chapter. After the second meiotic division of the spermatogenesis in *G. caespitosa*, the spermatids detached from the seminiferous epithelium and completed their entire spermiogenesis while floating freely in the germinal fluid of the male reproductive duct. The spermatids were independent from supporting cells and were indirectly supported by the secretory vesicles released from nurse cells. In comparison, spermiogenesis in most mammalian species occurs within the seminiferous epithelium and is completely dependent upon the adherent Sertoli cells. These nurse cells provide the differentiating sperm cells with essential nourishment, such as growth and anti-apoptotic factors and form the blood-testis barrier to support the movement of these sperm cells towards the lumen of seminiferous tubule during the differentiation process. Such dependence upon supporting cells renders mammalian spermiogenesis extremely difficult to replicate in artificial environments. Therefore, spermiogenesis in *G. caespitosa* and other similar polychaetes, which takes place while the cells are floating freely in the germinal fluid, is a convenient model to study the *in vitro* differentiation of spermatids, by which the molecular mechanisms underlying this process would be unlocked. On the other hand, the different steps of spermatid differentiation are particularly hard to identify in such polychaetes, because they have similar sizes to their spermatogenic precursors. Besides, rather than being properly arranged inside the seminiferous epithelium, spermatids in polychaetes are randomly distributed in the lumen of the germinal chamber and mixed with other spermiogenic cells at various stages of development. In light of these factors, spermiogenesis in a wide range of polychaetes has not been comprehensively investigated at the ultrastructural level.

Spermiogenesis is generally characterised by various morphological alterations in the spermatids, such as formation of the acrosome, condensation of the nucleus, elongation of flagellum and the activities of other organelles (e.g. Golgi complex and centrioles). In a large proportion of polychaetes, the origin of the acrosome has not been adequately described, because it is difficult to acquire favourable ultrathin sections through the relatively small acrosome in those randomly dispersed round spermatids. The spermiogenesis in *G. caespitosa* was temporally divided into three distinct phases: Golgi phase, which involves the formation of proacrosomal vacuole and flagellum; acrosomal phase, during which a substantial portion of acrosome differentiation took place and a mitochondrial sheath formed surrounding the initial segment of the flagellum; and maturation phase, during which the acrosome migrated to the pole opposite to the flagellum and accomplished its final differentiation, the nucleus was fully condensed and the excess cytoplasm was eliminated.

In *G. caespitosa*, the acrosome first appeared as a cluster of single membrane-bound proacrosomal vesicles situated at the posterior pole of the spermatids and in close apposition to the concave surface of the Golgi complex (**Figure 3.1B**). Involvement of the Golgi complex during the formation of the proacrosome has been confirmed in many other polychaetes [e.g. *Phragmatopoma lapidosa* (Eckelbarger, 1984) and *Capitella* spp. (Eckelbarger and Grassle, 1987)], and avian [e.g. *Coturnix coturnix japonica* (Lin and Jones, 1993)] and mammalian species [e.g. *Ornithorhynchus anatinus* (Lin and Jones, 2000)]. In these species, including *G. caespitosa*, the proacrosomal vacuole forms similarly through the fusion of the proacrosomal vesicles. The proacrosomal vacuole in *Ornithorhynchus anatinus* (Lin and Jones, 2000) and many other mammals approaches the nuclear envelope and lodges into a concavity formed at the anterior pole of the nucleus.

After the lodgement of the proacrosome, it transforms into a cap-shaped structure covering about two thirds of the nuclear surface; this process is known as the cap phase of spermiogenesis in mammals. In contrast, the cap phase does not exist in the spermiogenesis of *G. caespitosa* and other polychaetes [e.g. *Phragmatopoma lapidosa* (Eckelbarger, 1984) and *Vanadis formosa* and *Krohnia lepidota* (Rice and Eckelbarger, 1989)]. The acrosome in these polychaetes is relatively free and never attaches to the nuclear membrane during the entire spermiogenesis. During the Golgi phase of spermiogenic process in *G. caespitosa*, a pair of centrioles was first found residing adjacent to both the nuclear membrane and the Golgi complex (**Figure 3.1A and B**), which is consistent with that in the step 1 spermatid of the mammal *Ornithorhynchus anatinus* (Lin and Jones, 2000). In both species, the two centrioles gradually migrate towards the plasma membrane and the distal centriole becomes docked with the cell membrane where it subsequently gives rise to a formative flagellum. Simultaneously, the orientation of the two centrioles transforms from parallel to perpendicular.

During the early acrosomal phase, an implantation fossa was formed at the posterior pole of the nucleus, followed by the insertion of the proximal centriole. The implantation fossa in both *G. caespitosa* and *Ornithorhynchus anatinus* is relatively shallow compared with that in other polychaetes [e.g. *Marenzelleria viridis* (Rice, 1981)], the depth of whose implantation fossa accounts for approximately half length of the longitudinal diameter of the nucleus. However, the proximal centriole in *G. caespitosa* made contact with the fossa by extending its microtubules into it, whereas in the mammalian species the centriole directly attaches to the implantation fossa.

After insertion of the proximal centriole into the implantation fossa, the mitochondria sheath started to form, as indicated by changes in the number, size and position of the

mitochondria. From the Golgi phase to the early acrosomal phase, small spherical mitochondria, which were initially randomly dispersed in the cytoplasm, fused with each other to form larger spherical-shaped mitochondria that migrated towards the posterior end of the spermatids. Fusion of mitochondria has been recognised as a common process during the spermiogenesis in polychaetes and is necessary for the reduction of mitochondrial number and the subsequent formation of the mitochondrial sheath (Purschke and Fursman, 2005). During step 3 of spermiogenesis in *G. caespitosa*, larger rod-shaped mitochondria, which were twice as large as the small spherical mitochondria started to appear (**Figure 3.3A**), suggesting the occurrence of mitochondrial fusion in the spermatids. Interestingly, the fused mitochondria in polychaetes became lodged into depressions formed at the posterior end of the nucleus. Such adherence of mitochondria to concave recesses in the envelope has also been found common in a wide range of polychaetes [e.g. *Marenzelleria viridis* (Bochert, 1996) and *Phragmatopoma lapidosa* (Eckelbarger, 1984)]. During the late acrosomal phase, the fused mitochondria formed the mitochondria sheath surrounding the principal segment of the flagellum. In polychaetes, the fully differentiated ect-aquasperm usually encompasses a short midpiece containing four to six spherical mitochondria encircling the centrioles. Such an intimate relationship between the centrioles and mitochondria may permit fast diffusion of ATP, which is essential for the sperm movement (Eckelbarger and Grassle, 1987). Comparatively, in *Ornithorhynchus anatinus* (Lin and Jones, 2000) and many other mammalian species, the spermatozoa contain a large number of mitochondria, which forms a relatively long midpiece at the junction of the nucleus and the flagellum.

In *Ornithorhynchus anatinus*, both the acrosome and flagellum initially appeared at the anterior end of the cytoplasm and the flagellum subsequently migrated towards the

opposite end where it became associated with the implantation fossa (Lin and Jones, 2000). However, in *G. caespitosa*, the flagellum remained located at the posterior end of the spermatids, where the acrosome first appeared and the mitochondrial sheath later formed. Moreover, instead of the flagellum migrating to the pole opposite the acrosome, the acrosome in the spermatids of *G. caespitosa* was the one that migrated. Acrosome migration during spermiogenesis has also been discovered in many other polychaetes, such as *Marenzelleria viridis* (Bochert, 1996), *Phragmatopoma lapidosa* (Eckelbarger, 1984) and *Capitella* spp. (Eckelbarger and Grassle, 1987). In these species, including *G. caespitosa*, the acrosome forms and migrates from the posterior end of the cytoplasm to the anterior end. The migration generally initiates on completion of nuclear condensation and is accomplished prior to the final differentiation of the acrosome. Similar to many other polychaetes, migration of the acrosome in *G. caespitosa* happened while it was in intimate association with the cytoplasmic membrane (Franzén and Rice, 1988). By contrast, in *Ornithorhynchus anatinus* and most other mammalian species, after the lodgement in a concave recess at the anterior aspect of the nucleus, the acrosome persists adhering to the nuclear membrane throughout the entire spermiogenic process (Lin and Jones, 2000).

The spermatozoa of *G. caespitosa* have been identified as a typical ect-aquasperm, which is associated with its broadcast-spawning strategy and external fertilisation mode (Franzén and Rice, 1988). Although the acrosome of ect-aquasperm varies in their morphology and size, it is generally indented towards the anterior end of the cytoplasm in most cases. The indentation of the acrosome forms a subacrosomal space containing granular subacrosomal materials. In *G. caespitosa*, the subacrosomal space was not filled with granular material until the lower end of the ring-like structure closely approached

the apex of the nucleus. Sparsely distributed fibrillary materials were observed along the base of the subacrosomal space in *G. caespitosa* and in some other polychaetes, such as *Phragmatopoma lapidosa* (Eckelbarger, 1984) and *S. tetraceros* (Selim *et al.*, 2005). These electron-dense fibrillary materials have been described as subacrosomal filaments, which are presumed to be actin that, in turn, plays an important role in the acrosome reaction during fertilisation (Eckelbarger, 1984). The acrosome in the spermatozoa of *G. caespitosa* exhibited a cap-like appearance, which is similar to acrosomal morphology in several other polychaete species [e.g. *Hydroides dianthus*, *Serpula vermicularis*, *Vermiliopsis infundibulum* (Gherardi *et al.*, 2011) and *Spirobranchus tetraceros* (Selim *et al.*, 2005)].

Nuclear condensation was generally accomplished during the acrosomal phase of spermiogenesis in *G. caespitosa*. Microtubules were found running around the nucleus in the spermatids of *G. caespitosa* and other polychaetes, such as *Streblospio benedicti* (Rice, 1981) and in *Ornithorhynchus anatinus* (Lin and Jones, 2000). The bundles of microtubules, or the manchette, have been demonstrated to play a role in shaping the nucleus in polychaetes [e.g. *Krohnia lepidota* (Rice and Eckelbarger, 1989) and *Capitella* spp. (Eckelbarger and Grassle, 1987)]. Instead of happening simultaneously, the compaction of the chromatin in the spermatids of *G. caespitosa* occurs prior to the shrinkage of the nuclear envelope. The heterochromatin first aggregates into an irregular-shaped chromatin block attaching to the posterior end of the inner nuclear membrane, where the implantation fossa is formed (**Figure 3.7A**). While the nuclear membrane remained spherical in appearance, the chromatin block already became transformed into an approximate oval shape. The nuclear membrane started to form an oval shape after completion of chromatin condensation (**Figure 3.8A**). The pattern of chromatin

aggregation at the posterior nucleus and slight asynchronicity between chromatin condensation and shrinkage of the nuclear membrane have also been observed in older spermatids of *Phragmatopoma lapidosa* (Eckelbarger, 1984). Such asynchronicity is reflected in the presence of a gap containing sparse euchromatin between the condensed chromatin block and nuclear envelope. Noticeably, dramatic chromatin aggregation and shaping occurred after adherence of the spherical mitochondria to the nuclear envelope. Franzén and Rice (1988) suggested that the chromatin condensation during this period might be mediated by these mitochondria associated with the nuclear membrane. In a considerable number of polychaete species, such as *Polydora* spp. (Gao *et al.*, 2014) and *Streblospio benedicti* (Rice, 1981), chromatin condensation involves heterochromatin transforming from a fibrillary or lamellar structure into homogeneously electron-dense material during late spermiogenesis. However, the homogeneous chromatin in spermatozoa is transformed from granular materials in several other polychaetes, such as in *Amathys lutzii* (Blake and Van Dover, 2005), *Aonides oxycephala* (Radashevsky *et al.*, 2011) and *Terebrasabella heterouncinata* (Simon and Rouse, 2005). In *G. caespitosa*, the fully condensed chromatin in the sperm nucleus retained a densely packed granular texture, as has been observed in other polychaetes such as *Sabella spallanzanii* (Giangrande *et al.*, 2000), *Gorgoniapolynoe caeciliae* (Eckelbarger *et al.*, 2005) and *Methanoaricia dendrobranchiata* (Eckelbarger and Young, 2002).

The sperm nucleus in *G. caespitosa* presented an oval-shaped appearance, which is relatively short compared with the elongated nucleus in other polychaetes. Indeed, the ect-aquasperm of most polychaetes, including *G. caespitosa*, present a nucleus that is only slightly elongated and approximately oval in shape. Sperm nuclei are more elongated in ent-aquasperm and introsperm, possibly because elongation of the nucleus is associated

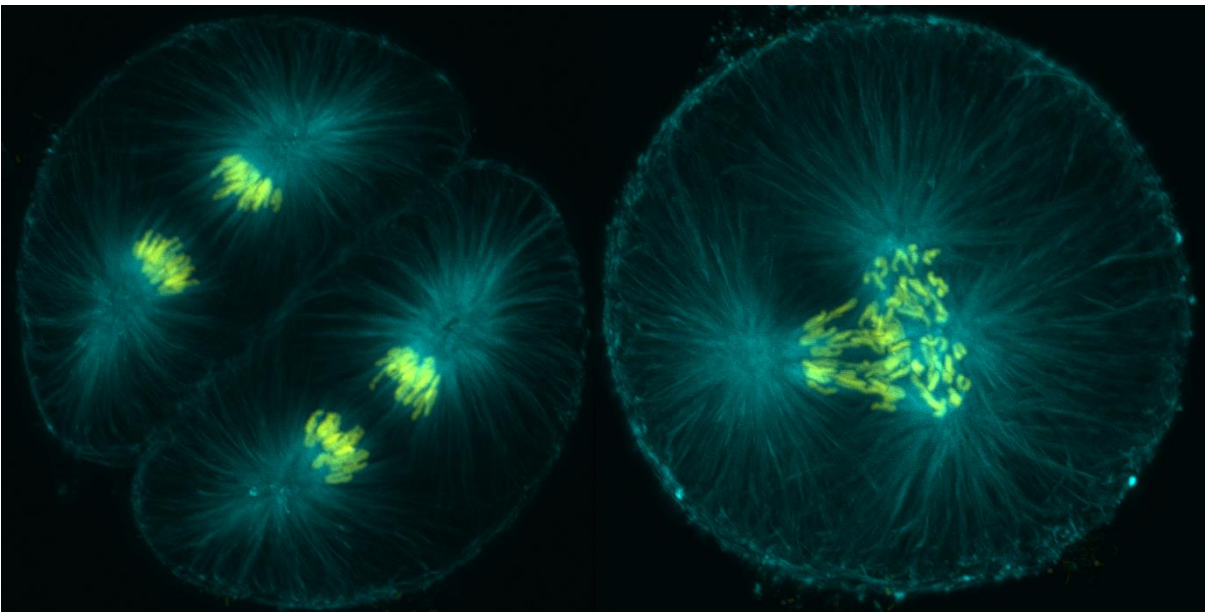
with sperm storage in the female reproductive ducts and internal fertilisation in such species (Franzén and Rice, 1988).

In marine polychaetes, sperm motility is activated by changes in intracellular pH. Differently, in mammals, newly formed spermatozoa, or testicular spermatozoa, lack the capacity of progressive movement and fertilisation. Spermiogenesis in these higher animals is concluded at spermiation, during which the elongated spermatozoa detach from the seminiferous epithelium and travel along the lumen of the seminiferous tubule in the testicular fluid towards the ductus epididymis. During subsequent passage through the epididymis, the spermatozoa accomplish their final maturation, including the completion of sperm morphogenesis and acquisition of the ability to move and fertilise oocytes.

This study also included a preliminary trial of reproducing the differentiation of spermatids *in vitro* and succeeded in demonstrating that step 1-3 spermatids were able to differentiate into step 7-9 spermatids in both male germinal fluid (a natural culture medium) and 10% foetal bovine serum in RPMI 1640 medium (an artificial culture medium). The *in vitro* culture of spermatids conducted in this study not only provides a fundamental basis for the future investigation, but also confirms that spermiogenesis in this species is dependent on intrinsic programming in the germline. The failure of spermatid differentiation in female and boiled male germinal fluids suggests that the essential regulators of spermiogenesis in *G. caespitosa* are gender-specific and contain key proteins. As no similar cell culture attempt has been conducted on the spermatids of invertebrates, more works are expected to be carried out to reveal the mechanism underlying spermiogenesis using the *G. caespitosa* model. In future studies, male and female germinal fluids could be analysed respectively by mass spectrometry to determine the nature of potential drivers of spermatid differentiation that are unique to the male tract.

Chapter 4

Dibutyl phthalate-impaired spermatozoa induced
cytoskeletal disruption in the early embryogenesis of
Galeolaria caespitosa



4.1 Overview

In this chapter, the toxic effects of dibutyl phthalate (DBP) on early embryogenesis of a sessile marine invertebrate *Galeolaria caespitosa* has been investigated and the mechanisms of how DBP-impaired spermatozoa led to embryonic arrest and malformation were uncovered. Through embryotoxicity tests, we observed DBP-induced sperm dysfunction that subsequently led to a decreased ability to initiate normal embryogenesis and an increased occurrence of malformed embryos exhibiting a particular pattern of abnormality. After the first cleavage, one blastomere in these malformed embryos was able to carry out further mitoses, while the other one arrested. The fluorescence staining of microtubules, chromosomes and actin filaments demonstrated that the mitotic spindles in the malformed embryos were irregularly bent, shortened and unable to anchor to the cortex, which resulted in defective segregation of chromosomes. Within the non-dividing blastomeres, karyokinesis was found to continue at a slow pace as indicated by the presence of multiple sets of abnormal mitotic spindles. However, cytokinesis had been disrupted in these arrested cells due to a failure to assemble contractile actin ring, as a result of which half of the embryos remained as one larger cell. The lucigenin-dependent chemiluminescence assay revealed that DBP suppressed the activity of superoxide dismutase in the spermatozoa. Using immunocytochemical techniques, we discovered that the DBP-treated spermatozoa were subject to lipid peroxidation which was immunolocalised at the acrosomal and neck regions. The lipid peroxidation occurring at the acrosome would be expected to result in a failure of the acrosome reaction, which would, in turn, generate an anticipated decrease in the success of fertilisation and subsequent embryogenesis. Lipid peroxidation at the sperm neck caused sperm centriole damage by modifying the protein structure. The oxidised sperm

centrioles were inherited by the embryos and consequently induced a disruption of cytoskeletal proteins during the early embryonic cleavage. This research highlights the necessity of environmentally friendly disposal of plasticisers and supports the utilisation of abnormal embryogenesis in *G. caespitosa* as an indicator of phthalate esters in coastal waters.

4.2 Introduction

Phthalate esters, or phthalic acid esters (PAEs), are one of the most commonly utilised industrial chemicals, predominantly applied as plasticisers for improving the durability, elasticity and flexibility of high molecular weight polymers. These compounds are employed as additives for manufacturing of an extensive range of products, such as construction materials, home furnishings, food packaging, clothing, cosmetics and medical products. During the processing, utilisation and disposal of these products, PAEs will be gradually released into the environment, inducing sublethal effects on both wildlife and humans. Due to their lipophilicity, PAEs tend to concentrate in the surface water and sediment after entering the marine environment and accumulate more readily in marine invertebrates who have a comparatively low metabolic capacity (van Wezel *et al.*, 2000).

This study investigated the adverse effects of dibutyl phthalate (DBP) on early embryogenesis in *G. caespitosa* when its gametes being exposed to up to 20 mg/L of DBP and uncovered mechanisms underlying the resultant embryonic arrest and malformation. Although DBP is usually below the limit of detection in the environments with less human activity, high concentrations of DBP have been found in the surface water and sediment samples obtained from polluted areas. For example, the chemical analyses of a surface

water sample from Kuils River, South Africa and a sediment sample from Zhonggang River, Taiwan revealed that DBP had been found in extremely high concentrations of 34.52 ± 0.75 mg/L and 30.3 mg/kg respectively (Olujimi *et al.*, 2012; Yuan *et al.*, 2002). Such levels of DBP contamination are much higher than the concentrations tested in this study.

4.3 Materials and Methods

4.3.1 Sample collection and maintenance

Aggregations of *Galeolaria caespitosa* were collected freshly between February and May at low tides from intertidal rock revetments at Nobbys Beach (32°55'46"S, 151°47'28"E), Newcastle East, New South Wales, Australia. The tubeworms were transported to the laboratory within 1 h after the collection and maintained in an aerated polyethylene bucket with natural seawater obtained from the collection site. Samples were reared at constant room temperature of 20 ± 2 °C and supplied with a 12-h light/12-h dark illumination cycle. All experiments were conducted within 10 days of sample collection.

4.3.2 Toxicity tests

4.3.2.1 Gamete collection and preparation

G. caespitosa were carefully extracted from their calcareous tubes with fine forceps. Adult male and female *G. caespitosa* tubeworms were transferred to two petri dishes filled with 0.22- μ m-filtered natural seawater (FSW). The genders can be distinguished by creamy white colour of male abdomens and bright orange colour of female abdomens. *G. caespitosa* spontaneously releases its gametes on being exposed to seawater. After spawning for 10 min, sperm and oocytes were collected respectively using plastic transfer pipettes. The sperm density was calculated using a haemocytometer for further dilutions into the designated concentrations.

According to a series of pilot experiments conducted by Ross and Bidwell (Ross and Bidwell, 2001) on *G. caespitosa*, a high concentration of spermatozoa would induce polyspermy while a low sperm concentration would lead to incomplete fertilisation. To maximise the fertilisation rates for the untreated control, in the current study, the final

concentration of spermatozoa in test solutions was $\sim 6 \times 10^4$ cells/mL. The final concentration of oocytes was no less than 5×10^3 cells/mL to ensure a sufficient number of embryos for scoring. The final volume of all test solutions was 30 mL, which had been demonstrated as the lowest test volume that could result in a development rate of over 95% (Ross and Bidwell, 2001).

Dibutyl phthalate (DBP) was purchased from Sigma Aldrich (Castle Hill, Australia) with a purity over 99%. DBP stock solutions were prepared in absolute acetone at a concentration of 100 g/L and serially diluted with FSW. Due to the presence of acetone in the test solutions, its toxicity to the spermatozoa and oocytes was tested in the first place. In this test, the gametes were exposed to 1% (v/v) acetone in FSW, which was higher than any concentration of acetone applied during the following toxicity tests. The toxicity of acetone was reflected by the percentage of the embryos that successfully entered the 2-cell stage at 1.5 h after fertilisation.

4.3.2.2 Sperm-exposure tests

During sperm-exposure tests, freshly collected spermatozoa were treated with graded concentrations of DBP at 0.02, 0.2, 2 and 20 mg/L respectively in 1.5 mL Eppendorf tubes. The total volume of spermatozoa in each treatment was 1 mL. After 15 min incubation at room temperature, the 1 mL DBP-treated sperm solutions were directly added to 29 mL freshly collected oocytes in FSW in 50 mL autoclaved conical flasks. Given the possibility that DBP might induce time-dependent effect on the early embryogenesis, the percentages of embryos that successfully reached the 2-, 4-, 8- and 16-cell were respectively scored at 1.5, 2, 2.5 and 3 h after adding the DBP-treated spermatozoa to oocytes. The scoring was conducted under a light microscope at 20 \times magnification, during which the first one hundred embryos observed were examined. The

unfertilised, arrested or malformed embryos were all identified as unsuccessful development. Immature oocytes with a pronounced germinal vesicle were omitted during the calculation of development rates. The percentages of malformed embryos were also recorded for each treatment at each time point. Images of the malformed embryos were captured under a Zeiss Axiovert S100 inverted microscope with a Zeiss AxioCam MRm camera (Carl Zeiss, Oberkochen, Germany).

4.3.2.3 Oocyte-exposure tests

Since the DBP was not removed from the sperm solution during the sperm-exposure test, the oocytes were exposed to low concentrations of DBP (≤ 1.3 mg/L). In order to clarify if the resultant embryonic arrest and malformation originated from DBP-induced sperm or oocyte dysfunction, an oocyte-exposure test was also conducted.

In this test, the oocytes were exposed to graded concentrations of DBP (2.5, 5, 10, 15 and 20 mg/L) for 15 min at room temperature. The removal of the DBP from the oocyte solutions was accomplished by allowing the oocytes to settle, replacing the supernatant with FSW and resuspending the oocytes thoroughly. This washing process was repeated for three times prior to the addition of freshly collected spermatozoa. The percentages of embryos that successfully reached the 8-cell stage were scored at 2.5 h after mixing spermatozoa with the DBP-treated oocytes.

4.3.3 Confocal microscopy

The methods for embryo fixation and fluorescent staining of microtubules, actin filaments and chromosomes were adapted from Foe and von Dassow (2008) and optimised for *G. caespitosa*.

4.3.3.1 Fixation of embryos

Unless otherwise specified, all chemicals used during the embryo fixation were of analytical grade and purchased from Sigma Aldrich (Castle Hill, Australia). The embryos were fixed in 100 mM HEPES, 50 mM EGTA, 10 mM MgSO₄, 2% formaldehyde, 0.2% glutaraldehyde (ProSciTech, Queensland, Australia), 0.2% acrolein and 0.2% Triton X-100 in distilled water. In order to allow EGTA to dissolve completely, the pH of the fixative was adjusted to 8.0 using KOH. The final pH was adjusted to 7.4 using hydrochloric acid and the osmolality of the fixative was adjusted to about 1,100 mOsm/kg using dextrose. The embryos were fixed for 24 h at 4 °C. To avoid incomplete fixation, the embryos were resuspended for several times during the 24 h period of fixation. After the fixation, the embryos were washed three times with 0.1% (v/v) Triton X-100 in PBS (PBT), followed by another three washes in PBS to eliminate the detergent. The embryos were then transferred to freshly made 0.1% sodium borohydride in PBS to minimise glutaraldehyde-induced autofluorescence. The embryos were allowed to sit uncapped in a 50 mL Falcon tube for 2 h until bubbling ceased. After three washes in PBT, the embryos were blocked with 5% goat serum in PBT for 12 h at 4 °C. Prior to staining, the embryos were washed in PBS for additional three times and stored in PBS at 4 °C.

4.3.3.2 Fluorescent staining of microtubules, chromosomes and actin filaments

For microtubule staining, the fixed embryos were initially treated with primary antibody 1:1000 rat anti- α -tubulin (YL 1/2 clone; Abcam, Cambridge, United Kingdom) in PBT with 0.1% bovine serum albumin (BSA; Sigma Aldrich, Castle Hill, Australia) for 24 h at 4 °C. The embryos were then washed three times in PBT and stained with the secondary antibody 1:500 goat anti-rat IgG (H+L) secondary antibody conjugated with Alexa Fluor[®] 568 (Thermo Fisher Scientific, North Ryde, Australia) in PBT with 0.1%

BSA for 24 h at 4 °C. After three washes in PBT, the chromosomes were visualised by staining the embryos with 1:500 Hoechst 33342 (Thermo Fisher Scientific, North Ryde, Australia) in PBT with 0.1% BSA for 2 h at 4 °C. After three washes in PBT, the actin filaments were stained with 5 µL/mL BODIPY[®] FL phalloidin (Thermo Fisher Scientific, North Ryde, Australia) in PBT for 12 h at 4 °C. The embryos were finally washed once in PBS for 20 min before being mounted.

To prepare a semi-permanent slide for the stained embryos, the coverslips were treated with Vaseline[®] petroleum jelly (Unilever, Sydney, Australia) along each edge to make continuous jelly ledge. The fixed embryos were mixed thoroughly in a small amount of ProLong[®] Diamond Antifade Mountant (Thermo Fisher Scientific, North Ryde, Australia). A drop of the antifading mountant containing a small number of embryos was then placed at the centre of poly-L-lysine coated microscope slides. The coverslip was then placed over the liquid droplet with its Vaseline side down. The chamber was sealed by lightly pressing each edge of the coverslip against the microscope slide. The prepared semi-permanent slides were stored away from light in a slide storage box (ProSciTech, Queensland, Australia).

The embryos were examined under an Olympus FV1000 laser scanning confocal microscope (Olympus, Macquarie Park, Australia) with a 60× oil immersion objective lens. All confocal images were captured using Olympus FV10-ASW 4.2 Viewer software (Olympus, Macquarie Park, Australia).

4.3.4 Sperm analyses

4.3.4.1 Sperm motility assay

As the sperm solution obtained by exposing the worms to seawater usually contains a considerable number of spermatids, the sperm motility was counted manually. During this assay, freshly collected spermatozoa were treated with graded concentrations of DBP (0.02, 0.2, 2 and 20 mg/L) for 15 min at room temperature. The final concentration of spermatozoa in test solutions was $\sim 1 \times 10^5$ cells/mL. The scoring was conducted under a light microscope with phase-contrast optics at 40 \times magnification, during which the first a hundred spermatozoa encountered were examined. The spermatozoa exhibited a forward movement were identified as motile, while the ones with no active movement as immotile.

4.3.4.2 Sperm DNA damage assay

The method of flow cytometric analysis of sperm DNA damage was adapted from De Juiis et al. (2009). The generation of 8-hydroxy-2'-deoxyguanosine (8-OH-dG) was utilised as a biomarker for oxidative DNA damage. During this assay, the spermatozoa were initially treated with graded concentrations of DBP (0.02, 0.2, 2 and 20 mg/L) in artificial seawater (ASW; 28.32 g NaCl, 0.77 g KCl, 5.41 g MgCl₂·6H₂O, 7.13 g MgSO₄·7H₂O, 1.18 g CaCl₂ and 0.2 g NaHCO₃ in 1 L distilled water) for 15 min at room temperature. After the DBP treatments, all sperm samples were washed twice by centrifuging at 600 g for 7 min, replacing the supernatant with ASW. The washed spermatozoa were then treated with 1 mM H₂O₂ and 1 mM CuSO₄ in 100 μ L ASW for 1 h at room temperature as a positive control. After two washes in ASW, the sperm samples were resuspended in 100 μ L 2 mM dithiothreitol (DTT) in ASW and incubated for 30 min at room temperature. After being washed once in ASW, the spermatozoa were then

fixed in 100 μ L 4% paraformaldehyde in ASW for 15 min at 4 °C. After fixation, the spermatozoa were washed twice in ASW and then stored in 0.1 M glycine in ASW at 4 °C for no more than one week. The fixed spermatozoa were washed once in ASW and permeabilised in 100 μ L 0.1% (v/v) Triton X-100 in ASW at room temperature for 3 min. Prior to the immunofluorescent staining, the anti-8-OH-dG reagent conjugated with fluorescein isothiocyanate (FITC) supplied in Calbiochem OxyDNA Assay Kit (Calbiochem, California, USA) was diluted to 1:50 in 'Wash Solution' (Calbiochem OxyDNA Assay Kit, Calbiochem, California, USA). The FITC-conjugated solution was purified by adding approximately 1 mg activated charcoal powder and incubating at room temperature for 1 h. The charcoal-treated reagent was then centrifuged at 16,060 g for 5 min and the supernatant was transferred to a clean 1.5 mL Eppendorf tube. This process was repeated for at least twice to remove the charcoal completely from the OxyDNA reagent. After the permeabilisation, the unstained control was resuspended in 50 μ L 'Wash Solution' while all other samples were resuspended in 50 μ L charcoal-treated 1:50 FITC-conjugated reagent in 'Wash Solution'. After 1 h staining at room temperature, the spermatozoa were washed once in ASW and were then transferred to 5 mL FACS tubes and examined under a BD FACSCalibur™ flow cytometer (BD Biosciences, North Ryde, Australia).

4.3.4.3 Assessment of superoxide dismutase activity in spermatozoa

The method for assessing the activity of superoxide dismutase (SOD) is adapted from Aitken et al. (Aitken *et al.*, 1996), which was able to detect the low activity of SOD in spermatozoa. Unless otherwise specified, all chemicals used in the SOD assessment were of analytical grade and purchased from Sigma Aldrich (Castle Hill, Australia). Prior to the assessment, a reaction mixture containing 13 mL of 1.33 mM

diethylenetriaminepentaacetic acid, 0.5 mL of 1 mg catalase (5000 IU) and 1.7 mL of 1.8 mM xanthine in K_3PO_4 buffer (0.05 M, pH 7.8) was freshly prepared.

During the assay, freshly collected spermatozoa were treated with graded concentrations of DBP at 0.625, 1.25, 2.5, 5, 10 and 20 mg/L respectively in 1.5 mL Eppendorf tubes for 15 min at room temperature. The DBP was then removed from the test solutions by centrifuging at 500 g for 5 min and replacing the supernatant with FSW. The FSW in the sperm samples was then replaced by 50 μ L 0.5 mM phenylmethylsulfonyl fluoride in K_3PO_4 buffer, with a final sperm density of 2×10^6 cells/mL. These sperm samples were respectively added to 400 μ L of the previously prepared reaction mixture in 1.5 mL Eppendorf tubes. To each Eppendorf tube, 5 μ L Triton X-100 and 4 μ L 25 mM lucigenin in DMSO were introduced. After 5 min incubation, 50 μ L xanthine oxidase was added to each tube and the luminescence signals were monitored and measured over the following 15 min on a Berthold Biolumat LB9500T luminometer (Berthold, Bad Wildbad, Germany).

4.3.4.4 Immunocytochemical analysis of lipid peroxidation in the spermatozoa

Freshly collected spermatozoa were treated with graded concentrations of DBP at 0.625, 1.25, 2.5, 5, 10 and 20 mg/L respectively for 15 min and fixed in 2.5% (v/v) paraformaldehyde in FSW for 2 h at room temperature. After three washes in 0.1 M phosphate buffered saline (PBS; pH 7.4), the sperm samples were resuspended in PBS with a final concentration of 2×10^6 cells/mL and 10 μ L of the sperm suspension was smeared onto poly-L-lysine-coated microscope slides and allowed to sit for at least 15 min at room temperature until the spermatozoa became completely dried. The air-dried spermatozoa were then rehydrated in PBS and permeabilised in ice-cold absolute methanol at -20 °C for 15 min. After being washed once in PBS, the spermatozoa were

blocked with 5% goat serum in PBS at room temperature for 2 h and were then probed with 1:100 rabbit anti-4-hydroxynonenal (HNE) polyclonal antibody (Jomar Life Research, Caribbean Park, Australia) in PBS for 1 h at room temperature. The sperm samples were then washed in PBS for three times and stained with 1:100 goat anti-rabbit IgG (H+L) secondary antibody conjugated with Alexa Fluor® 488 (Thermo Fisher Scientific, North Ryde, Australia) in PBS for another 1 h. After additional three washes in PBS, spermatozoa were covered with a small drop of ProLong® Diamond Antifade Mountant (Thermo Fisher Scientific, North Ryde, Australia). Both the subcellular immunolocalisation of 4-HNE on spermatozoa and the percentages of 4-HNE positive spermatozoa were investigated under a Zeiss Axioplan II fluorescence microscope (Carl Zeiss, Sydney, Australia) with a wavelength of 530 nm.

4.3.4.5 Toxic effect of 4-HNE on sperm functions

To confirm whether the embryonic malformation was caused by the DBP-induced lipid peroxidation, freshly collected spermatozoa were directly treated with graded concentrations of 4-HNE (Sigma Aldrich, Castle Hill, Australia) at 100, 200 and 400 µM respectively in FSW for 15 min at room temperature, followed by the addition of oocytes. The final concentrations of spermatozoa and oocytes and the final volume of the test solutions were consistent with the prior toxicity tests. The percentages of embryos that successfully reached the 8-cell stage and the percentages of malformed embryos were recorded 2.5 h after fertilisation using the using the aforementioned scoring method.

4.3.5 Statistical analysis

The adverse effects of DBP and 4-HNE on the early embryogenesis in *G. caespitosa* were evaluated on datasets consisting of at least three replicates. The statistical differences

between the rates of successfully developed embryos/malformed embryos in different treatments were analysed using one-way analysis of variance (ANOVA). The presence of a dose-dependent relationship between the toxicant concentrations and the percentages of successfully developed embryos/malformed embryos was also determined using ANOVA. The ANOVA was further applied to assess if DBP induced a time-dependent inhibition of early embryonic development. The difference was recognised as statistically significant if the P value was less than 0.05. All statistical analyses were performed using Microsoft Excel 2013 (Microsoft Corporation, Redmond, USA).

4.4 Results

Due to the broadcast-spawning strategy and sedentary lifestyle that *G. caespitosa* exhibits, its gametes are directly exposed to toxic pollutants in the ambient water before, during and after fertilisation. Such chronic exposure of gametes to marine toxicants may affect their normal function and result in defective early embryogenesis. In this study, adverse effects on early embryogenesis following respective exposure of spermatozoa and oocytes to DBP were analysed to uncover whether the resultant disruption of embryonic development originated from DBP-induced impairment of spermatozoa or oocyte function. Following these initial toxicity tests, the study then focused on revealing the mechanisms by which DBP caused embryonic arrest and abnormality through pre-fertilisation exposure.

4.4.1 DBP caused embryogenesis arrest and malformation by impairing the male germline

As DBP was dissolved in acetone before serial dilutions into the designated concentrations, an acetone control was tested in the first instance. Freshly collected spermatozoa and oocytes were mixed together after being respectively treated with 1% (v/v) acetone in filtered natural seawater (FSW), which was higher than any acetone concentration applied in the following tests on DBP toxicity. **Figure 4.1** demonstrated that 1% acetone was unable to induce any adverse effect on the early embryogenesis, as approximately 90% of the embryos in the acetone-treated group successfully reached 2-cell stage, which had no significant difference compared with the untreated control ($P > 0.05$).

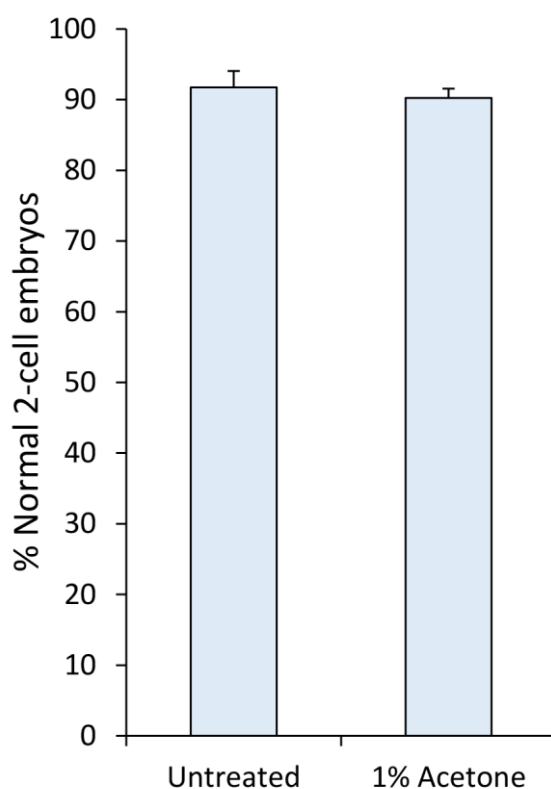


Figure 4.1 Exposure of gametes to 1% (v/v) acetone had no adverse effect on the early embryogenesis in *G. caespitosa*. To determine the effect of low-level acetone on the early embryogenesis, spermatozoa and oocytes were treated with 1% acetone in FSW respectively for 15 min prior to fertilisation. No significant difference was detected between the untreated and acetone-treated groups in terms of the percentages of embryos that successfully developed into two cells at 1.5 h after fertilisation ($P > 0.05$).

During the oocyte-exposure tests, the oocytes were treated with 2.5, 5, 10, 15 and 20 mg/L DBP for 15 min. After the removal of DBP, the treated oocytes were mixed with freshly collected spermatozoa in FSW. The impact of DBP on oocyte function was determined by the percentages of the resultant embryos that successfully reached the 8-cell stage at 2.5 h after fertilisation. As shown in **Figure 4.2**, exposure of oocytes to DBP caused significant decrease in the success of embryogenesis only at the concentration of 20 mg/L ($P < 0.001$). No morphologically abnormal embryo development was detected at any point during the oocyte-exposure tests. Therefore, any defective embryogenesis induced

by low levels of DBP (< 20 mg/L) in the following sperm-exposure tests should all be attributed to DBP-induced sperm impairment.

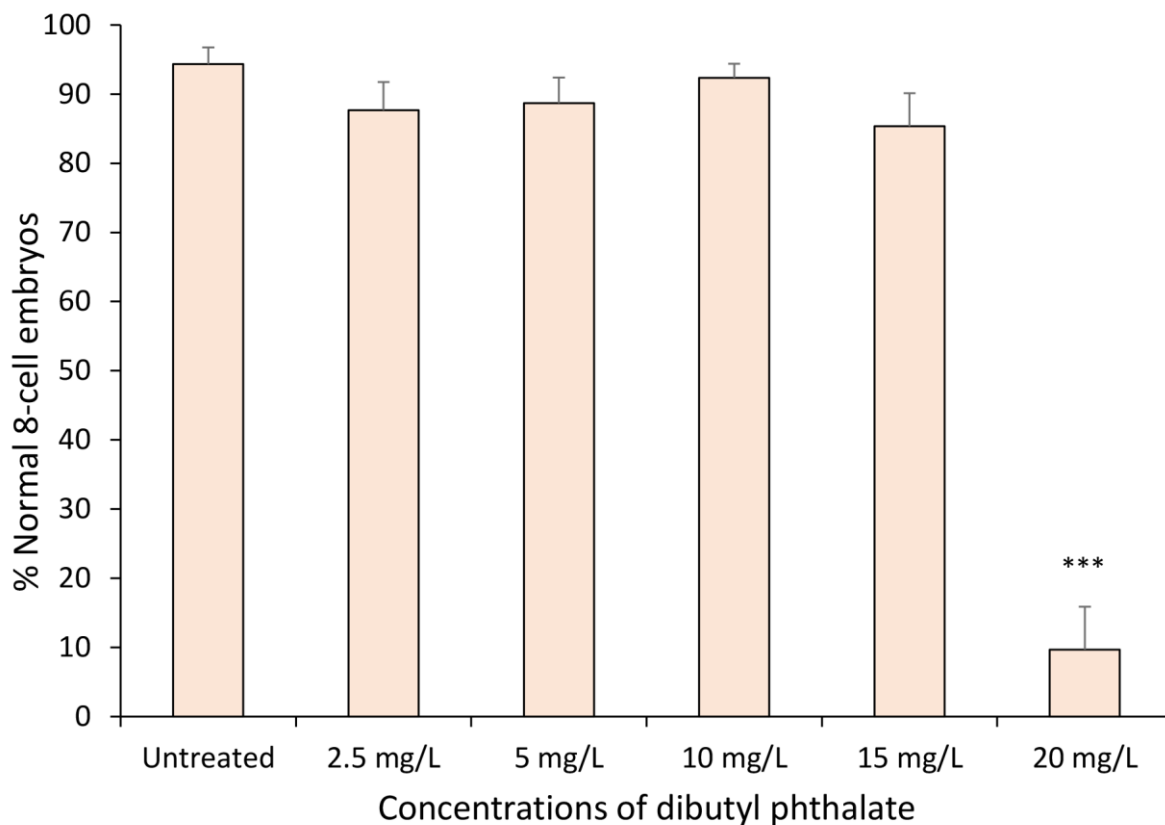


Figure 4.2 Exposure of oocytes to the graded concentrations of DBP had no adverse effect on the early embryogenesis except for the concentration at 20 mg/L. During the oocyte-exposure tests, the oocytes were initially treated with graded concentrations of DBP for 15 min. Before the addition of freshly collected spermatozoa, the residual DBP was removed by allowing the oocytes to settle and replacing the supernatant with FSW. Exposure of oocytes to DBP resulted in no significant adverse impact on the early embryogenesis until the chemical concentration reached 20 mg/L. ***, $P < 0.001$.

Regarding the sperm-exposure tests, the spermatozoa were treated with 0.02, 0.02, 2 and 20 mg/L DBP for 15 min, followed by the addition of freshly collected oocytes. The impact of DBP on sperm function was manifested in the success rates of subsequent embryonic development at 2-, 4-, 8- and 16-cell stages. When the spermatozoa were exposed to increasing concentrations of DBP, the inhibitory effects that the chemical

posed on the success of embryogenesis increased in a dose-dependent manner (**Figure 4.3**; ANOVA, $P < 0.001$). The DBP-induced toxicity effect was statistical significant at concentrations of 0.2 mg/L or greater ($P < 0.05$). While the untreated samples exhibited high rates of normal development of about 90%, exposure of spermatozoa to 0.2 mg/L DBP resulted in significant decreased percentages of approximately 70% ($P < 0.05$). After the spermatozoa were treated with 2 mg/L DBP, only about 30% of the embryos were able to proceed through the normal early development ($P < 0.01$). Further, exposure of spermatozoa to 20 mg/L DBP resulted in extremely low development rates of less than 5% (**Figure 4.3**; $P < 0.001$). These data indicated that the capacity of spermatozoa to activate normal embryonic development was dramatically reduced as the DBP concentration increased with this capacity being completely suppressed at 20 mg/L.

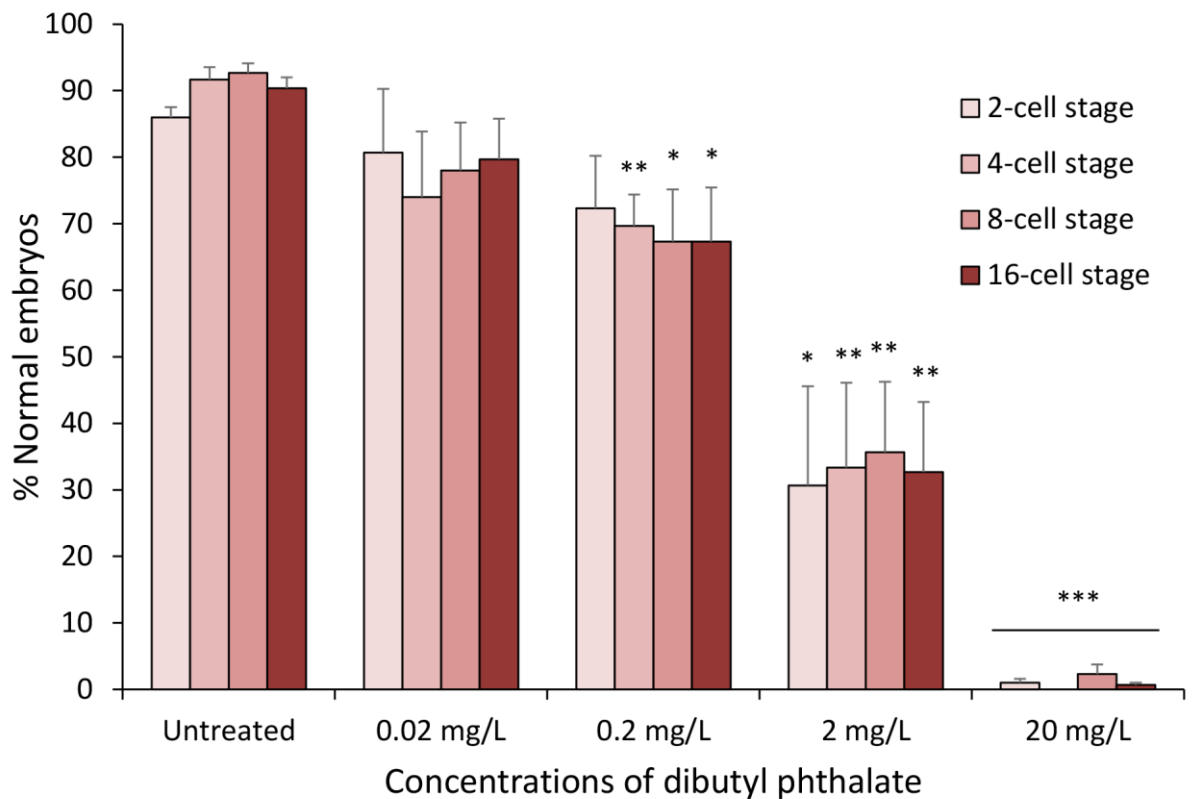


Figure 4.3 Exposure of spermatozoa to the graded concentrations of DBP resulted in decrease of normal development rates. Spermatozoa were exposed to graded concentrations of DBP for 15 min prior to the addition of untreated oocytes. With the increase of tested DBP concentrations, the percentages of normal embryos reduced in a dose-dependent manner (ANOVA, $P < 0.001$). The inhibitory effects of DBP on the embryogenesis success were statistical significant at concentrations of 0.2 mg/L and higher ($P < 0.05$). *, $P < 0.05$; **, $P < 0.01$; ***, $P < 0.001$.

Exposure of spermatozoa to the graded concentrations of DBP not only resulted in a decreased success of early development, but also resulted in an elevated incidence of morphologically abnormal embryos (**Figure 4.4**). As shown in **Figure 4.4**, no abnormal embryo was detected in all groups at 2-cell stage, suggesting all embryonic malformations occurred during the second cleavage. From 4-cell stage, with the concentrations of DBP increased from 0 to 2 mg/L, the percentages of malformed embryos increased in a dose-dependent manner (**Figure 4.4**; ANOVA, $P < 0.001$). Exposure of spermatozoa to 2 mg/L DBP resulted in an elevated rate of abnormal development of less than 10%, compared with no malformed embryos was detected in the untreated samples. No malformed embryo was observed in 20 mg/L DBP-treated samples, where the capacity of spermatozoa to activate normal embryogenesis was mostly suppressed and the majority of the embryos remained undeveloped.

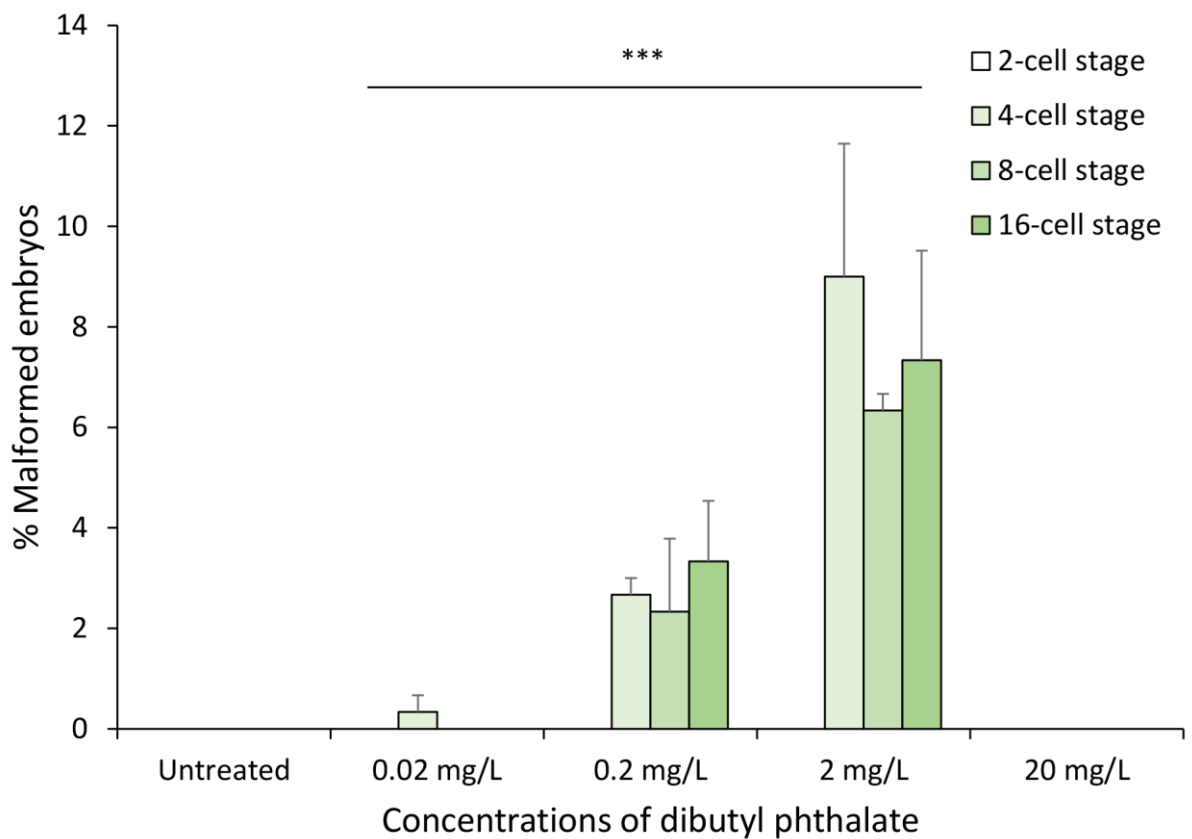


Figure 4.4 Exposure of spermatozoa to the graded concentrations of DBP resulted in increased incidence of malformed embryos. During the sperm-exposure test, the percentages of morphologically abnormal embryos were respectively recorded at 2- to 16-cell stages of the early embryogenesis. No malformed embryo was observed in all treatments at 2-cell stage. From 4-cell stage, with the concentrations of DBP elevated from 0 to 2 mg/L, the occurrence of embryonic malformations increased in a dose-dependent manner (ANOVA, $P < 0.001$). No abnormal embryo was detected in the untreated and the 20 mg/L DBP-treated samples. ***, $P < 0.001$.

During the sperm-exposure tests, the oocytes were exposed to low concentrations of DBP ranging from 0.0013 to 1.3 mg/L as the chemical was not eliminated from the treated spermatozoa. As revealed by the oocyte-exposure tests, exposure of oocytes to such low levels of DBP was not able to induce any embryonic arrest or malformation. Therefore, the malformed embryos detected during the sperm-exposure tests were all attributed to the DBP-induced sperm dysfunction.

4.4.2 DBP-impaired spermatozoa produced malformed embryos with a typical pattern of abnormality

Under normal conditions, the fertilised oocytes divided into two and four blastomeres during the first two cleavages. These blastomeres within the 2- and 4-cell embryos exhibited an equal volume and a symmetrical arrangement (**Figure 4.5A** and **B**). From the third cleavage, the spiral arrangement of the blastomeres became apparent, during which the spindle was shifted in an oblique angle within the dividing blastomeres and the newly formed blastomeres came to lie over the furrows between their parent blastomeres (**Figure 4.5C** and **D**). As a result, the blastulae of *G. caespitosa* exhibited a rather symmetrical appearance containing similar-sized small blastomeres (**Figure 4.5E**).

The toxicity tests demonstrated that exposure of spermatozoa to low concentrations of DBP would result in increased rates of embryonic arrest and abnormality. Interestingly, a typical pattern of embryonic malformation was observed among the abnormal embryos. The first cleavage of the abnormal embryos appeared normal under light microscope, during which the fertilised oocyte bisected symmetrically into two equal-sized blastomeres (**Figure 4.5F**). However, following the second cleavage, one of the blastomeres in these abnormal embryos stopped dividing, while the other blastomere was able to undergo the further cleavage. As a consequence, they appeared as 3-cell embryos containing one large blastomere and two smaller equal-sized blastomeres after the second division (**Figure 4.5G**). Likewise, during the third and fourth cleavages, half of the malformed embryos was occupied by one large undeveloped blastomere and the other half contained four and eight equal-sized small blastomeres respectively (**Figure 4.5H** and **I**). Such a unique pattern persisted in the malformed blastula, which contained a large blastomere and a clump of small equal-sized blastomeres (**Figure 4.5J**).

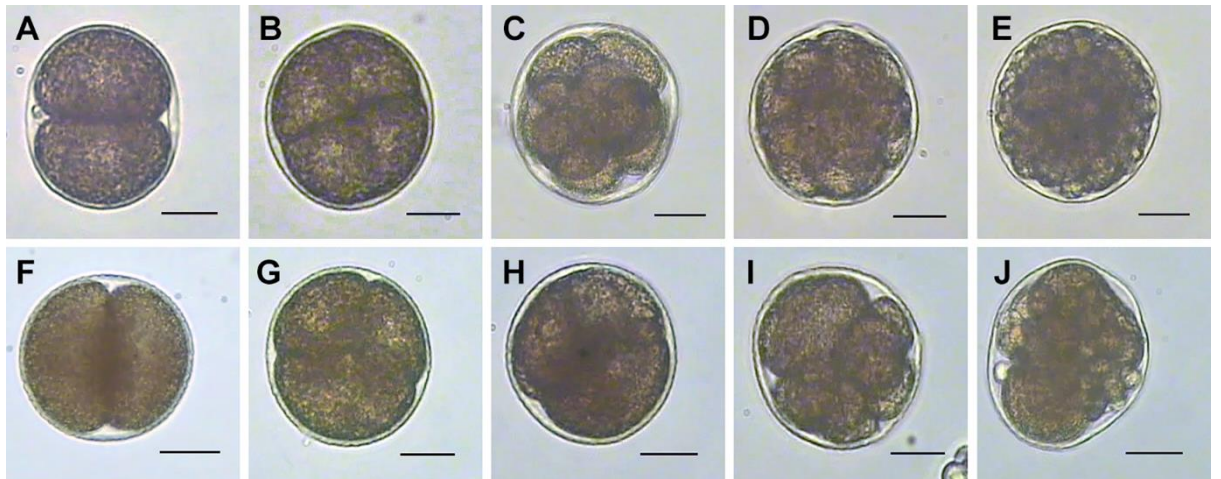


Figure 4.5 DBP-impaired spermatozoa produced malformed embryos with a typical pattern of abnormality. (A - E) A normal embryo underwent the first four mitotic divisions and developed into a blastula. (A) The first cleavage occurred approximately 1.5 h after fertilisation, during which the fertilised oocyte bisected into two equal-sized blastomeres. (B) The second cleavage occurred about 2 h after fertilisation, during which the two blastomeres divided synchronously and symmetrically into four equal-sized blastomeres. (C) About 2.5 h after fertilisation, the normal embryo was committed to the third mitotic division, during which eight blastomeres were produced and arranged into the spiral pattern. (D) The fourth cleavage took place approximately 3 h after fertilisation, during which an embryo containing 16 similar-sized blastomeres was produced. (E) Within 5 h after insemination, the fertilised oocyte divided into a blastula which was characterised by a spherical mass of similar-sized small blastomeres. (F - J) Malformed embryos derived from the DBP-treated spermatozoa underwent the first four mitotic divisions and developed into an abnormal blastula. (F) After the first cleavage, the malformed embryo appeared as a normal 2-cell embryo containing two equal-sized blastomeres. (G) During the second division, one blastomere in the malformed embryo was at rest, while the other blastomere divided into two equal-sized blastomeres. (H) After the third cleavage, the non-dividing blastomere remained undeveloped and occupied half volume of the abnormal embryo, while the dividing blastomeres developed into four smaller blastomeres. (I) After the fourth cleavage, half of the malformed embryo was still occupied by the large non-dividing blastomere, whereas the other half was filled with eight smaller blastomeres. (J) At the end of the embryonic cleavage, an abnormal blastula formed. The non-dividing blastomere remained occupying half volume of the blastula, while the other half was densely packed with smaller similar-sized blastomeres. Scale bars = 20 μ m.

4.4.3 The typically malformed embryos contained abnormal mitotic spindles and underwent defective chromosome segregation during the first cleavage

Microscopic observation of the malformed embryos demonstrated that these embryos failed to carry out normal mitotic divisions at early cleavage stages. Therefore, the microtubules, actin filaments and chromosomes in the early embryos were selectively stained to determine whether a disruption in the cellular cytoskeleton attributed to such an abnormality originating from DBP-induced sperm impairment.

During the metaphase and anaphase of the first cleavage, the astral microtubules in the normal embryos protruded from each spindle pole and continuously elongated in all directions until their tips were completely anchored to the cortex (**Figure 4.6A**). Meanwhile, a bundle of kinetochore microtubules also protruded from each spindle pole with their tips gradually approximating towards the centre of the embryo where they ultimately bound to the centromeres of the chromosomes. With the assistance of the kinetochore microtubules, the chromosomes became strictly aligned along the equatorial plate of the embryo (**Figure 4.6B**). At late metaphase and early anaphase, the chromosomes broke up into sister chromatids and these chromatids became perpendicular to the equatorial plate (**Figure 4.6C**). During anaphase, the sister chromatids were evenly drawn to opposite ends of the embryo with the shortening of the kinetochore microtubules with segregation occurring synchronously among each pair of chromatids (**Figure 4.6D**).

The spindle fibres in the normal embryos exhibited a naturally curved appearance. They were properly organised into radial arrays extended from the centrosomes with their distal termini firmly anchoring to the cortex (**Figure 4.6**). In contrast, the spindle fibres in DBP-induced abnormal embryos were shortened, aberrantly bent and incompletely anchored

to the cortex (**Figure 4.6E**). Such a disordered arrangement of spindle fibres would result in instability of the spindle apparatus, which in turn led to errors in the subsequent spindle-involved activities, including the alignment of chromosomes (**Figure 4.6F**) and segregation of sister chromatids (**Figure 4.6G and H**). As shown in **Figure 4.7F**, at the first metaphase, instead of rigidly aligning along the equatorial plate, the chromosomes (white arrowheads) in the abnormal embryos were partially distributed away from the equatorial plate, with the connected kinetochore microtubules prematurely shortening and improperly orienting towards the peripheral regions of the equatorial plate. In contrast to the chromosomes of normal embryos which were uniformly perpendicular to the equatorial plate at the late metaphase/early anaphase (**Figure 4.6C**), the chromosomes in the abnormal embryo were inconsistently distributed and segregated (**Figure 4.6G**). Notably, while the majority of the chromatids were perpendicular to the equatorial plate and not yet separated, a solitary chromatid appeared at the south of the equatorial plate (white arrowhead) and no paired sister chromatid could be observed (**Figure 6G**). Therefore, the chromatids were segregated unequally and asynchronously in the embryo. Such an unequal and asynchronous segregation of chromatids was also observed during the first anaphase, reflected by the three chromatids (white arrowheads) being separated away from the equatorial plate, while the other chromatids were just beginning to separate. Such disrupted chromosome segregation during the metaphase of the first cleavage led to the production of two blastomeres with abnormal chromosome numbers, creating a state of aneuploidy.

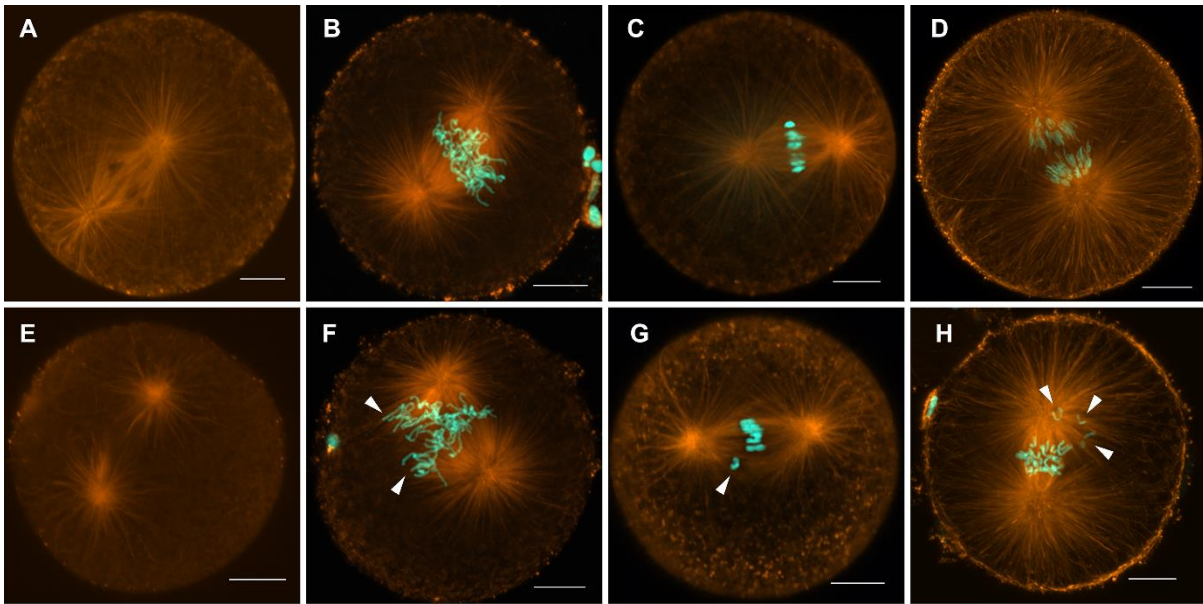


Figure 4.6 Confocal micrographs depicting the distribution of microtubules and chromosomes in normal embryos and malformed embryos created by DBP-impaired spermatozoa during the first mitotic division. The microtubules and chromosomes were visualised using anti- α -tubulin (orange) and Hoechst 33342 (cyan) respectively. Scale bars = 20 μ m. **(A)** At the metaphase of the first cleavage, the spindle fibres in the normal embryo were well arranged around each spindle pole with a naturally curved appearance and their tips were internally attached to the cortex. **(B)** At early metaphase of the first mitotic division, the centromeres of the chromosomes in the normal embryo were connected by the kinetochore microtubules and strictly aligned along the equatorial plate of the embryo. **(C)** At late metaphase and early anaphase, the sister chromatids were perpendicular to the equatorial plate and ready to be separated by the kinetochore microtubules towards each end of the embryo. **(D)** During anaphase, the paired chromatids were separated from one another evenly and synchronously. Each chromatid was strictly situated opposite to its sister. **(E)** In the DBP-induced abnormal embryo, the spindle fibres were irregularly bent, shortened and partially unanchored to the cortex. **(F)** At the first metaphase, the chromosomes in the abnormal embryo were randomly distributed at the centre of the embryo and failed to align properly along the equatorial plate. The kinetochore microtubules connecting to the disorganised chromosomes were prematurely shortened and directed to the peripheral regions away from the equatorial plate. **(G)** At late metaphase and early anaphase, the chromosomes in the abnormal embryo were irregularly distributed along the equatorial plate, indicating the unequal segregation of the chromosomes. **(H)** At early anaphase, the chromatids failed to segregate evenly and synchronously, with three chromatids being solitarily isolated from the paired sister chromatids at the equatorial plate. Thus two aneuploidy blastomeres were produced after the first cleavage.

In normal embryonic development, the chromosomes were separated evenly and synchronously by the spindle apparatus containing two sets of microtubules. During the second cleavage, the segregation of chromosomes was precisely synchronised between the two blastomeres (**Figure 4.7A and B**). The malformed embryos derived from DBP-impaired spermatozoa displayed a typical 3-cell arrangement after the second division (**Figure 4.7C**). Such abnormality was caused by one of the two blastomeres being unable to carry out the mitotic divisions, while the other one failed to divide further and remained as one large blastomere. Although the arrested blastomere was unable to carry out cell division (i.e. cytokinesis), according to observations made with a confocal microscope, nuclear division (i.e. karyokinesis) was still proceeding in the cytoplasm. After the second cleavage, the dividing blastomere accomplished the first telophase and bisected symmetrically into two smaller daughter cells, whereas the non-dividing blastomere was retarded at the metaphase of the first cleavage (**Figure 4.7D**). After the third cleavage, the dividing blastomeres moved on to the metaphase of the fourth cleavage, while the arrested blastomere was still at the anaphase of the second cleavage. Thus, the non-dividing blastomere in malformed embryos was still able to undergo the karyokinesis but proceeded asynchronously at a slow pace.

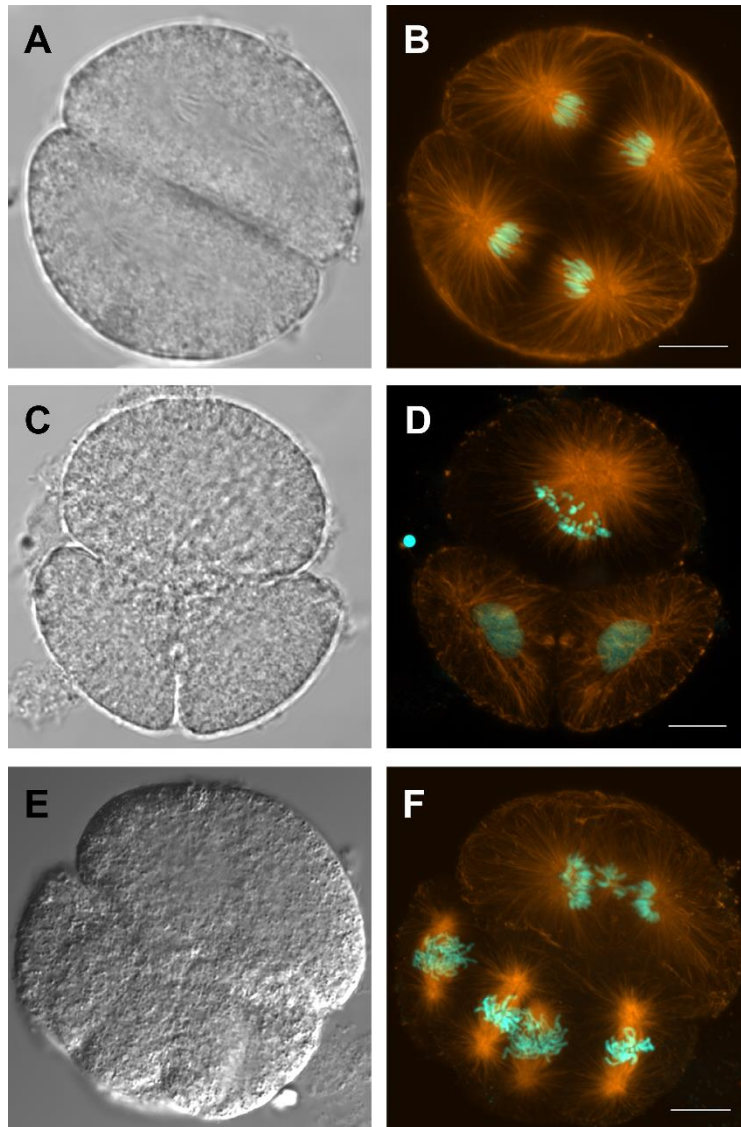


Figure 4.7 Light and confocal micrographs showing the distribution of microtubules and chromosomes in normal embryos undergoing the second cleavage and malformed embryos created by DBP-impaired spermatozoa undergoing the second and fourth cleavages. The microtubules and chromosomes were visualised using anti- α -tubulin (orange) and Hoechst 33342 (cyan) respectively. Scale bars = 20 μ m. **(A - B)** A normal embryo at the anaphase of the second cleavage. The chromosomes were segregated evenly and synchronously in the two blastomeres. **(C - D)** A malformed embryo undergoing the second cleavage. The non-dividing blastomere remained at rest after the first cleavage, while the other blastomere divided into two smaller daughter cells, which collectively formed a typical 3-cell malformed embryo. According to the morphology of the chromatin, the non-dividing and the other divided blastomeres exhibited asynchronous cleavage. The karyokinesis was retarded at the metaphase in the arrested blastomere, while the other two daughter cells already completed their telophase of the second cleavage. **(E - F)** An abnormal embryo undergoing the metaphase of the fourth cleavage. After the third

cleavage, while the dividing blastomeres divided into four smaller cells occupying half of the embryo, the other half was occupied by one large cytokinesis-arrested blastomere, in which the karyokinesis was proceeding in the cytoplasm. However, the karyokinesis of the arrested blastomere was retarded at the second anaphase, while the dividing blastomere had already reached the metaphase of the fourth cleavage.

4.4.4 The non-dividing blastomere in the typically malformed embryos was unable to assemble contractile actin ring during the second cleavage

Forming a ring of actin microfilaments is a necessary mechanical agent for cytokinesis. In order to determine whether the contractile ring occurred in the blastomeres of the abnormal embryos induced by the DBP-treated spermatozoa, the actin microfilaments were visualised by fluorescence-conjugated phalloidin in a typical 3-cell malformed embryo (**Figure 4.8A**). After the second cleavage, typical abnormal embryos contained only three blastomeres (**Figure 4.8A**). A contractile actin ring of the third cleavage was observed in each of the two dividing blastomeres (**Figure 4.8B and C**), indicating these cells continued to undergo the cytokinesis. By contrast, in the non-dividing blastomere, neither the contractile rings for the second cleavage, nor for the third cleavage were detected (**Figure 4.8B and C**). This study therefore suggested that the disruption of cytokinesis in the arrested blastomere was caused by a failure to form the contractile actin ring.

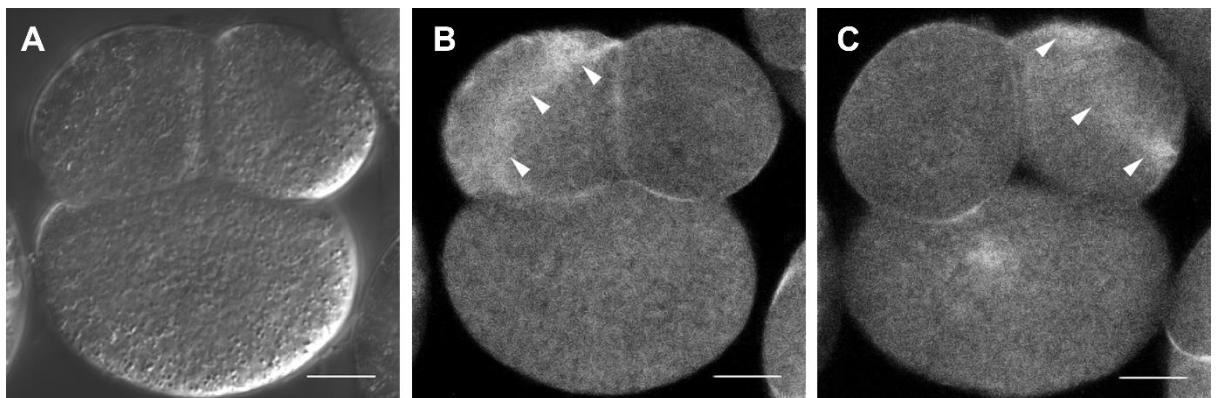


Figure 4.8 Confocal micrographs showing the contractile actin ring failed to form in the non-dividing blastomere of a malformed embryo created by DBP-impaired spermatozoa. The actin filaments were visualised using BODIPY® FL phalloidin (grey). Scale bars = 20 µm. (A) Light micrograph of a typical 3-cell malformed embryo. (B - C) Two confocal micrographs captured at different level showing the presence of actin filaments in the two smaller blastomeres of the 3-cell embryo. Distinct contractile actin rings could be observed in the two dividing blastomeres, which appeared as a white band along the equatorial plate. No sign of contractile actin ring was observed in the non-dividing blastomere, indicating a failure to form the contractile ring.

4.4.5 DBP induced acrosome and centriole damage in the spermatozoa which respectively led to embryonic arrest and malformation

As revealed by the sperm- and oocyte-exposure tests, within the test concentration range, the decreased success of early embryogenesis and the elevated occurrence of abnormal embryos were all attributable to DBP-induced sperm dysfunction. The confocal microscopic studies further demonstrated that fertilisation involving DBP-impaired spermatozoa resulted in defective spindle microtubules. In the embryos of *G. caespitosa*, the spindle microtubules originated from the centrioles that were inherited from the male germline during fertilisation. Therefore, the embryonic malformation was possibly derived from DBP-mediated impairment of the sperm centriole. Given the above implications, we conducted a series of sperm analyses to uncover the mechanism of how the DBP-induced sperm dysfunction led to embryonic arrest and abnormality.

4.4.5.1 DBP did not affect the sperm motility

The sperm motility assay was conducted to determine if the dose-dependently decreased success of embryogenesis was caused by DBP-induced sperm motility loss in the sperm-exposure test. In the absence of DBP, about 79% of the spermatozoa exhibited motility of various grades (**Figure 4.9**); the majority of these motile spermatozoa displayed a

forward and fast movement, while a small number of the motile spermatozoa swam sluggishly or in circles. In the DBP-treated samples, the spermatozoa also displayed rapid progressive movement. The addition of DBP to the spermatozoa had no statistically significant effect on the sperm motility, which exhibited similar motility rates of approximately 77%.

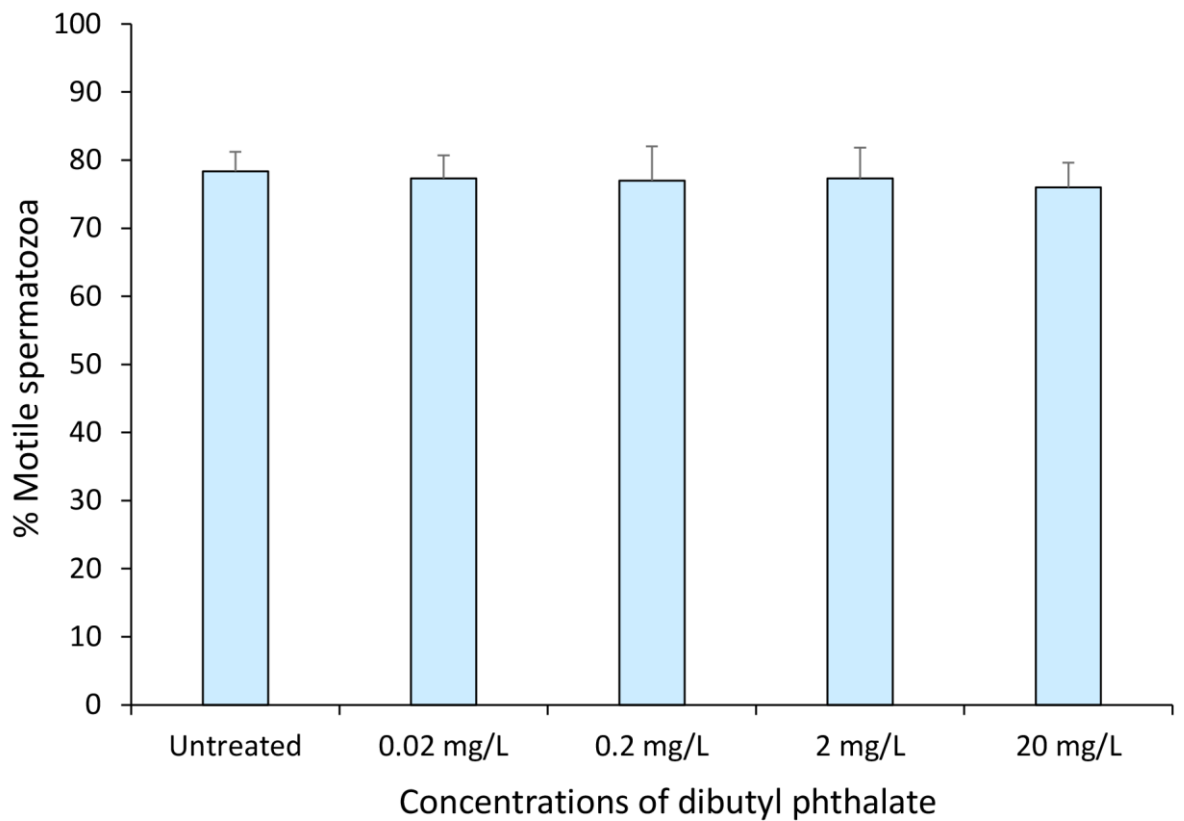


Figure 4.9 DBP did not cause sperm motility loss. According to the data analyses between the motility rates of untreated and DBP-treated samples, no statistically significant difference was detected, indicating DBP did not induce sperm motility loss within the designated concentration range.

4.4.5.2 DBP did not induce significant sperm DNA damage

Whether exposure of spermatozoa to graded concentrations of DBP would result in oxidative DNA damage was determined by measuring the expression of the biomarker 8-hydroxy-2'-deoxyguanosine (8-OH-dG) using flow cytometry. As shown in **Figure 4.10**, no significant difference was detected between the levels of 8-OH-dG expressed in untreated and DBP-treated groups ($P > 0.05$), suggesting the degree of oxidative DNA damage in the spermatozoa did not change with the increase of DBP concentration.

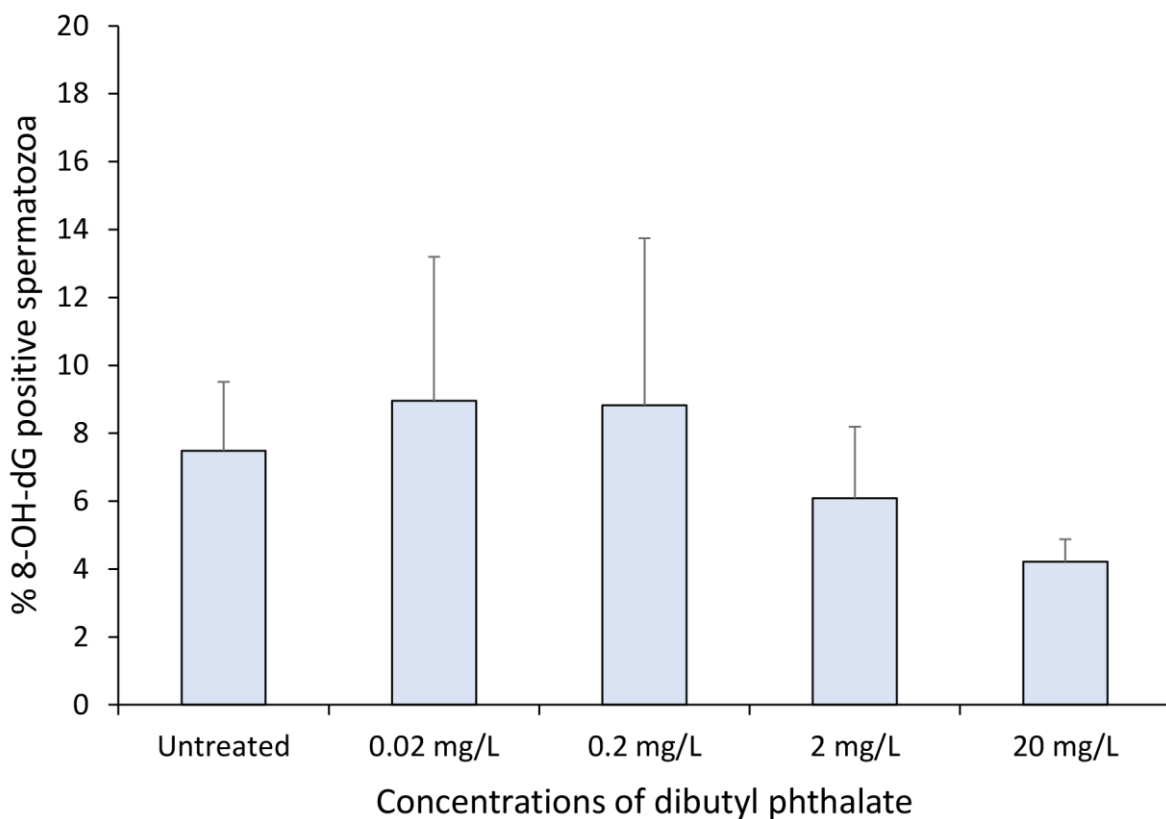


Figure 4.10 DBP did not induce oxidative DNA damage in the spermatozoa. The sperm samples were treated with graded concentrations of DBP and probed with FITC-conjugated anti-8-OH-dG to measure the level of oxidative DNA damage. Within the tested concentration range, DBP was unable to induce statistically significant elevation of oxidative DNA damage in the spermatozoa.

4.4.5.3 DBP inhibited the activity of superoxide dismutase in the spermatozoa

The activity of superoxide dismutase (SOD) in the DBP-treated spermatozoa was reflected by the intensity of chemiluminescence signals. By plotting the concentrations of DBP against the intensity of chemiluminescence signals in the spermatozoa, it was obvious that a strong correlation existed between the two parameters ($R^2 = 0.700$; **Figure 4.11**). As the concentration of DBP increased from 0 to 5 mg/L, the DBP-induced inhibitory effect on the SOD activity became increasingly stronger, with the 5 mg/L DBP-treated spermatozoa giving high luminescence signals that were nearly twice as much as the signals detected in the untreated sample (**Figure 4.11**). When the DBP concentration increased from 5 to 20 mg/L, the inhibitory effect on the SOD activity was slightly decreased, reflected by the slightly decreased signal intensity. Nevertheless, the intensity of luminescence signals detected in these treatments was still higher than that of the lower DBP concentrations ranging from 0 to 2.5 mg/L, demonstrating that high DBP concentrations (5 to 20 mg/L) still induced an inhibitory effect on the activity of SOD.

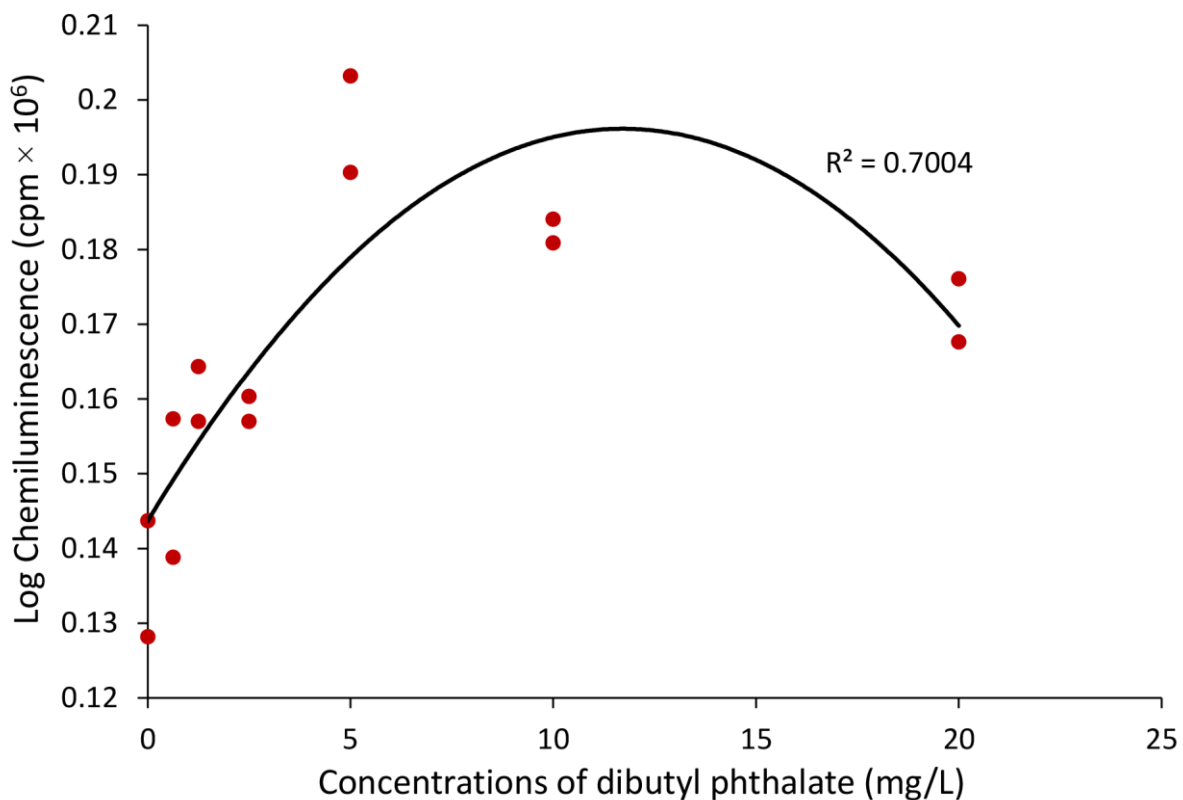


Figure 4.11 DBP inhibited the activity of SOD in the spermatozoa. With the concentration of DBP increased from 0 to 5 mg/L, the intensity of luminescence signal was dramatically increased, indicating the activity of SOD in the spermatozoa decreased with the elevation of DBP concentration. The intensity of luminescence signal reached its peak at 5 mg/L of DBP treatment and was slightly reduced when the concentration of DBP increased further.

4.4.5.4 DBP induced lipid peroxidation in the acrosome and sperm neck

The biomarker 4-HNE was applied to detect if lipid peroxidation occurred in the DBP-impaired spermatozoa. To achieve a more precise determination of immunolocalisation in the spermatozoa, the detailed ultrastructure of a spermatozoon in *G. caespitosa* was supplied in **Figure 4.12A**.

The spermatozoa which were not subject to lipid peroxidation exhibited no fluorescent staining (**Figure 4.12B**). In the DBP-impaired spermatozoa, lipid peroxidation was generally detected at the acrosomal region and the sperm neck. Based on the positions of

the fluorescent labels, these 4-HNE positive spermatozoa could be divided into three types: the ones whose neck region being solely labelled (**Figure 4.12C and D**); the ones with only the acrosomal region being highlighted (**Figure 4.12E**); and the ones being labelled at both the neck and acrosomal regions (**Figure 4.12F**).

With the assist of the ultrastructure of spermatozoa in *G. caespitosa*, it was clear that in the neck-labelled spermatozoa, the anti-4-HNE bound to the initial segment of the sperm flagellum, rather than the adjacent cytoplasmic membrane or the mitochondria in the midpiece (**Figure 4.12A**). Such fluorescence pattern was further confirmed by the immunofluorescent labelling displayed in a decapitated 4-HNE positive spermatozoon in **Figure 4.12D**. In this spermatozoon, two individual fluorescent spots were observed at the anterior tip of the flagellum (**Figure 4.12D**), indicating that lipid peroxidation happened in the centrioles. The spermatozoa being solely labelled at the acrosomal region exhibited an arc-shaped fluorescent signal lining the anterior region of the acrosome (**Figure 4.12E**). Instead of the acrosome itself being labelled, the fluorescence targeted the cytoplasmic membrane at the acrosomal region. Apart from these two patterns of fluorescent labelling, a considerable amount of DBP-treated spermatozoa was stained at both the acrosomal and neck regions (**Figure 4.12F**), indicating the lipid peroxidation occurred at both positions simultaneously.

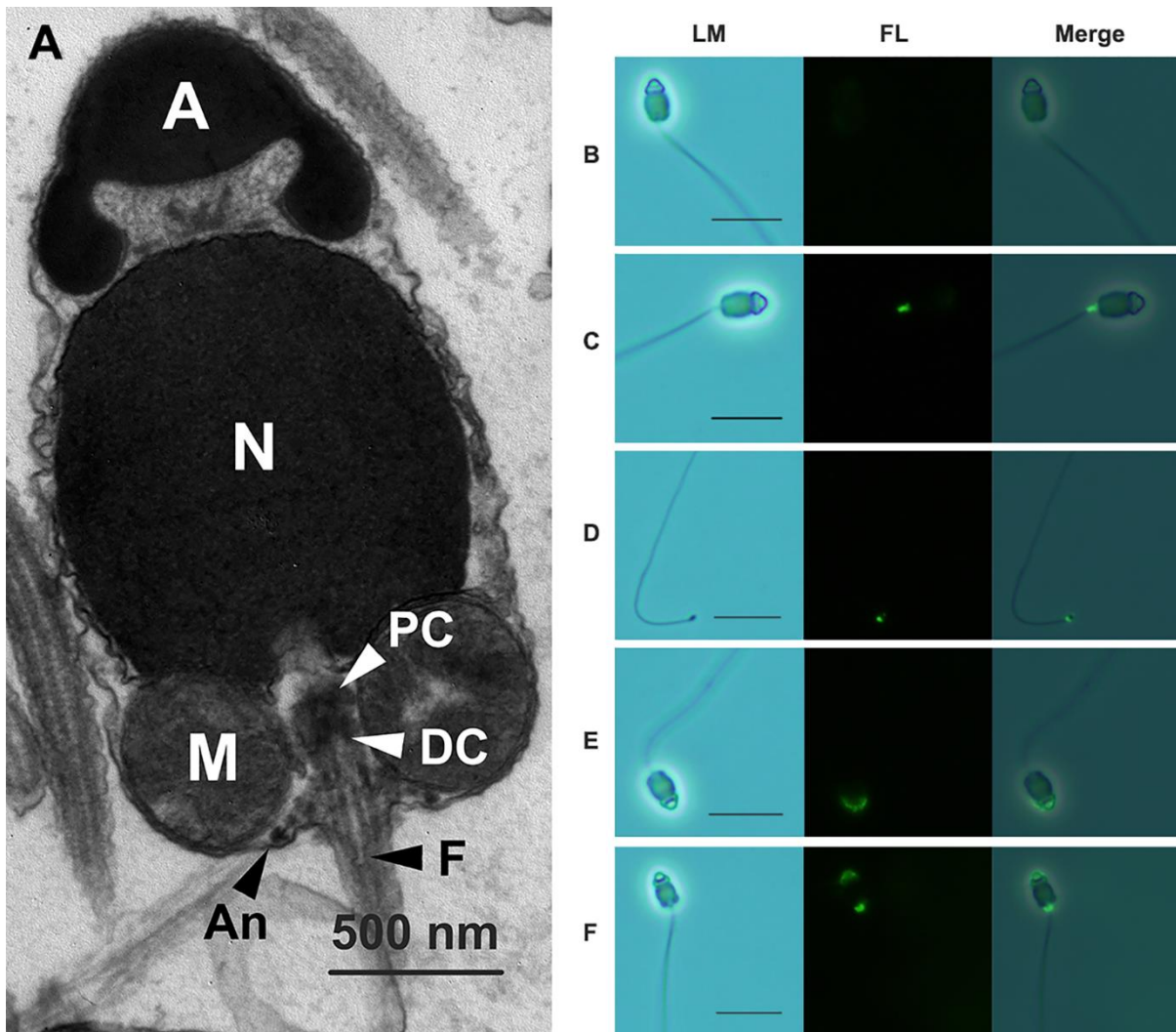


Figure 4.12 DBP induced lipid peroxidation on the sperm neck and acrosomal regions revealed by the biomarker 4-HNE. The sperm samples were treated with graded concentrations of DBP and probed with anti-4-HNE antiserum. On the left panel, the immunolocalisation was displayed in an order of the light microscope image (LM), the fluorescence microscope image (FL) and the overlay of the brightfield and fluorescence images (Merge). Scale bars = 10 µm. (A) Transmission electron micrograph of a spermatozoon in *G. caespitosa*. The ultrastructure of spermatozoa was provided to achieve a more precise determination of immunolocalisation. In the spermatozoon, the sperm head was comprised of a cap-like acrosome (A), an oval-shaped nucleus (N) and a short midpiece containing four spherical mitochondria (M). The proximal centriole (PC) was surrounded by the mitochondria and in close proximity to the implantation fossa located at the posterior end of the nucleus. The distal centriole (DC) oriented perpendicularly to the proximal centriole and formed a formative flagellum (F). A ring-shaped annulus (An) was located intracellularly at the junction of the midpiece and flagellum. (B) An untreated spermatozoon with no fluorescent staining. (C) A DBP-impaired spermatozoon with its neck region being solely

labelled. In the neck-labelled spermatozoa, the anti-4-HNE targeted the initial segment of the flagellum. **(D)** A decapitated 4-HNE positive spermatozoon showing the fluorescence targeted the anterior portion of the flagellum. Remarkably, two individual fluorescent spots were observed at the initial segment of the tail, suggesting the centrioles were targeted by the anti-4-HNE. **(E)** A DBP-treated spermatozoon with its acrosomal region being labelled. Instead of the acrosome itself being labelled, the fluorescent signal in these spermatozoa appeared an arc-shape and targeted the cytoplasmic membrane surrounding the acrosomal region. **(F)** A DBP-treated spermatozoon with both its neck and acrosomal regions being labelled. A considerable portion of DBP-treated spermatozoa was labelled simultaneously at both the neck and acrosomal regions, indicating both regions were subjected to DBP-induced lipid peroxidation.

According to the immunolocalisation of 4-HNE in the DBP-impaired spermatozoa, lipid peroxidation mainly occurred at the acrosomal region and sperm neck. To determine if such patterns of 4-HNE expression were correlated with the concentrations of DBP that the spermatozoa were exposed to, the percentages of acrosome- and neck-positive spermatozoa were scored respectively. As a portion of the spermatozoa were simultaneously labelled at both regions, the total percentages of 4-HNE positive spermatozoa, regardless of the fluorescence pattern, were also recorded.

As shown in **Figure 4.13**, the amount of lipid peroxidation expressed at the acrosomal region of DBP-treated spermatozoa was significantly higher than the untreated control when the concentration of DBP was at 2.5 mg/L and higher. The increase in 4-HNE expression at the sperm neck became statistically significant when the concentration of DBP was equal or higher than 5 mg/L. Moreover, the amount of lipid peroxidation expressed in the spermatozoa, regardless of the location of expression, was significantly increased when the spermatozoa were exposed to 5 and 20 mg/L of DBP. Overall, the exposure of spermatozoa to increasing concentrations of DBP resulted in the percentages of acrosome-positive, neck-positive and total-positive spermatozoa all increasing in a

dose-dependent manner, suggesting the DBP-induced lipid peroxidation in the spermatozoa became more severe with the elevation of DBP concentration.

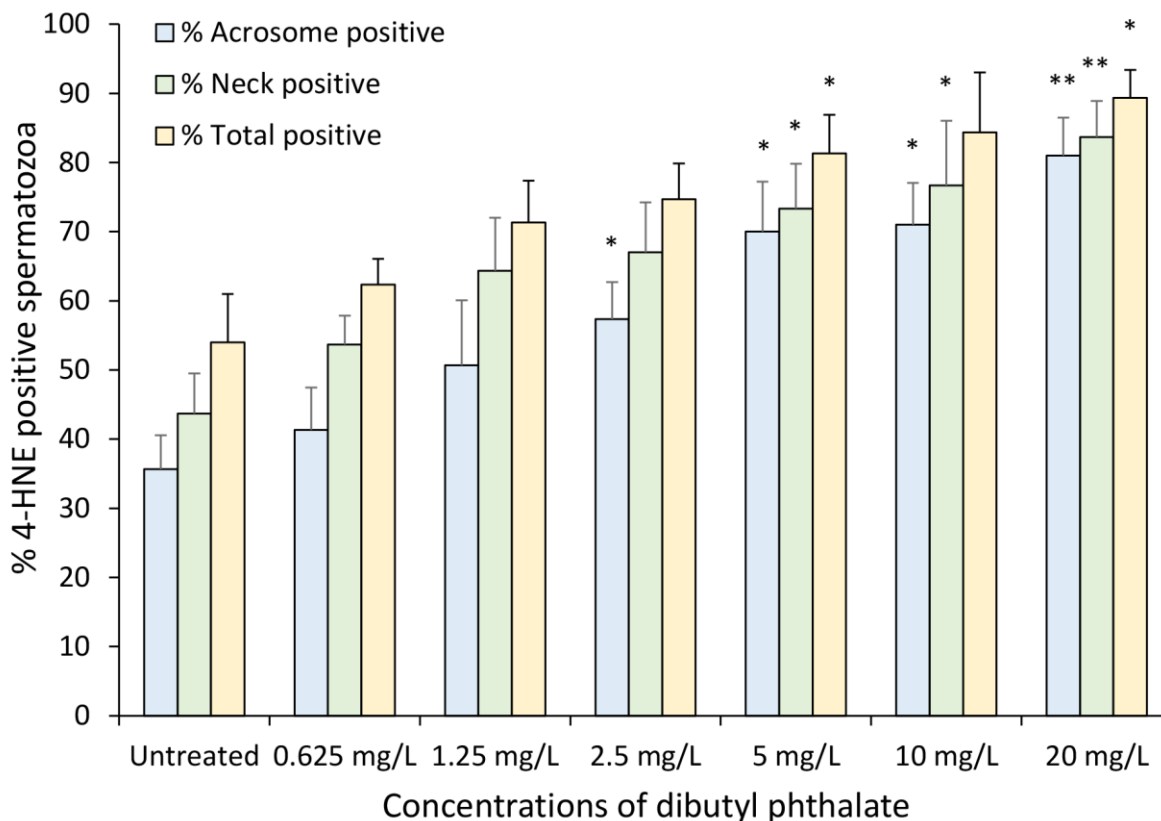


Figure 4.13 DBP-induced lipid peroxidation in the spermatozoa increased with the elevation of the DBP concentration. The sperm samples were treated with graded concentrations of DBP and probed with anti-4-HNE antiserum. In this column graph, the acrosome/neck positive columns indicated the percentages of spermatozoa that were labelled at the acrosomal/neck region and the total positive columns represented the total percentages of spermatozoa that were 4-HNE positive, regardless of the location of the fluorescent labelling. Based on the data analysis, with the elevation of the DBP concentration, the percentages of spermatozoa that were acrosome, neck and total positive were all increased in a dose-dependent manner (acrosome positive, $P < 0.01$; neck positive, $P < 0.05$; total positive, $P < 0.05$). *, $P < 0.05$; **, $P < 0.01$.

4.4.5.5 4-HNE-treated spermatozoa produced malformed embryos with the typical pattern of abnormality

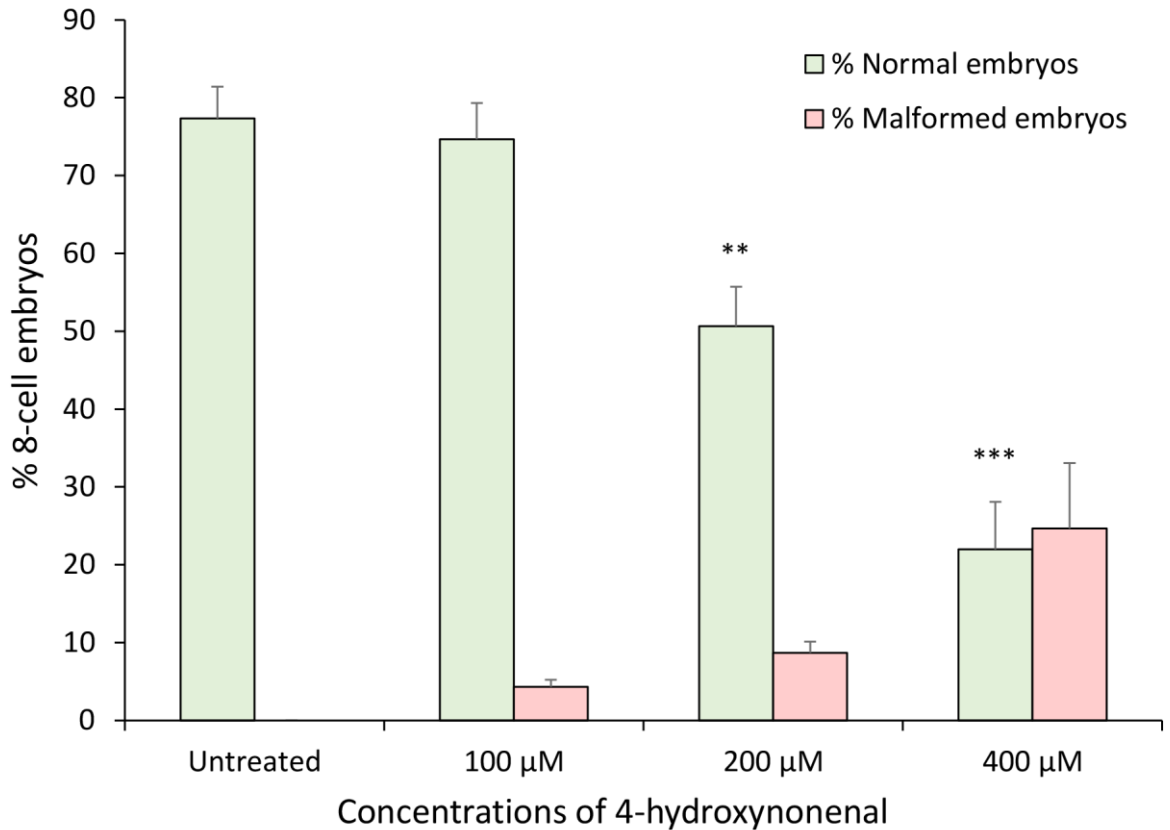


Figure 4.14 4-HNE-impaired spermatozoa led to decreased success of embryogenesis and increased incidence of the typical embryonic malformation. Spermatozoa were initially exposed to 4-HNE for 15 min, followed by the addition of freshly collected oocytes. The rates of normal developed embryos and malformed embryos with the typical abnormal morphology were respectively scored at 8-cell stage. The exposure of spermatozoa to graded concentrations of 4-HNE resulted in a significant dose-dependent suppression of normal early development ($P < 0.001$). With the elevation of 4-HNE concentration, the occurrence of the typical malformed embryos also increased in a dose-dependent manner ($P < 0.001$). Note, the red columns only represented the percentages of the embryos that exhibited the common pattern of abnormality; arrested embryos or abnormal embryos with a different pattern of abnormality were not included. **, $P < 0.01$; ***, $P < 0.001$.

To determine whether the typical embryonic abnormalities described earlier could be attributed to the DBP-induced production of 4-HNE, the effects of exposing spermatozoa

to graded concentrations of 4-HNE on subsequent early embryogenesis were assessed. As illustrated in **Figure 4.14**, as the concentration of 4-HNE increased from 0 to 400 μM , the percentage of embryos that successfully developed into normal 8-cell embryos declined in a dose-dependent manner ($P < 0.001$). The 4-HNE-induced inhibitory effect on the success of embryogenesis became apparent when the concentration was higher than 100 μM .

The majority of the 4-HNE-induced abnormal embryos exhibited the same defective morphological pattern as recorded during the DBP toxicity testing. Likewise, after undergoing the first mitotic division, one blastomere of the 4-HNE-induced abnormal embryo was unable to carry out further cleavage, while the other one continuously divided as usual. As the concentration of 4-HNE increased from 100 to 400 μM , the occurrence of the typical malformed embryos increased in a dose-dependent manner ($P < 0.001$; **Figure 4.14**). Remarkably, the incidence of typical abnormal embryos at 400 μM of 4-HNE treatment reached an extremely high percentage of about 25%, which was even higher than the average rate of normal developed embryos in the same treatment group.

4.5 Discussion

The majority of marine polychaetes, including *G. caespitosa*, are broadcast-spawners which shed their gametes directly into the surrounding water column where subsequent fertilisation occurs. This spawning strategy renders their gametes continuously exposed to hazardous substances in the local environment before, during and after fertilisation. Such pre-fertilisation exposure to contaminants may cause sperm or oocyte dysfunction, which, in turn, might lead to a disturbance in both fertilisation and other post-fertilisation events such as embryogenesis, larval development and larval settlement. This study has clearly demonstrated that the damage observed following exposure to DBP is mediated *via* the male not the female germline. This paternally-mediated pathway for pollutant-induced embryonic disruption has been neglected by the majority of traditional embryotoxicity tests on broadcast-spawning species, where the toxicants were mainly applied to fertilised eggs or developing embryos. Since embryos are less susceptible to pollutant-damage than gametes, these prior toxicity studies may have underestimated the deleterious effects that such chemicals may have upon the related biosphere. Besides, notwithstanding the large number of toxicity tests which have been conducted on marine invertebrates using a wide range of toxic chemicals, very few studies looked into the underlying mechanism that led to the decreased rates of embryonic development or the increased occurrence of malformed embryos.

Comparative toxicities of six representative PAEs, including benzyl butyl phthalate (BBP), diallyl phthalate (DAP), dibutyl phthalate (DBP), diethyl phthalate (DEP), dimethyl phthalate (DMP) and dioctyl phthalate (DOP) were examined by our laboratory on the early embryogenesis of *G. caespitosa* (see **Chapter 5** for details). Based on the severity of the disruption that 20 mg/L of these PAEs caused on the early development,

their toxicity order has been determined as follows: DBP > BBP \approx DAP > DOP > DEP \approx DMP. Among these six compounds, the DBP-treated samples exhibited the most significant inhibitory effect on the success of early development and a highest incidence of embryonic malformations.

In the research described in this chapter, the effects of a widely used plasticiser DBP on the normal functioning of spermatozoa and oocytes were examined in conjunction with the normality of subsequent early embryonic development. Since oocyte exposure to low concentrations of DBP (≤ 15 mg/L) neither suppressed the success of embryogenesis nor caused any embryonic malformation, the decreased success of early development and increased occurrence of malformed embryos observed in the sperm-exposure test were all attributed to the DBP-induced sperm impairment. Interestingly, the malformed embryos created by DBP-impaired spermatozoa exhibited a uniform pattern of abnormality. After undergoing the first cleavage as usual, one of the two blastomeres in the malformed embryos stopped dividing, while the other blastomere was able to carry out further mitotic divisions. As a result, the malformed embryos appeared as a 3-cell embryo after the first two divisions. Such a unique pattern of embryonic abnormality was also observed when the spermatozoa of *G. caespitosa* were exposed to other representative endocrine disrupting compounds (EDCs), including BBP, DAP, DBP, DEP, DMP, DOP and bisphenol A. These compounds, along with DBP might share a similar mechanism for creating malformed embryos. Therefore, the current research provides a model for how acute exposure of spermatozoa to EDCs induces sperm damage, which then causes cytoskeletal disruptions in early embryogenesis.

Utilising confocal microscopy, we discovered that the DBP-impaired spermatozoa created malformed embryos with defective spindle fibres, which were shortened,

irregularly bent and unable to anchor to the cortex. Morphologically abnormal spindle apparatus has been demonstrated to cause defective segregation of chromosome in the early embryos of rodent species (Burrue *et al.*, 2013). Indeed, we found that the chromosomes in the malformed embryos failed to align properly along the equatorial plate and the chromosomes were irregularly segregated, as reflected in the solitary/unpaired chromatids found in these embryos. Such errors during the alignment and segregation of chromatids were derived from the spindle fibres incompletely anchoring to the cortex, which rendered the spindle apparatus physically unstable and unable to separate homologous chromosomes properly. During embryogenesis, the fidelity of chromosome segregation must be maintained stringently so as to guarantee faithful inheritance of genetic materials. Defective chromosome segregation leads to a state of genomic instability (i.e. aneuploidy), which is characterised by an increased occurrence of chromosome nondisjunction or abnormal chromosome number (Draviam *et al.*, 2004). As demonstrated in this study, the malformed embryos experienced defective segregation of chromosomes during the first cleavage, which resulted in the production of two potentially aneuploid blastomeres. The blastomere experiencing chromosome loss might not be able to carry out the further development resulting in compromised embryonic viability. In this study, we discovered that the arrested blastomere experienced retarded karyokinesis and was unable to carry out normal cytokinesis. The lack of cytokinesis in the non-dividing blastomere was, in turn, caused by a failure to form the contractile actin ring. The spindle microtubules are not only responsible for the regulation of chromosome segregation, but are also involved in dictating the positions of the cleavage furrows and contractile actin ring (Straight and Field, 2000). The microtubules must communicate with the cortex to mark the position for the assembly of cleavage furrows, guide the actin and myosin to assemble at this site

and stimulate the ingression of the cleavage furrow (Straight and Field, 2000). The failure to assemble contractile ring in the arrested blastomere might also be attributed to the spindle fibres failing to communicate with the cortex through a proper microtubule anchoring process.

Paternal inheritance of centrosome (including the centrioles and pericentriolar matrix) at fertilisation has been found in most species, except for the mouse embryos, where the maternal centrosome forms bipolar spindles during embryonic cleavages (Sathananthan *et al.*, 1996; Schatten *et al.*, 1986). Since the sperm centrosome acts as the microtubule-organising centre during embryogenesis, any defect in the microtubule spindle might be derived from dysfunction of the paternal centriole. Given this implication, we investigated the mechanisms underlining the DBP-induced sperm damage.

Phthalate esters have been repeatedly found to induce negative impacts on the scavenging process of reactive oxygen species (ROS) by inhibiting the activity of antioxidant enzymes [e.g. BBP (Mankidy *et al.*, 2013), DBP (Farombi *et al.*, 2007; Mankidy *et al.*, 2013) and DOP (Wang *et al.*, 2012)]. In the present study, using lucigenin-dependent chemiluminescence, we found that DBP suppressed the activity of SOD in the spermatozoa ($R^2 = 0.70$). This antioxidant enzyme plays an important role in the defence against oxidative stress that superoxide anions pose on biological systems. The assay conducted by Prasanth *et al.* (2009) revealed that SOD exposure to DBP would result in the activity of this enzyme declining proportionately to the concentration of DBP that was introduced. Their molecular docking studies demonstrated that DBP is able to bind to the active site of SOD by forming hydrogen bonds with the active site residue R143. This residue is crucial in the binding of ROS during its conversion to hydrogen peroxide and molecular oxygen. Therefore, DBP hydrogen bonded to R143 occupies the binding site

of ROS, thereby leading to complete or partial inhibition of the activity of this enzyme (Prasanth *et al.*, 2009).

Apart from the PAEs, a broad range of environmental contaminants have been found to induce peroxidative damage in marine organisms. Spermatozoa are extraordinarily vulnerable to such stress due to their capacity to spontaneously generate ROS as well as their abundant endowment with polyunsaturated fatty acids and DNA, both of which are major substrates for free radical attack (Aitken and Clarkson, 1987; Aitken *et al.*, 1989). Because of their extremely limited cytoplasmic space, spermatozoa contain limited amounts of cytosolic antioxidant enzymes (e.g. catalase, SOD and glutathione peroxidase) that protect somatic cells from oxidative damage (Aitken *et al.*, 2010a). As indicated by Alvarez *et al.* (1987), the rates of lipid peroxidation in human spermatozoa exhibited a strong positive correlation ($R = 0.97$) with the SOD activity, suggesting this antioxidant acts as the primary enzymatic defence that compensates lipid peroxidation in spermatozoa. In the current study, with the increase of DBP concentration, the activity of SOD declined, resulting in a potential increase in the bioavailability of superoxide anions. The elevated amount of superoxide radicals would, in turn, be expected to initiate lipid peroxidation by converting to the protonated form and abstracting an allylic hydrogen from a polyunsaturated side chain to create a lipid radical (McCord, 2008). Indeed, according to our immunocytochemical analysis, elevated expressions of 4-HNE in the spermatozoa were detected in high concentrations of DBP treatments, indicating that the suppression of SOD activity was negatively related to the degree of lipid peroxidation in the spermatozoa. The study conducted by Farombi *et al.* (2007) also demonstrated that DBP induced testicular damage in rats by inhibiting the level of ROS scavenging enzymes,

such as glutathione, catalase and SOD, in turn, resulted in an elevated level of lipid peroxidation manifested in increased levels of testicular malondialdehyde (MDA).

In human spermatozoa, lipid peroxidation is usually accompanied with the generation of the electrophilic aldehyde 4-HNE, which targets the mitochondria in the midpiece and decreases mitochondrial membrane potential, which in turn leads to sperm motility loss (Aitken *et al.*, 2012b; Kasai *et al.*, 2002). Interestingly, in *G. caespitosa*, although the high concentration DBP-treated spermatozoa were subject to lipid peroxidation, their motility was not affected. Immunolocalisation analysis indicated that the production of 4-HNE occurred at both the plasma membrane at the acrosomal region and the sperm neck. As learnt from the ultrastructure of spermatozoa, the neck region of sperm in this species resides between the midpiece and the flagellum. The fluorescent pattern clearly indicated that the midpiece had never been targeted by 4-HNE, possibly suggesting why motility was unimpaired; instead, it was the junction of midpiece and flagellum that was labelled. The lack of an effect on motility is important and supported by data obtained on sperm motility in response to DBP in the European pikeperch, *Sander lucioperca* (L.), which also exhibits external fertilisation. In this species, concentrations of DBP up to 10 mg/L did not decrease sperm motility (Jarmolowicz *et al.*, 2010).

ROS-induced sperm DNA damage may also be a mechanism leading to abnormal sperm function and impaired embryonic development, given previous studies demonstrating that PAEs are able to induce DNA fragmentation in human spermatozoa (Duty *et al.*, 2003; Hauser *et al.*, 2007). However, DBP was found to induce no significant sperm DNA damage in this study. In the majority of animal species, except for mammals, the early cleavage of embryos is solely dependent on maternal proteins and mRNAs stored in the oocyte. During these early stages of embryogenesis, the zygotic genome is not activated

and does not participate in the regulation of cell division. The maternally stored mRNAs gradually diminish during the first several embryonic cleavages, after which the control of embryonic development transits from the maternal to the zygotic genome (Barckmann and Simonelig, 2013). In this case, even if the sperm DNA has been damaged, it would not affect the rapid early mitotic divisions of the embryos, during which the zygotic genome has not yet been activated. Therefore, the embryonic arrest and abnormality occurred at early cleavages would not be expected to originate from phthalate-induced paternal DNA damage.

The immunofluorescence detected in association with the plasma membrane at the acrosomal region demonstrated the elevated binding of 4-HNE at this site. Since these spermatozoa had never been exposed to the jelly coats of *G. caespitosa* oocytes, they were not acrosome-reacted. Instead of facilitating the upcoming sperm-oocyte interaction, the lipid peroxidation occurring in these spermatozoa would be expected to decrease membrane fluidity and jeopardise membrane integrity. In this case, the fertilisation-related activities that are highly dependent on the membrane fluidity (e.g. sperm-oocyte fusion, acrosome reaction) would be negatively affected (Aitken *et al.*, 1989; Griveau *et al.*, 1995), thereby resulting in the failure of sperm incorporation and a subsequent decrease in the success of embryogenesis (**Figure 4.3**).

Excessive production of intracellular ROS can alter protein structure by modifying the side chains of amino acid, resulting in functional changes in the protein (Cabiscol *et al.*, 2010). The end products of lipid peroxidation, 4-HNE and MDA themselves can also cause protein damage by forming stable adducts with cysteine, lysine, or histidine residues and thereby impair protein structure and function (Schutt *et al.*, 2003). In the current study, conspicuous expression of 4-HNE was detected at the neck region where

the sperm centrioles reside. An elevated amount of 4-HNE binding to this site would be expected to cause damage to the centrosome, which contains abundant proteins in the pericentriolar matrix, and thereby impairing the normality of cell division in the embryo.

In conclusion, this study assessed the toxic effect of a widely used plasticiser, DBP, on the normal functioning of spermatozoa and oocytes as well as subsequent early embryogenesis in a potential bio-indicator species *G. caespitosa*. Through the toxicity tests, we demonstrated that DBP-induced sperm dysfunction, led to significant embryonic arrest and malformation with a uniform pattern. By conducting a series of sperm analyses, we further uncovered that DBP could suppress the activity of SOD in the spermatozoa, which caused lipid peroxidation at both the acrosomal and neck regions of the cell. It is held that lipid peroxidation occurring in the acrosomal region of the spermatozoa would result in a failure of the acrosome reaction, which would in turn account for the observed decrease in rates of fertilisation and subsequent embryo development. The lipid peroxidation observed at the sperm neck, on the other hand, is held to cause sperm centriole damage by modifying protein structure. The oxidised sperm centriole inherited by the embryo during fertilisation, has been observed to generate microtubule disruption resulting in errors during chromosome alignment and segregation. The incomplete microtubule anchoring to the cortex and chromosome loss in the blastomeres might attribute to the observed retarded karyokinesis and failure to assemble the contractile actin ring. The results obtained from this study support our proposal that the abnormal embryogenesis in *G. caespitosa* can be used as a sensitive indicator for phthalate-induced marine pollution. Apart from an environmental concern about the use and disposal of plasticisers, this study also highlights the significant role that sperm centriole plays in the

normal functioning of spermatozoa and in the success of the subsequent embryonic development.

Chapter 5

Effects of bisphenol A, alkylphenols and phthalate esters on the early embryogenesis in *Galeolaria caespitosa*

5.1 Overview

In this chapter, the toxic effects of endocrine disrupting compounds bisphenol A (BPA), six alkylphenols [APs; butylphenol (BP), pentylphenol (PP), hexylphenol (HP), heptylphenol (HPP), octylphenol (OP) and nonylphenol (NP)] and six phthalate esters [PAEs; benzyl butyl phthalate (BBP), diallyl phthalate (DAP), DBP, diethyl phthalate (DEP), dimethyl phthalate (DMP) and dioctyl phthalate (DOP)] were examined on early embryogenesis in the marine invertebrate *Galeolaria caespitosa*. The overall purpose of these studies was to determine the feasibility of using the gametes and early stages of embryonic development in this species as indicators for pollution monitoring. By conducting sperm- and oocyte-exposure tests, all chemicals were found to decrease the rate of early embryogenesis by impairing the male germline. Except for the six APs, exposure of spermatozoa to BPA and PAEs resulted in elevated incidences of embryonic malformation and the resultant malformed embryos exhibited a common pattern of abnormality, as was previously observed during the DBP toxicity testing. By calculating the chemical concentrations that disabled half the number of the embryos from undergoing normal development (IC_{50}), the toxicity order of APs and PAEs were as follows: HP > NP > HPP > OP > BP > PP; DBP > BBP > DAP > DOP > DEP > DMP. While the APs with higher molecular weights tended to induce more severe inhibitory effects on embryogenesis, the toxicity of PAEs was not necessarily related to their molecular mass. By making comparisons with the EC_{50}/LC_{50} of other species based on various experimental endpoints, it was clear that the spermatozoa and early development of *G. caespitosa* could serve as sensitive indicators to BPA, HP, HPP, OP, NP and DBP. Although species with high sensitivity can be readily found for each chemical, the toxicity studies conducted in this chapter provided a rapid and repeatable method for the detection

of tested chemicals in *G. caespitosa*. Specifically, the atypical pattern of embryonic development observed during BPA and PAEs, was a highly sensitive indicator for the presence of these two estrogen-like compounds.

5.2 Introduction

A large variety of man-made chemicals are capable of adversely affecting the wellbeing of marine organisms. Bisphenol A (BPA) is one of the most important industrial chemicals synthesised for manufacturing polycarbonate plastics, epoxy resin production, and other products such as specialty resins and flame retardants (Haubruge *et al.*, 2000; Nakagawa and Tayama, 2000; Özlem and Hatice, 2008; Sajiki and Yonekubo, 2003; Sakaue *et al.*, 2001). It usually enters the environment through permitted discharges of treated industrial wastewater into terrestrial, freshwater, and marine environments (Özlem and Hatice, 2008).

Among a large variety of alkylphenols (APs), nonylphenol (NP) and octylphenol (OP) has attracted the attention of researchers in recent years due to the toxic effects of these chemicals on living organisms (Kim *et al.*, 2006). NPs are utilised in lubricant oil, cosmetics, emulsifiers, plastics, latex paints, household and industrial detergents, and paper and textile industries (Arslan *et al.*, 2007). OPs are employed in electrical insulating varnishes, ethoxylated resins, printing inks, pesticide formulations, water-based paints and textile auxiliaries, as well as for emulsion polymerization (Arslan and Parlak, 2007; Arslan *et al.*, 2007). It has been estimated that approximately 300,000 tons of APs are produced per year, 60% of which is discharged into the aquatic environment where it is converted into the biodegradation products NP and OP (Arslan and Parlak, 2007). These chemicals enter the environment predominantly as industrial and domestic waste and as effluent from waste treatment plants, but contamination also occurs directly *via* pesticide practices. Apart from the surfactant toxicity associated with NP and OP, these compounds are also endocrine disrupting compounds that can mimic hormones in vertebrates (Arslan *et al.*, 2007; Kim *et al.*, 2006). Toxicity studies indicated that these chemicals can also

induce significant damage on the developing embryos and larvae of marine invertebrates. Due to the lipophilic property of these APs, they are readily accumulated in aquatic species and are commonly found in sediments. OP is classified as a very toxic chemical to aquatic organisms, because it is not easily degraded in the environment and has been readily detected in surface waters. Furthermore, NPs are relatively easily degraded in the environment to form short-chained nonylphenol ethoxylates (NPEs), which are even more toxic to organisms (Arslan and Parlak, 2007).

The current study aimed to analyse the sensitivity of spermatozoa in *G. caespitosa* to a wide range of common marine pollutants (BPA, APs and phthalate esters), as reflected in the subsequent success of embryogenesis. Through these toxicological studies, the feasibility of using *G. caespitosa* as bio-indicator species could be assessed.

5.3 Materials and Methods

5.3.1 Sample collection and maintenance

Aggregations of *Galeolaria caespitosa* were collected from Nobbys Beach and maintained in the laboratory as described in **Section 4.3.1, Chapter 4**. Likewise, all toxicity tests were conducted within 10 days of sample collection.

5.3.2 Toxicity tests

The gametes of *G. caespitosa* were prepared and all toxicity tests were performed as described in **Section 4.3.2.1, Chapter 4**.

Bisphenol A (BPA), the six alkylphenols [APs; butylphenol (BP), pentylphenol (PP), hexylphenol (HP), heptylphenol (HPP), octylphenol (OP) and nonylphenol (NP)] and the six phthalate esters [PAEs; butyl benzyl phthalate (BBP), diallyl phthalate (DAP), dibutyl phthalate (DBP), diethyl phthalate (DEP), dimethyl phthalate (DMP) and dioctyl phthalate (DOP)] were all purchased from Sigma Aldrich (Castle Hill, Australia) with a purity over 98%. The stock solutions of PAEs were prepared in absolute acetone at a concentration of 100 g/L and serially diluted with filtered natural seawater (FSW). BPA and APs were dissolved in dimethyl sulfoxide (DMSO) to make stock solutions at a concentration of 10 g/L before serial dilutions into designated concentrations. The test concentrations of BPA used in this study were 1.25, 2.5, 5 and 10 mg/L and those of APs were 0.005, 0.05, 0.5 and 5 mg/L. The test concentrations of PAEs were displayed in **Table 5.1**. Except for DOP, the concentrations of all other PAEs were predetermined based on the dose-response curve obtained from pilot studies. The maximal concentration of DOP was set at 20 mg/L because DOP could not be dissolved in FSW at concentrations higher than 20 mg/L even with the assistance of the vehicle, acetone.

Table 5.1 Test concentrations of the six phthalate esters.

	Test concentrations (mg/L)			
BBP	3.125	6.25	12.5	25
DAP	3.125	6.25	12.5	25
DBP	0.02	0.2	2	20
DEP	20	40	60	80
DMP	25	50	100	200
DOP	5	10	15	20

As DMSO was utilised during BPA and APs toxicity testing, its toxicity to the spermatozoa and oocytes was examined in the first instance. The gametes were exposed to 1% (v/v) DMSO in FSW, which was higher than any DMSO concentration applied during all toxicity tests. The toxicity of DMSO was reflected by the percentage of the embryos that successfully entered the 8-cell stage at 2.5 h after fertilisation.

Same as the DBP toxicity testing conducted in **Chapter 4**, sperm-exposure tests and oocyte-exposure tests were conducted respectively for each tested chemical and the percentages of embryos that successfully reached the 2-, 4-, 8- and 16-cell were respectively scored at 1.5, 2, 2.5 and 3 h after the sperm-oocyte binding. The success rates of embryogenesis were scored as described in **Section 4.3.2.2, Chapter 4**. Again, the unfertilised, arrested or malformed embryos were all identified as unsuccessful development and immature oocytes with a pronounced germinal vesicle were omitted during the calculation of development rates. Images of the malformed embryos were

captured under the Zeiss Axiovert S100 inverted microscope equipped with a Zeiss AxioCam MRm camera (Carl Zeiss, Oberkochen, Germany).

5.3.3 Statistical analysis

The adverse effects of BPA, APs and PAEs on early embryogenesis in *G. caespitosa* were evaluated on datasets consisting of at least three replicates. The statistical differences between the rates of successfully developed embryos in different treatments were analysed using the one-way analysis of variance (ANOVA). The presence of a dose-dependent relationship between the toxicant concentrations and the percentages of successfully developed embryos/malformed embryos was also determined using ANOVA. The difference was recognised as statistically significant if the P value was less than 0.05. The median inhibition concentrations (IC₅₀) for the early embryonic development of *G. caespitosa* were estimated by Probit analysis (Finney, 1971). All statistical analyses were performed using Microsoft Excel 2013 (Microsoft Corporation, Redmond, USA).

5.4 Results

The success rates of embryogenesis were recorded at 2-, 4-, 8- and 16-cell stages respectively to cover the possibility that the toxicants examined induced time-dependent effects on early embryonic development. According to the results obtained from the toxicity tests, all tested chemicals were unable to induce time-dependent disturbances on the success of embryogenesis. Therefore, in this section, the statistics obtained at 8-cell stage were utilised to demonstrate the adverse effects that each chemical induced on early embryogenesis; the data obtained at all other three time points are all supplied in the **Appendix**.

In addition, except for dibutyl phthalate (DBP), all other oocyte-exposure tests conducted in this study revealed that the test concentrations applied during the sperm-exposure tests did not affect oocyte function (see **Appendix**). Thus, the embryonic arrests and abnormalities observed during the sperm-exposure tests were all attributed to the chemical-induced sperm impairment.

As bisphenol A (BPA) and alkylphenols (APs) were all dissolved in DMSO before serial dilutions into the designated concentrations, a vehicle control was tested in the first instance. Freshly collected spermatozoa and oocytes were mixed together after being respectively treated with 1% (v/v) DMSO in filtered natural seawater (FSW), which was higher than any DMSO concentration applied in the following tests. **Figure 5.1** demonstrated that 1% DMSO was unable to induce any adverse effect the early embryogenesis, as approximately 90% of the embryos in the DMSO-treated group successfully developed to the 2-cell stage, which was not significantly different from the value of untreated control ($P > 0.05$).

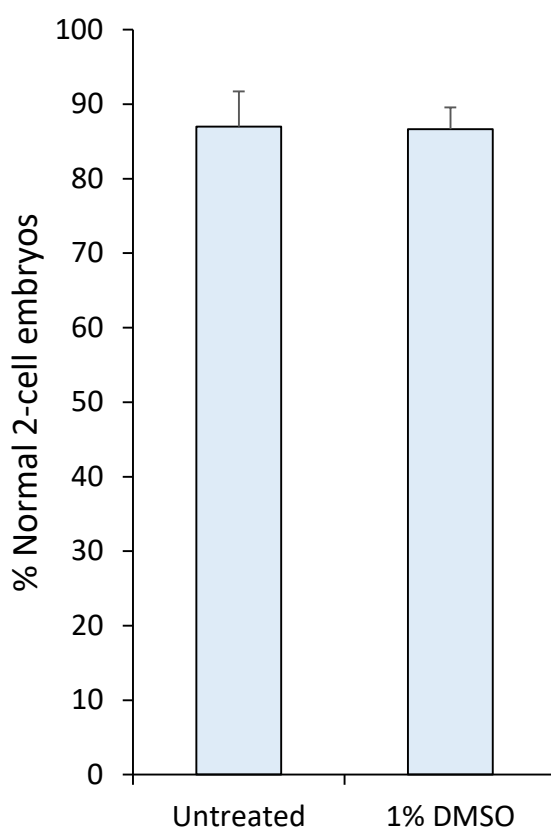


Figure 5.1 Exposure of gametes to 1% (v/v) DMSO had no adverse effect on the early embryogenesis in *G. caespitosa*. To determine the effect of low-level DMSO on the early embryogenesis, spermatozoa and oocytes were treated with 1% DMSO in FSW respectively for 15 min prior to fertilisation. No significant difference was detected between the untreated and the vehicle solution-treated groups in terms of the percentages of embryos that successfully developed into two cells at 1.5 h after fertilisation ($P > 0.05$).

5.4.1 Bisphenol A

During the BPA toxicity testing, the spermatozoa were exposed to 1.25, 2.5, 5 and 10 mg/L BPA for 15 min, followed by the addition of freshly collected oocytes. The impact of BPA on sperm function was determined by assessing the success of subsequent embryonic development at the 8-cell stage. When the spermatozoa were exposed to increasing concentrations of BPA, the inhibitory effects that the chemical generated on the success of embryogenesis increased in a dose-dependent manner (ANOVA, $P < 0.001$). The BPA-induced toxicity effect was statistical significant at concentrations of

2.5 mg/L or greater ($P < 0.05$; **Figure 5.2**). While the untreated samples exhibited high rates of normal development of about 80%, exposure of spermatozoa to 2.5 mg/L BPA resulted in the development rate decreasing by half ($P < 0.05$). After the spermatozoa were treated with 5 mg/L BPA, only about 15% of the embryos were able to develop into normal 8-cell embryos ($P < 0.01$). Furthermore, exposure of spermatozoa to 10 mg/L BPA resulted in no embryo being capable of proceeding through normal development ($P < 0.001$; **Figure 5.2**). These data indicated that the capacity of spermatozoa to activate normal embryonic development was dramatically reduced as the BPA concentration increased with this capacity being completely suppressed at 10 mg/L BPA.

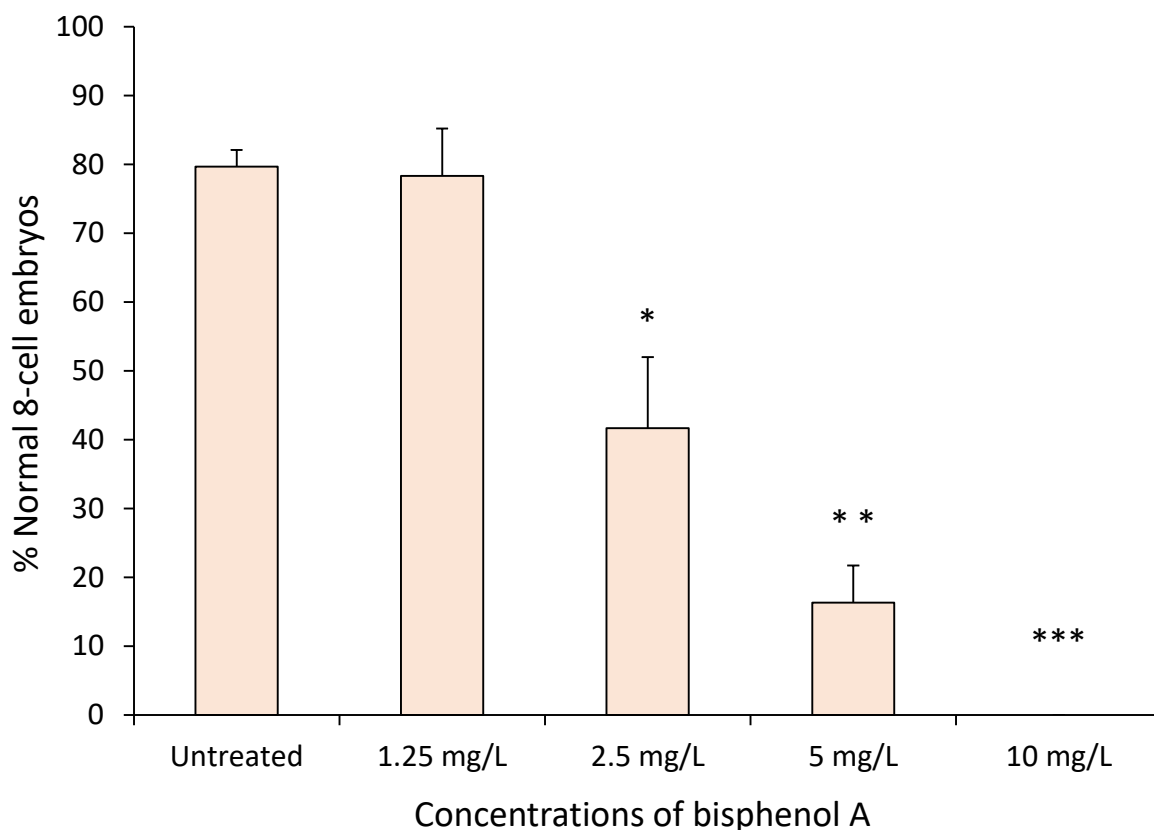


Figure 5.2 Exposure of spermatozoa to the graded concentrations of BPA resulted in decreases of normal development rates. Spermatozoa were exposed to graded concentrations of BPA for 15 min prior to the addition of untreated oocytes. With the increase of BPA concentration, the percentages of normal developed embryos reduced in a dose-dependent manner

(ANOVA, $P < 0.001$). The inhibitory effects of DBP on the embryogenesis success were statistically significant at concentrations of 2.5 mg/L and higher ($P < 0.05$). *, $P < 0.05$; **, $P < 0.01$; ***, $P < 0.001$.

By plotting the concentrations of BPA against the percentages of normally developed embryos, a strong negative linear relationship was revealed ($R^2 = -0.8596$). Based on the linear regression, the IC_{50} value, or the concentration of BPA that would lead to half of the embryos being unable to undergo normal development, was estimated to be 2.94 mg/L. The extrapolation of such IC_{50} values facilitated a comparative assessment of the sensitivity of the early development in *G. caespitosa* to each chemical.

The BPA toxicity testing revealed that BPA-induced sperm impairment resulted in a high incidence of abnormal embryonic development. Most of the abnormal embryos exhibited an irregular shape without a specific pattern (white asterisks, **Figure 5.3**); however, there was still a considerable portion of them displaying a common pattern of abnormality (black asterisks, **Figure 5.3**). Such abnormality was consistent with the one discovered during DBP toxicity testing (**Section 4.4.2, Chapter 4**), that was, after the first division, half of the embryo was not able to divide any longer, while the other half was still able to carry out the further cytoplasmic divisions.

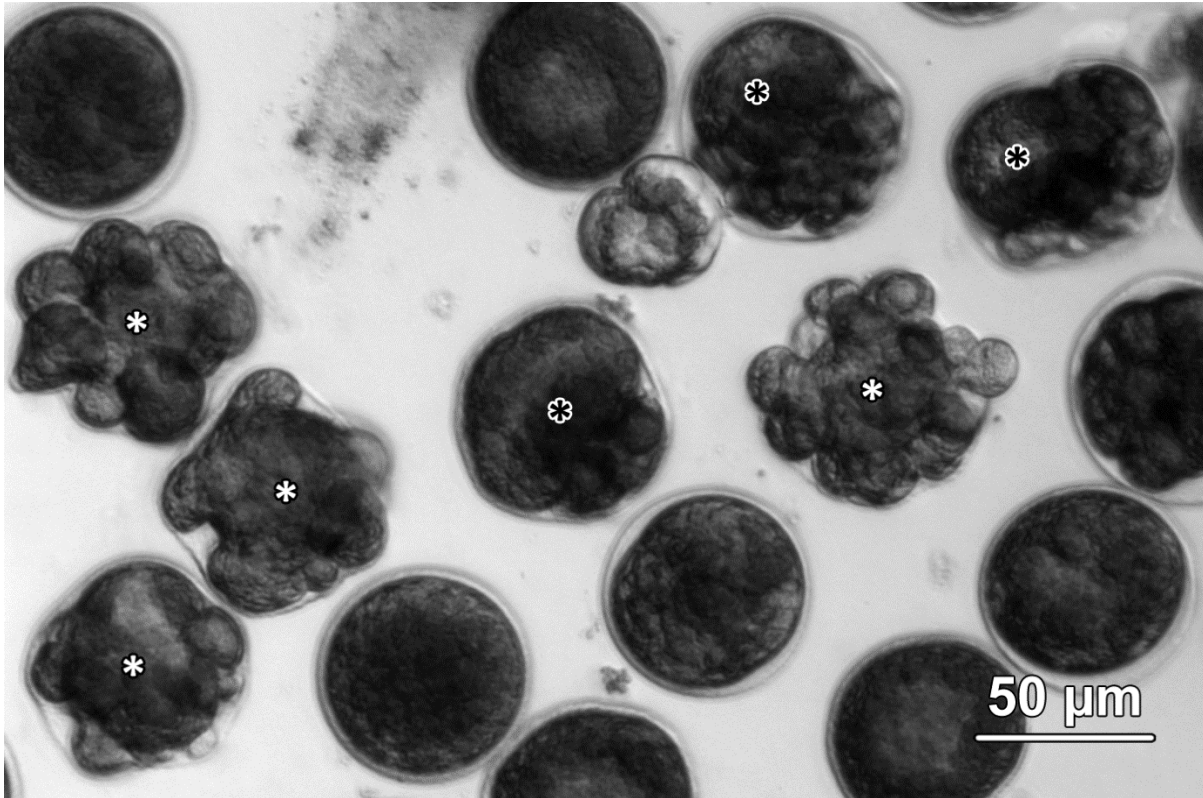


Figure 5.3 Exposure of spermatozoa to BPA led to an elevated incidence of malformed embryos. The spermatozoa were treated with 5 mg/L BPA and the image was captured at 3 h after fertilisation. Malformed embryos were labelled with black and white asterisks (*). A portion of the malformed embryos exhibited the typical embryonic malformation observed during DBP toxicity testing (black asterisks, *). After the first cleavage, half of the malformed embryo was at rest, while the other half underwent further mitoses.

5.4.2 Alkylphenols

Six APs were examined during this study, including butylphenol (BP), pentylphenol (PP), hexylphenol (HP), heptylphenol (HPP), octylphenol (OP) and nonylphenol (NP). The gametes of *G. caespitosa* were all exposed to graded concentrations of APs at 0.005, 0.05, 0.5 and 5 mg/L respectively.

5.4.2.1 Butylphenol

Exposure of spermatozoa to BP caused no significant effect on subsequent early embryogenesis ($P > 0.05$) until the concentration increased to 5 mg/L ($P < 0.001$; **Figure 5.4**). The ANOVA indicated that the embryogenesis success reduced in a dose-dependent manner ($P < 0.001$) with increasing concentrations of BP. The results also gave a strong negative correlation between the concentrations of BP applied to the spermatozoa and the percentages of the embryos undergoing the normal development ($R^2 = -0.9814$). Based on the linear regression, the IC_{50} value was extrapolated to be 11.72 mg/L. In addition, no obvious morphologically abnormal embryo was observed in the untreated or treated groups. At 3 h after fertilisation, the embryos that failed to develop to eight cells all appeared unfertilised or arrested at earlier stages.

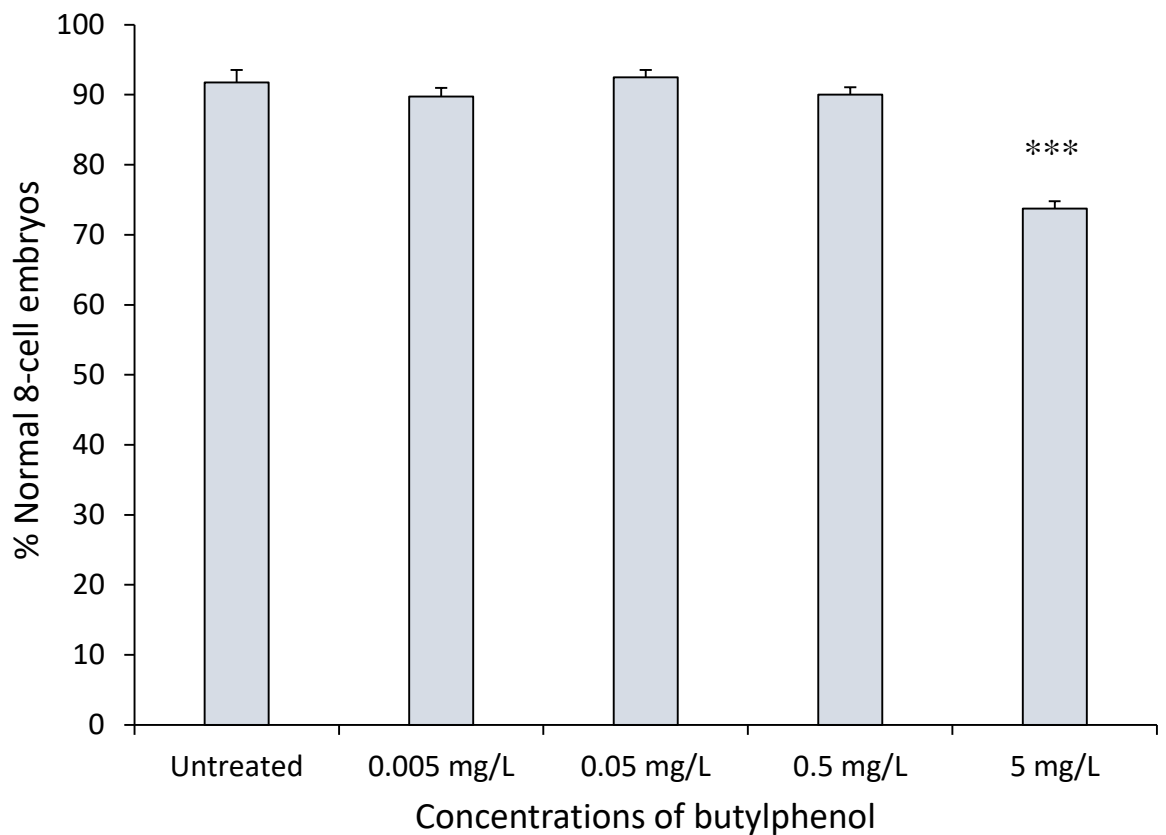


Figure 5.4 Exposure of spermatozoa to the graded concentrations of BP caused no significant effect on the early development until the concentration increased to 5 mg/L ($P < 0.001$). With the increase of the BP concentration, the success rate of early development decreased in a dose-dependent manner ($P < 0.001$). ***, $P < 0.001$.

5.4.2.2 Pentylphenol

Similar to the response of the early embryogenesis to BP, exposure of spermatozoa to PP also resulted in no significant effect when the concentration was or less than 0.5 mg/L. The 5 mg/L PP-treated group exhibited a significantly lower rate of embryogenesis, that was still approximately 80% ($P < 0.01$; **Figure 5.5**), compared with the untreated sample which had a successful embryogenesis rate of over 90%. Similarly, the percentage of successfully developed embryos decreased in a dose-dependent manner (ANOVA, $P < 0.001$) with the increase of PP concentration. Based on the negative linear relationship obtained from these statistics ($R^2 = -0.6571$), the IC_{50} value was found to be 24.96 mg/L. Such a high IC_{50} value suggested that the spermatozoa of *G. caespitosa* had a relatively low sensitivity to this compound. Moreover, no malformed embryo was detected during this test.

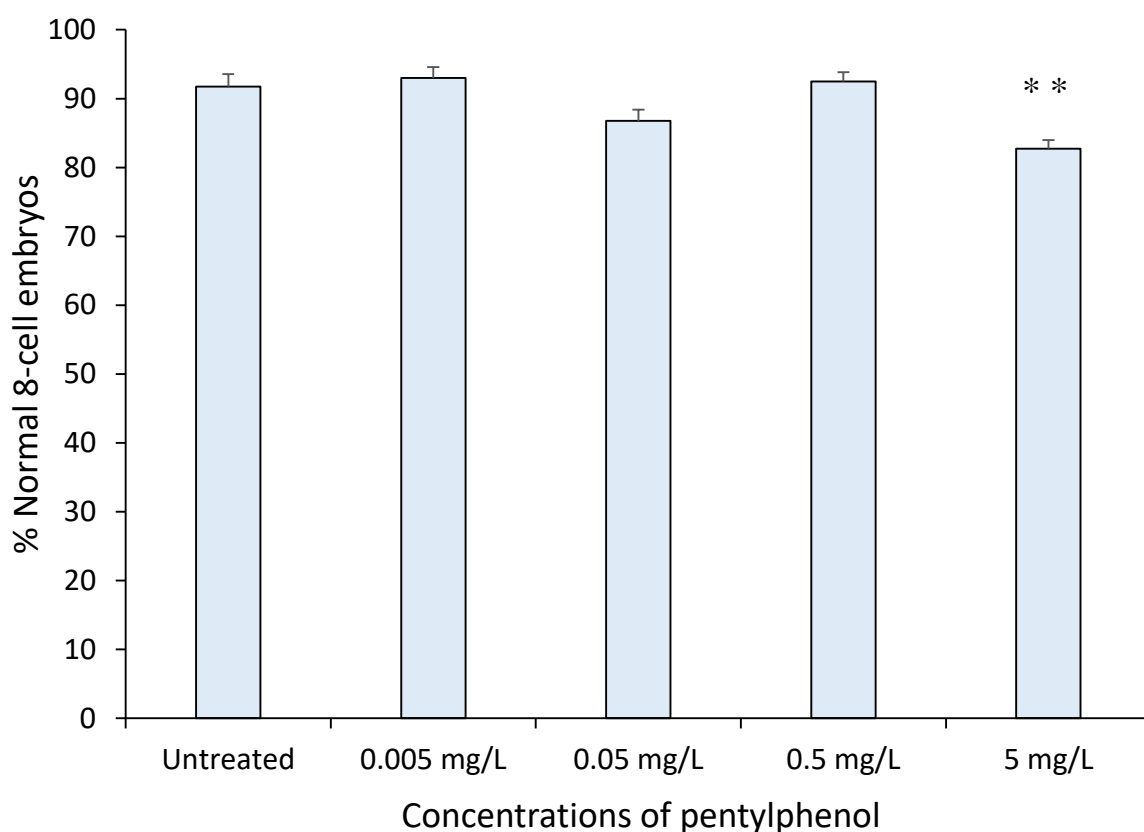


Figure 5.5 Exposure of spermatozoa to graded concentrations of PP resulted in no significant effect on the early embryogenesis until the concentration reached 5 mg/L ($P < 0.01$). The success of early embryonic development decreased with the increase of the concentration of PP (ANOVA, $P < 0.001$). **, $P < 0.01$.

5.4.2.3 Hexylphenol

Distinct from the previous two APs, exposure of spermatozoa to HP resulted in significantly decreased rates of successful embryogenesis when the concentration was higher than 0.005 mg/L (**Figure 5.6**). Remarkably, the 0.05, 0.5 and 5 mg/L HP-treated groups all exhibited statistically significant lower percentages of normally developed embryos ($P < 0.001$). Moreover, the success rate of normal early development reduced in a dose-dependent manner when the concentration of HP increased (ANOVA, $P < 0.001$). Exposure of spermatozoa to 5 mg/L HP resulted in only about 10% of the embryos being able to proceed through normal development whereas the untreated control gave an

embryogenesis success rate of over 90%. Based on the negative linear relationship obtained from these data, the IC₅₀ value was determined to be 2.2 mg/L, which was much lower than that of the previous two APs. Notwithstanding such high sensitivity to this chemical, no malformed embryos were observed during this toxicity study.

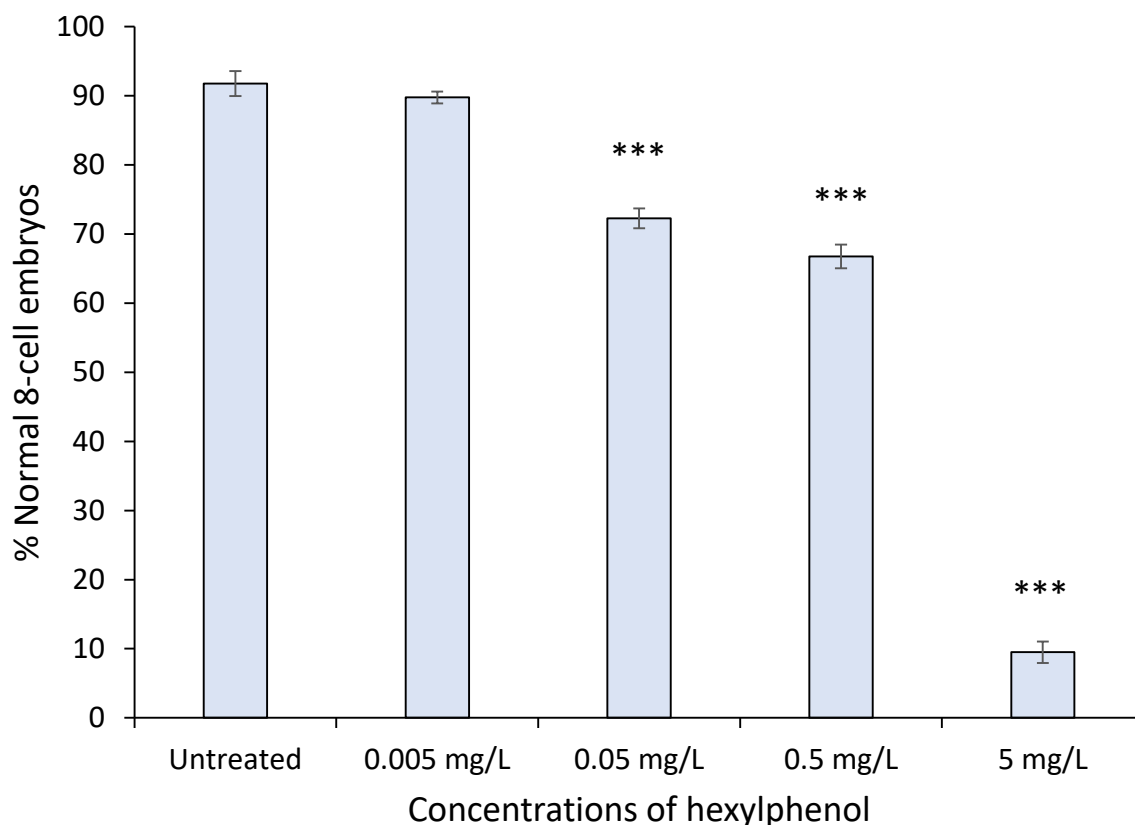


Figure 5.6 Exposure of spermatozoa to the graded concentrations of HP resulted in decreases of normal development rates. With the increase of HP concentration, the percentages of normal developed embryos reduced in a dose-dependent manner (ANOVA, $P < 0.001$). The inhibitory effects of HP on the embryogenesis success were statistically significant at concentration of 0.05 mg/L or higher ($P < 0.001$). ***, $P < 0.001$.

5.4.2.4 Heptylphenol

Exposure of spermatozoa to increasing concentrations of HPP resulted in a continuous decrease in the average rate of embryonic development. This decrease became apparent once the concentration reached 0.5 mg/L ($P < 0.01$; **Figure 5.7**). Similar to 5 mg/L of HP

treatment, the same concentration of HPP also dramatically suppressed the percentage of normally developed embryos to an extremely low level of less than 10%. Likewise, the results obtained from the HPP toxicity testing gave a negative linear relationship ($R^2 = -0.9887$), by which the IC_{50} value was estimated to be 2.29 mg/L. In addition, no distinct embryonic malformations were detected throughout the HPP toxicity testing.

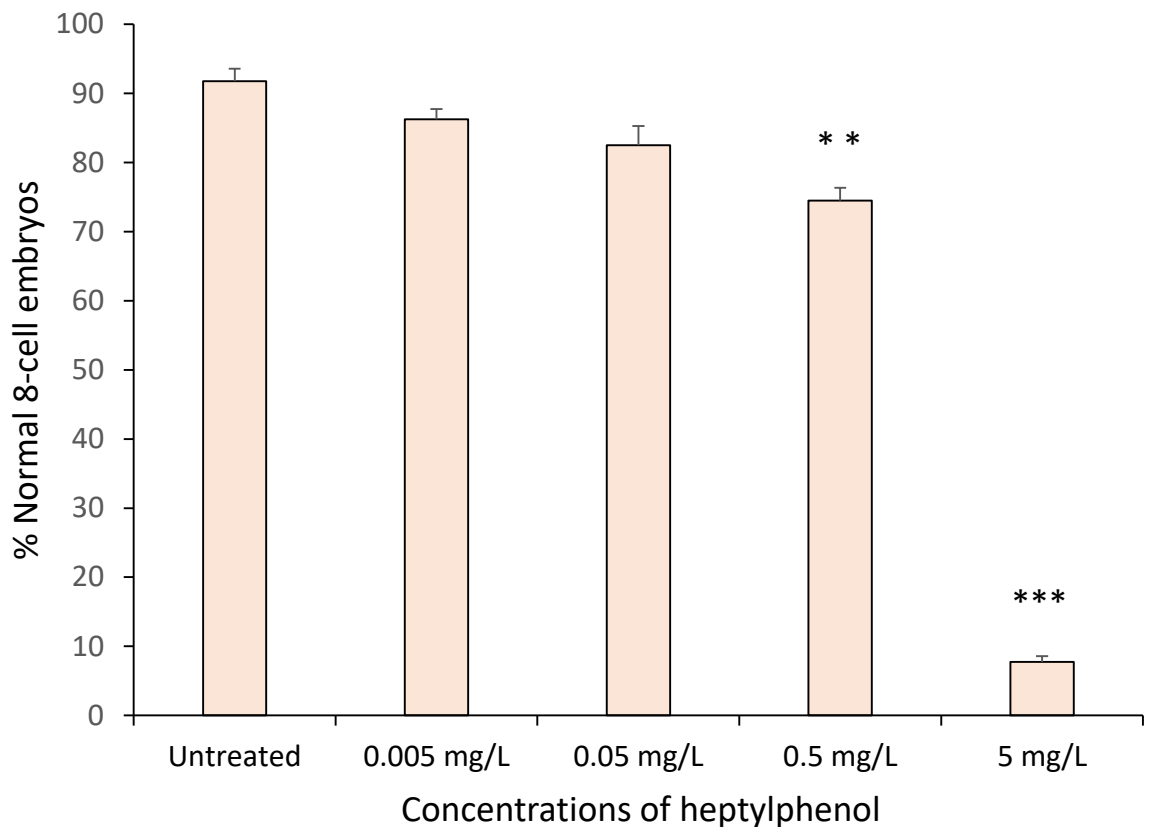


Figure 5.7 Exposure of spermatozoa to the graded concentrations of HPP resulted in decreased success rates of early embryogenesis. With the elevation of the concentration of HPP, the percentages of normal developed embryos decreased in a dose-dependent manner (ANOVA, $P < 0.001$). The inhibitory effects of HPP on the embryogenesis success were statistically significant at concentrations of 0.5 mg/L and higher ($P < 0.01$). **, $P < 0.01$; ***, $P < 0.001$.

5.4.2.5 Octylphenol

Spermatozoa exposed to OP at doses less than 5 mg/L had no adverse effect on the subsequent embryogenesis ($P > 0.05$; **Figure 5.8**). However, once the concentration of

OP reached 5 mg/L, the success rate of embryogenesis was dramatically decreased to a low percentage of approximately 15% ($P < 0.001$). Overall, the success of embryogenesis decreased in a dose-dependent manner in concert with increases in the concentration of OP (ANOVA, $P < 0.001$). By plotting the OP concentrations against percentage embryogenesis success, a negative linear correlation was observed ($R^2 = -0.9958$). By utilising the equation obtained from the linear regression, the IC_{50} value was estimated to be 2.61 mg/L.

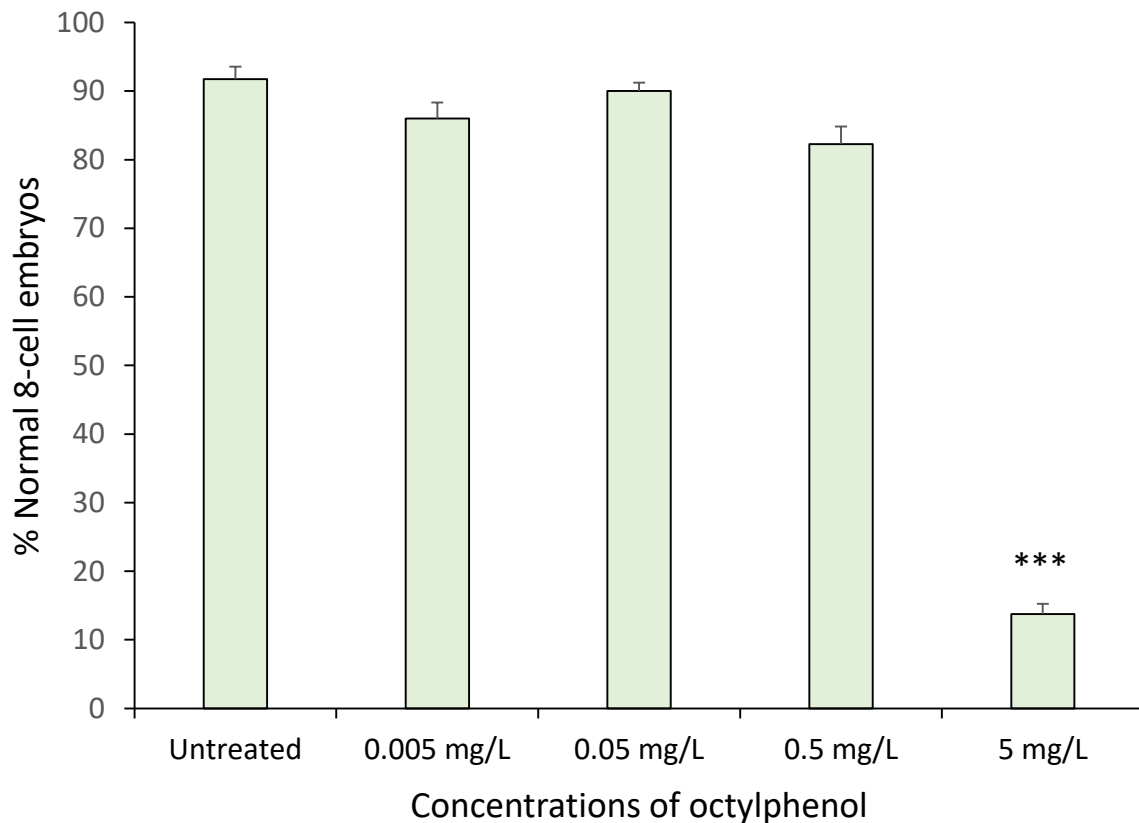


Figure 5.8 Exposure of spermatozoa to graded concentrations of OP resulted in no significant effect on the early embryogenesis until the concentration increased to 5 mg/L ($P < 0.001$). The success of early embryonic development reduced in a dose-dependent manner with the increase of the dose of OP (ANOVA, $P < 0.001$). ***, $P < 0.001$.

5.4.2.6 Nonylphenol

As shown in **Figure 5.9**, pre-fertilisation exposure of the spermatozoa to increasing concentrations of NP resulted in the success rates of subsequent embryogenesis decreasing in a dose-dependent manner (ANOVA, $P < 0.001$). Such a dose-dependent response was manifested in a negative linear relationship when the concentrations of NP were plotted against the resultant development rates ($R^2 = -0.9686$); thereby, the approximate IC_{50} value of NP was calculated to be 2.22 mg/L. More specifically, the inhibitory effects of sperm exposure to NP on subsequent embryogenesis success became statistically significant when the concentration of NP reached 0.05 mg/L ($P < 0.01$). Remarkably, the success rate of embryonic development was decreased to only about 5% when the spermatozoa were treated with 5 mg/L NP. Similar to all other APs, exposure of spermatozoa to NP was not able to induce malformations in early embryonic development.

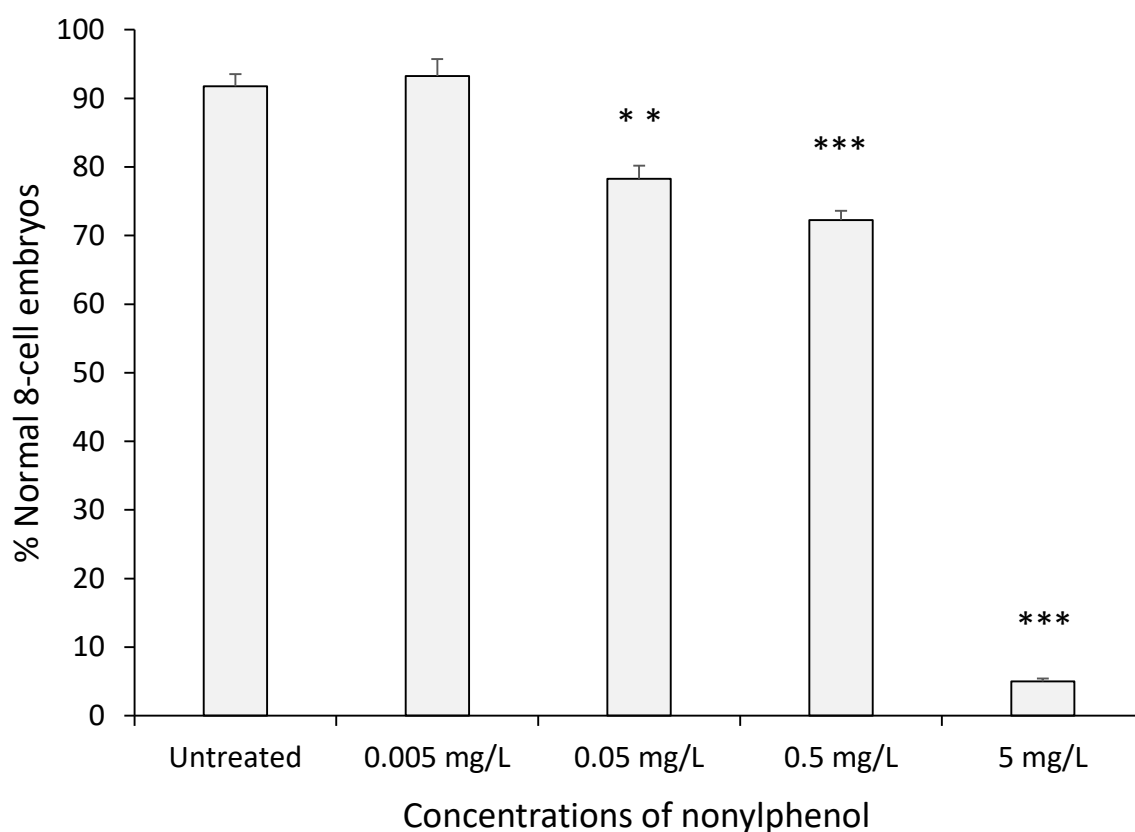


Figure 5.9 Exposure of spermatozoa to the graded concentrations of NP resulted in decreases of normal development rates. With the increase of NP concentration, the success rates of early embryogenesis decreased in a dose-dependent manner (ANOVA, $P < 0.001$). The inhibitory effects that OP posed on the development rates became apparent at concentrations of 0.05 mg/L and higher ($P < 0.01$). **, $P < 0.01$; ***, $P < 0.001$.

Based on the IC_{50} values secured for the six APs examined, a toxicity order could be determined as follows: HP > NP > HPP > OP > BP > PP. While the first four most toxic APs exhibited similar IC_{50} values ranging from 2.2 to 2.3 mg/L, the last two had much higher IC_{50} values of 11.72 and 24.96 mg/L respectively.

5.4.3 Phthalate esters

Six PAEs were examined during this study, including benzyl butyl phthalate (BP), diallyl phthalate (DAP), DBP, diethyl phthalate (DEP), dimethyl phthalate (DMP) and dioctyl phthalate (DOP).

5.4.3.1 Benzyl butyl phthalate

Freshly collected spermatozoa were treated with graded concentrations of BBP at 3.125, 6.25, 12.5 and 25 mg/L respectively for 15 min followed by the addition of healthy oocytes. The percentage of developed normal embryos decreased in a dose-dependent manner with the increase of BBP concentration (ANOVA, $P < 0.001$). The BBP-induced suppression of early embryogenesis was statistically significant at the concentrations equal and higher than 3.125 mg/L ($P < 0.01$; **Figure 5.10**). The untreated samples exhibited a high percentage of embryogenesis success of about 95%. When the spermatozoa were exposed to 6.25, 12.5 and 25 mg/L of BBP, the subsequent rates of early embryogenesis were dramatically decreased to approximately 60%, 30% and 10% respectively. By plotting the BBP concentrations against embryogenesis success, a negative linear correlation was observed ($R^2 = -0.935$). Based on the equation obtained from the linear regression, the IC_{50} value was determined to be 10.9 mg/L. Noticeably, BBP-treated spermatozoa led to an increased occurrence of malformed embryos, compared with the complete absence of malformations in untreated samples.

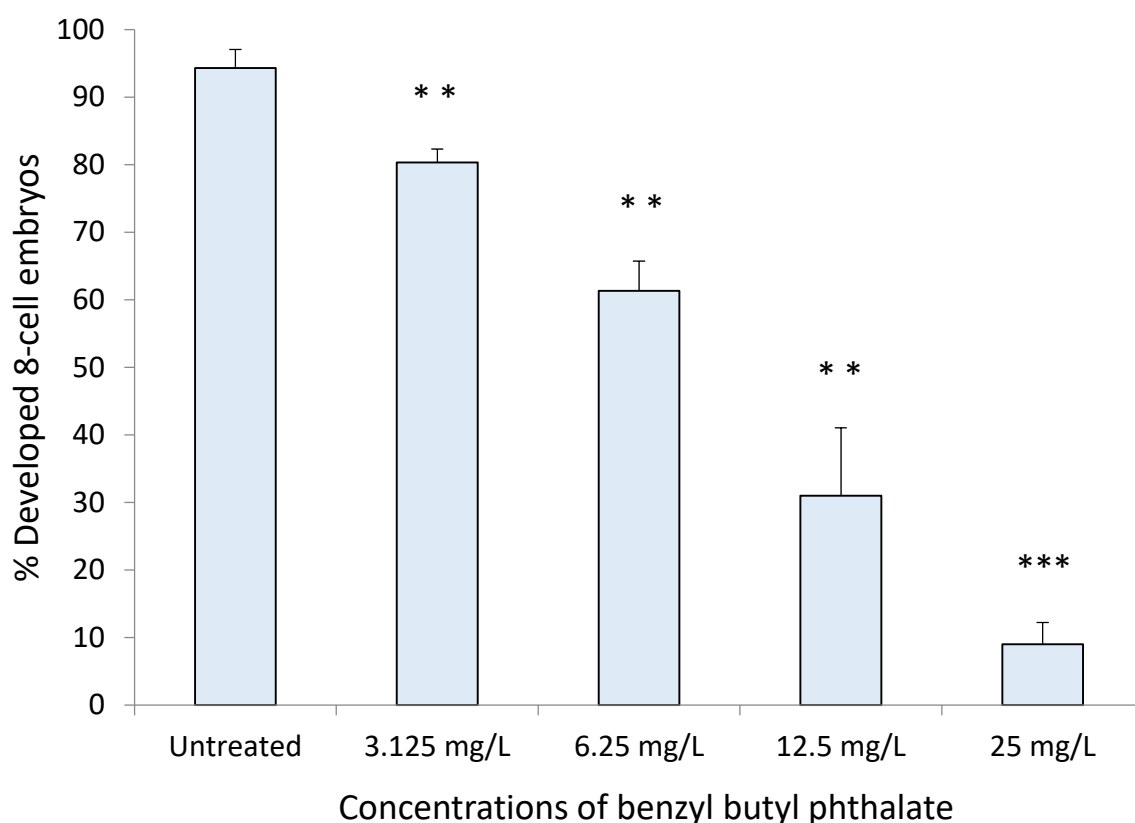


Figure 5.10 Exposure of spermatozoa to the graded concentrations of BBP resulted in the decrease of subsequent embryogenesis success. The inhibitory effect that BBP posed on the success rates of embryonic development became apparent when the concentration reached 3.125 mg/L. Overall, the percentage of normally developed embryos decreased in a dose-dependent manner with the increase of BBP concentration (ANOVA, $P < 0.001$). **, $P < 0.01$; ***, $P < 0.001$.

5.4.3.2 Diallyl phthalate

Spermatozoa were exposed to same concentrations of DAP as used during the BBP toxicity testing, after which freshly collected oocytes were introduced for fertilisation. Overall, with the elevation of DAP concentration, the percentage of normally developed embryos decreased in a dose-dependent manner (ANOVA, $P < 0.001$). The inhibitory effects that DAP caused on the embryogenesis success became apparent when its concentration was 6.25 mg/L or higher ($P < 0.01$; **Figure 5.11**). Specifically, 12.5 mg/L DAP-treated spermatozoa resulted in nearly half of the embryos failing to undergo the

normal embryogenesis while 25 mg/L DAP decreased the embryogenesis rate to around 10%. A strong negative linear relationship was detected between the concentrations of DAP applied to the spermatozoa and the success rates of early embryogenesis ($R^2 = -0.9988$). Based on the linear regression, the IC_{50} value of DAP was estimated to be 13.82 mg/L, which was slightly higher than that of BBP.

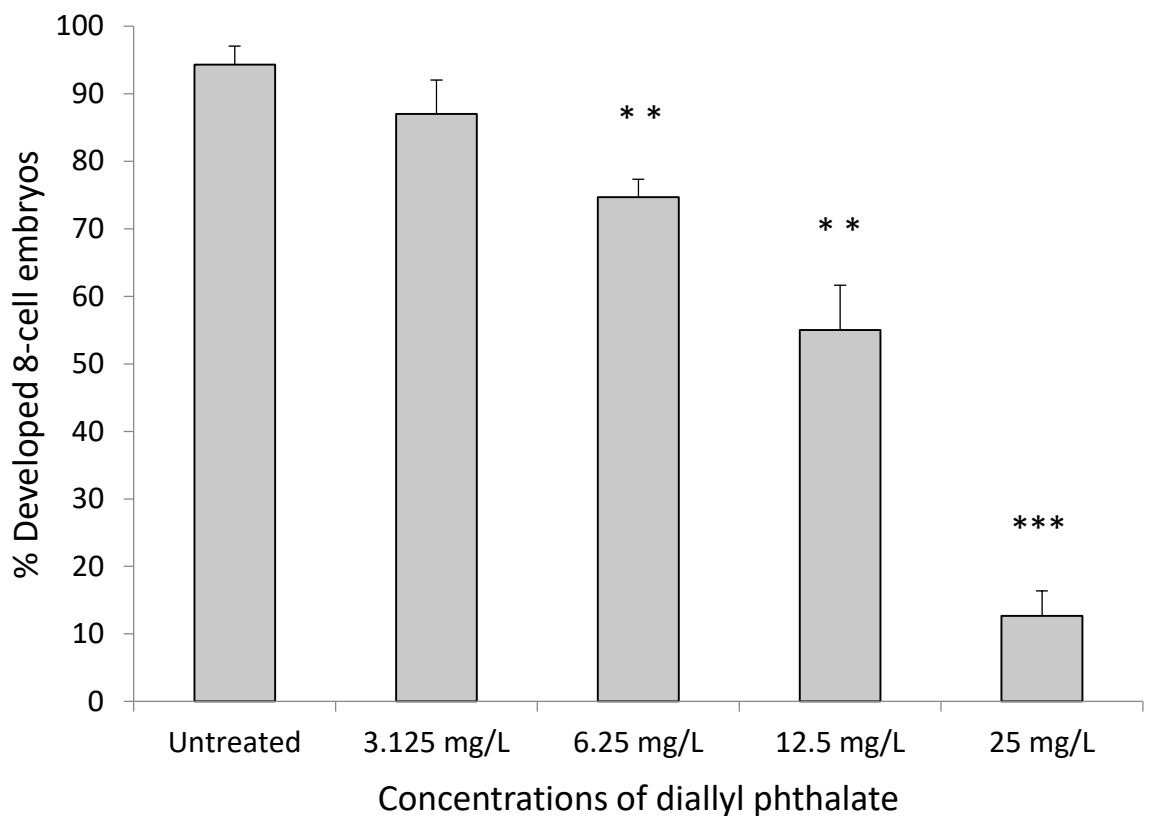


Figure 5.11 Exposure of spermatozoa to the graded concentrations of DAP caused the decrease of early embryonic development in a dose-dependent manner (ANOVA, $P < 0.001$). When the spermatozoa being exposed to 6.25, 12.5 and 25 mg/L, the percentages of normally developed embryos were reduced to approximately 70%, 55% and 10% respectively, which were significantly lower than that of the untreated sample (~ 95%). **, $P < 0.01$; ***, $P < 0.001$.

5.4.3.3 Dibutyl phthalate

In this test, spermatozoa were treated with 0.02, 0.2, 2 and 20 mg/L of DBP for 15 min, after which the treated spermatozoa were directly mixed with freshly collected oocytes.

With increasing concentrations of DBP, the percentage of normally developed embryos decreased in a dose-dependent manner (ANOVA, $P < 0.001$). While the untreated samples exhibited a high rate of embryogenesis success exceeding 90%, the 0.2 mg/L DBP-treated spermatozoa resulted in a significantly decreased development rate of approximately 65% ($P < 0.05$; **Figure 5.12**). When the DBP concentration increased to 2 mg/L, the success of embryogenesis further dropped to around 35%. Remarkably, 20 mg/L DBP resulted in almost all of the embryos remaining undeveloped. By plotting the concentrations of DBP against the rates of normally developed embryos, a strong negative linear relationship was observed ($R^2 = -0.7465$). Based on this linear regression equation, the IC_{50} value was estimated to be 5.9 mg/L, which was nearly half the IC_{50} value recorded for the previous two PAEs.

Among all the tested toxicants in this study, within the range of tested concentrations applied during sperm-exposure tests, DBP was the only one that induced a significant reduction in the embryogenesis success by impairing the female germline (**Figure 4.2, Chapter 4**). Moreover, exposure of spermatozoa to 0.2 and 2 mg/L of DBP induced an elevated incidence of morphologically abnormal embryos. These malformed embryos displayed a specific pattern of abnormality (**Figure 4.5, Chapter 4**), which was consistent with the pattern observed during BPA toxicity testing (black asterisks, **Figure 5.2**).

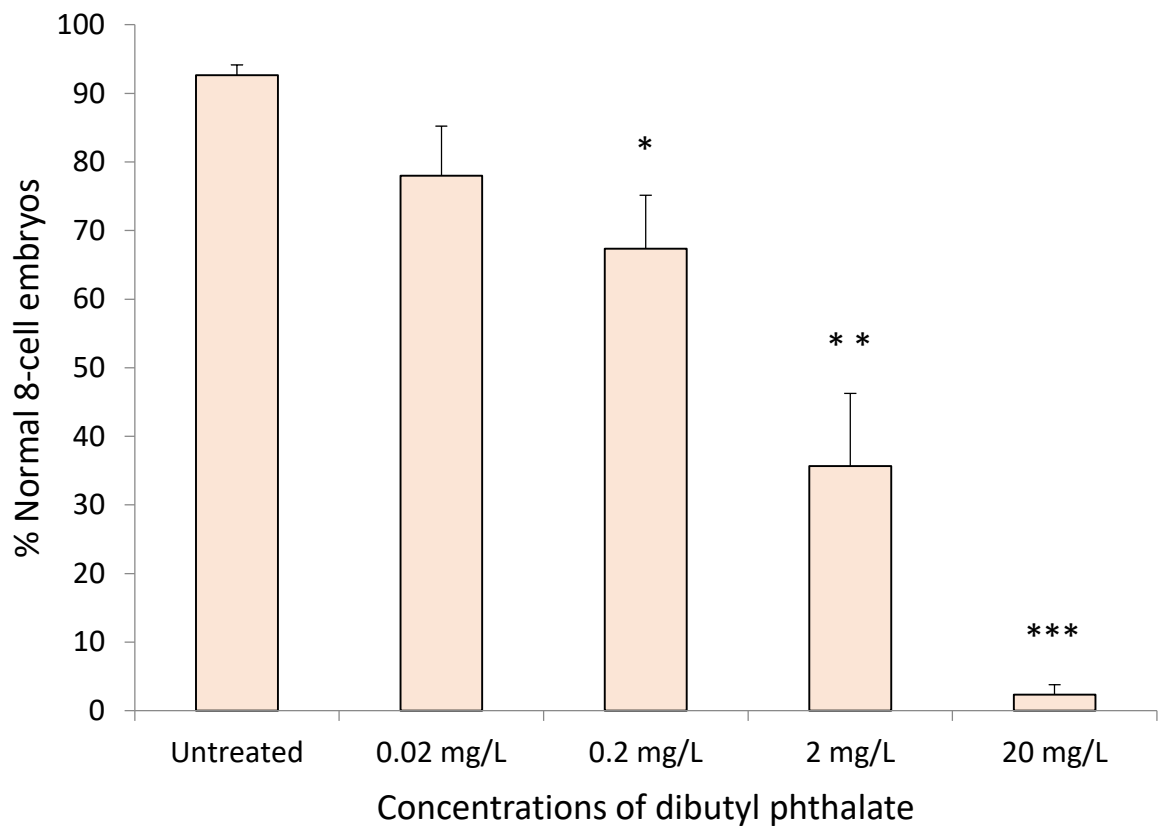


Figure 5.12 Exposure of spermatozoa to the graded concentrations of DBP led to decreased percentages of normally developed embryos. The inhibitory effect that DBP posed on the success rates of embryonic development became apparent when the concentration reached 0.2 mg/L. Overall, the percentage of normally developed embryos decreased in a dose-dependent manner with the increase of DBP concentration (ANOVA, $P < 0.001$). *, $P < 0.05$; **, $P < 0.01$; ***, $P < 0.001$.

5.4.3.4 Diethyl phthalate

Prior to the addition of freshly collected oocytes, spermatozoa of *G. caespitosa* were exposed to graded concentrations of DEP at 20, 40, 60 and 80 mg/L for 15 min. Exposure of spermatozoa to 20 mg/L resulted in a significant decrease in embryonic development to about 80% ($P < 0.05$), compared with the untreated samples which gave a high percentage of normally developed embryos approximating to 95% (**Figure 5.13**). When the spermatozoa were treated with 80 mg/L of DEP, the success rate of early embryogenesis decreased to nearly 30% ($P < 0.001$). Overall, with increasing DEP

concentrations, the subsequent rates of normal embryonic development decreased in a dose-dependent manner (ANOVA, $P < 0.001$), and was manifested in a strong negative linear relationship between the two parameters ($R^2 = -0.977$). According to the equation obtained from such linear correlation, the IC_{50} value was estimated to be 58.21 mg/L. Similar to all other PAEs, exposure of spermatozoa to DEP also resulted in an increased incidence of malformed embryos.

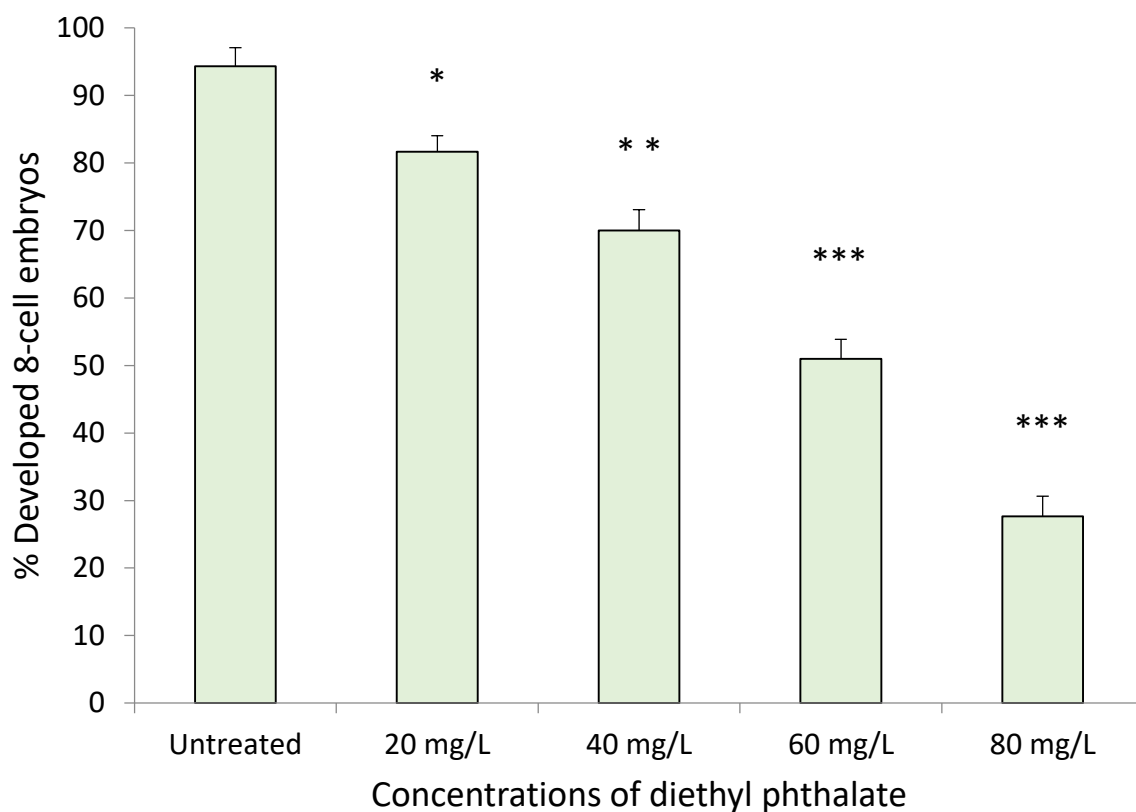


Figure 5.13 Spermatozoa being exposed to the graded concentrations of DEP resulted in decreased success rates of early embryogenesis. With the concentration of DEP increased from 0 to 80 mg/L, the percentage of normally developed embryos decreased in a dose-dependent manner (ANOVA, $P < 0.001$). While the untreated control displayed a high embryogenesis success of about 95%, the 20, 40, 60 and 80 mg/L of DEP-treated samples resulted in decreased rates of ~ 80%, 70%, 50% and 30% respectively. *, $P < 0.05$; **, $P < 0.01$; ***, $P < 0.001$.

5.4.3.5 Dimethyl phthalate

Regarding the DMP toxicity testing, the spermatozoa were treated with relatively high concentrations of DMP up to 200 mg/L, generating a dose-dependent decrease of embryonic development with increasing DMP concentrations (ANOVA, $P < 0.001$). The DMP-induced reduction in development rates became apparent when the concentrations were equal to or higher than 50 mg/L. When the spermatozoa being exposed to 200 mg/L of DMP, the subsequent percentage of normally developed embryos was decreased to about 5% ($P < 0.001$; **Figure 5.14**). Similar to other PAEs, an obvious negative linear relationship was detected between the dose of chemical applied and subsequent embryogenesis success ($R^2 = -0.9778$), generating an IC_{50} value of around 94.98 mg/L. Although the gametes of *G. caespitosa* were less sensitive to DMP, within the tested range of concentrations, the DMP-treated spermatozoa still gave rise to an increased number of malformed embryos.

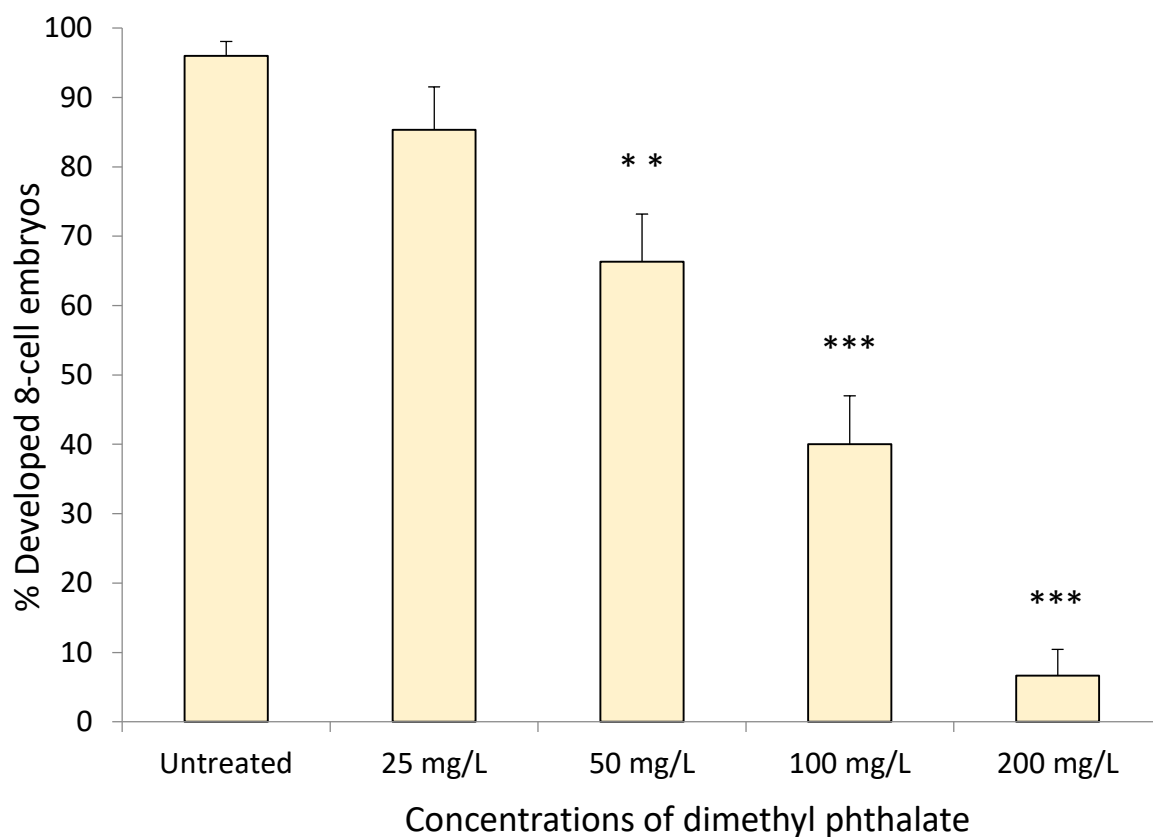


Figure 5.14 Exposure of spermatozoa to the graded concentrations of DMP resulted in decreased percentages of normally developed embryos. The inhibitory effect that DMP induced on the success rates of embryogenesis became significant when its concentration reached 50 mg/L. With the increase of DMP concentration, the percentage of successfully developed embryos decreased in a dose-dependent manner (ANOVA, $P < 0.001$). **, $P < 0.01$; ***, $P < 0.001$.

5.4.3.6 Dioctyl phthalate

During the DOP toxicity testing, spermatozoa were treated with up to 20 mg/L DOP, as this chemical was not able to dissolve in seawater when the concentration was higher than 20 mg/L, even with the help of the solvent, acetone. When the concentration of DOP increased from 0 to 20 mg/L, the success of embryogenesis decreased in a dose-dependent manner (ANOVA, $P < 0.001$). Compared with the untreated control, which gave a high percentage of normally developed embryos of over 90%, spermatozoa exposed to 20 mg/L of DOP resulted in a decrease to around 65% ($P < 0.01$; **Figure 5.15**). By plotting

the concentrations of DOP against the percentage of normally developed embryos, a strong negative linear correlation was revealed ($R^2 = -0.9605$). In light of this linear regression equation, the IC_{50} value of DOP was determined to be 30.26 mg/L; similar to other studied PAEs, DOP was able to induce malformed embryos *via* an action on the spermatozoa.

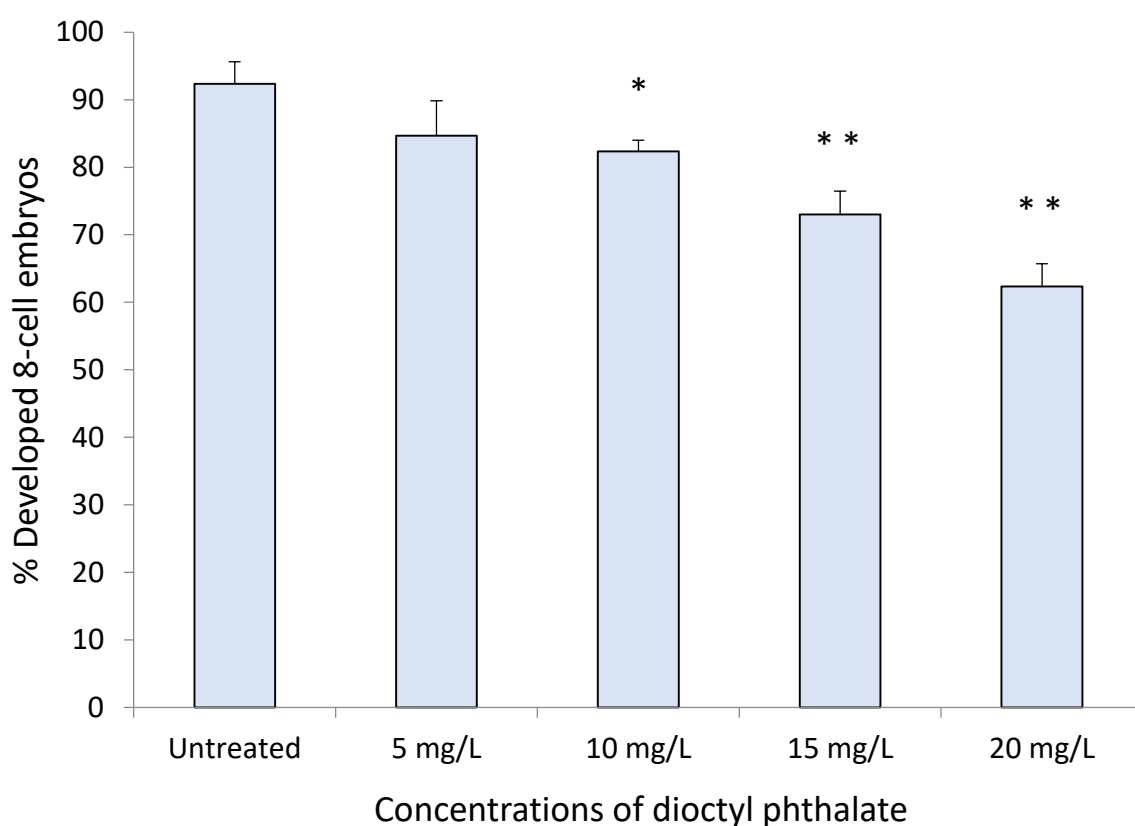


Figure 5.15 Exposure of spermatozoa to the graded concentrations of DOP caused the decrease of early embryonic development in a dose-dependent manner (ANOVA, $P < 0.001$). When the spermatozoa being exposed to 10, 15 and 20 mg/L, the percentages of normally developed embryos were significantly reduced to approximately 80%, 75% and 65% respectively. *, $P < 0.05$; **, $P < 0.01$.

Based on the IC_{50} values obtained from the above sperm toxicity tests, a toxicity order can be described as follows: DBP > BBP > DAP > DOP > DEP > DMP.

5.5 Discussion

To assess the feasibility of using the gametes and subsequent embryogenesis of *G. caespitosa* as indicators of marine contamination, the toxicity of various representative marine pollutants, including bisphenol A, six alkylphenols and six phthalate esters was examined.

5.5.1 Bisphenol A

The spermotoxicity tests revealed that exposure of spermatozoa to graded concentrations of BPA resulted in decreased success rates of early embryogenesis and an increased incidence of malformed embryos in *G. caespitosa*. The dose of BPA that prevented half of the embryos from developing normally (IC₅₀) was about 2.94 mg/L.

As previously reviewed by Staples *et al.* (1998), the toxic effects of BPA have been studied on a wide range of aquatic organisms, such as microorganisms, algae, invertebrates and fish. However, these studies were dedicated to investigating the lethal endpoint (i.e. mortality) or various sub-lethal endpoints (e.g. changes in growth, behaviour and reproduction) on the basis of acute or chronic exposure to BPA. Regardless of the endpoints that the EC₅₀/LC₅₀ values are based on, the majority of them were higher than 2.94 mg/L, which was the median effective value obtained from spermotoxicity tests of *G. caespitosa*. There were still several toxicity studies for BPA which exhibited lower EC₅₀/LC₅₀ values than those observed for this *G. caespitosa* model, such as 96-h EC₅₀ based on the various chlorophyll A fluorescence (1.8 mg/L) and cell count (1 mg/L) of a marine algae *Skeletonema costatum*, 96-h EC₅₀ based on the cell growth (2.5 mg/L) of a freshwater algae *Selenastrum capricornutum* and 96-h LC₅₀ based on the mortality (1.1 mg/L) of the Mysid shrimp *Mysidopsis bahia*. Even though these studies exhibited

higher sensitivities to BPA than the embryogenesis success in *G. caespitosa*, they still have drawbacks to be used as models for the detection of BPA-related contamination due to their prolonged period of incubation.

The levels of BPA in unpolluted aquatic environments are generally found less than 1 µg/L in China [29 - 64 ng/L, Songhua River (Shao *et al.*, 2008)], Germany [0.05 - 249 ng/L, North Sea (Jonkers *et al.*, 2010)], Japan [20.2 - 30.1 ng/L, Tokyo Bay (Hashimoto *et al.*, 2005)], the Netherlands [10 - 330 ng/L (Belfroid *et al.*, 2002)], Spain [52 - 219 ng/L, Granada (González-Casado *et al.*, 1998)], United Kingdom [5.3 - 24 ng/L, Sussex (Liu *et al.*, 2004)] and United States [9 - 44 ng/L, Bayou River (Boyd *et al.*, 2004)]. Such environmental levels of BPA are much lower than the concentrations tested in the current study, which were ranging from 1.25 to 10 mg/L. Nevertheless, elevated levels of BPA were found in aquatic regions that were situated in close proximity to domestic or industrial wastewater treatment plants and hazardous waste disposal sites. The industrial effluents sampled from Toronto, Canada contained relatively high concentrations of BPA up to 0.15 mg/L (Lee and Peart, 2000) and the maximum level of BPA detected in the effluents obtained from paper recycling plants in Shizuoka, Japan was 0.37 mg/L (Fukazawa *et al.*, 2001).

The mechanisms underlying the BPA-induced defects in embryonic development have not been studied adequately. The research conducted by Zhou *et al.* (2011b) provided a preliminary investigation of the possible mechanisms that were involved in the BPA-mediated disturbance of embryonic development in abalone (*Haliotis diversicolor supertexta*). Similar to the results obtained from the current study, exposure of abalone gametes to BPA resulted in decreased embryo hatchability, increased embryonic malformation and suppressed metamorphosis behaviour of the larvae.

Through measurement of the activities of Na⁺/K⁺-ATPase (sodium-potassium pump) and Ca²⁺/Mg²⁺-ATPase (calcium-magnesium pump) in the BPA-treated embryos, Zhou *et al.* (2011b) found that with increasing BPA concentrations, the activities of both enzymes also increased dramatically (P < 0.05). As the main biological role of Na⁺/K⁺- or Ca²⁺/Mg²⁺-pump was to maintain the electrochemical gradients of these ions across the plasma membrane (Haynes, 1983), the BPA-induced changes in these enzyme activities disrupted the normal ionic equilibrium and osmoregulation in this organism. Moreover, Ca ion was also recognised as a key signalling molecule in early development, acting as a second messenger regulating cell differentiation and proliferation. It has also been demonstrated that tributyltin-induced alteration of calcium signalling could be a potential mechanism for developmental toxicity in sea urchin embryos (Roepke *et al.*, 2005).

By analysing the activity of peroxidase (Px) and the level of malondialdehyde (MDA) in the BPA-treated abalone embryos, Zhou *et al.* (2011b) also discovered that BPA significantly suppressed the activity of Px at concentrations of 2 mg/L and higher (P < 0.05) and induced the production of MDA in the embryos (P < 0.05). Therefore, it was also possible that by inhibiting the activities of ROS-scavenging enzymes, BPA induced oxidative damage in the abalone embryos, which caused lipid peroxidation of polyunsaturated fatty acids, as indicated by the elevated intracellular amount of MDA. Under such BPA-induced oxidative stress, the embryos experienced a decreased potential for development (Zhou *et al.*, 2011b).

Interestingly, Arkhipenko Yu *et al.* (1985) demonstrated that lipid peroxidation would suppress the activity of Na⁺/K⁺-ATPase and the inhibitory effect on the enzyme activity was linearly dependent on the amount of MDA accumulated intracellularly. Moreover, BPA has been repeatedly identified as a putative ATPase inhibitor, for example inhibiting

the activity of Ca²⁺-ATPase in the sarcoplasmic reticulum of skeletal muscle cells (Logan-Smith *et al.*, 2001) and the spermatozoa of sea urchin (Ardón *et al.*, 2009). Therefore, the results provided by Zhou *et al.* (2011b) referring to the accumulation of MDA in the face of increases in the activities of ion-ATPases are difficult to reconcile.

Using an RT-PCR technique, Zhou *et al.* (2011b) found that the exposure of abalone embryos to BPA resulted in overexpression of cyclin B (*CB*) and cyclin-dependent kinase 1 (*CDK1*) genes and down-regulation of the prohormone convertase 1 (*PCI*) gene. *CB* is known as a ubiquitous regulatory protein that controls the cell cycle in eukaryotes. It forms *CB/CDK1* complex, or the M-phase promoting factor that accelerates the onset of mitosis and regulates the dynamics of microtubule action (Masaki *et al.*, 2000; Pines, 2006, Stiffler *et al.*, 1999). BPA has previously been found to interfere with the assembly of microtubules which, in turn, led to mitotic arrest and aberrant mitotic spindles (Metzler and Pfeiffer, 1995; Ochi, 1999). Furthermore, BPA-induced disruption of the cytoskeleton has been deemed responsible for embryonic arrest and malformation in toxicity studies (Charles *et al.*, 2002). Moreover, the over-expression of *CDK* gene was demonstrated to perturb early development and delay tissue-specific differentiation in the African clawed frog (Richard-Parpaillon *et al.*, 2004). Based on the findings obtained from PCR analysis, Zhou *et al.* (2011b) proposed that the up-regulation of the two genes might induce retardation of metaphase by destabilising the microtubules, further prolonging the time required to form a functional spindle. As indicated by Ramakrishnan and Wayne (2008), BPA-caused changes in the starting time of mitosis that in turn reduced embryo hatchability and hatching time in the medaka fish *Oryzias latipes*. Therefore, the BPA-mediated disruption of mitosis could be a possible cause of defective embryogenesis in abalone. As demonstrated by Zhou and Cai (2010), *PCI* was involved

in the post-translational processing of steroid hormones and the regulation of reproductive behaviour in abalone. It has been demonstrated that hormonal signals are involved in regulating embryogenesis in some aquatic invertebrates, such as Crustaceans [*Cancer antennarius*, *Carcinus maenas* and *Menippe mercenaria* (Subramoniam, 2000)] and Gastropods [*Lymnaea stagnalis* (Kudikina, 2011)]. Furthermore, hormones were also demonstrated to affect the cell cycle regulatory apparatus such as *CB/CDKI* complex (Pestell et al., 1999). In light of such considerations, Zhou *et al.* (2011b) believed that the BPA-induced interference in endogenous hormone regulation might also occur in abalone embryos, disrupting the cell cycle and ultimately impairing early development.

As observed during the BPA toxicity testing, the BPA-impaired spermatozoa resulted in an elevated occurrence of embryonic malformation and a portion of the malformed embryos exhibited the same pattern of abnormality that we observed in the DBP-treated samples. Zhou *et al.* (2011b) has provided several possible mechanisms for the BPA-mediated embryonic arrest and abnormality in abalone; however, those mechanisms may not be applicable to the embryonic defects in *G. caespitosa*, because instead of the spermatozoa, the fertilised oocytes were exposed to the chemical in their study. Nevertheless, the mechanisms established by Zhou *et al.* (2011b) may possibly explain that how 20 mg/L DBP completely inhibited the embryonic development by inducing oocyte dysfunction (**Figure 4.2, Chapter 4**). Given the similarity between the morphologies of BPA- and DBP-induced malformed embryos, the mechanism underpinning the involvement of BPA-impaired spermatozoa in abnormal embryonic development might be similar to that of the DBP, described in detail in the previous chapter.

5.5.2 Alkylphenols

Most ecotoxicological studies have been performed to investigate the toxicity of octylphenol (OP) and nonylphenol (NP), which are the most representative marine contaminants, accounting for about 60% of the biodegradation products of alkylphenol ethoxylates (APEs). Similar to BPA, the levels of APs in unpolluted aquatic environments are below the limit of detection. However, in areas near the primary source of pollution such as waste treatment plants, elevated levels could still be detected [e.g. 0.33 mg/L OP, United States (Snyder et al., 1999); 0.644 mg/L NP, Spain (Ahel et al., 1994); and 13.7 mg/L NP, Italy (Marcomoni et al., 2009)].

The toxic effect of OP recorded at the 4-cell stage (see **Appendix**) revealed that 0.05 mg/L of OP was the lowest dose that induced a significant reduction in subsequent embryogenesis in *G. caespitosa*. This concentration was lower than the 0.33 mg/L OP detected in the wastewater sample obtained from United States. Likewise, the lowest NP concentration that induced a significant decrease in the success rate of early embryogenesis was also 0.05 mg/L, which was lower than the NP detected in the above mentioned polluted water samples. Therefore, the embryogenesis of *G. caespitosa* can be regarded as a sufficiently sensitive indicator of both OP and NP toxicity.

The toxicity of alkylphenols on the embryogenesis in *G. caespitosa* was positively correlated with the molecular weight of the chemicals, that is, the alkylphenols with highest molecular weights exhibited the greatest toxicity. Specifically, the alkylphenols with molecular masses ranging from 178.27 to 220.35 g/mol resulted in low IC₅₀ values of less than 3 mg/L, while pentylphenol (PP) and butylphenol (BP), whose molecular weights were 164.24 and 150.22 g/mol, exhibited high IC₅₀ values of 24.96 and 11.72

mg/L. In fact, as revealed by Ghirardini *et al.* (2001), the toxicity of APs is determined by their alkyl chain length and branching, i.e. the presence of alkyl side chains. Indeed, compared with PP and BP, NP have many more alkyl side chains, thus exhibits more serious toxicity than the formers.

5.5.3 Phthalate esters

The toxic effects of PAEs were well demonstrated in various aquatic species including microorganisms, algae, invertebrates and fish. Similar to BPA, previous toxicity studies regarding PAEs also focused on a range of experimental endpoints such as mortality, growth inhibition, reproductive disorder and immobility through acute, short-term and long-term exposure (Staples *et al.*, 1997). Regardless of the differences between these studies, they were all dedicated to evaluating the toxicity of PAEs and assessing the sensitivity of the tested organisms to certain PAEs as manifested in the EC₅₀/LC₅₀ values obtained.

The marine and freshwater algae, *Skeletonema costatum* and *Selanastrum capricornutum* both exhibited high sensitivities to benzyl butyl phthalate (BBP) based on different types of endpoints. For example, the 96-h EC₅₀ value based on Chlorophyll A of *Skeletonema costatum* was 0.11 mg/L, which was much lower than the IC₅₀ value of 10.9 mg/L obtained from studying embryogenesis in *G. caespitosa*. A range of fish (e.g. *Cymatogaster aggregate*, *Parophrys vetulus*, *Oncorhynchus mykiss*) also exhibited promising vulnerability to BBP, as reflected by the low 96-h LC₅₀ values of approximately 1 mg/L. The abalone *Haliotis diversicolor supertexta* also displayed a higher vulnerability to BBP compared with *G. caespitosa*, as indicated by a 9-h EC₅₀ value of 2.65 mg/L based on the success of embryogenesis.

The toxicity of diallyl phthalate (DAP) has not been adequately studied in aquatic species. Nevertheless, the Golden Orfe *Leuciscus idus melanotus* exhibited a remarkable sensitivity to DAP manifested in a 48-h LC₅₀ value of 0.4 mg/L, which was lower than the IC₅₀ value of 13.82 mg/L based on changes in embryogenesis of *G. caespitosa*. On the other hand, the sensitivity of *G. caespitosa* to DAP was still stronger than another invertebrate the water flea *Daphnia magna*, which had a 24-h LC₅₀ value of 26 mg/L.

As reviewed by Staples *et al.* (1997), a wide range of tested organisms generally gave sensitive responses to DBP, resulting in the EC₅₀/LC₅₀ values ranging from 0.02 (96-h EC₅₀ based on cell counts of marine algae *Gymnodinium breve*) to 6.47 mg/L (96-h LC₅₀ value of rainbow trout *Oncorhynchus mykiss*). While the embryogenesis of *G. caespitosa* exhibited a moderate IC₅₀ value of 5.9 mg/L, the embryogenesis of the abalone was less sensitive to DBP, with a higher EC₅₀ value of 8.37 mg/L.

The toxicity of diethyl phthalate (DEP) has been adequately studied in different species, which provided various degrees of sensitivities manifested in different EC₅₀ values ranging from 3 (96-h growth rate of marine algae *Gymnodinium breve*) to 132 mg/L (48-h growth inhibition of Protozoa *Tetrahymena pyriformis*). While the EC₅₀ value obtained from the success of embryogenesis in the abalone was 39.13 mg/L, the EC₅₀ value based on embryogenesis in *G. caespitosa* was much higher (58.21 mg/L).

Toxicity tests on a variety of organisms generally revealed low sensitivities to dimethyl phthalate (DMP), as reflected by the relatively high EC₅₀ values ranging from 26.1 (96-h changes in Chlorophyll A fluorescence in *Skeletonema costatum*) to 537 mg/L (48-h growth inhibition of Protozoa *Tetrahymena pyriformis*). While embryogenesis in the abalone exhibited moderate sensitivity, as reflected in an EC₅₀ value of 39.13 mg/L,

embryogenesis of *G. caespitosa* displayed a low sensitivity, manifested in a much higher EC₅₀ value of 94.98 mg/L.

Information on the toxicity of dioctyl phthalate (DOP) has been limited to the water flea *Daphnia magna* and the fathead minnow *Pimephales promelas*, which provided 48-h and 96-h LC₅₀ values of 10 and 0.113 mg/L respectively. In contrast, the sensitivity of the embryogenesis in *G. caespitosa* was relatively low than compared with these two species, generating a high EC₅₀ value of 30.26 mg/L.

Collectively, *G. caespitosa* generally displayed a moderate sensitivity to the six PAEs relative to other aquatic organisms tested including microorganisms, algae, invertebrates and fish. Given that PAE-disrupted embryogenesis in *G. caespitosa* gave rise to a typical pattern of embryonic abnormality and the response of embryogenesis to the presence of toxic substances could be obtained within 3 h, the developmental process in *G. caespitosa* still have the potential to detect PAEs, particularly DBP in the marine environment.

The mechanism by which DBP-impaired spermatozoa generated embryonic arrest and malformation has been adequately elucidated in **Chapter 4**. As exposure of spermatozoa to PAEs resulted in a common pattern of abnormality, it is very likely that all the PAEs share a similar mechanism in disrupting the embryogenesis by impairing centriolar function in the male germline. In addition to the model previously established, Zhou *et al.* (2011a) generated preliminary data on the mechanisms by which exposure of fertilised abalone oocytes to PAEs led to defective embryogenesis. Similar to the mechanism they established for BPA-induced embryonic disruption (Zhou *et al.*, 2011b), PAEs were also found to decrease the level of Px and induce the production of MDA in the embryos. These chemicals, particularly DBP, were able to induce the overexpression of cytochrome

P450 3A (*CyP3A*) and glutathione peroxidase (*GPx*) genes and knock down the expression of 17 β hydroxysteroid dehydrogenase 12 (*17 β -HsD 12*) gene. The up-regulation of *CyP3A* and *GPx* demonstrated that PAE induced changes in the status of antioxidants in the embryos, which disrupted the intracellular pro-oxidative/anti-oxidative balance. Such disruption possibly led to oxidative stress in the embryos, which in turn resulted in teratogenesis of abalone embryos (Zhou *et al.*, 2011a). The gene *17 β -HsD 12* participates in steroid biosynthesis, which is important for development, growth and reproduction (Mindnich *et al.*, 2004). This gene has been demonstrated as a key regulator of early embryonic development of the Arctic charr *Salvelinus alpinus*, facilitating the maintenance of steroid homeostasis in developing embryos (Khan *et al.*, 1997). In light of these considerations, Zhou *et al.* (2011a) proposed that down-regulation of the gene may interfere with the steroid biosynthesis during abalone embryogenesis, thereby causing defects during early development. These mechanisms established by Zhou *et al.* (2011a) are still preliminary and have to be independently verified before we can start to develop a comprehensive and coherent model of PAE-induced embryonic disruption.

Chapter 6

General discussion and future directions

6.1 General discussion

This PhD project has made contributions to improve our understanding of male reproductive biology in an important species of aquatic annelids and the reproductive toxicity of several compounds including the plasticisers, phthalate esters.

6.1.1 Established a comprehensive model of male reproductive system and spermatogenesis in broadcast-spawning polychaetes

The first part of this PhD project was designed to elucidate the functional and gross anatomy of the male reproductive system as well as the general pattern of spermatogenesis in the marine invertebrate *G. caespitosa*. Spermatogenesis in a wide range of polychaetes has been described, however, a large portion of these published studies have failed to provide a comprehensive model of sperm production and development. Since a substantial portion of spermatogenesis occurs while the differentiating germ cells are floating freely in the germinal fluid, identification of the various germ cell types in polychaetes becomes particularly challenging and time-consuming. Apart from distinct morphological events (e.g. formation of the synaptonemal complex or elongation of the sperm flagellum) which occur during sperm development, the size and relative position of germ cells have been widely used to identify different types/stages of spermatogenic cells in mammalian species. In relation to the spermatogenesis in polychaetes, the position and size of the freely floating germ cells cannot be regarded as the primary indicator for the determination of a cell type and caution should be exercised particularly for the species whose spermatocytes and spermatids are all liberated into the coelomic cavity.

While spermatogenesis has been well studied in higher order animals, the pattern of germ cell differentiation in invertebrates should be also described in detail so as to acquire a more comprehensive understanding of the reproductive biology of these species. Given that the pattern of spermatogenesis in polychaetes has been demonstrated to correlate with their reproductive traits and even phylogenetic positions (Rouse, 1999), the study of male reproductive function including insights into how spermatogenesis and sperm differentiation are organized and regulated has become particularly important.

6.1.2 Discovered the similarities between the male reproductive system of vertebrates and invertebrates

A comparative study of the male reproductive biology was incorporated into this project, in order to establish parallels between the male reproductive system in this simple annelid and human beings were discovered for the first time. In most studied polychaetes, the location and basic structure of the male gonads have been described, but the migration of the germ cells within their reproductive systems has never been documented. The differentiating germ cells are released to the coelomic cavity after undergoing mitoses, however the coelomic cavity is still a very structured environment; for example, the step 1 spermatids were rarely observed in the compartments close to main sperm duct (or vas deferens). Similar to the testis in higher animals, different parts of the male reproductive system in polychaetes exhibit different structure, house different types of germ cells and perform different functions. Different from most other species, broadcast-spawning invertebrates need to produce large numbers of gametes to maintain a high level of reproductive success as fertilisation is largely dependent upon flows within in the water column randomly bringing the gametes together. Elucidation of male reproductive system facilitates a deeper understanding of how reproduction in the broadcast-spawners is

organised and provides information for comparative study of reproductive system between species with different reproductive characteristics.

6.1.3 Demonstrated that the differentiation of spermatids was intrinsically programmed

The detachment of spermatogenic cells from the seminiferous epithelium and the entire process of spermiogenesis was found to occur in the lumen of the germinal chamber as has been previously documented in other polychaete species [e.g. *Marenzelleria viridis* (Bochert, 1996), *Parergodrilus heideri* (Purschke, 2002), *Phragmatopoma lapidosa* (Eckelbarger, 1984)]. However, the potential of the cell-free differentiation process has been neglected until the current study occurred. Understanding the mechanisms that lead to the differentiation of male germ cells from diploid spermatogonial stem cells through mitotic and meiotic divisions to mature haploid spermatozoa has been a major quest for many decades. As the entire process of spermatogenesis in mammalian species occurs in the recesses of Sertoli cells, the recapitulation of this process *in vitro* is extremely challenging. Although significant information on the regulation of spermatogenesis has been acquired through manipulation of the genome, an *in vitro* model is still required to generate a full understanding of this complex differentiation process. The ultrastructural observations described in this study alongside the experimental induction of limited spermiogenesis in a simple culture medium collectively demonstrate that the entire spermatogenic/spermiogenic process in this species of polychaetes was self-determined, without the need for close association with a somatic nurse cell. This study therefore suggests that this particular species of polychaete might be a convenient model to study cellular differentiation in the male germ line, particularly when it comes to the complex process of spermiogenesis.

6.1.4 Unlocked the mechanism of embryonic disruption originated from phthalate ester-induced sperm impairment

The damage induced by a large variety of hazardous substances in mammalian spermatozoa has been extensively investigated by previous toxicological studies (Chitra *et al.*, 2003; Duty *et al.*, 2003). Comparatively speaking, the far-reaching disruption that such toxicant-induced sperm impairments might impose on embryogenesis has not been as well studied as direct damage to the spermatozoa in terms of motility and DNA integrity. This lack of focus on embryogenesis reflects the obvious constraints of the use of human embryos in laboratory research and the limited number of oocytes that mammals can produce. Moreover, the mouse model is not reflective of the possible disruption that may occur in human embryos in the face of any cytoskeletal disruption since it has been demonstrated that the mouse embryo used its maternal centrosome to form bipolar spindles during embryo cleavage while the maternal centrosomes in humans remain non-functional during embryogenesis (Schatten *et al.*, 1985). *G. caespitosa* is a promising model for the study of sperm damage-related embryonic disruption since it produces a virtually unlimited number of viable spermatozoa and oocytes and is able to accomplish the early embryonic cleavages within 5 h. During the analysis of phthalate-induced sperm impairment, high concentrations of DBP were found to be incapable of inducing a loss of sperm motility or cause significant oxidative DNA damage in *G. caespitosa*, distinct from previous investigations on the spermatozoa of humans and other mammals (Duty *et al.*, 2003; Hauser *et al.*, 2007). This study then established a novel mechanism that might explain the resultant embryonic malformation: DBP was found to cause sperm centriolar damage by inducing intracellular lipid peroxidation, leading to cytoskeletal disruption in the subsequent embryogenesis. The toxicant-induced disruption

of sperm centriole integrity and function is an entirely novel finding that has not been previously reported. This organelle is inherited by the oocytes during sperm incorporation and is rather important during embryogenesis given the vital role that it plays in assembling and organising microtubules. This study therefore highlighted the important role that the centrioles play in male fertility and embryogenesis and highlighted their vulnerability to attacks by electrophilic lipid aldehydes.

6.1.5 Demonstrated the sensitivity of spermatozoa to a range of marine pollutants

In the last portion of this PhD project, the sensitivity of spermatozoa in *G. caespitosa* was studied through a series of sperm toxicity tests. During this study, several of the tested chemicals were found to be able to induce significant reductions in subsequent embryogenesis including distinct patterns of malformation at concentrations lower than the level detected in highly polluted environments. Therefore, combined with a number of other attributes that *G. caespitosa* presents, the gametes of this species can be regarded as sensitive indicators for certain chemicals in marine environments giving this species some potential as an experimental model for the study of male reproductive biology and chemical toxicity.

6.2 Future directions

6.2.1 Investigate the self-renewal process of spermatogonial stem cells in *G. caespitosa*.

An important future goal in this research will be to analyse the kinetics of spermatogenesis, in order to reveal the pattern of spermatogonial stem cell self-renewal and differentiation, using a radioisotope labelling technique. In these studies,

aggregations of *G. caespitosa* will be maintained in an aerated tank with filtered seawater containing ^3H -thymidine. Reproductively mature male *G. caespitosa* will be isolated from their tubes every two hours and fixed using routine TEM sample preparation. The ages of *G. caespitosa* are roughly determined according to their sizes and the numbers of abdominal segments. To minimise probable differences in the reproductive system between ages, the various phases of spermatogonial development will be only determined and calculated in *G. caespitosa* which are of similar age. Ultimately the cycles of spermatogonial differentiation and renewal will be estimated according to the average ratios between spermatogonia in different phases of development and primary spermatocytes. The duration of the entire spermatogenic process will also be determined according to the presence of isotope-labelled spermatozoa. Furthermore, daily sperm output can be calculated by making comparisons between the amounts of isotope-labelled spermatogonia/primary spermatocytes at different time points.

6.2.2 Optimise the system for differentiating spermatids *in vitro*

Proteins in male and female body fluid will be segmented using SDS-PAGE gel to investigate if some specific protein bands appear exclusively in the male one. Analytical mass spectrometry will also be used to compare the proteomic structure of germinal fluid from both sexes. The determination of obtained protein candidates will be achieved using the sequencing database of *Capitella teleta* (Polychaeta: Capitellidae), which is the only annelid worm whose gene has been fully sequenced. To narrow down the protein candidates, male germinal fluid will also be fractionated using size-exclusion chromatography. Spermatids will then be cultured in these different protein fractions in order to determine the approximate molecular mass of proteins supporting differentiation. The fractions which are found to facilitate the differentiation of spermatids will then be

further examined using mass spectrometry. In these studies, the salinity, pH and osmolality of the germinal fluid will also be carefully controlled to simulate the *in vivo* environment.

6.2.3 Investigate the changes that DBP-induced in sperm centrioles

The sperm centrioles, as well as the pericentriolar material in the spermatozoa will be collected and analysed to determine the changes that DBP induces on the centrioles. As the centrioles have never been studied in this species, it may be better to use a higher mammal model to conduct this analysis, which will also provide more profound insights into the DBP-induced sperm damage in mammalian species. Once again mass spectrometry will be extremely helpful in determining the molecular features of the 4-HNE adducts that so effectively compromise centriolar function.

6.2.4 Assess the sensitivity of *G. caespitosa* to effluents in laboratory and field studies

Polluted seawater samples will be collected from different sites along Australian South-eastern coast and assessed using the *G. caespitosa* model established during my PhD project. As part of these studies, aggregations of *G. caespitosa* will be collected from polluted areas or be reared in polluted seawater samples for certain periods of time and the impacts on reproductive function as a consequence of whole body exposure will then assessed. Via such studies, the true potential of *G. caespitosa* as a sensitive bio-indicator species will be determined.

References

- Adams, S. M. (2005). Assessing cause and effect of multiple stressors on marine systems. *Mar Pollut Bull* **51**:649-657. doi: 10.1016/j.marpolbul.2004.11.040
- Ahn, I.-Y., Kang, J., and Kim, K.-W. (2001). The effect of body size on metal accumulations in the bivalve *Laternula elliptica*. *Antarct Sci* **13**:355-362. doi: 10.1017/S0954102001000505
- Aitken, R. J., Baker, M. A., De Iuliis, G. N., and Nixon, B. (2010a). New Insights into Sperm Physiology and Pathology. In U.-F. Habenicht and J.R. Aitken (eds) *Fertility Control*. Springer Berlin Heidelberg, Berlin, Heidelberg, pp. 99-115.
- Aitken, R. J., Buckingham, D. W., Carreras, A., and Stewart Irvine, D. (1996). Superoxide dismutase in human sperm suspensions: Relationship with cellular composition, oxidative stress, and sperm function. *Free Radic Biol Med* **21**:495-504. doi: 10.1016/0891-5849(96)00119-0
- Aitken, R. J., and Clarkson, J. S. (1987). Cellular basis of defective sperm function and its association with the genesis of reactive oxygen species by human spermatozoa. *J Reprod Fertil* **81**:459-469. doi: 10.1530/jrf.0.0810459
- Aitken, R. J., Clarkson, J. S., and Fishel, S. (1989). Generation of reactive oxygen species, lipid peroxidation, and human sperm function. *Biol Reprod* **41**:183-197. doi: 10.1095/biolreprod41.1.183
- Aitken, R. J., De Iuliis, G. N., Finnie, J. M., Hedges, A., and McLachlan, R. I. (2010b). Analysis of the relationships between oxidative stress, DNA damage and sperm vitality in a patient population: development of diagnostic criteria. *Human Reproduction* **25**:2415-2426. doi: 10.1093/humrep/deq214
- Aitken, R. J., Fisher, H. M., Fulton, N., Gomez, E., Knox, W., Lewis, B., and Irvine, S. (1997). Reactive oxygen species generation by human spermatozoa is induced by exogenous NADPH and inhibited by the flavoprotein inhibitors diphenylene iodonium and quinacrine. *Molecular Reproduction and Development* **47**:468-482. doi: 10.1002/(SICI)1098-2795(199708)47:4<468::AID-MRD14>3.0.CO;2-S
- Aitken, R. J., Jones, K. T., and Robertson, S. A. (2012a). Reactive Oxygen Species and Sperm Function—In Sickness and In Health. *Journal of Andrology* **33**:1096-1106. doi: 10.2164/jandrol.112.016535
- Aitken, R. J., Ryan, A. L., Curry, B. J., and Baker, M. A. (2003). Multiple forms of redox activity in populations of human spermatozoa. *Molecular Human Reproduction* **9**:645-661. doi: 10.1093/molehr/gag086
- Aitken, R. J., Whiting, S., De Iuliis, G. N., McClymont, S., Mitchell, L. A., and Baker, M. A. (2012b). Electrophilic Aldehydes Generated by Sperm Metabolism Activate Mitochondrial Reactive Oxygen Species Generation and Apoptosis by

Targeting Succinate Dehydrogenase. *J Biol Chem* **287**:33048-33060. doi: 10.1074/jbc.M112.366690

Alvarez, J. G., Touchstone, J. C., Blasco, L., and Storey, B. T. (1987). Spontaneous Lipid Peroxidation and Production of Hydrogen Peroxide and Superoxide in Human Spermatozoa Superoxide Dismutase as Major Enzyme Protectant Against Oxygen Toxicity. *J Androl* **8**:338-348. doi: 10.1002/j.1939-4640.1987.tb00973.x

Andrews, J., and Anderson, D. (1962). The development of the polychaete *Galeolaria caespitosa* Lamarck (Fam. Serpulidae). *Proc Linn Soc N S W* **87**:185-188.

Ardón, F., Rodríguez-Miranda, E., Beltrán, C., Hernández-Cruz, A., and Darszon, A. (2009). Mitochondrial inhibitors activate influx of external Ca²⁺ in sea urchin sperm. *Biochimica et Biophysica Acta (BBA) - Bioenergetics* **1787**:15-24. doi: 10.1016/j.bbabi.2008.10.003

Arkhipenko Yu, V., Meerson, F. Z., Sazontova, T. G., and Kagan, V. E. (1985). Mode of lipid peroxidation-induced inhibition of Na, K-ATPase. *Acta Physiol Pharmacol Bulg* **11**:70-78.

Arslan, O. C., and Parlak, H. (2007). Embryotoxic effects of nonylphenol and octylphenol in sea urchin *Arbacia lixula*. *Ecotoxicology* **16**:439-444. doi: 10.1007/s10646-007-0147-z

Arslan, O. C., Parlak, H., Oral, R., and Katalay, S. (2007). The Effects of Nonylphenol and Octylphenol on Embryonic Development of Sea Urchin (*Paracentrotus lividus*). *Archives of Environmental Contamination and Toxicology* **53**:214-219. doi: 10.1007/s00244-006-0042-2

Au, D. (2004). The application of histo-cytopathological biomarkers in marine pollution monitoring: a review. *Mar Pollut Bull* **48**:817-834. doi: 10.1016/j.marpolbul.2004.02.032

Barckmann, B., and Simonelig, M. (2013). Control of maternal mRNA stability in germ cells and early embryos. *Biochim Biophys Acta* **1829**:714-724. doi: 10.1016/j.bbagr.2012.12.011

Baumber, J., Ball, B. A., Gravance, C. G., Medina, V., and Davies-Morel, M. C. (2000). The effect of reactive oxygen species on equine sperm motility, viability, acrosomal integrity, mitochondrial membrane potential, and membrane lipid peroxidation. *Journal of andrology* **21**:895-902.

Bayr, H. (2005). Reactive oxygen species. *Critical Care Medicine* **33**:S498-S501. doi: 10.1097/01.ccm.0000186787.64500.12

Beal, M. F. (1995). Aging, energy, and oxidative stress in neurodegenerative diseases. *Annals of Neurology* **38**:357-366. doi: 10.1002/ana.410380304

- Beiras, R., Bellas, J., Fernández, N., Lorenzo, J., and Cobelo-García, A. (2003). Assessment of coastal marine pollution in Galicia (NW Iberian Peninsula); metal concentrations in seawater, sediments and mussels (*Mytilus galloprovincialis*) versus embryo–larval bioassays using *Paracentrotus lividus* and *Ciona intestinalis*. *Mar Environ Res* **56**:531-553. doi: 10.1016/S0141-1136(03)00042-4
- Belfroid, A., van Velzen, M., van der Horst, B., and Vethaak, D. (2002). Occurrence of bisphenol A in surface water and uptake in fish: evaluation of field measurements. *Chemosphere* **49**:97-103. doi: 10.1016/S0045-6535(02)00157-1
- Berlett, B. S., and Stadtman, E. R. (1997). Protein Oxidation in Aging, Disease, and Oxidative Stress. *Journal of Biological Chemistry* **272**:20313-20316. doi: 10.1074/jbc.272.33.20313
- Birch, G. (2000). Marine pollution in Australia, with special emphasis on central New South Wales estuaries and adjacent continental margin. *Int J Environ Pollut* **13**:573-607. doi: 10.1504/IJEP.2000.002334
- Blake, E. A., and Van Dover, C. L. (2005). The reproductive biology of *Amathys lutzi*, an ampharetid polychaete from hydrothermal vents on the Mid-Atlantic Ridge. *Invertebr Biol* **124**:254-264. doi: 10.1111/j.1744-7410.2005.00022.x
- Blanc, E. M., Keller, J. N., Fernandez, S., and Mattson, M. P. (1998). 4-hydroxynonenal, a lipid peroxidation product, impairs glutamate transport in cortical astrocytes. *Glia* **22**:149-160. doi: 10.1002/(SICI)1098-1136(199802)22:2<149::AID-GLIA6>3.0.CO;2-2
- Bloom, W., and Fawcett, D. (1975). A textbook of histology. W. B. Saunders, Philadelphia, pp. 805-855.
- Bochert, R. (1996). An electron microscopic study of spermatogenesis in *Marenzelleria viridis* (Verrill, 1873) (Polychaeta: Spionidae). *Acta Zool* **77**:191-199. doi: 10.1111/j.1463-6395.1996.tb01263.x
- Boening, D. W. (1999). An evaluation of bivalves as biomonitors of heavy metals pollution in marine waters. *Environ Monit Assess* **55**:459-470. doi: 10.1023/a:1005995217901
- Boyd, G. R., Palmeri, J. M., Zhang, S., and Grimm, D. A. (2004). Pharmaceuticals and personal care products (PPCPs) and endocrine disrupting chemicals (EDCs) in stormwater canals and Bayou St. John in New Orleans, Louisiana, USA. *Science of The Total Environment* **333**:137-148. doi: 10.1016/j.scitotenv.2004.03.018
- Bremner, J. (2008). Species' traits and ecological functioning in marine conservation and management. *J Exp Mar Biol Ecol* **366**:37-47. doi: 10.1016/j.jembe.2008.07.007
- Bührmann, C., Westheide, W., and Purschke, G. (1996). Spermatogenesis and sperm ultrastructure in the interstitial syllid *Petitia amphophthalma* (Annelida, Polychaeta). *Ophelia* **45**:81-100. doi: 10.1080/00785326.1996.10432464

- Burger, J., and Gochfeld, M. (2004). Marine Birds as Sentinels of Environmental Pollution. *EcoHealth* **1**:263-274. doi: 10.1007/s10393-004-0096-4
- Burrue, V., Klooster, K. L., Chitwood, J., Ross, P. J., and Meyers, S. A. (2013). Oxidative damage to rhesus macaque spermatozoa results in mitotic arrest and transcript abundance changes in early embryos. *Biol Reprod* **89**:72, 71-11. doi: 10.1095/biolreprod.113.110981
- Cabiscol, E., Tamarit, J., and Ros, J. (2000). Oxidative stress in bacteria and protein damage by reactive oxygen species. *International microbiology : the official journal of the Spanish Society for Microbiology* **3**:3-8.
- Cabiscol, E., Tamarit, J., and Ros, J. (2010). Oxidative stress in bacteria and protein damage by reactive oxygen species. *Int Microbiol* **3**:3-8.
- Chen, J. J., and Yu, B. P. (1994). Alterations in mitochondrial membrane fluidity by lipid peroxidation products. *Free Radical Biology and Medicine* **17**:411-418. doi: 10.1016/0891-5849(94)90167-8
- Chevion, M., Berenshtein, E., and Stadtman, E. R. (2000). Human studies related to protein oxidation: protein carbonyl content as a marker of damage. *Free Radic Res* **33 Suppl**:S99-108.
- Chiarelli, R., and Roccheri, M. C. (2014). Marine invertebrates as bioindicators of heavy metal pollution. *Open J Met* **4**:14. doi: 10.4236/ojmetal.2014.44011
- Chitra, K. C., Latchoumycandane, C., and Mathur, P. P. (2003). Induction of oxidative stress by bisphenol A in the epididymal sperm of rats. *Toxicology* **185**:119-127. doi: 10.1016/S0300-483X(02)00597-8
- Chu, D. S., and Shakes, D. C. (2013). Spermatogenesis. In T. Schedl (ed) Germ cell development in *C. elegans*. Springer New York, New York, NY, pp. 171-203.
- Cooke, M. S., Evans, M. D., Dizdaroglu, M., and Lunec, J. (2003). Oxidative DNA damage: mechanisms, mutation, and disease. *The FASEB Journal* **17**:1195-1214. doi: 10.1096/fj.02-0752rev
- Cooper, T. G. (1986a). Epididymal Structure and Function The Epididymis, Sperm Maturation and Fertilisation. Springer Berlin Heidelberg, Berlin, Heidelberg, pp. 117-139.
- Cooper, T. G. (1986b). Maturation of Spermatozoa in the Epididymis The Epididymis, Sperm Maturation and Fertilisation. Springer Berlin Heidelberg, Berlin, Heidelberg, pp. 1-8.
- Cormack, D. H. (2001). Essential histology. Lippincott Williams & Wilkins, Maryland, USA, pp. 414-415.

- Cotter, E., O'Riordan, R., and Myers, A. (2003). A histological study of reproduction in the serpulids *Pomatoceros triqueter* and *Pomatoceros lamarckii* (Annelida: Polychaeta). *Mar Biol* **142**:905-914. doi: 10.1007/s00227-002-0987-2
- Crimaldi, J. P. (2012). The role of structured stirring and mixing on gamete dispersal and aggregation in broadcast spawning. *J Exp Biol* **215**:1031-1039. doi: 10.1242/jeb.060145
- Currie, D. R., McArthur, M. A., and Cohen, B. F. (2000). Reproduction and distribution of the invasive European fanworm *Sabella spallanzanii* (Polychaeta: Sabellidae) in Port Phillip Bay, Victoria, Australia. *Mar Biol* **136**:645-656. doi: 10.1007/s002270050724
- Davies, K. J. A. (1995). Oxidative stress: the paradox of aerobic life. *Biochemical Society Symposium* **61**:1-31. doi: 10.1042/bss0610001
- de Kretser, D. M., Loveland, K. L., Meinhardt, A., Simorangkir, D., and Wreford, N. (1998). Spermatogenesis. *Human Reproduction* **13**:1-8. doi: 10.1093/humrep/13.suppl_1.1
- de Lamirande, E., and Gagnon, C. (1995). Impact of reactive oxygen species on spermatozoa: a balancing act between beneficial and detrimental effects. *Human Reproduction* **10**:15-21. doi: 10.1093/humrep/10.suppl_1.15
- de Lamirande, E., Jiang, H., Zini, A., Kodama, H., and Gagnon, C. (1997). Reactive oxygen species and sperm physiology. *Reviews of Reproduction* **2**:48-54. doi: 10.1530/ror.0.0020048
- de Rooij, D. (2001). Proliferation and differentiation of spermatogonial stem cells. *Reproduction* **121**:347-354. doi: 10.1530/rep.0.1210347
- de Rooij, D. G., and Grootegoed, J. A. (1998). Spermatogonial stem cells. *Current Opinion in Cell Biology* **10**:694-701. doi: 10.1016/S0955-0674(98)80109-9
- Dean, H. K. (2008). The use of polychaetes (Annelida) as indicator species of marine pollution: a review. *Rev Biol Trop* **56**:11-38.
- Derraik, J. G. (2002). The pollution of the marine environment by plastic debris: a review. *Mar Pollut Bull* **44**:842-852. doi: 10.1016/S0025-326X(02)00220-5
- Desai, N., Sabanegh Jr, E., Kim, T., and Agarwal, A. (2010). Free Radical Theory of Aging: Implications in Male Infertility. *Urology* **75**:14-19. doi: 10.1016/j.urology.2009.05.025
- Doi, A. M., Pham, R. T., Hughes, E. M., Barber, D. S., and Gallagher, E. P. (2004). Molecular cloning and characterization of a glutathione S-transferase from largemouth bass (*Micropterus salmoides*) liver that is involved in the detoxification of 4-hydroxynonenal. *Biochemical Pharmacology* **67**:2129-2139. doi: 10.1016/j.bcp.2004.01.024

- Draviam, V. M., Xie, S., and Sorger, P. K. (2004). Chromosome segregation and genomic stability. *Curr Opin Genetics Dev* **14**:120-125. doi: 10.1016/j.gde.2004.02.007
- Duty, S. M., Singh, N. P., Silva, M. J., Barr, D. B., Brock, J. W., Ryan, L., Herrick, R. F., Christiani, D. C., and Hauser, R. (2003). The relationship between environmental exposures to phthalates and DNA damage in human sperm using the neutral comet assay. *Environ Health Perspect* **111**:1164-1169. doi: 10.1289/ehp.5756
- Eckelbarger, K., and Grassle, J. (1987). Spermatogenesis, sperm storage and comparative sperm morphology in nine species of *Capitella*, *Capitomastus* and *Capitellides* (Polychaeta: Capitellidae). *Mar Biol* **95**:415-429. doi: 10.1007/BF00409572
- Eckelbarger, K., Watling, L., and Fournier, H. (2005). Reproductive biology of the deep-sea polychaete *Gorgoniapolynoe caeciliae* (Polynoidae), a commensal species associated with octocorals. *J Mar Biol Assoc U K* **85**:1425-1433. doi: 10.1017/S0025315405012609
- Eckelbarger, K., Young, C., Llodra, E. R., Brooke, S., and Tyler, P. (2001). Gametogenesis, spawning behavior, and early development in the "iceworm" *Hesiocaeca methanicola* (Polychaeta: Hesionidae) from methane hydrates in the Gulf of Mexico. *Mar Biol* **138**:761-775. doi: 10.1007/s002270000510
- Eckelbarger, K. J. (1984). Ultrastructure of spermatogenesis in the reef-building polychaete *Phragmatopoma lapidosa* (Sabellariidae) with special reference to acrosome morphogenesis. *J Ultrastruct Res* **89**:146-164. doi: 10.1016/S0022-5320(84)80011-8
- Eckelbarger, K. J., and Young, C. M. (2002). Spermiogenesis and modified sperm morphology in the "seepworm" *Methanoaricia dendrobranchiata* (Polychaeta: Orbiniidae) from a methane seep environment in the Gulf of Mexico: implications for fertilization biology. *Biol Bull* **203**:134-143. doi: 10.2307/1543382
- Falkenberg, L. J., Havenhand, J. N., and Styan, C. A. (2016). Sperm Accumulated Against Surface: A novel alternative bioassay for environmental monitoring. *Mar Environ Res* **114**:51-57. doi: 10.1016/j.marenvres.2015.12.005
- Farombi, E. O., Abarikwu, S. O., Adedara, I. A., and Oyeyemi, M. O. (2007). Curcumin and kolaviron ameliorate di-n-butylphthalate-induced testicular damage in rats. *Basic Clin Pharmacol Toxicol* **100**:43-48. doi: 10.1111/j.1742-7843.2007.00005.x
- Foe, V. E., and von Dassow, G. (2008). Stable and dynamic microtubules coordinately shape the myosin activation zone during cytokinetic furrow formation. *J Cell Biol* **183**:457-470. doi: 10.1083/jcb.200807128
- Franzén, Å., and Rice, S. A. (1988). Spermatogenesis, male gametes and gamete interactions. *The ultrastructure of polychaeta. Microfauna Mar* **4**:309-333.

- Fukazawa, H., Hoshino, K., Shiozawa, T., Matsushita, H., and Terao, Y. (2001). Identification and quantification of chlorinated bisphenol A in wastewater from wastepaper recycling plants. *Chemosphere* **44**:973-979. doi: 10.1016/S0045-6535(00)00507-5
- Galloway, T. S., Sanger, R. C., Smith, K. L., Fillmann, G., Readman, J. W., Ford, T. E., and Depledge, M. H. (2002). Rapid assessment of marine pollution using multiple biomarkers and chemical immunoassays. *Environ Sci Technol* **36**:2219-2226. doi: 10.1021/es010300w
- Gao, Y., Zhang, T., Zhang, L., Qiu, T., Xue, D., and Yang, H. (2014). Ultrastructure developments during spermiogenesis in *Polydora ciliata* (Annelida: Spionidae), a parasite of mollusca. *Journal of Ocean University of China* **13**:1071-1077.
- Gartner, L. P., Hiatt, J. L., and Strum, J. M. (2010). Cell biology and histology. Lippincott Williams & Wilkins, Philadelphia, USA, pp. 311-315.
- Gharagozloo, P., and Aitken, R. J. (2011). The role of sperm oxidative stress in male infertility and the significance of oral antioxidant therapy. *Human Reproduction* **26**:1628-1640. doi: 10.1093/humrep/der132
- Gherardi, M., Lepore, E., Sciscioli, M., Mercurio, M., Licciano, M., and Giangrande, A. (2011). A study on spermatogenesis of three Mediterranean serpulid species. *Ital J Zool* **78**:174-181. doi: 10.1080/11250003.2010.529468
- Ghirardini, A. V., Novelli, A. A., Likar, B., Pojana, G., Ghetti, P. F., and Marcomini, A. (2001). Sperm cell toxicity test using sea Urchin *Paracentrotus lividus* Lamarck (Echinodermata: Echinoidea): Sensitivity and discriminatory ability toward anionic and nonionic surfactants. *Environmental Toxicology and Chemistry* **20**:644-651. doi: 10.1002/etc.5620200325
- Giangrande, A. (1997). Polychaete reproductive patterns, life cycles and life histories: an overview. In A. Ansell, R. Gibson, and M. Barnes (eds) *Oceanography and marine biology: an annual review*. Vol. 35. UCL Press, London, pp. 323-386.
- Giangrande, A., Licciano, M., and Musco, L. (2005). Polychaetes as environmental indicators revisited. *Mar Pollut Bull* **50**:1153-1162. doi: 10.1016/j.marpolbul.2005.08.003
- Giangrande, A., Licciano, M., Pagliara, P., and Gambi, M. (2000). Gametogenesis and larval development in *Sabella spallanzanii* (Polychaeta: Sabellidae) from the Mediterranean Sea. *Mar Biol* **136**:847-861. doi: 10.1007/s002279900251
- Goldberg, E. D., and Bertine, K. K. (2000). Beyond the mussel watch — new directions for monitoring marine pollution. *Sci Total Environ* **247**:165-174. doi: 10.1016/S0048-9697(99)00488-X
- González-Casado, A., Navas, N., del Olmo, M., and Vílchez, J. L. (1998). Determination of Bisphenol A in Water by Micro Liquid—Liquid Extraction Followed by

Silylation and Gas Chromatography—Mass Spectrometry Analysis. *Journal of Chromatographic Science* **36**:565-570. doi: 10.1093/chromsci/36.11.565

- Gopalakrishnan, S., Thilagam, H., and Raja, P. V. (2008). Comparison of heavy metal toxicity in life stages (spermioxicity, egg toxicity, embryotoxicity and larval toxicity) of *Hydroides elegans*. *Chemosphere* **71**:515-528. doi: 10.1016/j.chemosphere.2007.09.062
- Greenbaum, M. P., Iwamori, T., Buchold, G. M., and Matzuk, M. M. (2011). Germ Cell Intercellular Bridges. *Cold Spring Harbor Perspectives in Biology* **3**:a005850. doi: 10.1101/cshperspect.a005850
- Griveau, J. F., Dumont, E., Renard, P., Callegari, J. P., and Le Lannou, D. (1995). Reactive oxygen species, lipid peroxidation and enzymatic defence systems in human spermatozoa. *J Reprod Fertil* **103**:17-26. doi: 10.1530/jrf.0.1030017
- Gupta, G. S. (2005). Proteomics of spermatogenesis. Springer-Verlag, USA, pp. 1-20.
- Haglund, K., Nezis, I. P., and Stenmark, H. (2011). Structure and functions of stable intercellular bridges formed by incomplete cytokinesis during development. *Communicative & Integrative Biology* **4**:1-9. doi: 10.4161/cib.4.1.13550
- Halliwell, B., and Aruoma, O. I. (1991). DNA damage by oxygen-derived species Its mechanism and measurement in mammalian systems. *FEBS Letters* **281**:9-19. doi: 10.1016/0014-5793(91)80347-6
- Halliwell, B., and Chirico, S. (1993). Lipid peroxidation: its mechanism, measurement, and significance. *The American Journal of Clinical Nutrition* **57**:715S-724S.
- Halt, M. N., Kupriyanova, E. K., Cooper, S. J., and Rouse, G. W. (2009). Naming species with no morphological indicators: species status of *Galeolaria caespitosa* (Annelida: Serpulidae) inferred from nuclear and mitochondrial gene sequences and morphology. *Invertebr Syst* **23**:205-222. doi: 10.1071/IS09003
- Haschek, W. M., Rousseaux, C. G., and Wallig, M. A. (2010). Male Reproductive System Fundamentals of Toxicologic Pathology (Second edition). Academic Press, San Diego, pp. 553-597.
- Hashimoto, S., Horiuchi, A., Yoshimoto, T., Nakao, M., Omura, H., Kato, Y., Tanaka, H., Kannan, K., and Giesy, J. P. (2005). Horizontal and Vertical Distribution of Estrogenic Activities in Sediments and Waters from Tokyo Bay, Japan. *Archives of Environmental Contamination and Toxicology* **48**:209-216. doi: 10.1007/s00244-003-0205-3
- Haubruge, E., Petit, F., and Gage, M. J. G. (2000). Reduced sperm counts in guppies (*Poecilia reticulata*) following exposure to low levels of tributyltin and bisphenol A. *Proceedings of the Royal Society of London. Series B: Biological Sciences* **267**:2333-2337. doi: 10.1098/rspb.2000.1288

- Hauser, R., Meeker, J. D., Singh, N. P., Silva, M. J., Ryan, L., Duty, S., and Calafat, A. M. (2007). DNA damage in human sperm is related to urinary levels of phthalate monoester and oxidative metabolites. *Hum Reprod* **22**:688-695. doi: 10.1093/humrep/del428
- Hawkins, C. L., and Davies, M. J. (2001). Generation and propagation of radical reactions on proteins. *Biochimica et Biophysica Acta (BBA) - Bioenergetics* **1504**:196-219. doi: 10.1016/S0005-2728(00)00252-8
- Haynes, D. H. (1983). Mechanism of Ca²⁺ transport by Ca²⁺-Mg²⁺-ATPase pump: analysis of major states and pathways. *American Journal of Physiology - Gastrointestinal and Liver Physiology* **244**:G3-G12.
- Henrikson, R. C., and Mazurkiewicz, J. E. (1997). Histology. Lippincott Williams & Wilkins, Maryland, USA, pp. 394-395.
- Hess, R. A., and de Franca, L. R. (2008). Spermatogenesis and Cycle of the Seminiferous Epithelium. In C.Y. Cheng (ed) *Molecular Mechanisms in Spermatogenesis*. Springer New York, New York, NY, pp. 1-15.
- Higuchi, Y. (2003). Chromosomal DNA fragmentation in apoptosis and necrosis induced by oxidative stress. *Biochemical Pharmacology* **66**:1527-1535. doi: 10.1016/S0006-2952(03)00508-2
- Hilário, A., Young, C. M., and Tyler, P. A. (2005). Sperm storage, internal fertilization, and embryonic dispersal in vent and seep tubeworms (Polychaeta: Siboglinidae: Vestimentifera). *Biol Bull* **208**:20-28. doi: 10.2307/3593097
- Hollows, C. F., Johnston, E. L., and Marshall, D. J. (2007). Copper reduces fertilisation success and exacerbates Allee effects in the field. *Mar Ecol Prog Ser* **333**:51-60. doi: 10.3354/meps333051
- Hutchings, P. (1998). Biodiversity and functioning of polychaetes in benthic sediments. *Biodivers Conserv* **7**:1133-1145. doi: 10.1023/A:1008871430178
- Islam, M. S., and Tanaka, M. (2004). Impacts of pollution on coastal and marine ecosystems including coastal and marine fisheries and approach for management: a review and synthesis. *Mar Pollut Bull* **48**:624-649. doi: 10.1016/j.marpolbul.2003.12.004
- Jamieson, B. G. M., and Rouse, G. W. (1989). The spermatozoa of the Polychaeta (Annelida): An ultrastructural review. *Biol Rev* **64**:93-157. doi: 10.1111/j.1469-185X.1989.tb00673.x
- Jarmołowicz, S., Demska-Zakęś, K., Kowalski, R., Cejko, B., Glogowski, J., and Zakęś, Z. (2010). Impact of dibutyl phthalate and benzyl butyl phthalate on motility parameters of sperm from the European pikeperch Sander lucioperca (L.). *Arch Pol Fish* **18**:149. doi: 10.2478/v10086-010-0016-x

- Johnson, M. H., and Everitt, B. J. (2007). Essential reproduction. Blackwell Publishing, Victoria, Australia.
- Jones, R., and Lin, M. (1992). Spermatogenesis in birds. *Oxf Rev Reprod Biol* **15**:233-264.
- Jonkers, N., Sousa, A., Galante-Oliveira, S., Barroso, C. M., Kohler, H.-P. E., and Giger, W. (2010). Occurrence and sources of selected phenolic endocrine disruptors in Ria de Aveiro, Portugal. *Environmental Science and Pollution Research* **17**:834-843. doi: 10.1007/s11356-009-0275-5
- Kasai, T., Ogawa, K., Mizuno, K., Nagai, S., Uchida, Y., Ohta, S., Fujie, M., Suzuki, K., Hirata, S., and Hoshi, K. (2002). Relationship between sperm mitochondrial membrane potential, sperm motility, and fertility potential. *Asian journal of andrology* **4**:97-103.
- Kennedy, A. D., and Jacoby, C. A. (1999). Biological indicators of marine environmental health: meiofauna – a neglected benthic component? *Environ Monit Assess* **54**:47-68. doi: 10.1023/a:1005854731889
- Kierszenbaum, A. L., and Tres, L. (2015). Histology and cell biology: An introduction to pathology. Elsevier Saunders, Philadelphia, USA, pp. 611-621.
- Kim, S.-K., Kim, B.-K., Shim, J.-H., Gil, J.-E., Yoon, Y.-D., and Kim, J.-H. (2006). Nonylphenol and Octylphenol-Induced Apoptosis in Human Embryonic Stem Cells Is Related to Fas-Fas Ligand Pathway. *Toxicological Sciences* **94**:310-321. doi: 10.1093/toxsci/kfl114
- Koppers, A. J., Iuliis, G. N. D., Finnie, J. M., McLaughlin, E. A., and Aitken, R. J. (2008). Significance of Mitochondrial Reactive Oxygen Species in the Generation of Oxidative Stress in Spermatozoa. *The Journal of Clinical Endocrinology & Metabolism* **93**:3199-3207. doi: doi:10.1210/jc.2007-2616
- Kudikina, N. P. (2011). Effect of hormonal compounds on embryogenesis of the pond snail *Lymnaea stagnalis* (L., 1758). *Russian Journal of Developmental Biology* **42**:180-185. doi: 10.1134/s106236041103009x
- Kupriyanova, E. K. (2006). Fertilization success in *Galeolaria caespitosa* (Polychaeta: Serpulidae): gamete characteristics, role of sperm dilution, gamete age, and contact time. *Sci Mar* **70**:309-317. doi: 10.3989/scimar.2006.70s3309
- Kupriyanova, E. K., and Havenhand, J. N. (2005). Effects of temperature on sperm swimming behaviour, respiration and fertilization success in the serpulid polychaete, *Galeolaria caespitosa* (Annelida: Serpulidae). *Invertebr Reprod Dev* **48**:7-17. doi: 10.1080/07924259.2005.9652166
- Lau, M. C., Chan, K. M., Leung, K. M. Y., Luan, T. G., Yang, M. S., and Qiu, J. W. (2007). Acute and chronic toxicities of tributyltin to various life stages of the

- marine polychaete *Hydroides elegans*. *Chemosphere* **69**:135-144. doi: 10.1016/j.chemosphere.2007.04.016
- Lee, H.-B., and Peart, T. E. (2000). Bisphenol A contamination in Canadian municipal and industrial wastewater and sludge samples. *Water Quality Res J Canada* **35**:283-298.
- Lenz, A., Costabel, U., and Maier, K. (1996). Oxidized BAL fluid proteins in patients with interstitial lung diseases. *European Respiratory Journal* **9**:307-312.
- Leppänen, M. (1995). The role of feeding behaviour in bioaccumulation of organic chemicals in benthic organisms. *Ann Zool Fennici* **32**:247-255.
- Lewis, C., and Galloway, T. (2009). Reproductive Consequences of Paternal Genotoxin Exposure in Marine Invertebrates. *Environmental Science & Technology* **43**:928-933. doi: 10.1021/es802215d
- Lewis, C., and Galloway, T. (2010). Sperm toxicity and the reproductive ecology of marine invertebrates. *Integrated Environmental Assessment and Management* **6**:188-190. doi: 10.1002/ieam.23
- Licciano, M., Giangrande, A., and Gambi, M. C. (2002). Reproduction and simultaneous hermaphroditism in *Branchiomma luctuosum* (Polychaeta, Sabellidae) from the Mediterranean Sea. *Invertebr Biol* **121**:55-65. doi: 10.1111/j.1744-7410.2002.tb00129.x
- Lin, M., and Jones, R. (1993). Spermiogenesis and spermiation in the Japanese quail (*Coturnix coturnix japonica*). *J Anat* **183**:525-535.
- Lin, M., and Jones, R. (2000). Spermiogenesis and spermiation in a monotreme mammal, the platypus, *Ornithorhynchus anatinus*. *J Anat* **196**:217-232. doi: 10.1046/j.1469-7580.2000.19620217.x
- Lipshultz, L. I., Howards, S. S., and Niederberger, C. S. (2009). *Infertility in the Male*. Cambridge University Press, Cambridge, UK, pp. 81-83.
- Liu, R., Zhou, J. L., and Wilding, A. (2004). Simultaneous determination of endocrine disrupting phenolic compounds and steroids in water by solid-phase extraction–gas chromatography–mass spectrometry. *Journal of Chromatography A* **1022**:179-189. doi: 10.1016/j.chroma.2003.09.035
- Livingstone, D. R. (2001). Contaminant-stimulated Reactive Oxygen Species Production and Oxidative Damage in Aquatic Organisms. *Marine Pollution Bulletin* **42**:656-666. doi: 10.1016/S0025-326X(01)00060-1
- Livingstone, D. R. (2003). Oxidative Stress in Aquatic Organisms in Relation to Pollution and Aquaculture. *Revue Méd. Vét.* **154**:427-430.

- Logan-Smith, M. J., Lockyer, P. J., East, J. M., and Lee, A. G. (2001). Curcumin, a Molecule That Inhibits the Ca²⁺-ATPase of Sarcoplasmic Reticulum but Increases the Rate of Accumulation of Ca²⁺. *Journal of Biological Chemistry* **276**:46905-46911. doi: 10.1074/jbc.M108778200
- Long, E. R., MacDonald, D. D., Smith, S. L., and Calder, F. D. (1995). Incidence of adverse biological effects within ranges of chemical concentrations in marine and estuarine sediments. *Environ Manage* **19**:81-97. doi: 10.1007/BF02472006
- Lücht, J., and Pfannenstiel, H.-D. (1989). Spermatogenesis in *Platynereis massiliensis* (Polychaeta: Nereidae). *Helgolander Meeresunters* **43**:19-28. doi: 10.1007/BF02365547
- Lushchak, V. I. (2011). Environmentally induced oxidative stress in aquatic animals. *Aquatic Toxicology* **101**:13-30. doi: 10.1016/j.aquatox.2010.10.006
- Mankidy, R., Wiseman, S., Ma, H., and Giesy, J. P. (2013). Biological impact of phthalates. *Toxicol Lett* **217**:50-58. doi: 10.1016/j.toxlet.2012.11.025
- Marieb, E. N. (2000). Human Anatomy & Physiology. Benjamin-Cummings, San Francisco, USA.
- Markert, B. A., Breure, A. M., and Zechmeister, H. G. (2003). Bioindicators & biomonitors: principles, concepts and applications. In J.O. Nriagu (ed) Trace metals and other contaminants in the environment. Vol. 6. Elsevier, Kidlington, Oxford, UK, pp. 595-596.
- Marsden, J., and Anderson, D. (1981). Larval development and metamorphosis of the serpulid polychaete *Galeolaria caespitosa* Lamarck. *Mar Freshwater Res* **32**:667-680. doi: 10.1071/MF9810667
- Marshall, D., and Evans, J. (2005a). The benefits of polyandry in the free-spawning polychaete *Galeolaria caespitosa*. *J Evol Biol* **18**:735-741. doi: 10.1111/j.1420-9101.2004.00873.x
- Marshall, D., and Evans, J. (2005b). Does egg competition occur in marine broadcast-spawners? *J Evol Biol* **18**:1244-1252. doi: 10.1111/j.1420-9101.2005.00947.x
- Marshall, D. J., and Bolton, T. F. (2007). Sperm release strategies in marine broadcast spawners: the costs of releasing sperm quickly. *J Exp Biol* **210**:3720-3727. doi: 10.1242/jeb.008417
- McCord, J. M. (2008). Superoxide Dismutase, Lipid Peroxidation, and Bell-Shaped Dose Response Curves. *Dose-Response* **6**. doi: 10.2203/dose-response.08-012.McCord
- Melville, F., and Pulkownik, A. (2006). Investigation of mangrove macroalgae as bioindicators of estuarine contamination. *Mar Pollut Bull* **52**:1260-1269. doi: 10.1016/j.marpolbul.2006.02.021

- Minchinton, T. E. (1997). Life on the edge: conspecific attraction and recruitment of populations to disturbed habitats. *Oecologia* **111**:45-52. doi: 10.1007/s004420050206
- Mindnich, R., Möller, G., and Adamski, J. (2004). The role of 17 beta-hydroxysteroid dehydrogenases. *Molecular and Cellular Endocrinology* **218**:7-20. doi: 10.1016/j.mce.2003.12.006
- Misra, M. K., Sarwat, M., Bhakuni, P., Tuteja, R., and Tuteja, N. (2009). Oxidative stress and ischemic myocardial syndromes. *Medical Science Monitor* **15**:RA209-RA219.
- Moore, D. W., Dillon, T. M., and Suedel, B. C. (1991). Chronic toxicity of tributyltin to the marine polychaete worm, *Neanthes arenaceodentata*. *Aquatic Toxicology* **21**:181-198. doi: 10.1016/0166-445X(91)90072-H
- Musset, B., Clark, R. A., DeCoursey, T. E., Petheo, G. L., Geiszt, M., Chen, Y., Cornell, J. E., Eddy, C. A., Brzyski, R. G., and El Jamali, A. (2012). NOX5 in human spermatozoa: expression, function, and regulation. *Journal of Biological Chemistry* **287**:9376-9388. doi: 10.1074/jbc.M111.314955
- Nakagawa, Y., and Tayama, S. (2000). Metabolism and cytotoxicity of bisphenol A and other bisphenols in isolated rat hepatocytes. *Archives of Toxicology* **74**:99-105. doi: 10.1007/s002040050659
- Nordberg, J., and Arnér, E. S. J. (2001). Reactive oxygen species, antioxidants, and the mammalian thioredoxin system1. *Free Radical Biology and Medicine* **31**:1287-1312. doi: 10.1016/S0891-5849(01)00724-9
- Oatley, J. M., and Brinster, R. L. (2008). Regulation of spermatogonial stem cell self-renewal in mammals. *Ann Rev Cell Dev Biol* **24**:263-286. doi: 10.1146/annurev.cellbio.24.110707.175355
- Oliver, J., and Babcock, R. (1992). Aspects of the Fertilization Ecology of Broadcast Spawning Corals: Sperm Dilution Effects and in situ Measurements of Fertilization. *Biol Bull* **183**:409-417.
- Olujimi, O. O., Fatoki, O. S., Odendaal, J. P., and Daso, A. P. (2012). Chemical monitoring and temporal variation in levels of endocrine disrupting chemicals (priority phenols and phthalate esters) from selected wastewater treatment plant and freshwater systems in Republic of South Africa. *Microchemical Journal* **101**:11-23. doi: 10.1016/j.microc.2011.09.011
- Özlem, Ç. A., and Hatice, P. (2008). Effects of bisphenol A on the embryonic development of sea urchin (*Paracentrotus lividus*). *Environmental Toxicology* **23**:387-392. doi: 10.1002/tox.20349
- Parks, J. E., Lee, D. R., Huang, S., and Kaproth, M. T. (2003). Prospects for spermatogenesis in vitro. *Theriogenology* **59**:73-86. doi: 10.1016/S0093-691X(02)01275-X

- Phillips, B. T., Gassei, K., and Orwig, K. E. (2010). Spermatogonial stem cell regulation and spermatogenesis. *Phil Trans R Soc B* **365**:1663-1678. doi: 10.1098/rstb.2010.0026
- Pocklington, P., and Wells, P. G. (1992). Polychaetes Key taxa for marine environmental quality monitoring. *Marine Pollution Bulletin* **24**:593-598. doi: 10.1016/0025-326X(92)90278-E
- Poli, G., Schaur, R. J., Siems, W. G., and Leonarduzzi, G. (2008). 4-Hydroxynonenal: A membrane lipid oxidation product of medicinal interest. *Medicinal Research Reviews* **28**:569-631. doi: 10.1002/med.20117
- Prasanth, G. K., Divya, L. M., and Sadasivan, C. (2009). Effects of mono and di(n-butyl) phthalate on superoxide dismutase. *Toxicology* **262**:38-42. doi: 10.1016/j.tox.2009.04.036
- Purschke, G. (2002). Male genital organs, spermatogenesis and spermatozoa in the enigmatic terrestrial polychaete *Parergodrilus heideri* (Annelida, Parergodrilidae). *Zoomorphology* **121**:125-138. doi: 10.1007/s004350100050
- Purschke, G., and Fursman, M. C. (2005). Spermatogenesis and spermatozoa in *Stygocapitella subterranea* (Annelida, Parergodrilidae), an enigmatic supralittoral polychaete. *Zoomorphology* **124**:137-148. doi: 10.1007/s00435-005-0001-x
- Radashevsky, V. I., Alexandrova, Y. N., and Yurchenko, O. V. (2011). Spermiogenesis and spermatozoa ultrastructure of *Aonides oxycephala* (Annelida: Spionidae) from the Sea of Japan. *Invertebr Reprod Dev* **55**:168-174. doi: 10.1080/07924259.2011.553410
- Rainbow, P. S. (1995). Biomonitoring of heavy metal availability in the marine environment. *Mar Pollut Bull* **31**:183-192. doi: 10.1016/0025-326X(95)00116-5
- Rainbow, P. S. (2006). Biomonitoring of trace metals in estuarine and marine environments. *Aust J Ecotoxicol* **12**:107-122.
- Ravindranath, N., Dettin, L., and Dym, M. (2003). Mammalian Testes: Structure and Function. In D.R.P. Tulsiani (ed) Introduction to Mammalian Reproduction. Springer US, Boston, MA, pp. 1-19.
- Reish, D. J., Martin, J. M., Piltz, F. M., and Word, J. Q. (1976). The effect of heavy metals on laboratory populations of two polychaetes with comparisons to the water quality conditions and standards in Southern California marine waters. *Water Research* **10**:299-302. doi: 10.1016/0043-1354(76)90170-6
- Reunov, A. A., Yurchenko, O. V., Alexandrova, Y. N., and Radashevsky, V. I. (2010). Spermatogenesis in *Boccardiella hamata* (Polychaeta: Spionidae) from the Sea of Japan: sperm formation mechanisms as characteristics for future taxonomic revision. *Acta Zool* **91**:447-456. doi: 10.1111/j.1463-6395.2009.00435.x

- Rice, S. A. (1981). Spermatogenesis and sperm ultrastructure in three species of *Polydora* and in *Streblospio benedicti* (Polychaeta: Spionidae). *Zoomorphology* **97**:1-16. doi: 10.1007/BF00310099
- Rice, S. A., and Eckelbarger, K. J. (1989). An ultrastructural investigation of spermatogenesis in the holopelagic polychaetes *Vanadis formosa* and *Krohnia lepidota* (Polychaeta: Alciopidae). *Biol Bull* **176**:123-134. doi: 10.2307/1541579
- Roepke, T. A., Snyder, M. J., and Cherr, G. N. (2005). Estradiol and endocrine disrupting compounds adversely affect development of sea urchin embryos at environmentally relevant concentrations. *Aquatic Toxicology* **71**:155-173. doi: 10.1016/j.aquatox.2004.11.003
- Roosen-Runge, E. C. (1977). The process of spermatogenesis in animals. Cambridge University Press, Cambridge, UK, pp. 154-157.
- Ross, K., and Bidwell, J. (2001). A 48-h larval development toxicity test using the marine polychaete *Galeolaria caespitosa* Lamarck (Fam. Serpulidae). *Arch Environ Contam Toxicol* **40**:489-496. doi: 10.1007/s002440010201
- Rossi, S. S., and Neff, J. M. (1978). Toxicity of polynuclear aromatic hydrocarbons to the polychaete *Neanthes arenaceodentata*. *Marine Pollution Bulletin* **9**:220-223. doi: 10.1016/0025-326X(78)90297-7
- Rouse, G. W. (1998). The Annelida. In D.T. Anderson (ed) Invertebrate zoology. Oxford University Press, South Melbourne, pp. 196-200.
- Rouse, G. W. (1999). Polychaete sperm: phylogenetic and functional considerations. *Hydrobiologia* **402**:215-224. doi: 10.1023/a:1003700827759
- Rouse, G. W. (2005). Annelid sperm and fertilization biology. *Hydrobiologia* **535**:167-178.
- Sajiki, J., and Yonekubo, J. (2003). Leaching of bisphenol A (BPA) to seawater from polycarbonate plastic and its degradation by reactive oxygen species. *Chemosphere* **51**:55-62. doi: 10.1016/S0045-6535(02)00789-0
- Sakaue, M., Ohsako, S., Ishimura, R., Kurosawa, S., Kurohmaru, M., Hayashi, Y., Aoki, Y., Yonemoto, J., and Tohyama, C. (2001). Bisphenol-A Affects Spermatogenesis in the Adult Rat Even at a Low Dose. *Journal of Occupational Health* **43**:185-190. doi: 10.1539/joh.43.185
- Saliu, J. K., and Ovuorie, U. R. (2007). The artificial substrate preference of invertebrates in Ogbe Creek, Lagos, Nigeria. *Life Sci J* **4**:77-81.
- Sany, S. B. T., Hashim, R., Rezayi, M., Salleh, A., and Safari, O. (2014). A review of strategies to monitor water and sediment quality for a sustainability assessment of marine environment. *Environ Sci Pollut Res* **21**:813-833. doi: 10.1007/s11356-013-2217-5

- Sarkar, A., Ray, D., Shrivastava, A. N., and Sarker, S. (2006). Molecular biomarkers: their significance and application in marine pollution monitoring. *Ecotoxicology* **15**:333-340. doi: 10.1007/s10646-006-0069-1
- Sathananthan, A., Ratnam, S., Ng, S., Tarin, J., Gianaroli, L., and Trounson, A. (1996). The sperm centriole: its inheritance, replication and perpetuation in early human embryos. *Hum Reprod* **11**:345-356.
- Schatten, G., Simerly, C., and Schatten, H. (1985). Microtubule configurations during fertilization, mitosis, and early development in the mouse and the requirement for egg microtubule-mediated motility during mammalian fertilization. *Proceedings of the National Academy of Sciences* **82**:4152-4156.
- Schatten, H., Schatten, G., Mazia, D., Balczon, R., and Simerly, C. (1986). Behavior of centrosomes during fertilization and cell division in mouse oocytes and in sea urchin eggs. *Proc Natl Acad Sci U S A* **83**:105-109.
- Schlegel, P., Havenhand, J. N., Obadia, N., and Williamson, J. E. (2014). Sperm swimming in the polychaete *Galeolaria caespitosa* shows substantial inter-individual variability in response to future ocean acidification. *Mar Pollut Bull* **78**:213-217. doi: 10.1016/j.marpolbul.2013.10.040
- Schutt, F., Bergmann, M., Holz, F. G., and Kopitz, J. (2003). Proteins modified by malondialdehyde, 4-hydroxynonenal, or advanced glycation end products in lipofuscin of human retinal pigment epithelium. *Invest Ophthalmol Vis Sci* **44**:3663-3668. doi: 10.1167/iovs.03-0172
- Selim, S., Naby, F. A., Gab-Alla, A., and Ghobashy, A. (2005). Gametogenesis and spawning of *Spirobranchus tetraceros* (Polychaeta, Serpulidae) in Abu Kir Bay, Egypt. *Mediterranean Marine Science* **6**:89-98.
- Shao, X.-L., Ma, J., and Wen, G. (2008). Investigation of endocrine disrupting chemicals in a drinking water work located in Songhua River basin. *Chin J Environ Sci* **29**:2723-2728.
- Sharma, R., and Agarwal, A. (2011). Spermatogenesis: An Overview. In A. Zini and A. Agarwal (eds) *Sperm Chromatin: Biological and Clinical Applications in Male Infertility and Assisted Reproduction*. Springer New York, New York, NY, pp. 19-44.
- Sharma, R. K., and Agarwal, A. (1996). Role of reactive oxygen species in male infertility. *Urology* **48**:835-850. doi: 10.1016/s0090-4295(96)00313-5
- Sies, H. (1997). Oxidative stress: oxidants and antioxidants. *Experimental Physiology* **82**:291-295. doi: 10.1113/expphysiol.1997.sp004024
- Simon, C. A., and Rouse, G. W. (2005). Ultrastructure of spermiogenesis, sperm, and the spermatheca in *Terebrasabella heterouncinata* (Polychaeta: Sabellidae: Sabellinae). *Invertebrate Biology* **124**:39-49.

- Sindermann, C. J. (1979). Pollution-associated diseases and abnormalities of fish and shellfish: a review. *Fish Bull* **76**:717-749.
- Sofikitis, N., Giotitsas, N., Tsounapi, P., Baltogiannis, D., Giannakis, D., and Pardalidis, N. (2008). Hormonal regulation of spermatogenesis and spermiogenesis. *The Journal of Steroid Biochemistry and Molecular Biology* **109**:323-330. doi: 10.1016/j.jsbmb.2008.03.004
- Staples, C. A., Adams, W. J., Parkerton, T. F., Gorsuch, J. W., Biddinger, G. R., and Reinert, K. H. (1997). Aquatic toxicity of eighteen phthalate esters. *Environmental Toxicology and Chemistry* **16**:875-891. doi: 10.1002/etc.5620160507
- Staples, C. A., Dome, P. B., Klecka, G. M., Oblock, S. T., and Harris, L. R. (1998). A review of the environmental fate, effects, and exposures of bisphenol A. *Chemosphere* **36**:2149-2173. doi: 10.1016/S0045-6535(97)10133-3
- Straight, A. F., and Field, C. M. (2000). Microtubules, membranes and cytokinesis. *Curr Biol* **10**:R760-R770. doi: 10.1016/S0960-9822(00)00746-6
- Styan, C. A., Kupriyanova, E. K., and Havenhand, J. N. (2008). Barriers to cross-fertilization between populations of a widely dispersed polychaete species are unlikely to have arisen through gametic compatibility arms - races. *Evolution* **62**:3041-3055. doi: 10.1111/j.1558-5646.2008.00521.x
- Subramoniam, T. (2000). Crustacean ecdysteroids in reproduction and embryogenesis. *Comparative Biochemistry and Physiology Part C: Pharmacology, Toxicology and Endocrinology* **125**:135-156. doi: 10.1016/S0742-8413(99)00098-5
- Sutovsky, P., and Manandhar, G. (2006). Mammalian spermatogenesis and sperm structure: anatomical and compartmental analysis. In C.J.D. Jonge and C.L.R. Barratt (eds) *The sperm cell*. Cambridge University Press, New York, UK, pp. 7-10.
- Torres, M. A., Barros, M. P., Campos, S. C., Pinto, E., Rajamani, S., Sayre, R. T., and Colepicolo, P. (2008). Biochemical biomarkers in algae and marine pollution: a review. *Ecotox Environ Safe* **71**:1-15. doi: 10.1016/j.ecoenv.2008.05.009
- Tulsiani, D. (2003). Introduction to Mammalian Reproduction. Springer, US, pp. 27-31.
- Valavanidis, A., Vlahogianni, T., Dassenakis, M., and Scoullou, M. (2006). Molecular biomarkers of oxidative stress in aquatic organisms in relation to toxic environmental pollutants. *Ecotoxicology and Environmental Safety* **64**:178-189. doi: 10.1016/j.ecoenv.2005.03.013
- Van Dover, C. L., Trask, J., Gross, J., Knowlton, A., and Van Dover, C. (1999). Reproductive biology of free-living and commensal polynoid polychaetes at the

Lucky Strike hydrothermal vent field (Mid-Atlantic Ridge). *Mar Ecol Prog Ser* **181**:201-214. doi: 10.3354/meps181201

van Wezel, A. P., van Vlaardingen, P., Posthumus, R., Crommentuijn, G. H., and Sijm, D. T. H. M. (2000). Environmental risk limits for two phthalates, with special emphasis on endocrine disruptive properties. *Ecotox Environ Safe* **46**:305-321. doi: 10.1006/eesa.2000.1930

Vortsepneva, E. V., Zhadan, A. E., and Tzetlin, A. B. (2006). Spermiogenesis and sperm ultrastructure of *Asetocalamyzas laonicola* Tzetlin, 1985 (Polychaeta), an ectoparasite of the large spionid *Scolelepis* cf. *matsugae* Sikorsfi, 1994, from the White Sea. *Sci Mar* **70**:343-350. doi: 10.3989/scimar.2006.70s3343

Wang, W., Craig, Z. R., Basavarajappa, M. S., Gupta, R. K., and Flaws, J. A. (2012). Di (2-ethylhexyl) phthalate inhibits growth of mouse ovarian antral follicles through an oxidative stress pathway. *Toxicol Appl Pharm* **258**:288-295. doi: 10.1016/j.taap.2011.11.008

Ward, T. J., and Jacoby, C. A. (1992). A strategy for assessment and management of marine ecosystems: baseline and monitoring studies in Jervis Bay, a temperate Australian embayment. *Mar Pollut Bull* **25**:163-171. doi: 10.1016/0025-326X(92)90220-Z

Waring, J. S., Maher, W. A., and Krikowa, F. (2006). Trace metal bioaccumulation in eight common coastal Australian polychaeta. *J Environ Monit* **8**:1149-1157. doi: 10.1039/B612509N

Weston, P. D., Penry, L. D., and Gulmann, K. L. (2000). The role of ingestion as a route of contaminant bioaccumulation in a deposit-feeding polychaete. *Arch Environ Contam Toxicol* **38**:446-454. doi: 10.1007/s002449910059

Wilson, W. H. (1991). Sexual reproductive modes in polychaetes: classification and diversity. *Bull Mar Sci* **48**:500-516.

Wisely, B., and Blick, R. (1967). Mortality of marine invertebrate larvae in mercury, copper, and zinc solutions. *Mar Freshwater Res* **18**:63-72. doi: 10.1071/MF9670063

Wistuba, J., Stukenborg, J.-B., and Luetjens, C. M. (2007). Mammalian spermatogenesis. *Funct Dev Embryol* **1**:99-117.

Xing, M. (2012). Oxidative stress: a new risk factor for thyroid cancer. *Endocrine-Related Cancer* **19**:C7-C11. doi: 10.1530/erc-11-0360

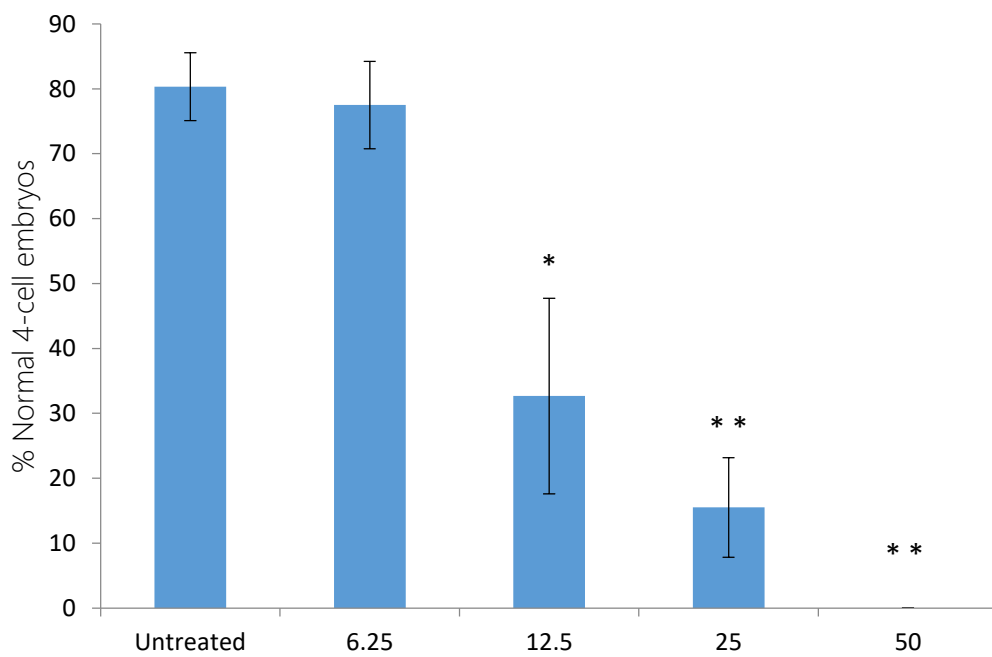
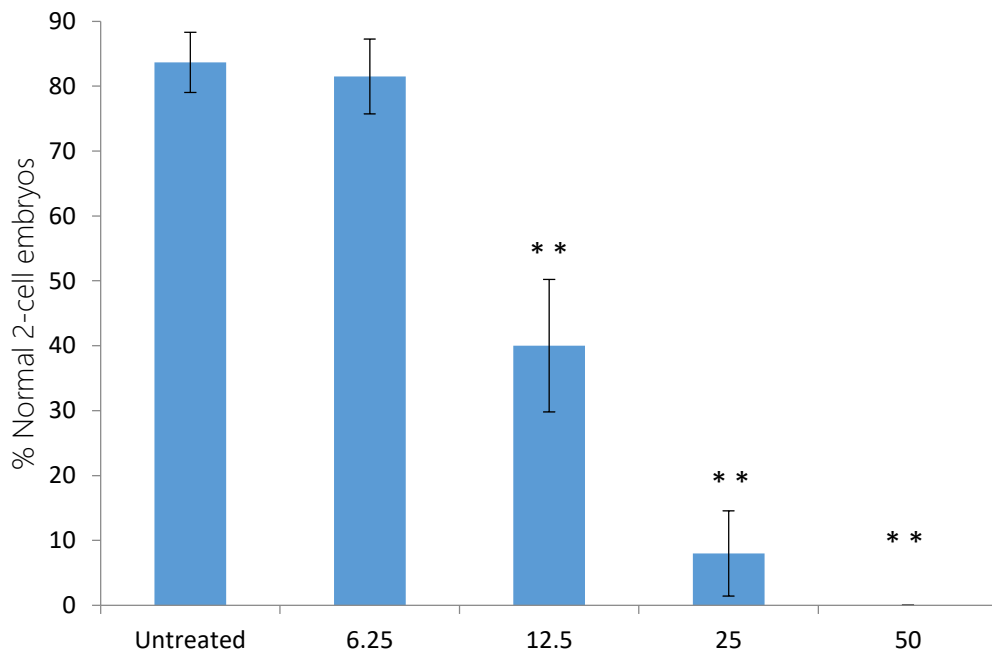
Yakes, F. M., and Van Houten, B. (1997). Mitochondrial DNA damage is more extensive and persists longer than nuclear DNA damage in human cells following oxidative stress. *Proceedings of the National Academy of Sciences* **94**:514-519.

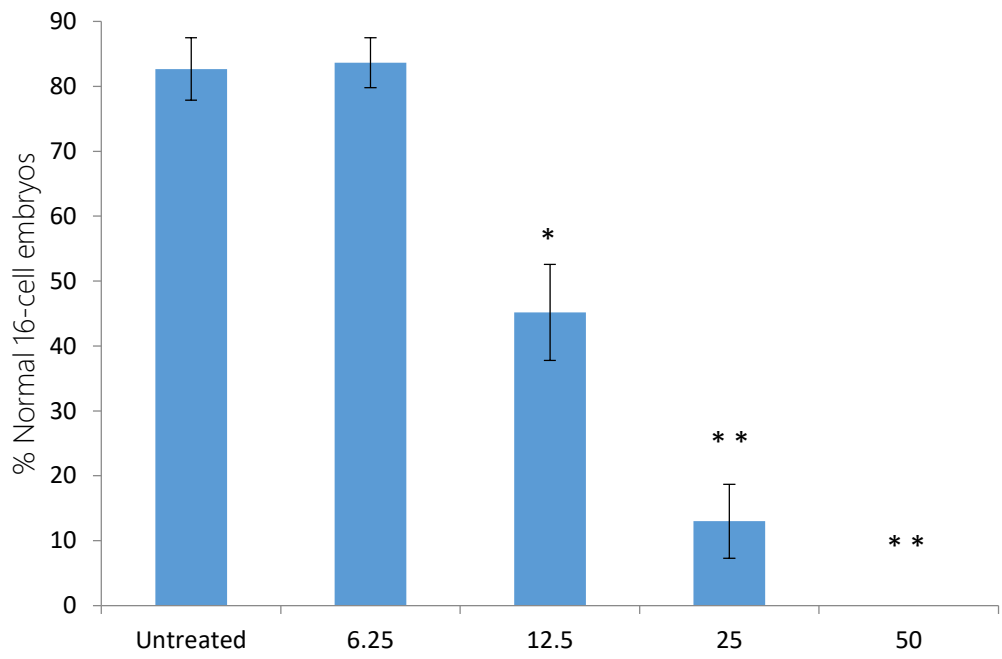
- Yuan, S. Y., Liu, C., Liao, C. S., and Chang, B. V. (2002). Occurrence and microbial degradation of phthalate esters in Taiwan river sediments. *Chemosphere* **49**:1295-1299. doi: 10.1016/S0045-6535(02)00495-2
- Zhou, F., Guo, H., Liu, Y., and Jiang, Y. (2007). Chemometrics data analysis of marine water quality and source identification in Southern Hong Kong. *Mar Pollut Bull* **54**:745-756. doi: 10.1016/j.marpolbul.2007.01.006
- Zhou, J., Cai, Z.-H., and Xing, K.-Z. (2011a). Potential mechanisms of phthalate ester embryotoxicity in the abalone *Haliotis diversicolor supertexta*. *Environmental Pollution* **159**:1114-1122. doi: 10.1016/j.envpol.2011.02.016
- Zhou, J., Zhu, X.-S., and Cai, Z.-H. (2011b). The impacts of bisphenol A (BPA) on abalone (*Haliotis diversicolor supertexta*) embryonic development. *Chemosphere* **82**:443-450. doi: 10.1016/j.chemosphere.2010.09.056

Appendix

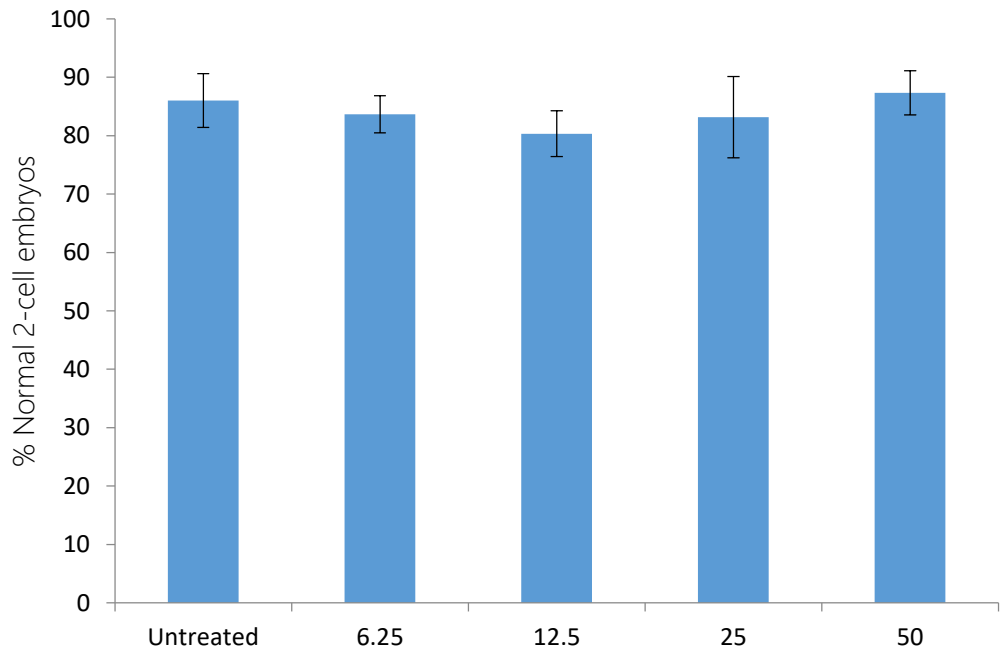
Toxicity tests for bisphenol A

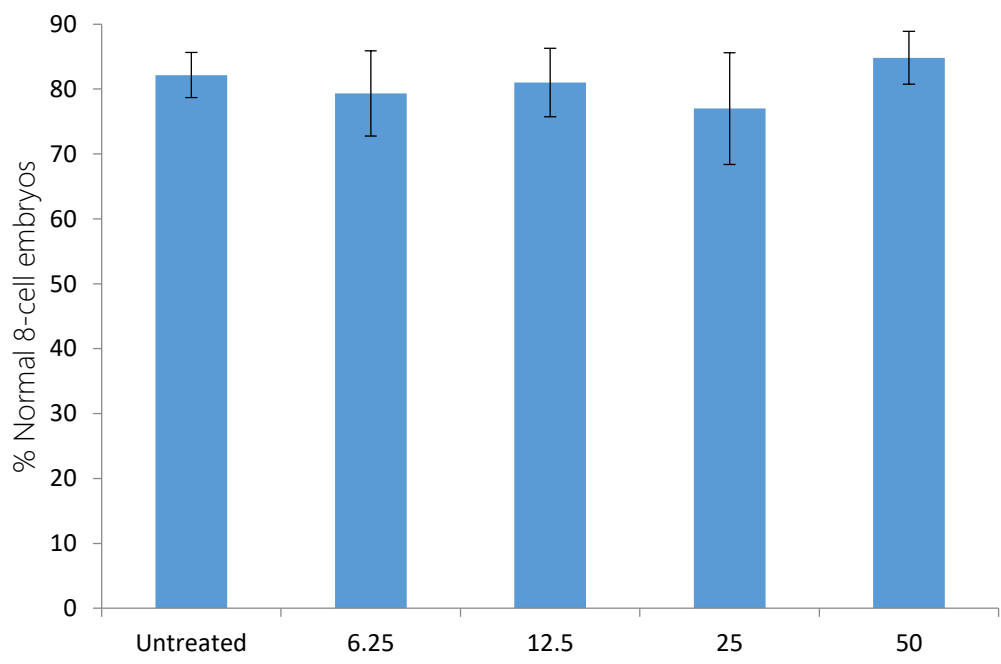
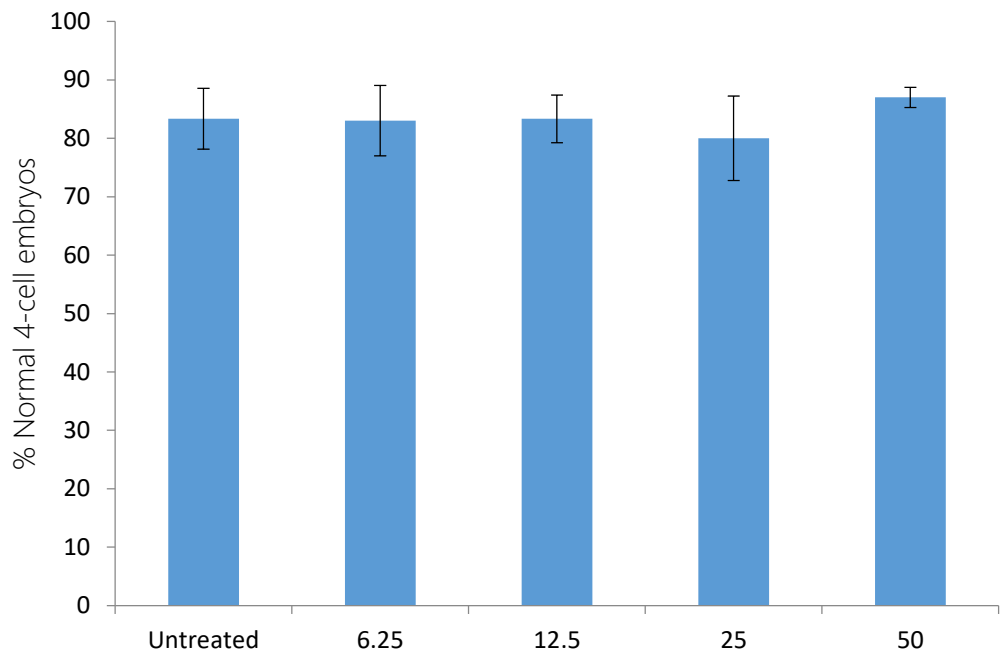
Sperm-exposure tests (Units: mg/L)

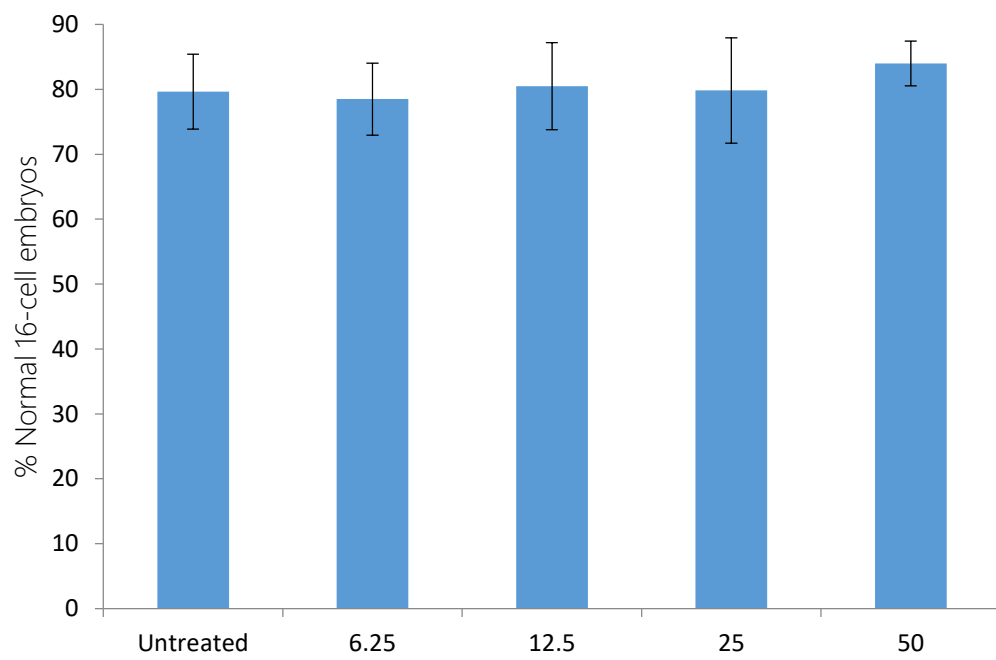




Oocyte-exposure tests (Units: mg/L)

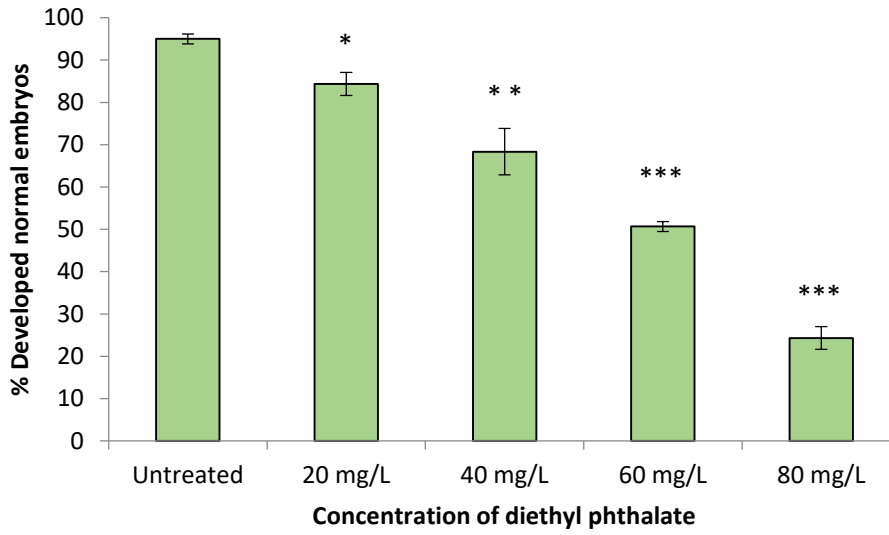




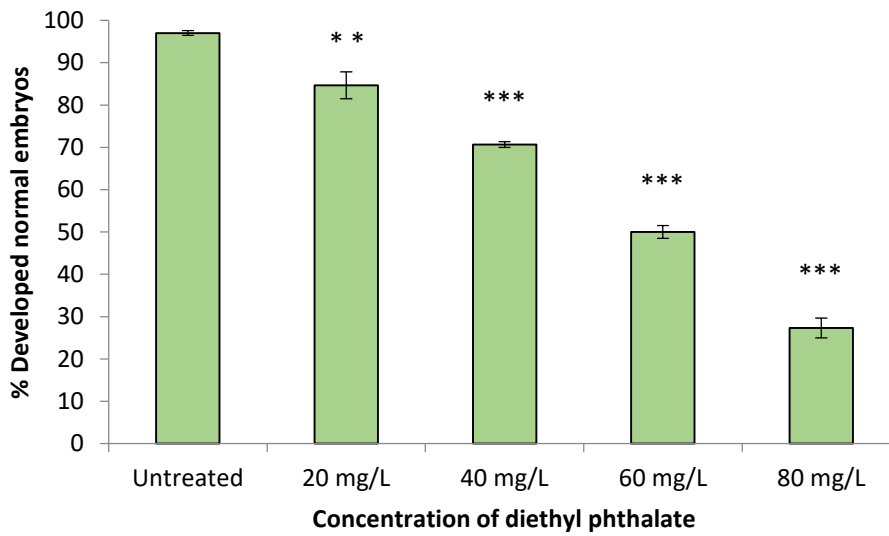


Diethyl Phthalate (Sperm-exposure)

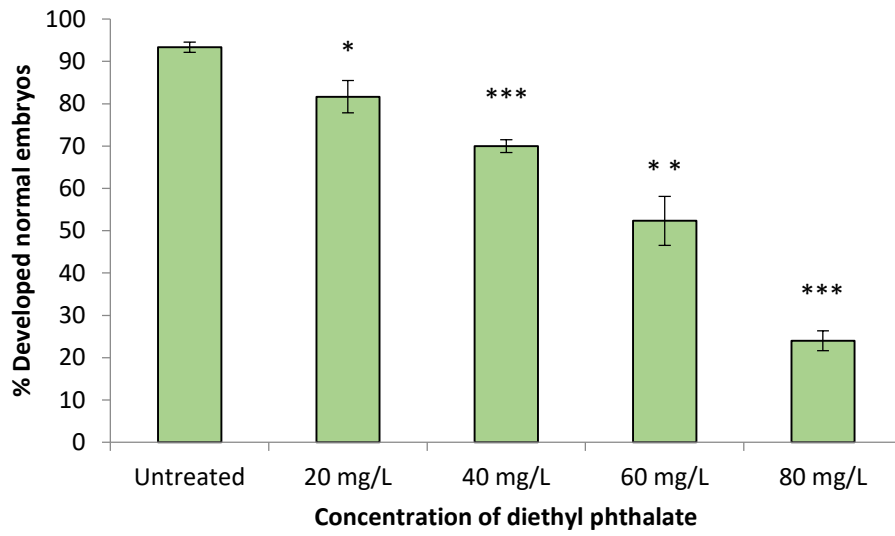
2-cell stage



4-cell stage

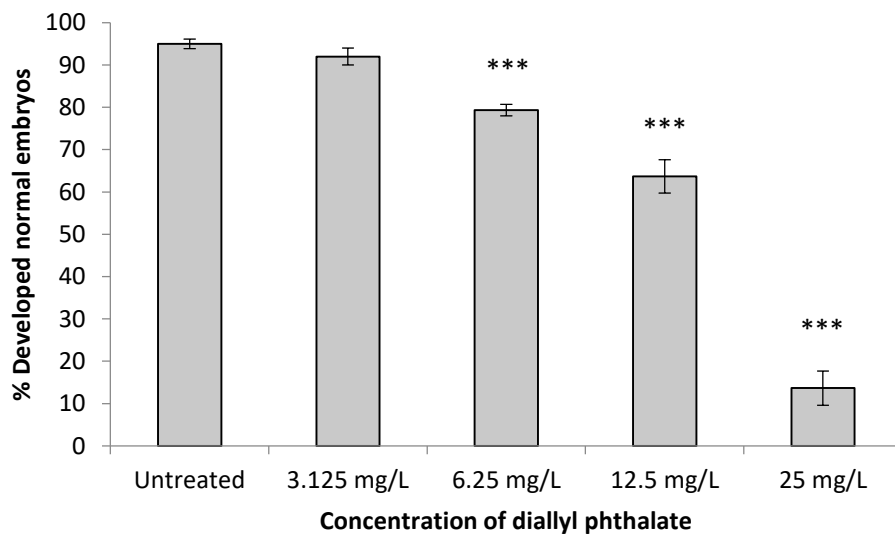


16-cell stage

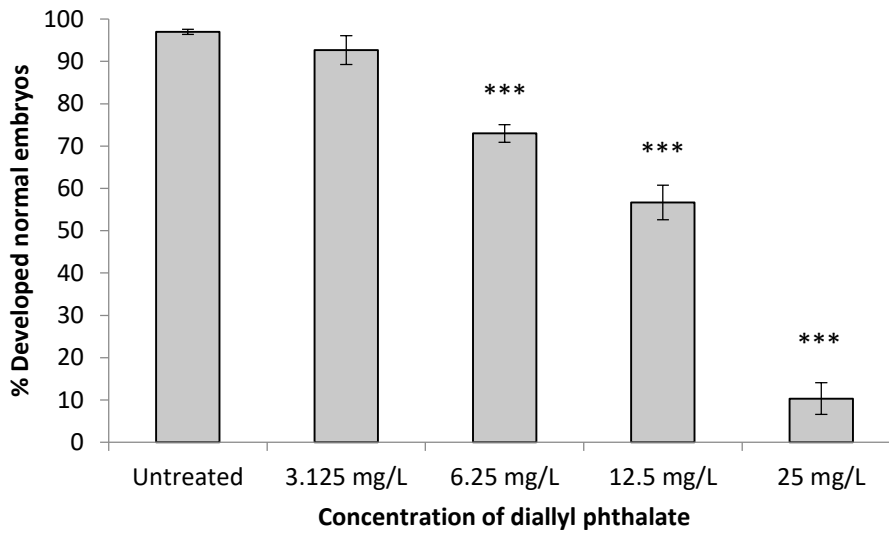


Diallyl phthalate (sperm-exposure)

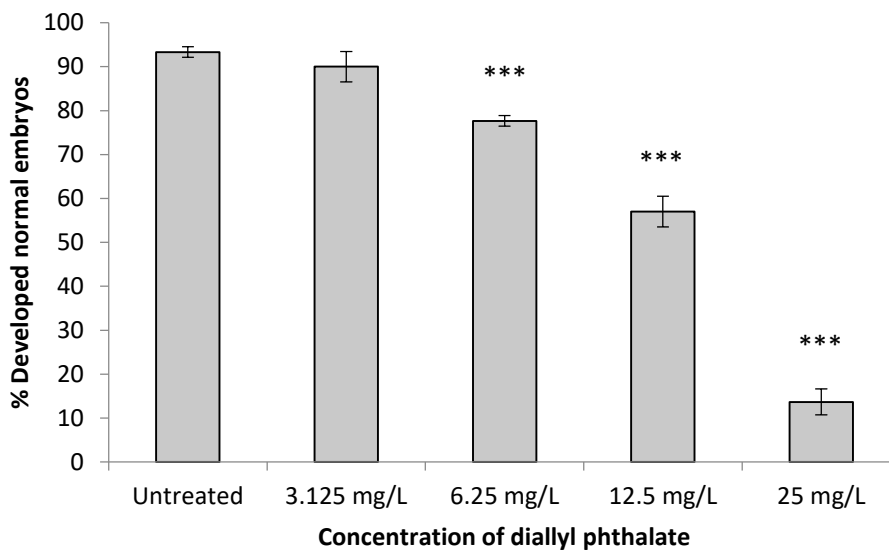
2-cell stage



4-cell stage

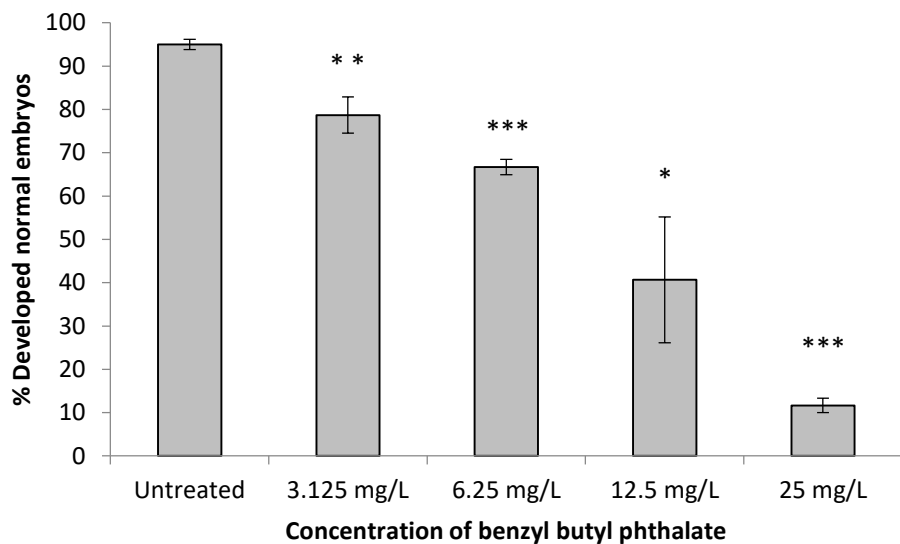


16-cell stage

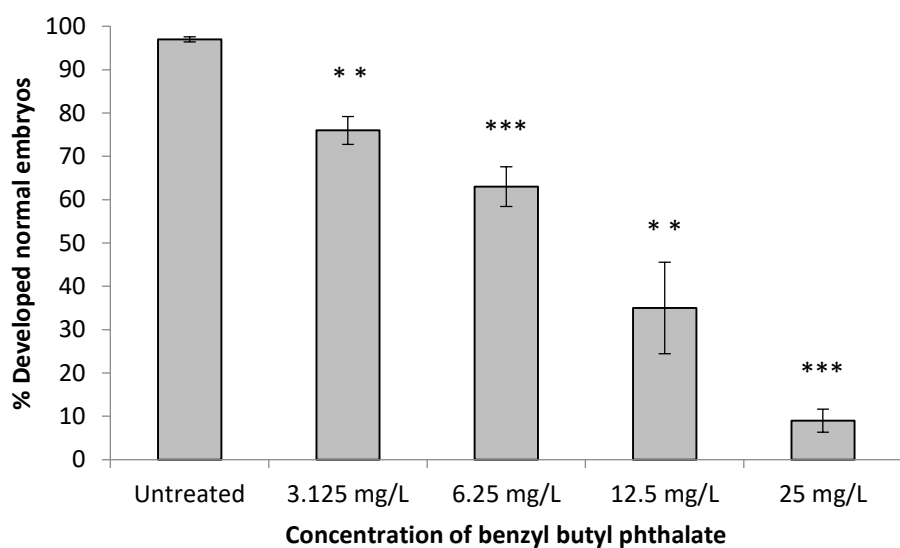


Benzyl butyl phthalate (sperm-exposure)

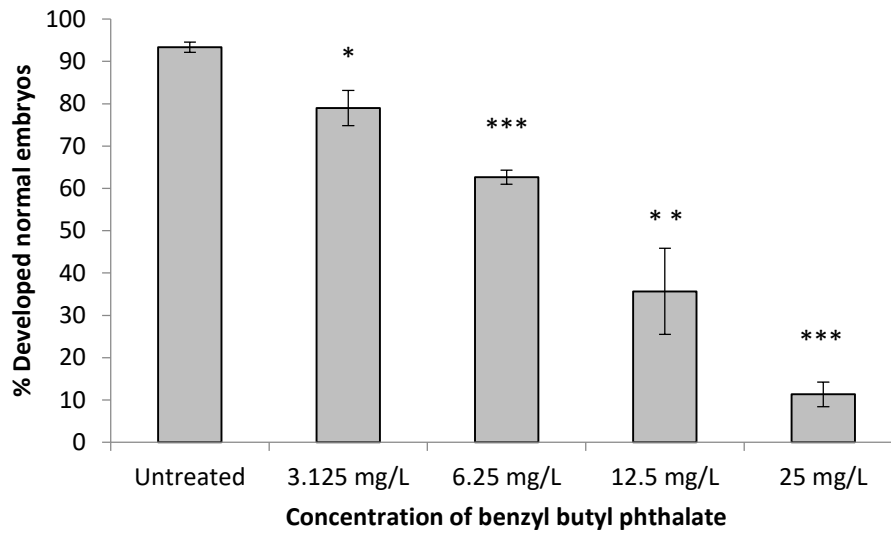
2-cell stage



4-cell stage

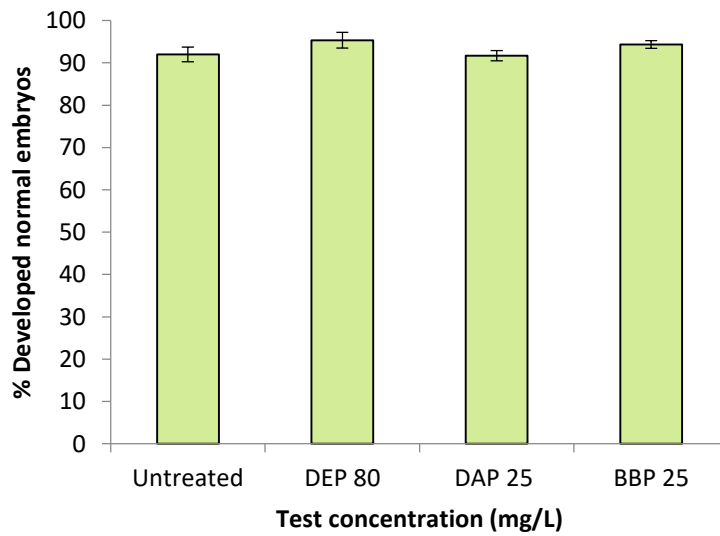


16-cell stage

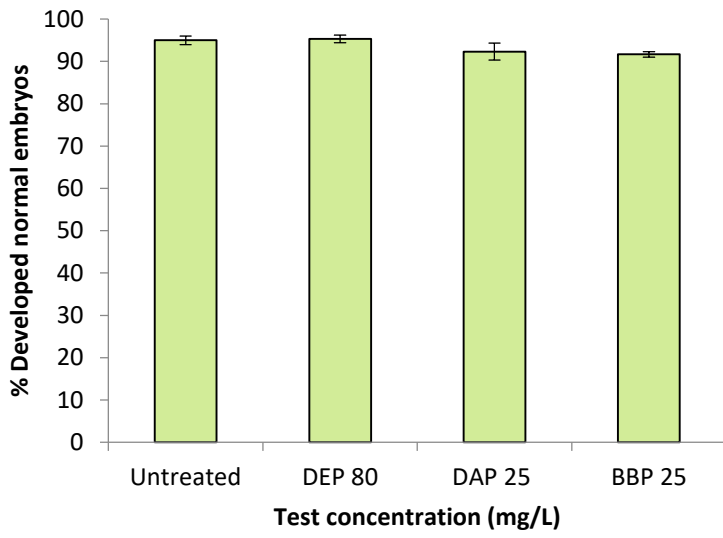


Diethyl phthalate, diallyl phthalate, benzyl butyl phthalate (oocyte-exposure)

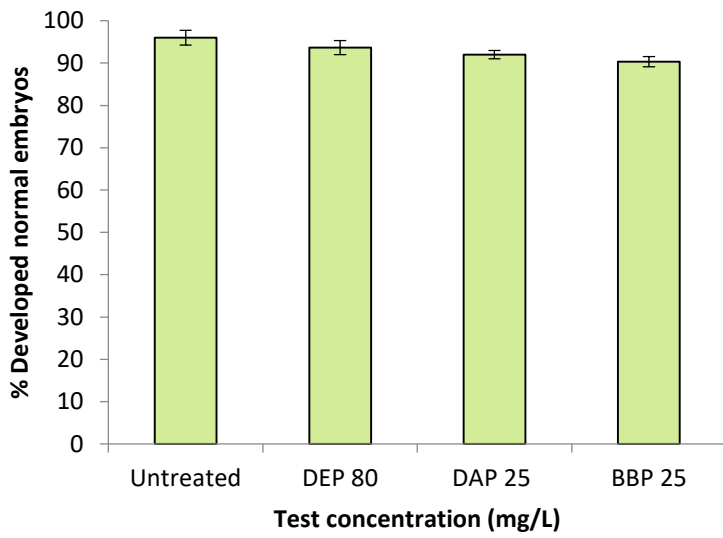
2-cell stage



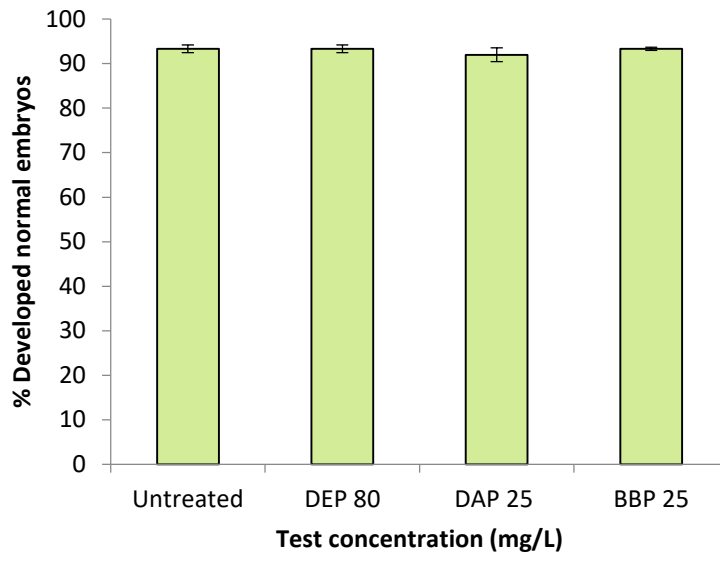
4-cell stage



8-cell stage

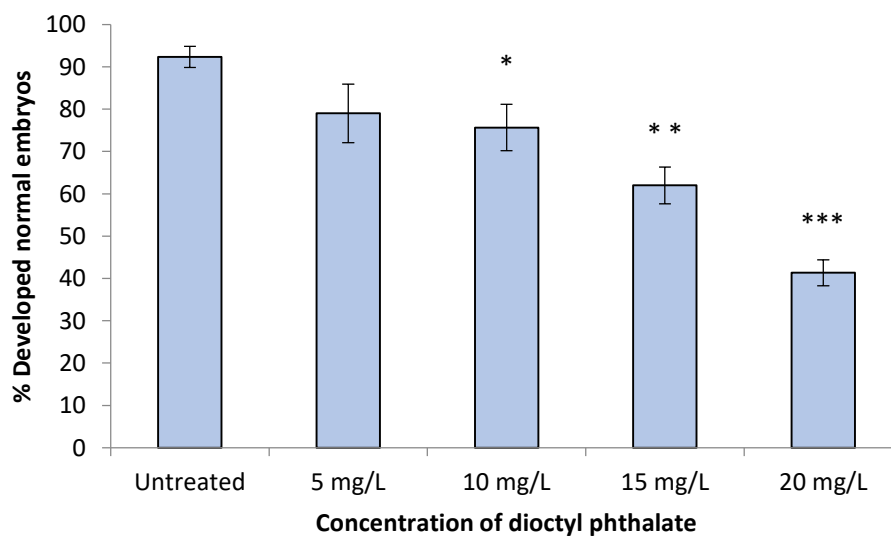


16-cell stage

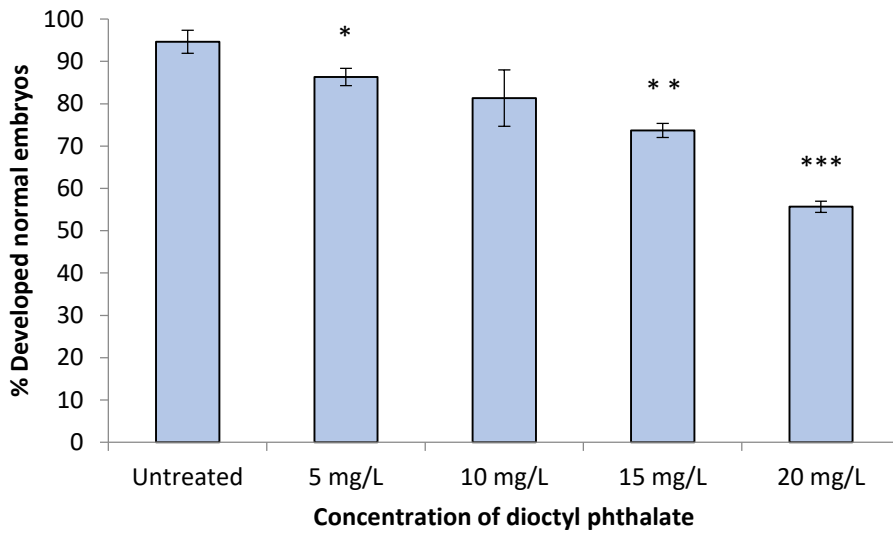


Diocetyl phthalate (sperm-exposure)

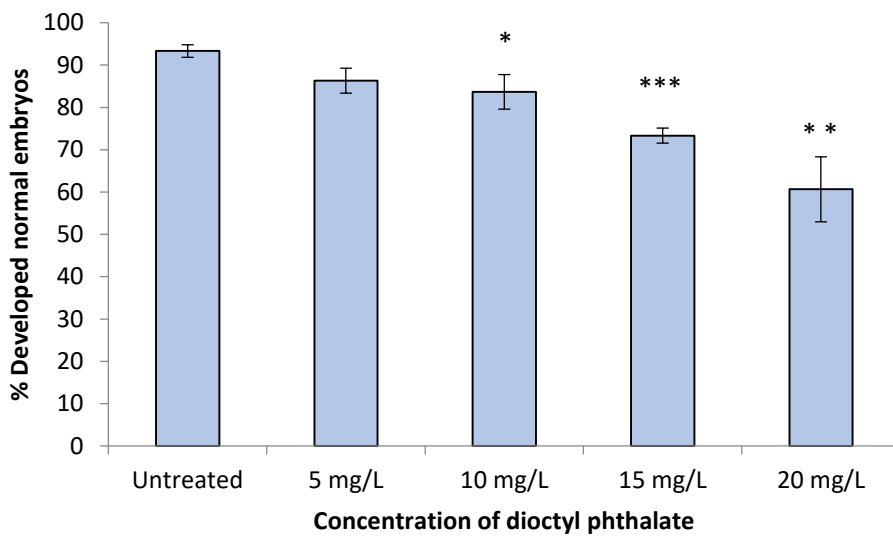
2-cell stage



4-cell stage

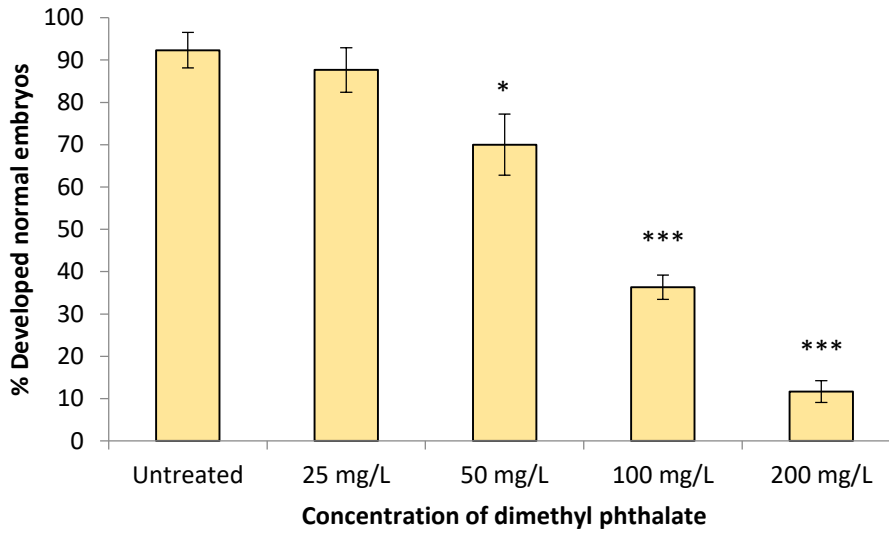


16-cell stage

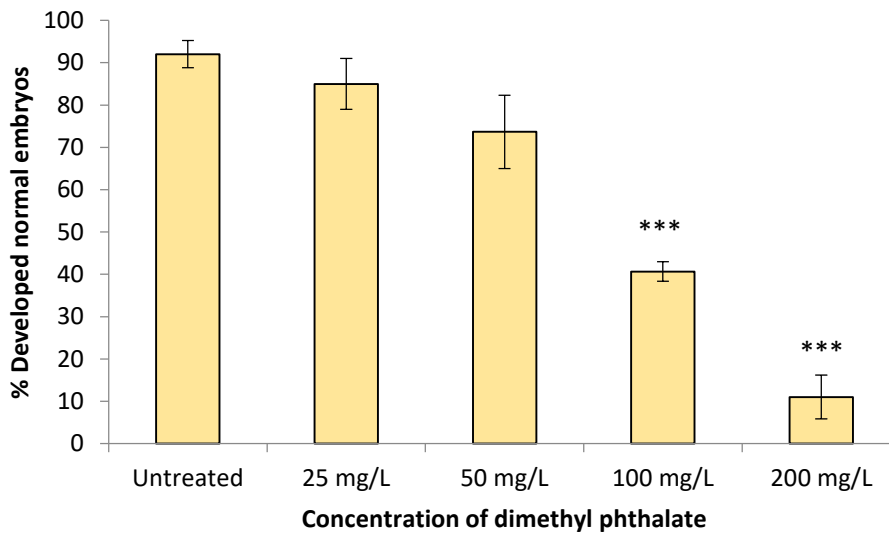


Dimethyl phthalate (sperm-exposure)

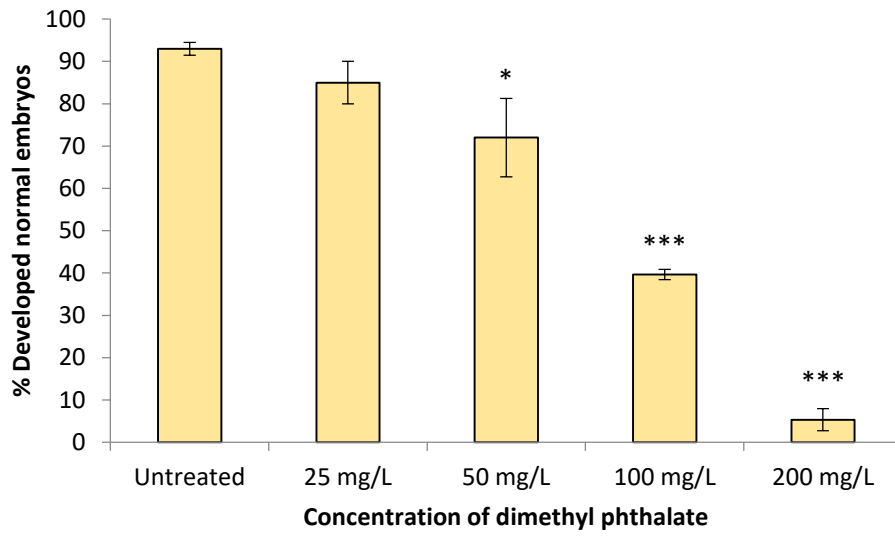
2-cell stage



4-cell stage

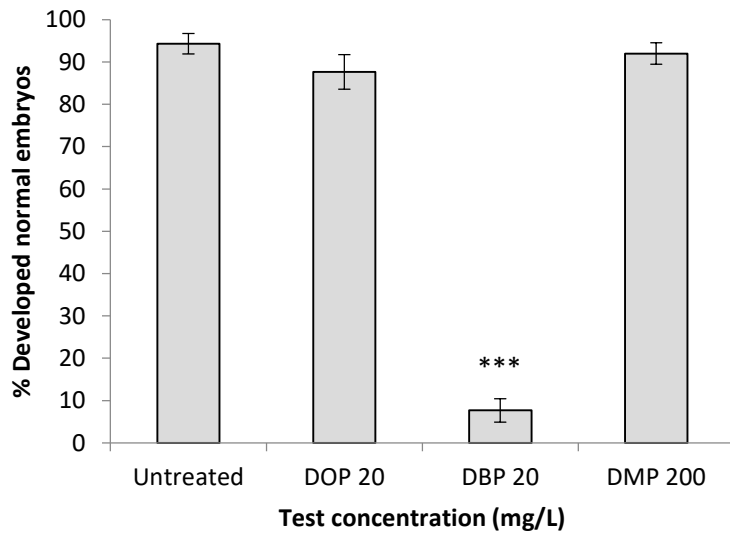


16-cell stage

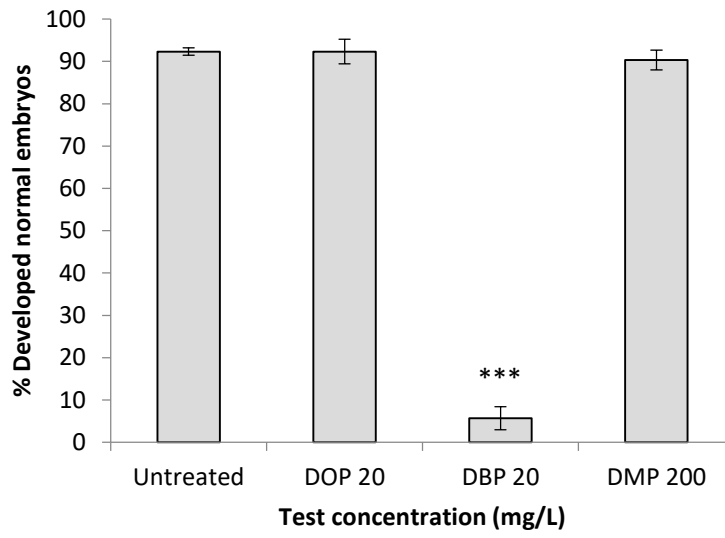


Diocetyl phthalate, dibutyl phthalate, dimethyl phthalate (oocyte-exposure)

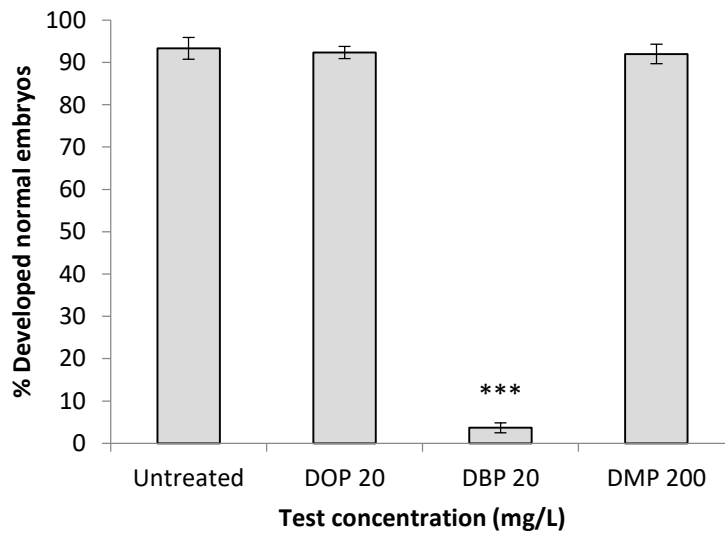
2-cell stage



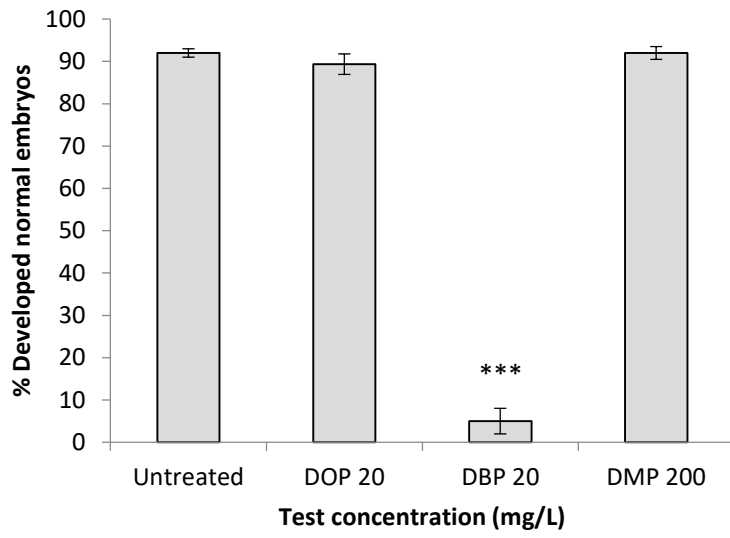
4-cell stage



8-cell stage



16-cell stage



Octylphenol (Sperm-exposure test)

